

Amazon hydrology from space: scientific advances and future challenges

Alice César Fassoni-Andrade¹, Ayan Santos Fleischmann², Fabrice Papa³, Rodrigo Cauduro Dias de Paiva⁴, Sly Wongchuig⁵, John M. Melack⁶, Adriana Aparecida Moreira⁷, Adrien Paris⁸, Anderson Ruhoff², Claudio Clemente Faria Barbosa⁹, Daniel Andrade Maciel⁹, Evlyn Márcia Leão de Moraes Novo¹⁰, Fabien Durand¹¹, Frederic Frappart¹², Filipe Aires¹³, Gabriel Medeiros Abrahão¹⁴, Jefferson Ferreira-Ferreira¹⁵, Jhan Carlo Espinoza³, Leonardo Laipelt², Marcos Heil Costa¹⁴, Raul Espinoza-Villar¹⁶, Stephane Calmant¹⁷, and Victor Pellet¹⁸

¹Institute of Geosciences, University of Brasília

²Universidade Federal do Rio Grande do Sul

³Institut de Recherche pour le Développement

⁴Instituto de Pesquisas Hidráulicas IPH, Universidade Federal do Rio Grande do Sul UFRGS, Porto Alegre, Brazil

⁵Univ. Grenoble Alpes, IRD, CNRS, Grenoble INP, Insitut des Géosciences de l'Environnement (IGE, UMR 5001)

⁶Earth Research Institute, University of California

⁷Instituto de Pesquisas Hidráulicas IPH, Universidade Federal do Rio Grande do Sul

⁸Université de Toulouse, CNRS, CNES, IRD, UPS

⁹Brazilian Institute of Space Research

¹⁰Instituto Nacional de Pesquisas Espaciais

¹¹IRD/LEGOS

¹²LEGOS

¹³LERMA

¹⁴Federal University of Viçosa

¹⁵Mamirauá Institute for Sustainable Development

¹⁶Universidad Nacional Agraria La Molina

¹⁷IRD

¹⁸The University of Tokyo

November 23, 2022

Abstract

As the largest river basin on Earth, the Amazon is of major importance to the world's climate and water resources. Over the past decades, advances in satellite-based remote sensing (RS) have brought our understanding of its terrestrial water cycle and the associated hydrological processes to a new era. Here, we review major studies and the various techniques using satellite RS in the Amazon. We show how RS played a major role in supporting new research and key findings regarding the Amazon water cycle, and how the region became a laboratory for groundbreaking investigations of new satellite retrievals and analyses. At the basin-scale, the understanding of several hydrological processes was only possible with the advent of RS observations,

such as the characterization of “rainfall hotspots” in the Andes-Amazon transition, evapotranspiration rates, and variations of surface waters and groundwater storage. These results strongly contribute to the recent advances of hydrological models and to our new understanding of the Amazon water budget and aquatic environments. In the context of upcoming hydrology-oriented satellite missions, which will offer the opportunity for new synergies and new observations with finer space-time resolution, this review aims to guide future research agenda towards an integrated monitoring and understanding of the Amazon water from space. Integrated multidisciplinary studies, fostered by international collaborations, set up future directions to tackle the great challenges the Amazon is currently facing, from climate change to increased anthropogenic pressure.

Amazon hydrology from space: scientific advances and future challenges

Alice César Fassoni-Andrade^{1,2,3}, Ayan Santos Fleischmann³, Fabrice Papa^{1,2}, Rodrigo Cauduro Dias de Paiva³, Sly Wongchuig⁴, John M. Melack⁵, Adriana Aparecida Moreira³, Adrien Paris^{6,1}, Anderson Ruhoff³, Claudio Barbosa⁷, Daniel Andrade Maciel⁷, Evlyn Novo⁷, Fabien Durand^{1,2}, Frédéric Frappart¹, Filipe Aires⁸, Gabriel Medeiros Abrahão⁹, Jefferson Ferreira-Ferreira¹⁰, Jhan Carlo Espinoza⁴, Leonardo Laipelt³, Marcos Heil Costa⁹, Raul Espinoza-Villar¹¹, Stéphane Calmant¹, Victor Pellet^{12,8}

¹ Laboratoire d'Etudes en Géophysique et Océanographie Spatiales (LEGOS), Université Toulouse, IRD, CNRS, CNES, UPS, Toulouse, France.

² Institute of Geosciences, University of Brasília (UnB), Campus Universitário Darcy Ribeiro, Brasília, Brazil.

³ Institute of Hydraulic Research, Federal University of Rio Grande do Sul (UFRGS), Porto Alegre, Brazil.

⁴ Univ. Grenoble Alpes, IRD, CNRS, Grenoble INP, Institut des Géosciences de l'Environnement (IGE, UMR 5001), 38000, Grenoble, France.

⁵ Earth Research Institute, University of California, Santa Barbara.

⁶ Ocean Next, La Terrasse, 38660 Grenoble, France.

⁷ Instrumentation Lab for Aquatic Systems (LabISA), Earth Observation Coordination of National Institute for Space Research (INPE), São José dos Campos, SP, Brazil.

⁸ Laboratoire d'Etudes du Rayonnement et de la Matière en Astrophysique et Atmosphères, Observatoire de Paris, UMR 8112, Paris, France.

⁹ Federal University of Viçosa (UFV), Viçosa, MG, Brazil.

¹⁰ Mamirauá Institute for Sustainable Development, Tefé, AM, Brazil.

¹¹ Departamento de Ordenamiento Territorial y Construcción, Universidad Nacional Agraria La Molina (UNALM), Av. La Molina s/n Lima 12, Perú.

¹² Institute of Industrial Science, The University of Tokyo, Tokyo, Japan.

Corresponding author: Alice Fassoni-Andrade (alice.fassoni@gmail.com, alice.fassoni@legos.obs-mip.fr)

Key points:

- Integrated view of scientific advances in Amazon hydrology with remote sensing
- Expected progresses to understand the water cycle, aquatic ecosystems and environmental changes with upcoming hydrology-oriented missions
- Need to translate advance knowledge from RS to support water management and environmental governance

38

39 **Abstract**

40 As the largest river basin on Earth, the Amazon is of major importance to the world's climate and
 41 water resources. Over the past decades, advances in satellite-based remote sensing (RS) have
 42 brought our understanding of its terrestrial water cycle and the associated hydrological processes
 43 to a new era. Here, we review major studies and the various techniques using satellite RS in the
 44 Amazon. We show how RS played a major role in supporting new research and key findings
 45 regarding the Amazon water cycle, and how the region became a laboratory for groundbreaking
 46 investigations of new satellite retrievals and analyses. At the basin-scale, the understanding of
 47 several hydrological processes was only possible with the advent of RS observations, such as the
 48 characterization of "rainfall hotspots" in the Andes-Amazon transition, evapotranspiration rates,
 49 and variations of surface waters and groundwater storage. These results strongly contribute to the
 50 recent advances of hydrological models and to our new understanding of the Amazon water
 51 budget and aquatic environments. In the context of upcoming hydrology-oriented satellite
 52 missions, which will offer the opportunity for new synergies and new observations with finer
 53 space-time resolution, this review aims to guide future research agenda towards an integrated
 54 monitoring and understanding of the Amazon water from space. Integrated multidisciplinary
 55 studies, fostered by international collaborations, set up future directions to tackle the great
 56 challenges the Amazon is currently facing, from climate change to increased anthropogenic
 57 pressure.

58

59 **Plain Language Summary**

60 The Amazon basin is the largest river basin in the world, characterized by complex hydrological
 61 processes that connect high rates of precipitation, extensive floodplains, dense tropical forests,
 62 complex topography, and large variations in freshwater storage and discharge. It plays a key role
 63 in the water, energy and carbon cycles and interacts with the global climate system. Earth
 64 observations have played a major role in supporting research in Amazon hydrology, and the
 65 characterization of several hydrological processes was only possible with the help of remote
 66 sensing data. The basin is now facing great risk under current climate change and increased
 67 anthropogenic pressure and the resulting environmental alterations require a better understanding
 68 of the overall basin's water cycle across scales. We review the strengths and limitations of
 69 observations from satellites in the context of the current and upcoming hydrology-oriented
 70 satellite missions, and we make recommendations for improving satellite observations of the
 71 Amazon basin water cycle, along with an interdisciplinary and stepwise approach to guide
 72 research for the next decades.

73

74 **Table of contents**

75

76	1. Introduction	3
77	2. Precipitation	8
78	3. Evapotranspiration	18

79	4. Surface water	26
80	4.1. Surface water elevation	26
81	4.2. Surface water extent	33
82	4.3. Floodplain and river channels topography	41
83	4.4. Water quality: Sediments, chlorophyll and colored dissolved organic matter	44
84	5. Total water storage and groundwater storage	50
85	6. Integrative and interdisciplinary studies	54
86	6.1. Water budget	54
87	6.2. Modeling the Amazon water cycle and its wetlands	58
88	6.3. Aquatic ecosystems	67
89	6.4. Environmental changes	71
90	7. Synthesis of scientific advances, future challenges and priorities	75
91	7.1. The Amazon Basin as a remote sensing laboratory for hydrology	78
92	7.2. The benefits of the lessons learnt in the Amazon to understand the hydrology of	
93	other large tropical river basins	82
94	7.3. Tackling the current knowledge gaps with future satellite missions	83
95	7.4. How to use RS-based scientific advances to foster water resources management in	
96	the Amazon basin?	88
97	7.5. Recommendations	90
98	Acknowledgments	91
99	Data Availability Statement	92
100	References	92

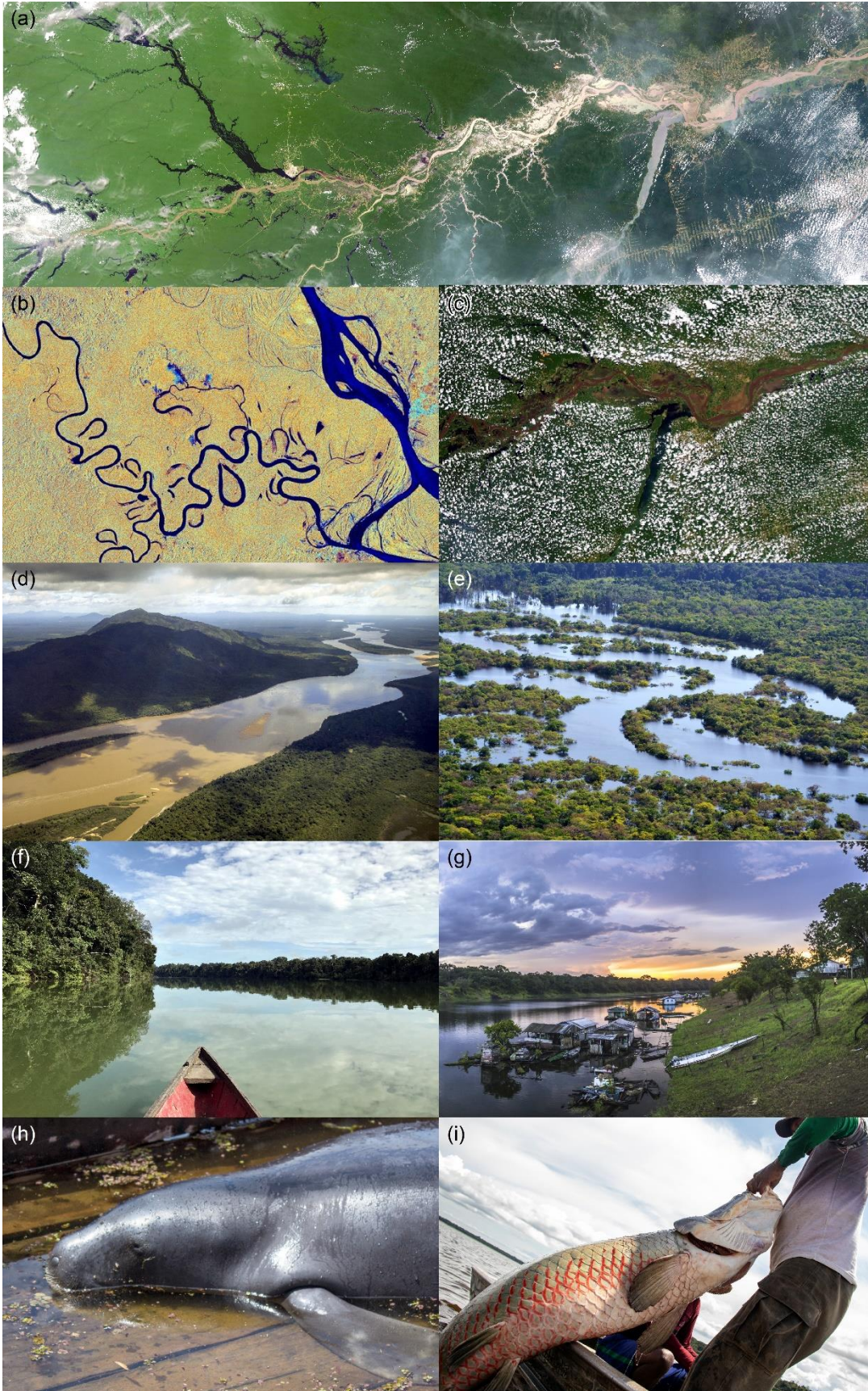
101

102 1. Introduction

103 The Amazon River basin (AB) is the major hydrological system of the world (~6 million
104 km²) with a diverse rivers, floodplains and wetlands (Latrubesse et al., 2017; **Figure 1**). It spans
105 over seven countries and it hosts four of the ten largest rivers in the world, namely the Solimões-
106 Amazonas, Madeira, Negro, and Japurá rivers (**Figure 2**). It receives high annual rainfall rates
107 (~2200 mm yr⁻¹, Builes-Jaramillo & Poveda, 2018; Espinoza et al., 2009) and around half of the
108 precipitation in the AB is recycled by local evapotranspiration (Salati et al., 1979; Satyamurty,
109 da Costa, & Manzi, 2013) providing moisture to southern parts of South America. The Amazon
110 River then flows into the Atlantic Ocean with an average annual discharge of 206 x 10³ m³s⁻¹
111 (Callède et al., 2010), amounting to almost 20% of the total global freshwater reaching the ocean
112 annually and exports the largest sedimentary supply to the ocean (1.1 x 10⁹ tons per year;
113 Armijos et al., 2020).

114 The high rates of precipitation, evapotranspiration, and large variations in freshwater
115 storage and river discharge make the AB a key player in the global climate system, with large
116 contributions to the water, energy, and carbon cycles (Gash et al., 2013; Nagy et al., 2016).
117 Amazon surface waters, for instance, are a major source and sink of carbon dioxide (Abril et al.,
118 2014; Amaral et al., 2020; Guilhen et al., 2020; Raymond et al., 2013; Richey et al., 2002) and
119 the largest natural geographic source of methane in the tropics (Kirschke et al., 2013; Melack et
120 al., 2004; Pangala et al., 2017; Pison et al., 2013). Seasonal variations in water contribute to the
121 formation of tropical forests (Leite et al., 2012), maintain high aquatic productivity (Melack &
122 Forsberg, 2001) and biodiversity (Junk, 1997; Junk et al., 2010), and influence fish distributions
123 and fisheries yield (Junk et al., 2010; Lobón-Cerviá et al., 2015). The AB hosts ~40% of the
124 world tropical forest and ~15% of global land biodiversity (Marengo et al., 2018). AB is the
125 home of local people that rely on rivers as transportation corridors, and utilize these
126 environments for their subsistence (A. B. Anderson et al., 1991; Campos-Silva et al., 2020; Endo
127 et al., 2016). AB also serves the broader South American population in terms of energy, food and
128 other forest products

129



131 **Figure 1.** (a) MODIS image of the central AB, characterized by large floodplains (Source:
 132 NASA catalog; <https://visibleearth.nasa.gov/images/62101/the-amazon-brazil/621041>); (b)
 133 Sentinel-1 image of rivers and lakes of the upper Solimões River (Source: ESA catalog;
 134 https://www.esa.int/ESA_Multimedia/Images/2020/09/Amazon_River); (c) MODIS image
 135 showing the reduced cloud cover over water bodies (Source: NASA catalog;
 136 <https://earthobservatory.nasa.gov/images/145649/mapping-the-amazon>); (d) Aerial view of Rio
 137 Branco (Photo by Thiago Laranjeira); (e) Floodplain during the high water (Photo by João Paulo
 138 Borges Pedro); (f) Channel (Photo by Jefferson Ferreira-Ferreira); (g) Community at the river
 139 bank (Photo by Thiago Laranjeira); (h) Manatee (Photo by Amanda Lelis); (i) Arapaima
 140 (Pirarucu) fish, the largest scaled freshwater in the world (Photo by Bernardo Oliveira).

141

142 The region is now facing risks under current climate and anthropogenic changes, and
 143 changes in Amazon hydrology could have substantial impacts globally (Jimenez et al., 2019). In
 144 the past decades, the AB experienced several intense climatic events, such as extreme droughts
 145 and floods, with no equivalent in the last 100 years (Barichivich et al., 2018; Marengo &
 146 Espinoza, 2016). Severe droughts can lead to environmental disturbances, from increased fire
 147 occurrence (Zeng et al., 2008) to abrupt shifts in fish assemblages (Röpke et al., 2017).
 148 Moreover, the accumulated negative impacts of increased human interventions across the region,
 149 such as damming (Forsberg et al., 2017; Latrubesse et al., 2017), deforestation (M. E. Arias et
 150 al., 2020; Coe et al., 2009; Leite-Filho et al., 2020; Leite et al., 2012), fires (Aragão et al., 2008;
 151 Xu et al., 2020; Zeng et al., 2008), and mining (Abe et al., 2019; Lobo et al., 2015), will possibly
 152 trigger major modifications that could affect the AB water cycle, although they provide a
 153 fundamental basis for calibrating and validating RS data.

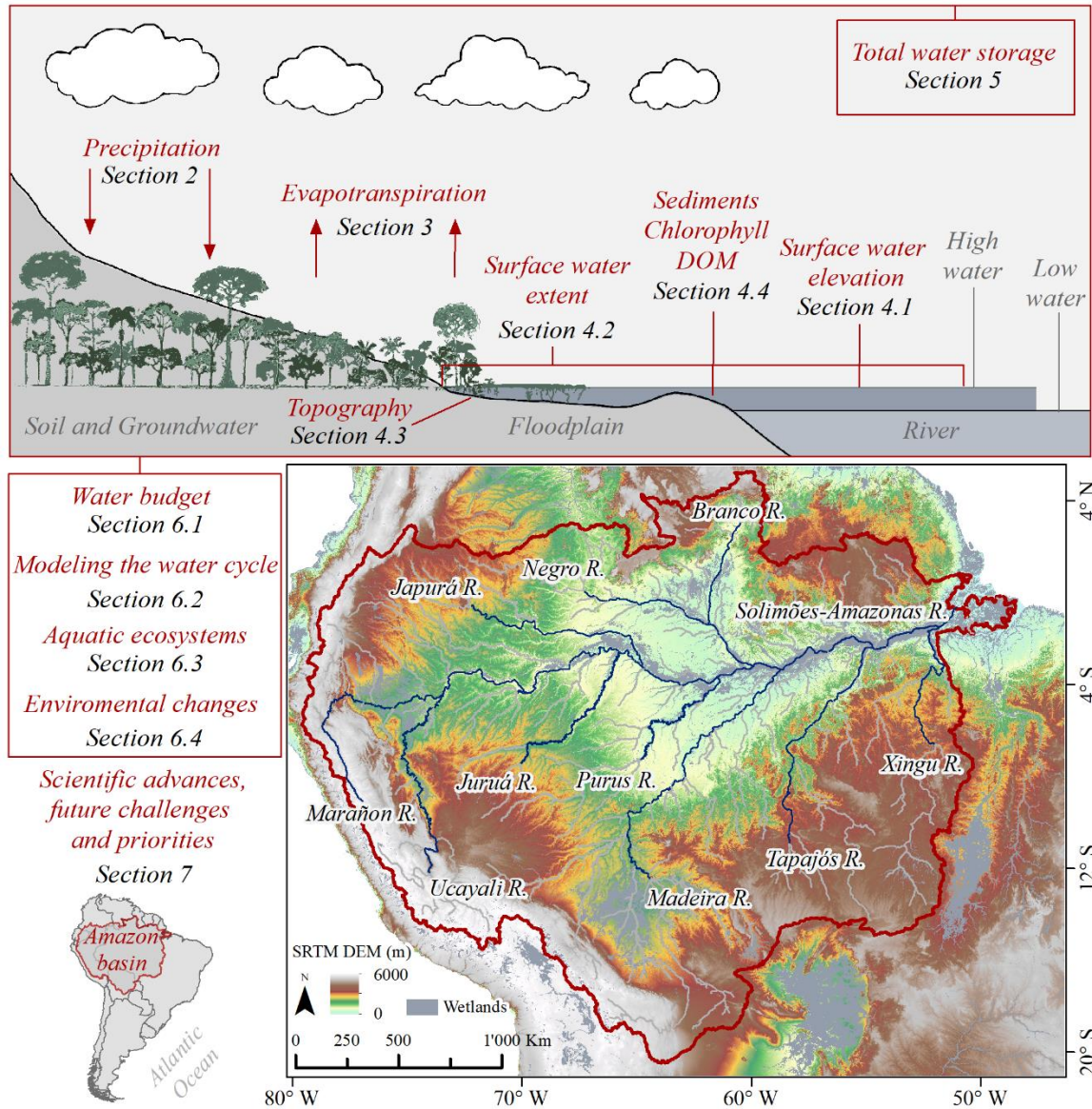
154 Characterizing and understanding the dynamics of the Amazon water cycle is of primary
 155 importance for climate and ecology research and for the management of global water resources.
 156 Consequently, there is a need for a comprehensive monitoring of the spatial-temporal dynamic of
 157 the Amazon water cycle components and how they interact with climate variability and
 158 anthropogenic pressure. In large and remote tropical watersheds such as the AB, in situ
 159 observational networks are difficult to operate and maintain, and they are not capable of
 160 monitoring all components of the water cycle.

161 While the AB was in the spotlight of international scientific discussion during the last
 162 decades, the understanding of AB hydrology coevolved with another groundbreaking field: the
 163 remote sensing (RS) of terrestrial water cycle. In this context, the AB has been an ideal
 164 laboratory for the seminal development of RS techniques with the advent of Earth Observation
 165 (EO) and these advances have fostered the scientific understanding of AB hydrology, ecosystems
 166 and environmental changes. For example, the first applications of altimeter and gravimetric
 167 satellites to characterize, respectively, surface water elevation (Guzkowska et al., 1990) and total
 168 water storage variations (Tapley et al., 2004) were performed in the AB due to its wide river and
 169 large spatial and temporal changes of freshwater. Pioneering RS applications also include
 170 microwave, Synthetic-Aperture Radar (SAR) and interferometric mapping of large scale flood
 171 inundation and characterization of sediment dynamics (Alsdorf et al., 2000; Hess et al., 2003;
 172 Mertes et al., 1993; Sippel et al., 1994). Since then, several applications using RS data have been
 173 carried out in other basins worldwide (e.g., Alsdorf et al., 2021). All these important
 174 developments have been carried out by a diverse community of scientists with different interests

175 and views on the AB water cycle, and surprisingly, there is a lack of review articles analyzing
176 the continuous growth of publications that make use of RS observations to study the hydrology
177 of the region.

178 Here we review the various achievements of more than three decades of scientific
179 advances on the hydrology of the AB from RS (**Figure 2**), and present perspectives, currently
180 fostered by an unprecedented availability of satellite observations and the upcoming launch of
181 dedicated hydrology satellites, such as the Surface Water and Ocean Topography (SWOT) or the
182 NASA-ISRO SAR mission (NISAR). This work reunited experts on RS of different hydrological
183 processes of the AB to review specific topics and discuss paths towards scientific advances as
184 well as the opportunities shaping this field for the next decades. Reviews account for
185 hydrological variables as precipitation, evapotranspiration, surface water elevation, surface water
186 extent, floodplain and river channels topography, water quality (e.g., estimation of sediments,
187 chlorophyll, and dissolved organic matter), total water storage and groundwater storage that are
188 presented in separate sections (**Figure 2**). Each section describes how the variable is retrieved
189 from RS observations, presents the scientific advances that have been achieved from this
190 information, as well as various applications in the AB and discusses future challenges. Then,
191 four sections are dedicated to the integration of RS data in the fields of water budget closure,
192 hydrological and hydraulic modelling, aquatic environments and environmental changes over the
193 Amazon. Section 7 summarizes the scientific advances, the knowledge gaps and the research
194 opportunities regarding AB hydrology and ecosystems, including the forthcoming satellite
195 missions. It also presents how the lessons learnt from AB experiences are benefiting other large
196 river basins worldwide. The two final parts discuss how to move forward from the scientific
197 advances toward a basin-scale water resources planning and new environment monitoring tools,
198 and highlight our recommendations that set forward the research agenda of Amazon hydrology
199 from space for the coming decade.

200



201
202 **Figure 2.** Location of the AB in South America, and representation of the hydrological variables
203 observed by RS techniques, with the respective section numbers as addressed in this review.

204
205 **2. Precipitation**

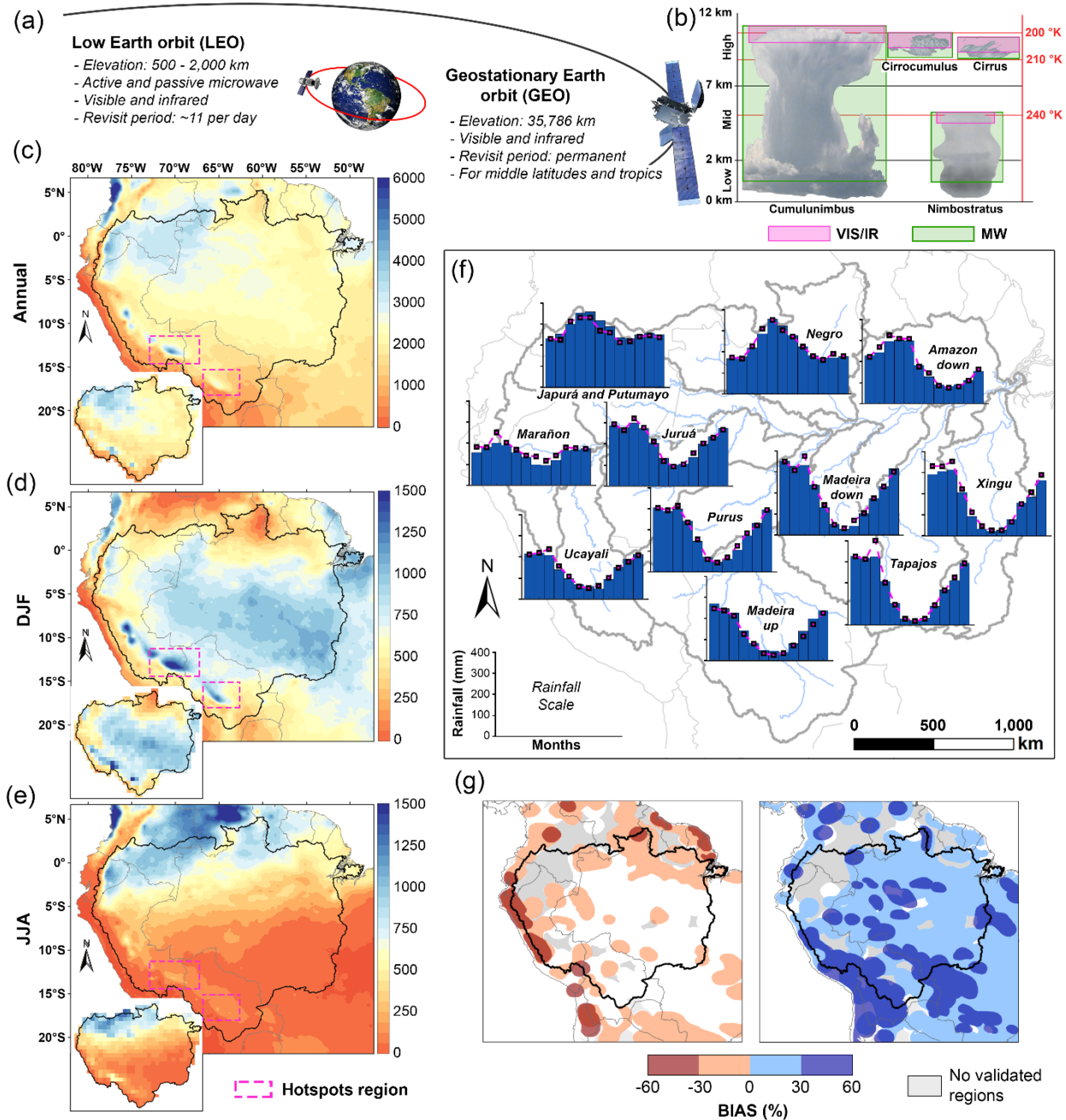
206 Precipitation is a crucial component of the water cycle (Bookhagen & Strecker, 2008; J.
207 C. Espinoza Villar, Ronchail, et al., 2009; Salati & Vose, 1984; Trenberth, 2011), characterized
208 by high spatial and temporal variability. In the AB, precipitation is related to complex
209 interactions of various large-scale physical and dynamic processes as well as local features,
210 which are responsible for the temporal and spatial distribution of precipitation (Figuroa &
211 Nobre, 1990). For instance, in addition to the orographic rains that occur in the transition
212 between the Andes mountains and the Amazon, the substantial transpiration from the forest
213 contributes to abundant water fluxes to the atmosphere, which eventually returns to the land as

214 recycled precipitation and contributes up to around 30% of the basin's rainfall (Bosilovich &
215 Chern, 2006; Eltahir & Bras, 1994; Van Der Ent et al., 2010; Fisher et al., 2009; Salati & Nobre,
216 1991; Staal et al., 2018; Yang & Dominguez, 2019; Zemp et al., 2014). This contribution is
217 normally presented as a convection process, which helps maintaining a climatological upper-
218 level, large-scale circulation known as the Bolivian high (Lenters & Cook, 1997; Virji, 1981),
219 and together with other related precipitation patterns are affected by both global-scale
220 phenomena (e.g., El Niño–Southern Oscillation -ENSO, Tropical Atlantic sea surface
221 temperature -SSTemp) and local forcing, such as land cover structures (Aceituno, 1988; Koren et
222 al., 2008; Leite-Filho et al., 2020; Lin et al., 2006).

223 Mainly because of its large extent, precipitation regimes in the AB differ from one region
224 to another in terms of seasonal pattern (**Figure 3c** to f) and on a more local scale, rainfall
225 regimes are highly variable in space (P. A. Arias et al., 2021; Espinoza et al., 2009). Therefore,
226 accurate and reliable rainfall measurements are crucial for the study of climate trends and
227 variability, and also for the management of water resources and weather, climate and
228 hydrological forecasting in this region (S. Jiang et al., 2012; X. Liu et al., 2017; Yilmaz et al.,
229 2005).

230 Gauge observations are traditionally used to measure precipitation directly at the land
231 surface (Kidd, 2001), and various large-scale datasets at different scales have been developed
232 from these in situ observations (A. Becker et al., 2013; Kidd et al., 2017). However, in situ
233 measurements have several drawbacks, such as incomplete cover over sparsely populated areas,
234 a common feature of Amazonian countries. In addition, the variability of rainfall means that the
235 measurements from in situ stations are typically not representative of the surrounding areas, or
236 may be inaccurate (Kidd et al., 2017; Prabhakara et al., 1986). In the AB, for instance, rainfall
237 stations are typically located in the cities, placed near to the main tributaries, and low density of
238 stations are observed in tropical forest and in regions not accessible. Therefore, the low density
239 of the rain gauge network and the lack of homogeneity in the time series prevent reliable
240 monitoring using ground data (Debortoli et al., 2015; Delahaye et al., 2015; J. C. Espinoza
241 Villar, Ronchail, et al., 2009; Ronchail et al., 2002). Collecting complementary observations to
242 in situ measurements is then fundamental to obtain estimation of rainfall over the continent's
243 surfaces (Van Dijk & Renzullo, 2011; Kidd & Levizzani, 2011; Wanders et al., 2014).

244



245

246 **Figure 3.** (a) Schematic representation of remote sensors for precipitation estimation on board
 247 satellites. (b) Illustration of the VIS/IR and MW coverage range for different cloud types.
 248 Precipitation climatology for (c) annual, (d) austral summer - DJF, and (e) austral winter - JJA
 249 from CHIRP v2 dataset (1981-2020) at 5 km spatial resolution and HOP dataset (1981-2009)
 250 (Espinoza et al., 2016; Guimberteau et al., 2012) in small boxes at left-bottom at ~100 km spatial
 251 resolution. (f) The annual regime for eleven large basins of the Amazon, based on HOP datasets
 252 (1981-2009) (bars) and the CHIRP based (1981-2020) in magenta lines. (g) Annual average
 253 negative (red scale) and positive (blue scale) bias of six precipitation RS-based and non-gauged-

254 corrected products in the AB for the period 2000-2016, adapted from (Beck, Vergopolan, et al.,
255 2017).

256

257 Satellite observations of precipitation have become available on a global scale in recent
258 decades. These satellites mainly use infrared (IR) and microwave (MW) sensors to provide
259 precipitation estimates using different techniques (Kidd & Huffman, 2011). The sensors used to
260 estimate precipitation can be classified in three categories (Prigent, 2010): (i) visible/IR (VIS/IR)
261 sensors on geostationary (GEO) and low Earth orbit (LEO) satellites, (ii) passive MW (PMW)
262 sensors on LEO satellites, and (iii) active MW (AMW) sensors on LEO satellites. Imaging
263 systems on GEO provide the rapid temporal update cycle needed to capture the growth and
264 decay of precipitating cloud systems on a scale of several kilometers. Current systems provide
265 rapid hourly updates in the VIS and IR spectrum, and for optically thick clouds the precipitation
266 can be inferred from the energy reflected by the clouds and the temperature of the cloud top,
267 respectively. MW based imagers on board LEO satellites are better suited than IR sensors for
268 quantitative measurements of precipitation due to the well-established physical connection
269 between the upwelling radiation and the underlying cloud precipitation structure (Turk et al.,
270 2000; **Figure 3a** and b).

271 From these sensors a diverse range of retrieval algorithms has been developed to estimate
272 precipitation, which require careful validation and provide information about their quality,
273 limitations and associated uncertainties. These algorithms are mainly divided into the so-called
274 “microwave-calibrated” and “morphing” methods (Huffman et al., 2007; Joyce et al., 2004; Kidd
275 et al., 2003; Marzano et al., 2004; Paola et al., 2012). However, there are differences among
276 these datasets due to shortcomings in the sources and in the generation of the products.
277 Therefore, LEO MW, GEO VIS/IR, gauge-based and reanalysis data have been blended together
278 to take advantage of the inherent relative benefits of each type of sensor and product (**Figure 3a**).
279 This can increase accuracy, coverage, spatial-temporal resolution, spatial homogeneity and
280 temporal continuity (Adler et al., 1994; Huffman et al., 1995; Joyce et al., 2004; Levizzani et al.,
281 2007; Sorooshian et al., 2002; Tapiador et al., 2004; Vicente et al., 1998; Xie et al., 2003).

282 In terms of operationally available datasets, these include the Tropical Rainfall
283 Measuring Mission (TRMM; Huffman et al., 2007), the Climate Hazards group InfraRed
284 Precipitation (CHIRP; Funk et al., 2015), the Precipitation Estimation from Remotely Sensed
285 Information using Artificial Neural Networks (PERSIANN; Ashouri et al., 2015), Integrated
286 Multi-satellite Retrievals for GPM (IMERG; Huffman, Bolvin, & Nelkin, 2015; Huffman,
287 Bolvin, Braithwaite, et al., 2015), Multi-Source Weighted-Ensemble Precipitation near-real-time
288 (MSWEP-NRT; Beck et al., 2018) and the Climate Prediction Center (CPC) morphing technique
289 (CMORPH; Joyce et al., 2004) products, among others. Although an increasing number of
290 precipitation data sets with higher spatial and temporal resolution have been constructed and
291 compared directly or through the application of hydrological models, uncertainty and
292 inconsistency are found among the different data sets (Beck et al., 2018; Beck, Vergopolan, et
293 al., 2017; Collischonn et al., 2008; Correa et al., 2017; Sun et al., 2018; Tapiador et al., 2017). A
294 summary of satellite-derived rainfall data sets currently available for the AB region is provided
295 in **Table 1**.

296

297 **Table 1.** Missions and products that provide rainfall estimates derived from RS data, including
 298 temporal-spatial resolution, data record, satellites used, algorithm retrieval and repository links
 299 (NRT - Near Real Time)

Name	Extended name	Satellite adjusted with	Coverage	Spatial resolution	Temporal resolution	Temporal coverage	Reference / Link
CMORPH v1.0	CPC MORPHing technique (CMORPH) V1.0	-	60° N/S	0.07°	30 min	1998–NRT	(Joyce et al., 2004; Joyce & Xie, 2011; Xie et al., 2017) www.cpc.ncep.noaa.gov
CMORPH-CRT v1.0	CPC MORPHing technique (CMORPH) bias corrected (CRT) V1.0	Gauge	60° N/S	0.07°	30 min	1998–2019	https://rda.ucar.edu/datasets/ds502.2 ftp://ftp.cpc.ncep.noaa.gov/precip/CMORPH_V1.0/CRT/
GSMaP-Std v6	Global Satellite Mapping of Precipitation (GSMaP) Moving Vector with Kalman MVK) Standard V6	-	60° N/S	0.1°	Hourly	2000–NRT	(Ushio et al., 2009) http://sharaku.eorc.jaxa.jp/GSMaP/
GSMaP-Std Gauge v7	Global Satellite Mapping of Precipitation (GSMaP) Moving Vector with Kalman (MVK) Standard gauge-corrected V7	Gauge	60° N/S	0.1°	Hourly	2000–NRT	/
IMERGHHE v06	Integrated Multi-satellitE Retrievals for GPM (IMERG) early run V06	-	Global	0.1°	30 min	2010–NRT	(Huffman, Bolvin, & Nelkin, 2015; Huffman, Bolvin, Braithwaite, et al., 2015; Tan et al., 2019)
IMERGDF v06	Integrated Multi-satellitE Retrievals for GPM (IMERG) final run V06	Gauge	Global	0.1°	Daily	06/2000 - present	https://gpm1.gesdisc.eosdis.nasa.gov/data/GPM_L3/GPM_3IMERGHHE.06/ https://gpm1.gesdisc.eosdis.nasa.gov/data/GPM_L3/GPM_3IMERGDF.06/
PERSIANN	Precipitation Estimation from Remotely Sensed Information using Artificial Neural Networks (PERSIANN)	-	60° N/S	0.25°	Hourly	03/2000–NRT	
PERSIANN-CCS	Precipitation Estimation from Remotely Sensed Information using Artificial Neural Networks (PERSIANN) Cloud Classification System (CCS)	-	60° N/S	0.04°	Hourly	01/2003–NRT	(Ashouri et al., 2015; Nguyen et al., 2019; Sorooshian et al., 2000) https://chrsdata.eng.uci.edu/
PERSIANN CDR v1R1	Precipitation Estimation from Remotely Sensed Information using Artificial Neural Networks (PERSIANN) Climate Data Record (CDR) V1R1	Gauge	60° N/S	0.25°	Daily	1983–present	
SM2RAIN-CCI v2	Rainfall inferred from European Space Agency's Climate Change Initiative (CCI) satellite near-surface soil moisture V2	Soil Moisture	Quasi Global / Land	0.25°	Daily	01/1998–12/2015	(Brocca et al., 2014; Ciabatta et al., 2018) https://zenodo.org/record/846260 https://doi.org/10.5281/zenodo.846259
SM2RAIN-ASCAT v1.2	Rainfall inferred from Advanced SCATterometer soil moisture	Soil Moisture	Global	12.5 km	Daily	2007-2019	(Brocca et al., 2019) https://doi.org/10.5281/zenodo.3635932
GPM+SM2RAIN v0.1	Rainfall inferred from ASCAT H113 H-SAF, SMOS L3 and SMAP L3 soil moisture	Soil Moisture	Global	0.25°	Daily	2007-2018	(Massari, 2020) https://doi.org/10.5281/zenodo.3854817

TMPA-3B42RT v7	TRMM Multi-satellite Precipitation Analysis (TMPA) 3B42RT V7	-	60° N/S	0.25°	3-hourly	03/2000–NRT	(Huffman et al., 2007) https://disc.gsfc.nasa.gov/datasets/TRMM_3B42RT_7/summary
TMPA-3B42 v7	TRMM Multi-satellite Precipitation Analysis (TMPA) 3B42 V7	Gauge	50° N/S	0.25°	3-hourly	12/1997–01/2020	https://disc.gsfc.nasa.gov/datasets/TRMM_3B42_7/summary
TMPA-3B43 v7	TRMM Multi-satellite Precipitation Analysis (TMPA) 3B43 V7	Gauge	50N-50S	0.25°	Monthly	1998-2020	(Huffman et al., 2010) https://disc2.gesdisc.eosdis.nasa.gov/data/TRMM_L3/TRMM_3B43_7/
GridSat v1.0	P derived from the Gridded Satellite (GridSat) B1 thermal infrared archive v02r01	-	< 50°	0.1°	3-hourly	1983–2016	(Knapp et al., 2011) https://www.ncdc.noaa.gov/gridsat/
ERA5 -HRES	European Centre for Medium-range Weather Forecasts ReAnalysis 5 (ERA5) High RESolution (HRES)	Reanalysis	Global	0.28° (~31 Km)	Hourly	2008–NRT	(Hersbach et al., 2018, 2020)
ERA5 – EDA	European Centre for Medium-range Weather Forecasts ReAnalysis 5 (ERA5) Ensemble Data Assimilation (EDA) ensemble mean	Reanalysis	Global	~0.56°	Hourly	2008–NRT	
ERA5-Land	European Centre for Medium-range Weather Forecasts ReAnalysis 5 (ERA5)	Reanalysis	Global	0.1°	Hourly	01/1981-present	https://cds.climate.copernicus.eu/cdsapp#!/dataset/reanalysis-era5-land
CHIRP v2.0	Climate Hazards group InfraRed Precipitation (CHIRP) V2.0	Reanalysis	50° N/S	0.05°	Daily	1981–NRT	(Funk et al., 2015) https://data.chc.ucsb.edu/products/CHIRP/daily/netcdf/
CHIRPS v2.0	Climate Hazards group InfraRed Precipitation with Stations (CHIRPS) V2.0	Gauge + Reanalysis	50° N/S	0.05°	Daily	01/1981-present	https://data.chc.ucsb.edu/products/CHIRPS-2.0/global_daily/netcdf/
GPCP-1DD v1.2	Global Precipitation Climatology Project (GPCP) 1-Degree Daily (1DD) Combination V1.2	Gauge	Global	1°	Daily	10/1996-11/2015	(Huffman et al., 2001, 2016) https://rda.ucar.edu/datasets/ds728.3
GPCP-PEN v2.2	Global Precipitation Climatology Project (GPCP) pentad precipitation analysis (PEN)	Gauge	Global	2.5°	5-daily	01/1979-06/2017	Xie, Pingping, R.F. Adler, G.J. Huffman, D. Bolvin (2011): Global Precipitation Climatology Project - Pentad, Version 2.2. NOAA National Climatic Data Center. [07-2020]. https://cmr.earthdata.nasa.gov/search/concepts/C1214566485-NOAA_NCEI http://apdr.c.soest.hawaii.edu/dchart/index.html?dsetid=e53e32f2c760e6375a4de86bd4718cba
MERRA-2	Modern-Era Retrospective Analysis for Research and Applications 2	Gauge + Reanalysis	Global	~0.5°	Hourly	1980-NRT	(Gelaro et al., 2017; Reichle et al., 2017)
MSWEP v2.2	Multi-Source Weighted-Ensemble Precipitation (MSWEP) V2.2	Gauge + Reanalysis	Global	0.1°	3-hourly	01/1979–NRT	(Beck et al., 2019; Beck, Van Dijk, et al., 2017) www.gloh2o.org
CMAP	CPC Merged Analysis of Precipitation (CMAP)	Gauge	Global	2.5°	Monthly	1979–present	(Huffman et al., 1997) ftp://ftp.cpc.ncep.noaa.gov/precip/cmap/

CPC-Global	CPC Unified Gauge-Based Analysis of Global Daily Precipitation	Gauge	Global	0.5°	Daily	2006-present	(M. Chen et al., 2008) https://ftp.cpc.ncep.noaa.gov/precip/CPC_UNI_PRCIP/
PISCOp v2.1	Peruvian Interpolated data of the SENAMHI's Climatological and hydrological Observations	Gauge + CHIRP v2.0	Peruvian Amazon	0.1°	Daily	01/1981 – 12/2016	(Aybar et al., 2019) https://piscoprec.github.io/

300

301 Precipitation information based on RS has contributed substantially in the last decades to
302 the understanding of key processes causing spatial and temporal variability of precipitation, as
303 well as local and regional atmospheric processes related to precipitations. These global or quasi
304 global data sets generally provide records of precipitation suitable for climate and hydrological
305 studies, such as hydrological reanalysis initiatives evaluated in the Amazon on regional (e.g.,
306 Correa et al., 2017; Wongchuig et al., 2019) and global scales (e.g. Balsamo et al., 2015; Rodell
307 et al., 2004; Van Huijgevoort et al., 2013). For instance, many studies have used satellite rainfall
308 databases to force hydrological models. One of the first studies was done in the Tapajós River
309 basin, one of the major tributaries of the AB, using TRMM precipitation estimates as input to a
310 precipitation-runoff model (Collischonn et al., 2008). In order to represent the interannual,
311 intraseasonal (30 to 70 days, Kiladis and Mo, 1998) and multidecadal series in the AB, different
312 research has been evaluated (Correa et al., 2017). Satellite-based data sets were also used in
313 water balance approaches to evaluate long term trends (Heerspink et al., 2020) and monthly
314 variations of runoff (Builes-Jaramillo & Poveda, 2018). In addition, hydrological extreme events
315 have been reported in the AB during last decades, which has been possible by using satellite-
316 based rainfall estimates (Barichivich et al., 2018; Espinoza et al., 2012; Gloor et al., 2013;
317 Marengo & Espinoza, 2016; Satyamurty, da Costa, Manzi, et al., 2013; Sena et al., 2012).
318 Applications of precipitation databases to understanding of the hydrologic cycle through
319 modeling is described in Section 6.2.

320 However, due to inconsistencies between different databases, several evaluations of
321 rainfall datasets were performed that consider the AB, from global evaluations (e.g. Beck et al.,
322 2018, 2017; Sun et al., 2018), only Amazon (e.g., Cavalcante et al., 2020; Correa et al., 2017;
323 Espinoza, Ronchail, et al., 2019; Haghtalab et al., 2020; Paca et al., 2019; Zubieta et al., 2019)
324 and in particular regions of Amazon (e.g., Avila-Diaz et al., 2020; Bookhagen & Strecker, 2008;
325 Chavez & Takahashi, 2017; Espinoza et al., 2015; Killeen et al., 2007; Manz et al., 2017; Paccini
326 et al., 2018; Zed Zulkafli et al., 2014; Getirana et al., 2011). These datasets perform differently
327 according to the region and the time scale analyzed, which will be described in the following
328 subsections together with the main scientific advances that have been elucidated.

329 **Figure 3c-e** show the cumulative rainfall for the annual, wet (DJF) and dry (JJA) period,
330 respectively, for the AB. In these figures the Hydro-geodynamics of the AB Observatory
331 (HYBAM) observed precipitation dataset (HOP), comprised of 752 daily rain gauge stations
332 throughout the AB at 1° spatial resolution (Espinoza et al., 2016; Guimberteau et al., 2012), and
333 the 5 km resolution CHIRP dataset, a non-gauged-corrected product, have been used.

334 Climatological studies in the AB that consider spatial patterns began in the 1980s. For
335 instance, the evaluation of the outgoing longwave radiation (OLR) from polar orbiting satellites
336 (mainly from NOAA), started in 1974, have been particularly useful for routine monitoring of
337 cloudiness and deep convection areas over the tropics with pioneering work by Gruber &
338 Krueger (1984) and Liebmann & Smith (1996). More regional rainfall patterns were revealed in

339 the transition between the Andes and the Amazon in the so-called "rainfall hotspots" region,
340 where rainfall can reach values higher than 6000 mm yr^{-1} , the highest rainfall in the AB (Chavez
341 & Takahashi, 2017; Espinoza et al., 2015). This region is among the rainiest areas in the world
342 according to the IMERG Grand Average Climatology dataset that covers June 2000 to May 2019
343 and has the world's largest squall lines (quasi-linear convective systems; Garstang et al., 1994).
344 Extreme vertical and horizontal structures occur due to the interactions between large-scale
345 atmospheric circulation and massive topography that affect atmospheric convection, producing
346 the rainfall hotspots during almost the whole year (Bookhagen & Strecker, 2008; J. C. Espinoza
347 Villar, Guyot, et al., 2009; Killeen et al., 2007). In addition, changes in forest cover in the
348 southern Amazon have been considered as a factor that may affect processes such as the
349 presence of convective cells, resulting in marked spatial and temporal variability (Durieux et al.,
350 2003; Funatsu et al., 2012; Laurance & Bruce Williamson, 2001; Staal et al., 2020).

351 **Figure 3f** shows the spatial distribution of the annual cycle of precipitation based on the
352 CHIRP and HOP datasets. Annual cycles of precipitation over the AB vary significantly, mainly
353 related to latitude, orography, and the influence of the large-scale atmospheric features (e.g.,
354 Intertropical Convergence Zone (ITCZ), South American Monsoon System (SAMS), South
355 Atlantic convergence zone (SACZ; J. C. Espinoza Villar, Ronchail, et al., 2009). The bias
356 performance of the datasets is shown in **Figure 3g**, which considers six non-gauged-corrected
357 datasets (PERSIANN-CCS, MSWEP-ng v2, CHIRP v2.0, CMORPH v1.0, SM2RAIN-ASCAT
358 and TMPA 3B42RT v7, adapted from Beck, Vergopolan, et al., 2017). The bias of total annual
359 rainfall for the period 2000-2016 is plotted for negative and positive values, where at least one of
360 these databases has detected an equal or greater value of bias. These satellite datasets were
361 validated for the AB against global and local in situ stations (e.g., GHCN, the Global Summary
362 of the Day (GSOD) database, the Latin American Climate Assessment & Dataset). The
363 evaluation of these datasets showed large biases in the occidental and southern AB, covered by
364 the Andean headwaters.

365 Over the Andes-Amazon transition region RS rainfall data have contributed to
366 understanding the main orographic processes related to anabatic and katabatic winds, which are
367 essential to explain the diurnal cycle of precipitation in this region (Junquas et al., 2018). In this
368 specific region the bias patterns of the datasets are in agreement with other research (Chavez &
369 Takahashi, 2017; Espinoza et al., 2015) only in the Peruvian rainfall hotspots, which
370 underestimated total annual precipitation by about 35% to 40% from the TRMM-PR data set for
371 the period 1998-2012. The general bias in some Andes regions can be explained, in part, by the
372 predominance of cirrus clouds (confused by satellites sensors with convective clouds such as
373 cumulonimbus that have similar cloud top temperature (Paredes Trejo et al., 2016; Thiemig et
374 al., 2013, **Figure 3b**), what occurs, for instance, over the east of the southern Andes mountains
375 (Altiplano Plateau, which extends between 15°S and 22°S). This mainly happens during the wet
376 austral summer (Barahona et al., 2017; Dinku et al., 2011; Viale et al., 2019), and where these
377 cloud formations are orographically dependent (Chavez & Takahashi, 2017; Giovannettone &
378 Barros, 2009; Junquas et al., 2018; Saavedra et al., 2020; Satgé et al., 2016, 2017).

379 Mesoscale circulation between land surface and large water bodies in the AB produce
380 river and coastal breeze. These systems affect the moisture transport and the spatial rainfall
381 pattern at local scale (Fitzjarrald et al., 2008; M. J. Santos et al., 2019; Silva Dias et al., 2004).

382 RS data helped to reveal that river breezes reduced rainfall over the Amazon water bodies (rivers
383 and large reservoirs) through the use of TRMM (Paiva et al., 2011).

384 Changes in land cover can produce complex mesoscale circulation patterns, including the
385 so-called “deforestation breeze” that can happen over small deforested patches but loses strength
386 at deforestation scales of around 100 km (Lawrence & Vandecar, 2015; Saad et al., 2010). These
387 deforestation-induced circulation patterns can significantly alter rainfall patterns at local to
388 continental scales, with such changes being observed over the AB in recent decades (Butt et al.,
389 2011; Khanna et al., 2017; Leite-Filho et al., 2019). The effects of deforestation on rainfall will
390 be further discussed in Section 6.4.

391 Remotely sensed data have been used to evaluate the temporal variability on different
392 time scales. For instance, spatial synoptic changes in rainfall patterns were evaluated using RS
393 information due to the heterogeneous spatial distribution of weather stations and inconsistent
394 temporal measurements of gauge data (Arvor et al., 2017; Silva Junior et al., 2018). Other studies
395 on a daily scale focused on evaluating the performance of the TMPA V7, TMPA RT, CMORPH
396 and PERSIANN datasets to represent the precipitation concentration index during the period
397 2001–2009 (Zubieta et al., 2019). This index is an indicator for temporal precipitation
398 distribution. The authors concluded that the best products (CMORPH and TMPA V7) can be an
399 alternative source of data to detect changes in daily precipitation concentration during dry or wet
400 seasons in regions of the AB that experience extreme events.

401 Considering that one of the main characteristics of convection processes in tropical
402 regions is their strong relationship with the diurnal cycle (Duvel & Kandel, 1985; Minnis &
403 Harrison, 1984), pioneer studies were performed since the 1990s for the understanding of
404 convective patterns in the AB. Based on nine years (1983–1991) of data from GEO IR satellites
405 (i.e., the B3 ISCCP product) with 3-h temporal resolution, Garreaud & Wallace (1997)
406 documented several features of the diurnal march of the frequency of convective cloudiness.
407 Data from SSM/I onboard the Defense Meteorological Satellite Program via application of the
408 Goddard Profiling algorithm were also used to characterize the climatology (10-yr) and the
409 diurnal variability (6-yr) of the rainfall in the AB (Negri et al., 2000). R. Oliveira et al. (2016)
410 evaluated two GPM products in order to reproduce the diurnal cycle of precipitation in the
411 central AB and obtained similar results to Angelis et al. (2004), who showed that rain tends to
412 occur mainly during the afternoon in the central AB.

413 Rainfall information from RS has helped to identify the time of wet season beginning and
414 ending (Wright et al., 2017), which is especially important because the prolongation of the dry
415 season increases the vulnerability of local ecosystems and agriculture to drought and fire events
416 (P. A. Arias et al., 2015; Fu et al., 2013; Marengo et al., 2011). One of the first RS-based
417 assessments found that the onset of the AB wet season typically occurs within a single month
418 (Horel et al., 1989). Negri et al. (1994) produced a regional precipitation climatology over the
419 AB during the wet season (January–May) using three years of the twice daily Special Sensor
420 Microwave/Imager (SSM/I) data. Changes in the seasonal cycle amplitude were also observed
421 with the TRMM data (Liang et al., 2020).

422 RS information supported important developments in the understanding of the processes
423 governing the seasonality of rainfall in the AB. The availability of satellite-derived precipitation,
424 OLR and reanalysis allowed the description of the thermally-driven seasonal patterns that form
425 the SAMS, which was previously not understood as a monsoon partly because it lacks the

426 classical seasonal inversion of absolute zonal winds (J. Zhou & Lau, 1998). An uncommon
427 characteristic of the monsoon over the AB elucidated by these RS products is that the onset of
428 rains occurs before the southward migration of the ITCZ, and that the Bolivian high pressure
429 zone characteristic of the SAMS is partly generated by the latent heat release from precipitation
430 over the AB before the traditional monsoon onset (Fu et al., 1999).

431 At seasonal to intraseasonal scales, OLR data from NOAA polar-orbiting satellites was
432 used to identify the intensity and spatial features of the SACZ in the Brazilian AB region (L. M.
433 V. Carvalho et al., 2004). The SACZ is a northwest-southwest convection band that extends from
434 the AB to the southeastern Atlantic Ocean, and its intensity and geographical distribution are
435 associated with extreme rainfall events in the southern AB. At the intraseasonal scale, the large-
436 scale Madden–Julian oscillation (MJO; Madden & Julian, 1994) has been established as the
437 dominant mode of variability across the tropics, modulating the SACZ and other climatological
438 features over the AB. Mayta et al. (2019) and Vera et al. (2018) used OLR data as a proxy of
439 convection to analyze the intraseasonal variability of precipitation in South America, and, in
440 particular, E. B. De Souza & Ambrizzi (2006) showed that the MJO is the main atmospheric
441 mechanism of rainfall variability on intraseasonal timescales over the eastern Amazon during the
442 wet season, which was confirmed through the use of rain gauge network by Mayta et al. (2019).
443 Moreover, RS information has contributed to understanding the mechanisms of atmospheric
444 circulation and rainfall datasets performance of seasonal and intraseasonal precipitation data sets.
445 For instance, in the Andes-Amazon transition region, particular atmospheric circulation patterns
446 (CP) were described by Paccini et al. (2018), where large underestimations of rainfall from
447 TRMM 3B42, TRMM 2A25 RP and CHIRPS occur when the CP is dominated by northerly
448 wind anomalies over tropical South America. In addition, large overestimations occur in the
449 southern Amazonia, during a CP with intermediate state between the northern and southern wind
450 anomalies and where the convergence of winds are predominant in the central and western
451 Amazon.

452 Changes in spatial and temporal distribution of rainfall in the AB may provide an
453 indicator of climate variability and in turn are an indicator of hydrological variability, including
454 extreme events, such as floods and droughts (e.g., Lewis et al., 2011; Marengo & Espinoza,
455 2016). Direct evaluation of these datasets have been done to assess the temporal evolution of
456 rainfall through analysis of occurrence indexes such as the dry-day frequency and the wet-day
457 frequency through the CHIRPS dataset (Espinoza, Ronchail, et al., 2019); or the assessment of
458 the trend in the length of the wet season in southern AB with the PERSIANN-CDR dataset
459 (Arvor et al., 2017). The interannual evolution of the hydrological processes was evaluated
460 through a water balance analysis by using CHIRPS dataset (Espinoza, Sörensson, et al., 2019). A
461 similar approach, the long-term surface water balance over the Andes-Amazonia system, was
462 performed by Builes-Jaramillo & Poveda (2018) through the use of in situ (precipitation from
463 GPCP and runoff from HYBAM) and RS-based information (evapotranspiration from
464 ORCHIDEE, GLEAM, MPI and MOD16), which pointed out that failures and scarcity of
465 information in the high Andes induce uncertainties and errors in the water budget. In addition,
466 CHIRPS v2.0 was used to analyze precipitation anomalies for the identification of spatial
467 patterns of drought over the AB related to the tropical Atlantic and Pacific SSTemp anomalies
468 and different ENSO events (Jimenez et al., 2019).

469 Rainfall estimations by RS since the 1980s in the AB have depicted more amounts of rain
470 in the north (Espinoza, Ronchail, et al., 2019; Paca et al., 2020; G. Wang et al., 2018) and lower
471 amounts in the south (Espinoza, Ronchail, et al., 2019; Leite-Filho et al., 2019). This north-south
472 contrasting pattern is translated to the hydrological behavior of the main basins that show an
473 intensification of the hydrological regime in the main course of the AB (Barichivich et al., 2018;
474 Heerspink et al., 2020).

475 AB characteristics pose unique challenges to satellite rainfall retrieval algorithms, both
476 from IR and MW sensors, considering the contrast in terms of orography, climate and changes in
477 vegetative cover. For IR, challenges occur mainly for warm orographic rains (shown north of
478 10°S), where fixed brightness temperature thresholds (cooler than warm orographic clouds) tend
479 to underestimate rainfall amounts. This would be happening in the hot-spots regions in the
480 Peruvian and Bolivian Andes-Amazon transition (Espinoza et al., 2015). For the MW algorithms,
481 rain overestimation comes from cold surfaces and ice over mountain tops which can be
482 interpreted as precipitation (Dinku et al., 2011; Toté et al., 2015).

483 Since satellite-based rainfall estimates are adjusted based on observations from rain
484 gauges, the accuracy of estimated rainfall values can be increased. However, this requires a
485 network of rain gauges with adequate spatial coverage in key areas of the Amazonia and high-
486 quality records for proper calibration and validation. In the case of in situ stations, some aspects
487 should be considered, for instance, that rainfall estimates are likely to be biased by river breeze at
488 some times of the year, as meteorological stations are usually located near large rivers and close
489 to most cities (Paiva, Buarque, et al., 2011; M. J. Santos et al., 2019; Silva Dias et al., 2004).

490 Current satellite-borne radar missions, such as TRMM Precipitation Radar, CloudSat's
491 Cloud Profiling Radar, or GPM Dual frequency Precipitation Radar, have low temporal
492 resolution, therefore are unable to observe the short-time evolution of weather processes. To
493 overcome this limitation, using only radars on LEO, it is necessary to have a constellation of
494 them. In recent years nanosatellites (e.g., SmallSat or CubeSat platforms) have the capability to
495 miniaturize, reduce cost and simultaneously preserve the fundamental requirements of their
496 larger and more expensive peers. In this sense, RainCube is a potential technology demonstration
497 mission to enable precipitation radar technologies on a low-cost platform (Peral et al., 2019).

498 Ground-based radars can measure the vertical structure of rain since its structure depends
499 on the type of rain, but with better temporal resolution than MW on board satellites (Kumar et
500 al., 2020). A recent example is the operational algorithm RAdar INfrared Blending algorithm for
501 Operational Weather monitoring, which merges ground radar network with VIS and IR images
502 from satellites to provide rainfall pattern and intensity over Italy (Adderio et al., 2020). New
503 methods have emerged that take advantage of the global cell phone network and its density to
504 estimate rainfall intensities, mainly in urban areas, but which can also be used in regions with
505 high topographical variability (Gosset et al., 2016; Overeem et al., 2013, 2016; van het Schip et
506 al., 2017), however they have not yet been explored in the AB. In general, monthly and annual
507 datasets are useful because they have an adequate agreement to the observations, but not with
508 daily and much less sub-daily data.

509

510 **3. Evapotranspiration**

511 Evapotranspiration (*ET*) has a considerable importance for the terrestrial climate system,
512 providing moisture to the atmosphere, linking the water, energy, and carbon cycles (Fisher et al.,
513 2017; M. Jung et al., 2010), and driving precipitation and temperature at local and regional scales
514 (Marengo et al., 2018). Studies have shown that around half of the precipitation in the AB is
515 recycled by local *ET* (Salati et al., 1979; Satyamurty, da Costa, & Manzi, 2013; Zemp et al.,
516 2017). In addition, Amazon *ET* constitutes an important source of moisture for southeastern
517 South America through atmospheric low-level (often referred to as “flying rivers”), providing
518 around 70% of the precipitation in this region (Van Der Ent et al., 2010; Pearce, 2020).
519 Especially during the dry season, Amazon *ET* seems to be more efficiently converted to
520 precipitation in the La Plata River Basin than local *ET* (J. A. Martinez & Dominguez, 2014).

521 With the advent of satellite observations, *ET* has been estimated at multiple spatial and
522 temporal scales. RS models to estimate *ET* can be divided into two main approaches: one based
523 on surface energy balance (SEB) and another using physical equations. One well known energy
524 balance models is the Surface Energy Balance Algorithm for Land (SEBAL), proposed by
525 Bastiaanssen (1995) to overcome most of the problems of the early surface energy balance
526 models, which were suitable only for local scale due to their dependence of local measurements
527 for calibration. Based on principles and methods adopted in SEBAL, R. G. Allen et al. (2007)
528 proposed the Mapping evapotranspiration at high Resolution with Internalized Calibration
529 (METRIC) algorithm, including an internal calibration using Inverse Modeling at Extreme
530 Conditions (CIMEC) and micrometeorological measurements to reduce computational biases
531 inherent to energy models that use RS data (R. G. Allen et al., 2007, 2011). Other surface energy
532 balance models were also proposed to use RS data, such as Surface Energy Balance Index
533 (SEBI; Menenti & Choudhury, 1993), Simplified Surface Energy Balance Index (S-SEBI;
534 Roerink et al., 2000), and Surface Energy Balance System (SEBS; Su et al., 2001).

535 SEB algorithms are generally defined as “One Source Surface Energy Balance” models,
536 since they do not distinguish between soil evaporation and canopy transpiration, whereas the
537 land surface is treated as a big leaf and as a single uniform layer (Tang et al., 2013; Ke Zhang et
538 al., 2016). In contrast, in the Two-Source Energy Balance (TSEB) models (Kustas & Norman,
539 1999; Norman et al., 1995), the soil-vegetation system is approximated as a two-layer model,
540 where the energy fluxes are partitioned into soil and vegetation components (Norman et al.,
541 1995). Based on the TSEB approach, the Atmosphere-Land Exchange Inverse model (Alexi) was
542 developed by Anderson et al. (1997), designed to represent land-atmosphere exchange over a
543 wide range of land cover conditions. Both approaches rely on thermal RS data, using
544 meteorological inputs as ancillary data (Ke Zhang et al., 2016).

545 RS models based on physical equations are generally divided into Penman-Monteith and
546 Priestley and Taylor equation-based approaches. Penman (1948) was the first to formulate an
547 equation to calculate evaporation based on a physical approach using two terms, an energy term
548 related to radiation and an aerodynamic term related to the vapor pressure deficit and wind speed
549 (Shuttleworth, 2012). While this equation represented open water evaporation, Monteith (1965)
550 presented an extension by adding surface and aerodynamic resistances, and thus the equation
551 became more consistent with estimation of *ET* from vegetated surfaces, resulting in the well-
552 known Penman-Monteith equation (Monteith & Unsworth, 2013). Based on this approach, the
553 MOD16 algorithm was formulated by Mu et al. (2007, 2011), previously proposed by Cleugh et
554 al. (2007), to calculate *ET* through the integrated use of global meteorological reanalysis and RS

555 data from the Moderate Resolution Imaging Spectroradiometer (MODIS) sensor, including leaf
 556 area index (LAI), fraction of absorbed photosynthetically active radiation (fPAR), albedo and
 557 land cover classification. Leuning et al. (2008) also proposed a similar *ET* algorithm based on
 558 this equation, the Penman-Monteith-Leuning (PML) using a simple biophysical model to
 559 calculate surface conductance from MODIS LAI. Another approach is the Priestley and Taylor
 560 equation (Priestley & Taylor, 1972). This model uses an empirical parameter to simplify the
 561 Penman-Monteith approach, minimizing the uncertainties related to estimating aerodynamic and
 562 surface resistances. Based on this equation, Fisher et al. (2008) developed the JPL-PT model, and
 563 Miralles et al. (2011) proposed the Global Land-Surface Evaporation Amsterdam Model
 564 (GLEAM), designed to estimate daily terrestrial evaporative fluxes and the root-zone soil
 565 moisture using maximum observations derived from RS (Martens et al., 2017). A summary of
 566 the main RS-based models to estimate *ET* in the South American tropics, with applications in the
 567 AB, is presented in **Table 2**.

568

569 **Table 2.** Summary of the main RS-based models to estimate ET, with applications in the
 570 Amazon (*Global applications including Amazon analysis)

Model	Physical principles	Spatial resolution	Usual RS sources	RS main drivers	Ancillary data	Model advantages	Model limitations	Applications in the AB
ALEXI (Anderson et al., 1997)	Surface Energy Balance	375 meters to 0.05°	GOES, MODIS, VIIRS	1) Thermal (land surface temperature) 2) Multispectral data (surface reflectance)	1) Meteorological (global reanalysis) 2) Surface data (land cover)	1) Energy fluxes are partitioned into soil and vegetation components 2) Representation of surface processes in areas with high water availability	1) High complexity for implementation 2) Require clear sky conditions 3) Require many meteorological variables	Paca et al. (2019)
BESS (Ryu et al., 2011)	Biophysical model	1 to 5 km	MODIS	1) Atmospheric data (aerosol, water vapor, cloud, atmospheric profile) 2) Surface properties (land surface temperature, land cover, LAI, albedo)	1) Meteorological (global reanalysis) 2) Surface data (global climates and vegetation)	1) Global spatial coverage and public data availability 2) Entirely independent from flux tower data, 3) Moderate spatial resolution to cover large areas 4) Multiple atmospheric and land surface data used as inputs 5) Linkage between carbon and water fluxes	1) Require many data (surface RS and meteorological variables) 2) Soil moisture effect and water evaporation from rainfall intercepted by the canopy are not explicitly include in the model 3) Complex terrain and heterogeneity of land surface are not considered, 4) Uncertainties in inputs datasets and gap-filling methods can influence in the results of the model.	Swann and Koven (2017)
MOD16 (Mu et al., 2007; 2011)	Physical approach - Penman-Monteith equation	500 meters to 0.05°		1) Vegetation phenology (LAI, fPAR) 2) surface properties (land cover, albedo)	Meteorological (global reanalysis)	1) Global spatial coverage and public data availability 2) Low complexity for implementation	1) Parametrizations of surface conductance 2) Require measured data for model calibration/parameterization	Baker and Spracklen (2019); da Silva et al. (2019); Maeda et al. (2017); Miralles et al. (2016)*; Oliveira et al.

							3) Limitations in areas with high soil and water evaporation 4) Moderate to high meteorological inputs	(2017); Swann and Koven (2017); Vergopolan and Fisher (2016); Xu et al. (2019), Paca et al. (2019)				
PML (Leuning et al., 2008)		500 meters						Zhang et al. (2016)*				
GLEAM (Miralles et al., 2011)	Physical approach - Priestley and Taylor equation	0.25°	AIRS, CERES, MODIS, multi-source soil moisture (ES-CCI), vegetation optical depth (VODCA)	1) Atmospheric data (radiation, precipitation, air temperature, lightning frequency) 2) surface properties (snow-water equivalent, soil moisture, vegetation cover fraction, vegetation optical depth)	Meteorological (global reanalysis)	1) Can be driven only with RS inputs 2) Moderate meteorological inputs requirements 3) Global spatial coverage and public data availability	1) Simplification of some physical processes 2) Over-dependence on water availability 3) Limitations in areas with high soil and water evaporation 4) Low spatial resolution	Baker and Spracklen (2019); Miralles et al. (2016)*, Paca et al. (2019), Wu et al. (2020)				
PT-JPL (Fisher et al., 2008)		1°	AVHRR, MODIS	Vegetation phenology (NDVI, SAVI)	Meteorological (global reanalysis) and Satellite land surface climatology	1) Global spatial coverage and public data availability 2) Can be driven only with RS data 3) Moderate meteorological inputs requirements	1) Simplification of some physical processes 2) Many ecophysiological parameterization 3) Limitations in areas with high soil and water evaporation 4) Low spatial resolution	Fisher et al., 2009; Miralles et al. (2016)*				
METRIC (Allen et al., 2007)	Surface Energy Balance	30 meters to 1 km	MODIS, Landsat	1) Thermal (land surface temperature) 2) multispectral data (surface reflectance)	Meteorological (from ground measurements to global meteorology)	1) Applications for regional scale in moderate to high spatial resolution 2) Less surface parameterization 3) Useful to evaluate land cover changes impacts 4) Low meteorological inputs requirements (SEBAL) 5) Higher accuracy in areas with ground measurements available (METRIC)	1) Require clear sky conditions 2) There is no distinguish between soil evaporation and canopy transpiration 3) Require the presence of hot and cold extreme conditions on the domain area 4) Domain-area dependence, with limitations for large-scale applications 5) Moderate to high meteorological inputs requirements (METRIC) 6) Higher uncertainty in data scarce areas (METRIC)	Khand et al. (2017), Numata et al. (2017), Nobrega et al. (2017)				
SEBAL (Bastiaanssen, 1995)			AVHRR, MODIS, Landsat, ASTER									Laipelt et al (2020); Oliveira et al. (2019), Nobrega et al. (2017)
SEBS (Su et al., 2001)			MODIS, Landsat								1) Accuracy related to land surface temperature 2) Low requirement for meteorological inputs	1) High requirement for surface parameterization 2) Moderate to high complexity for implementation

SSEBop (Senay et al., 2013)	Simplified surface energy balance					1) Low complexity for implementation 2) Global spatial coverage and public data availability	1) Simplified energy balance 2) Moderate to high meteorological inputs requirements (METRIC) 3) Higher uncertainty in data scarce areas	Paca et al. (2019), Senay et al. (2020)*
--------------------------------	-----------------------------------	--	--	--	--	---	---	--

571

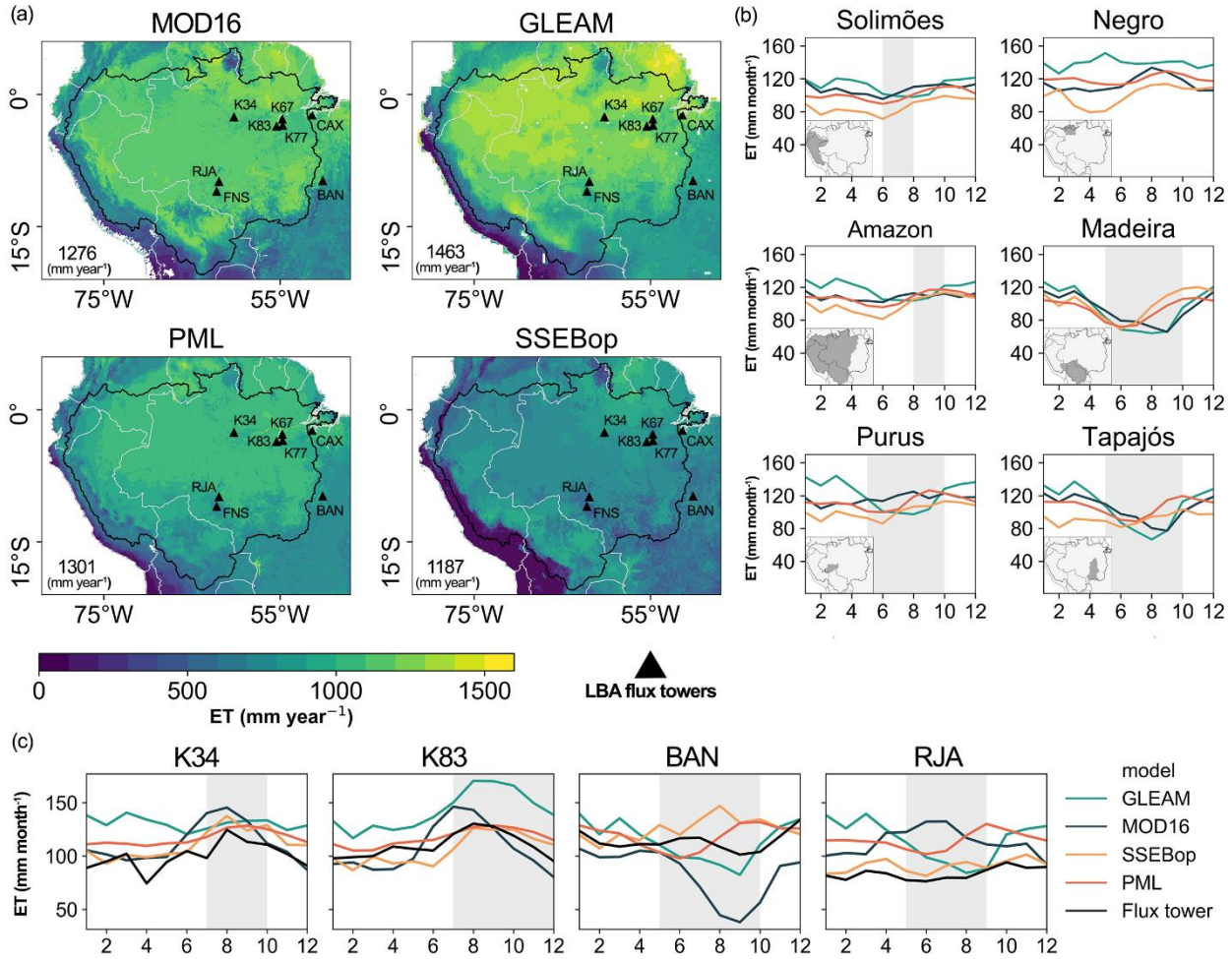
572 RS-based *ET* models have improved our understanding of *ET* processes worldwide,
573 allowing us to understand hydrological processes from local to large spatial and multiple
574 temporal scales. Energy balance models have the advantage to map *ET* at fine spatial resolution.
575 These models can estimate human impacts on the energy and water cycles and on the land-
576 surface interactions. However, since they are dependent on thermal RS data, they are generally
577 restricted to clear-sky or cloud-free conditions, which is a major drawback, especially in tropical
578 humid areas, such as the Amazon (Rocha et al., 2009). In addition, SEB models usually require
579 the presence of hot and cold conditions in the satellite domain area. This requirement is a
580 disadvantage since the selection of the hot and cold endmembers for internal calibration using
581 the CIMEC process on RS images can generate subjective results, especially under wet regions
582 such as the AB, where the selection of hot endmembers during both wet and dry seasons is a
583 challenge (Khand et al., 2017). Physically-based equations have the advantage to map *ET* at high
584 temporal resolution, enabling long-term and large-scale assessments of land-surface interactions.
585 However, some limitations include the uncertainty in parameterizing physical processes, as
586 surface resistance and conductance, and, therefore, are dependent on the use of look-up tables
587 biome-properties (Ruhoff et al., 2013). Error propagation derived from meteorological forcing
588 data is also an issue (Gomis-Cebolla et al., 2019; Miralles et al., 2016; Panday et al., 2015;
589 Talsma et al., 2018), since it can introduce large uncertainties in *ET* estimates, especially in the
590 tropics.

591 In the AB, the spatial and temporal drivers of *ET* are not fully understood, and these
592 uncertainties are reflected on how RS models estimate *ET* (Maeda et al., 2017; Sörensson &
593 Ruscica, 2018). *ET* measurements have provided valuable information about seasonality and
594 dynamics at local scales (Rocha et al., 2009). Some national initiatives, as the Brazilian National
595 Water Resource Information System (SINGREH) and the Meteorological Database for Research
596 from the Brazilian National Water and Sanitation Agency (ANA) and the National Institute of
597 Meteorology (INMET), respectively, and international research projects, as the Large-Scale
598 Biosphere-Atmosphere Experiment in Amazonia (LBA; E. A. Davidson & Artaxo, 2004),
599 provided standardized hydrometeorological and surface flux measurements to understand energy,
600 water and carbon exchanges across different tropical ecosystems (Gonçalves et al., 2013; Saleska
601 et al., 2013). However, due the high cost of eddy covariance measurements and maintenance
602 difficulties, there are only a few towers located across the basin, and these do not cover the
603 whole Amazon climate-vegetation complexity. Hence, through the calibration and validation of
604 RS-based *ET* models it has been possible to extend the spatial coverage of the *ET*, improving our
605 knowledge about seasonality and patterns in data scarce areas, covering long-term assessments.

606 RS models have shown that *ET* spatial pattern (**Figure 4a**), seasonality (**Figure 4b**), and
607 main *ET* drivers vary across the AB, with monthly averages rates ranging from 80 mm in the
608 southern part (including Madeira and Tapajos basin) up to 160 mm in the northern part of the

609 basin (Negro basin). Most models, as MOD16, usually show an increase in *ET* and forest
610 greenness as the dry season progresses in the northeastern and central Amazon, where equatorial
611 wet areas prevail, and spatial and temporal *ET* seasonality is mainly driven by incident radiation
612 and LAI (Maeda et al., 2017), corroborating with eddy covariance measurements (Christoffersen
613 et al., 2014), despite not all models agree with this pattern (**Figure 4c**). For instance, while
614 MOD16 *ET* seasonality is consistent with eddy covariance measurements (at K34 and K83),
615 with higher rates during the dry season, seasonality of the GLEAM model (at K34), peaking
616 during the wet season, implying that for wet regions in Amazon, this model has a dependence on
617 water availability, since GLEAM tends to follow the rainfall seasonality (Miralles et al., 2016).
618 Furthermore, in the south and southeastern parts of the AS (at Madeira and Tapajos basin), most
619 of the RS-based models consistently indicate a decrease in *ET* during the dry season, following
620 water availability (Maeda et al., 2017; H. J. F. da Silva et al., 2019). However, when RS-based
621 models estimates are compared to eddy covariance measurements (at local scale) or water
622 balance estimates (at large scale), the representation of the *ET* seasonality is still uncertain, since
623 most of the models are unable to consistently reproduce the seasonal cycles in tropical areas,
624 considering that multiple drivers operate simultaneously across the AB. Overall, in the tropics,
625 *ET* seasonality is mainly regulated by water and energy availability and how vegetation
626 assimilates both (Christoffersen et al., 2014; Restrepo-Coupe et al., 2013). Alternatively, in large
627 data scarce areas, estimating *ET* using multi-model ensembles and a dense observational network
628 across the Amazon, RS-based models can be improved through calibration and validation,
629 helping assess model uncertainties and to understand the land surface interactions in the tropics
630 (Gonçalves et al., 2013; Paca et al., 2019).

631



632
633
634
635
636
637
638
639

Figure 4. Spatial and temporal patterns of *ET* are differently represented by RS models. (a) Spatial variability of *ET* annual average (2003-2017) for GLEAM, SSEBop, MOD16 and PML models; the numbers on the lower left corner of each subplot represent the annual average *ET*. (b) *ET* seasonality for major Amazon sub-basins. (c) Monthly average comparison between estimates and eddy covariance measurements from the LBA project, using data from Saleska et al. (2013). The dry season is highlighted in gray as monthly precipitation rates < 100 mm month⁻¹

640 While flux tower measurements have shown, at local scales, that land cover changes can
641 impact water and energy fluxes (C. von Randow et al., 2004), large scale assessment with
642 satellites based on both energy balance and physical-based equations driven by vegetation
643 phenology and meteorological reanalysis have reinforced these findings (Baker & Spracklen,
644 2019; Khand et al., 2017; Laipelt et al., 2020; G. de Oliveira et al., 2019). All these studies
645 demonstrated significantly lower *ET* rates under pasture, agricultural, and deforested areas than
646 in primary and secondary forests (R. de C. S. von Randow et al., 2020). These results indicate
647 that less water returns to the atmosphere, thus affecting the precipitation recycling and
648 contributing to changes in the dry-to-wet season, possibly making the dry season longer (M. H.
649 Costa & Pires, 2010), while more of the precipitated water goes to runoff (Panday et al., 2015).
650 In addition, RS-based assessments demonstrated that drought events tend to affect anthropogenic

651 systems as pasture and agriculture areas more than primary and secondary forests, leading to an
652 increase in air temperature, and a decrease in LAI and *ET* (Baker & Spracklen, 2019; G. de
653 Oliveira et al., 2019). Results from MOD16 *ET* may assist in monitoring deforested areas in the
654 Brazilian Amazon (H. J. F. da Silva et al., 2019). However, global remotely sensed *ET*, such as
655 GLEAM, better reflect changes in vegetation greening and in air temperature increase than to
656 deforestation, may due the lack of deforestation account in these models (Wu et al., 2020).
657 Influence of land use changes on the water cycle will be discussed further in Section 6.4.

658 Our understanding about energy partitioning in the Amazon biome has improved through
659 RS models (Laipelt et al., 2020; G. de Oliveira et al., 2019). For example, high resolution *ET*
660 estimates using SEBAL in the south-western Amazon demonstrated significant differences
661 among energy and water fluxes in forests and non-forest areas, such as pasture and cropland. In
662 these anthropogenic areas, soil and sensible heat fluxes were from two to four times higher than
663 in forested areas (G. de Oliveira et al., 2019). In a transitional region between Amazon and
664 Cerrado biomes, converted areas can substantially change the energy and water fluxes, where
665 latent heat flux is the major component in forested areas, while in deforested areas an increase in
666 sensible heat flux is observed (Laipelt et al., 2020). These studies showed that change in land use
667 and land cover, can significantly affect *ET* rates, and observed *ET* rates was almost two times
668 lower in pasture than in tropical forest (Laipelt et al., 2020), and up to three times lower in non-
669 forested areas (G. de Oliveira et al., 2019).

670 Fisher et al. (2017) summarized in ten scientific questions the main outstanding
671 knowledge gaps for the *ET*-based science. To address these questions, *ET* estimations need to be
672 improved, aiming for high accuracy, high spatial and temporal scales, covering large spatial and
673 long-term monitoring. Recent research demonstrated that RS models can estimate *ET* with
674 reasonable accuracy and consistent agreement (Gomis-Cebolla et al., 2019; Martens et al., 2017;
675 Michel et al., 2016; Kun Zhang et al., 2019). However, for the individual *ET* components (soil
676 evaporation, transpiration, and interception), they diverge considerably (Miralles et al., 2016;
677 Talsma et al., 2018). For example, Miralles et al. (2016) showed that in tropical forests, soil
678 evaporation is almost non-existent in GLEAM and JPL models, whereas with MOD16 this
679 component may exceed transpiration. In the Amazon, canopy interception from JPL and MOD16
680 is nearly two times higher than in GLEAM model. Beyond the uncertainties related to canopy
681 transpiration and soil evaporation, open water evaporation and *ET* estimation over Amazon
682 wetlands is also a major knowledge gap. Wetland *ET* can be a complex process as it involves
683 fluxes at different vegetation conditions for transpiration, evaporation from water intercepted in
684 the canopy and from open and vegetated surface water. Changes in latent heat patterns over
685 water bodies (rivers, wetlands, lakes and artificial reservoirs) affect the local climate circulation
686 patterns through a breeze effect (Silva Dias et al., 2004), and have the potential to affect regional
687 climate through precipitation suppression over the wetlands and convection initiation over
688 wetland borders (Taylor et al., 2018). Wetland-upland differences in *ET* are still poorly
689 understood over the AB, and only a few in situ monitoring gauges are available on floodable
690 environments (Borma et al., 2009) that could be used for model validation. Improvements of
691 accuracy of *ET* components estimates lead us to better understand *ET* processes, and how these
692 components are impacted by changes in temperature, green-house gases concentration, and in the
693 hydrologic cycle (Fisher et al., 2017; Talsma et al., 2018).

694 Another challenge to satellite-based models overcome is to minimize the use of
695 parameterization and to improve input data accuracy. While the performance of Penman-
696 Monteith models can be strongly influenced by resistance parameterizations, Priestley and
697 Taylor models estimates have dependence on Priestley and Taylor parameter (α) parametrization,
698 as well as errors can also be related in both approaches by forcing data and algorithms structure
699 (Ershadi et al., 2015; Gomis-Cebolla et al., 2019). Moreover, measurements are still a significant
700 limitation. In the Amazon biome, there are only eight public flux towers with data available,
701 from the LBA project (Saleska et al., 2013), and they do not cover all vegetation and climate
702 complexity in the AB. In addition, when we are working on energy balance models, the main
703 challenge, especially in the Amazon, is the requirement of clear sky conditions. However recent
704 efforts to integrate microwave data to energy balance models are promising (Holmes et al.,
705 2018), since microwaves are less affected by cloud cover than the thermal infrared wavelength.

706 RS is now supported by a range of sensors and satellites which provide thermal infrared
707 images, and meteorological and surface observations, essential to estimate *ET*. In 2018 the
708 Ecosystem Spaceborne Thermal Radiometer Experiment on Space Station (ECOSTRESS)
709 mission was launched by National Aeronautics and Space Administration (NASA) and will
710 provide information about how vegetation responds to stress and how it uses water, focusing on
711 vegetation temperature measurement, allowing understanding of *ET* dynamics and processes at a
712 good temporal and spatial resolution (Fisher et al., 2017; Sheffield et al., 2018). Other missions
713 will improve *ET* estimates and will provide valuable information to validate current models. For
714 example, the Joint Polar Satellite System (JPSS), a mission from National Oceanic and
715 Atmospheric Administration (NOAA) and NASA, includes a range of sensors, such as the
716 Visible Infrared Imaging Radiometer Suite (VIIRS), that collect visible and infrared imagery,
717 providing useful global information to monitor vegetation, and as input to retrieval hydrological
718 variables (McCabe et al., 2017; Sheffield et al., 2018; L. Zhou et al., 2016). The Water Cycle
719 Observation Mission (WCOM) from China aims to acquire consistent measurements of the water
720 cycle components (Levizzani & Cattani, 2019; Shi et al., 2016). The FLouescence EXplorer
721 (FLEX) mission by European Space Agency, that will map vegetation fluorescence, providing
722 information about photosynthetic activity and vegetation stress and health, also helping to
723 improve constraints on transpiration (Drusch et al., 2017; McCabe et al., 2017). Beyond
724 continuity of Landsat (McCorkel et al., 2018) mission, will map long- term *ET* at high spatial
725 scale, and the Gravity Recovery and Climate Experiment (GRACE) Follow-on that will bring
726 significant opportunity to estimate *ET* with the water balance approach (Landerer et al., 2020).

727 RS has been crucial to improve our understanding of surface-atmosphere interactions
728 through *ET*, despite the challenges that still exist, and these future missions are an excellent
729 opportunity to address important scientific questions from *ET*-based science, allowing us to
730 improve techniques, approaches and our knowledge about *ET* processes and how the impact of
731 activities can affect the water cycle throughout the Earth, including the Amazon.

732

733 **4. Surface water**

734 **4.1. Surface water elevation**

735 Surface water is a key resource for all the communities living along the Amazon River.
736 Yet monitoring Surface Water Elevation (SWE) and discharge in the AB is a challenge. While

737 the AB is facing pressure on its water cycle due to human activities, the number of gauges
738 decreased globally in the last decades (Vörösmarty et al., 2000). This threatens our capacity to
739 understand natural and human-driven impacts of climate change on Amazonian rivers. Although,
740 to this date, no satellite mission have been designed specifically for retrieving inland water
741 elevations, remotely-sensed observations of SWE from radar altimetry are complementary to the
742 historical gauge network (Fekete et al., 2012) and improve monitoring of Amazonian rivers
743 (Calmant & Seyler, 2006; J. S. Da Silva et al., 2014).

744 The AB has become an ideal laboratory for pioneering studies that have demonstrated the
745 capacity of retrieving accurate SWE at particular locations from radar echoes and adapted
746 retracking procedures. The first studies over the AB used observations from Seasat (Sea Satellite
747 from NASA), launched in 1978, to derive the low water gradient of the Amazon main stem
748 (Guzkowska et al., 1990).

749 The configuration of the satellite altimeter orbit defines the intersections between the
750 satellite ground tracks and the river reaches, the so-called virtual stations (VSs), where SWE can
751 be estimated. At a given VS, the SWE is retrieved through the inversion of the signal round-trip
752 propagation time that provides the range. Several uncertainty corrections (due to delay in the
753 propagation caused by the atmosphere, dynamics of Earth's surface, etc.) must be applied to this
754 range to retrieve the SWE. Stammer & Cazenave (2017) provide an extensive discussion on
755 SWE estimation from satellite altimetry and the associated errors. Since the first satellites, the
756 accuracy of the orbit, which depends on the density of the atmosphere and on the resolution of
757 the gravitational field, has improved, and is now around one centimeter (against sixty
758 centimeters for Seasat). Yet calculating the correct range remains challenging, as it is necessary
759 to track (on board) or retrack (on the ground) the altimetric waveform (Frappart et al., 2006),
760 using algorithms to best fit the highly variable distribution of the echo energy bounced back by
761 the different types of surfaces in the satellite field of view (Calmant et al., 2016).

762 Since the first studies using Seasat data, we now have more than 30 years of monitoring
763 of inland waters by satellite altimetry. After Seasat came GEodetic and Oceanographic SATellite
764 (GEOSAT), that was used by Koblinsky et al. (1993) to retrieve SWE time series over the AB,
765 with uncertainties ranging from 0.19 to 1.09 m compared to in situ data. The European Remote
766 Sensing satellite (ERS-1; launched in 1991) initiated a long family of satellites that followed the
767 same 35-day repeat orbit (ERS-1, ERS-2, ENVISAT -Environmental Satellite, and SARAL -
768 Satellite with ARgos and ALtika), which covered the 1991-2016 period. A major advance was
769 made by the Observations des Surfaces Continentales par Altimetrie Radar (OSCAR) project,
770 that evaluated the ICE-2 specific retracking of radar echoes for ice caps (Legresy et al., 2005) for
771 ERS-1, ERS-2 and ENVISAT, and promoted its delivery in the Geophysical Data Records.

772 The retracking of radar echoes was analyzed by Frappart et al. (2006, 2016) and J. S. Da
773 Silva et al. (2010) over 70 ERS-2 and ENVISAT VSs and a large range of river widths (from
774 tens of meters to kilometers). They reported that the proper selection of the data considered as
775 representative of the water body is as important as the choice of the retracking algorithm. The
776 data from the 10-day repeat orbit of Topex/Poseidon (T/P) and Jason-2/3 have also been assessed
777 in the AB. Seyler et al. (2013) highlighted the gain of Jason-2 (ranging from 2008 to 2016 on its
778 nominal orbit) in comparison to T/P (from late 1992 to 2005), with an uncertainty around 0.35
779 m, possibly due to the sensor's better capacity to discriminate the surrounding floodplain from
780 the river.

781 All these missions operated in low resolution mode, i.e., the footprint on ground is large
 782 (some kilometers, depending on radar operating band) and the echoes returning to the antenna
 783 are influenced by the surroundings. The SAR mode, active on Sentinel-3 satellites, allows a
 784 reduction of the surrounding contributions by slicing the disc illuminated by the echo at a given
 785 time (Raney, 1998). This reduction provides a much better along track resolution, however it
 786 does not resolve some issues such as cross-track sloping measurements (Bercher et al., 2013).
 787 The addition of a second antenna, as on Cryosat-2, allows the SAR Interferometric mode to
 788 correct these cross-track measurements, hence allowing an improvement in the accuracy of SWE
 789 time series. However, Croysat-2 is not popular for SWE monitoring over rivers since its orbit
 790 shifts around 7 km every month and comes back to the same place every 369 days. Indeed, most
 791 of the studies on the use of satellite altimetry in the AB have focused on repetitive orbits, even
 792 though some studies have explored the use of missions in drifting or long-term repetitive ones
 793 and found good accuracy for SWE monitoring (e.g., Bogning et al., 2018). Such missions,
 794 instead of providing a SWE observation on a 10-day or almost monthly basis with a large
 795 intertrack distance at the equator (between 60 km and 100 km), provide a much denser spatial
 796 span but with observations separated from another in time. The use of ICESat (Ice, Cloud, and
 797 land Elevation Satellite) laser altimetry data was investigated by Hall et al. (2012). They
 798 concluded that this mission can be a valuable source of data for monitoring rivers from the AB,
 799 with accuracies of some tens of centimeters when compared to gauges. The ICESat mission was
 800 continued by ICESat-2, launched in 2018. Studies by Bercher et al. (2013) and L. Jiang et al.
 801 (2017) concluded that the SAR mission CryoSat-2 offers new opportunities to monitor narrow
 802 rivers in the AB, and should help linking the present and future altimetry missions.

803 The differential interferometry technique with SAR data allows obtaining information
 804 about changes in surface displacements, such as topographic changes. Centimeter-scale
 805 measurements of water level changes throughout inundated floodplain vegetation using
 806 interferometric SAR were obtained over the Amazon floodplains for the first time (Alsdorf et al.,
 807 2000; Alsdorf, Birkett, et al., 2001; Alsdorf, Smith, et al., 2001). This estimation is possible due
 808 to the radar pulse interactions with the water surface and the trunks of flooded vegetation causing
 809 a double-bounce path (Alsdorf et al., 2000; Hess et al., 1995). H. Lee et al., 2020 and
 810 Mohammadimanesh et al. (2018) reviewed the methods and limitations of the technique for
 811 applications in wetlands.

812 To date, SWE information is available as raw data and as processed data. Some groups or
 813 institutions provide processed SWE time series (see **Table 3**). Each dataset provides SWE on
 814 selected water bodies, all over the world or in specific regions, and have different objectives in
 815 terms of operability. Processing and filtering procedures vary between each group, and time
 816 series of the same VSs can vary from one group to another.

817

818 **Table 3.** Datasets of surface water elevation time series over the water bodies

Name	Producer	Weblink	Reference	Target	Delivery time
G-REALM	USDA NASA	https://ipad.fas.usda.gov/cropexplorer/global_reservoir/Default.aspx#SatelliteRadarAltimetry	(Birkett et al., 2017)	Lakes and reservoirs	NTC

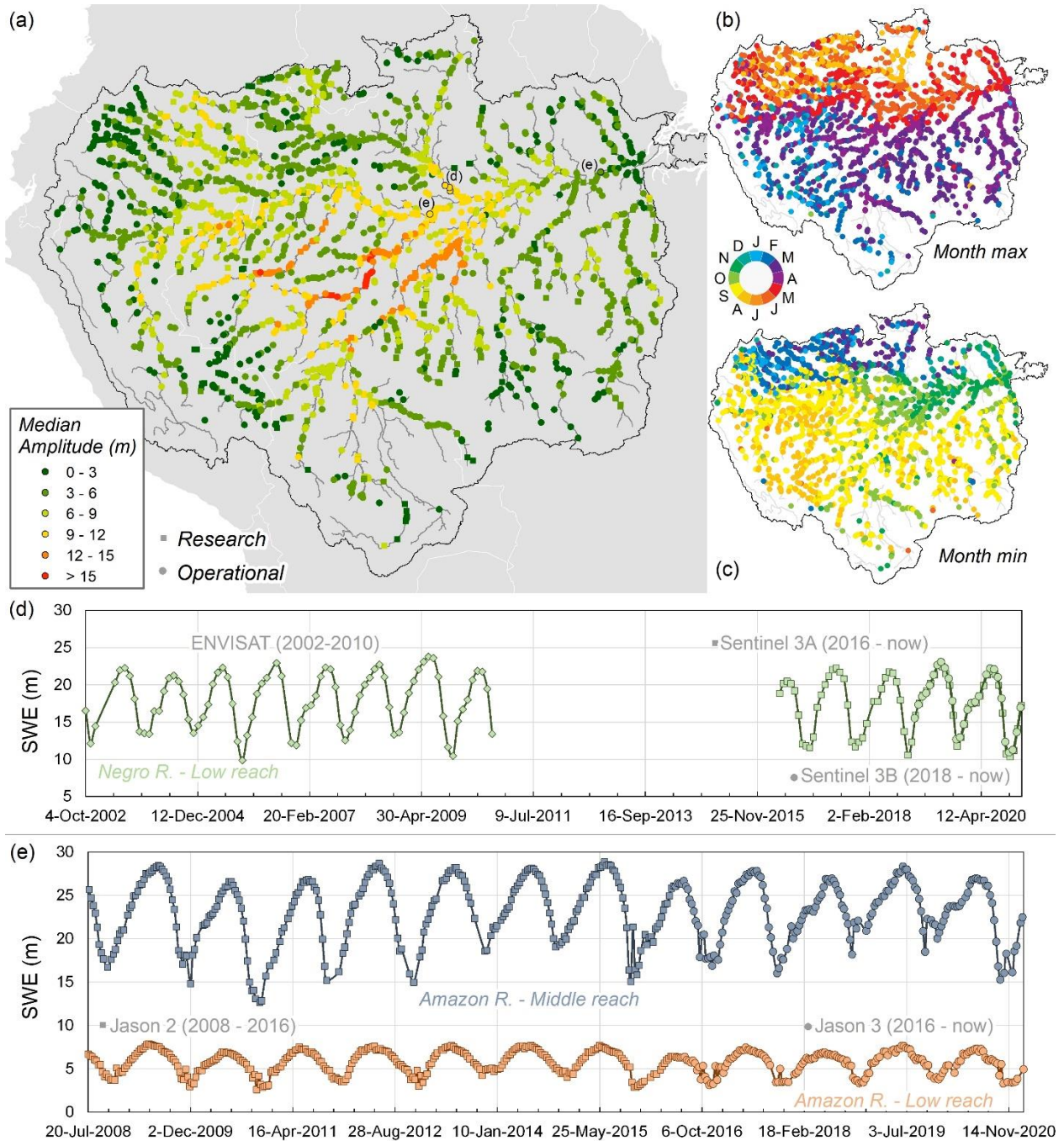
River & Lake	De Montfort University	http://altimetry.esa.int/riverlake/shared/main.html	(Berry et al., 2005)	Rivers, Lakes and reservoirs	SCT (discontinued)
DAHITI database	German Geodetic Research Institute	https://dahiti.dgfi.tum.de/en/	(Schwatke et al., 2015)	Rivers, lakes reservoirs and wetlands	NTC & reanalysis
GRRATS product	Ohio State University	https://podaac.jpl.nasa.gov/dataset/PRESWOT_HYDRO_GRRATS_L2_VIRTUAL_STATION_HEIGHTS_V2	(Coss et al., 2020)	Rivers	Reanalysis only
Hidrosat	ORE-HYBAM and ANA	http://hidrosat.ana.gov.br/	(J. C. Carvalho et al., 2015)	Rivers	NTC
Hydroweb	IRD/LEGOS, CNES (French Space Agency), and Universidade do Estado de Amazonas	http://hydroweb.theia-land.fr/	(Crétaux et al., 2011; J. S. Da Silva et al., 2010)	Rivers, lakes and reservoirs	STC & reanalysis

819 STC: Slow-Time Critical - delivered at maximum after three days; NTC: Non-Time Critical -
820 delivered typically within one month.

821

822 **Figure 5** provides the location of all virtual stations in the AB from the Hydroweb
823 website. **Figure 5a** is a representation of the median amplitude of SWE at each VS. Amplitude of
824 SWE measured by the satellites is lower in the headwaters (0-3 m) and medium size rivers (3-6
825 m) compared to Solimões-Amazonas main stem and its tributaries (9 - 12 m). Largest values are
826 found for the Purus River (> 15 m), a right bank tributary. **Figure 5b** and **c** provide the mean
827 month for high and low flows, respectively, indicating the influence of rainfall partition in the
828 northern and southern parts of the basin and the gradual shift due to the flood travel time along
829 the rivers and floodplains (~ 1- 3 months). **Figure 5d** and **e** provide multi-mission SWE time
830 series ranging from 2002 to now with ENVISAT and Sentinel3-B and from 2008 to 2020 with
831 Jason-2 and Jason-3, respectively. It shows the strong seasonal signal of the gradual flood of the
832 Amazon rivers, and interannual variability of maximum and minimum stages.

833



834

835 **Figure 5.** a) Location of the virtual stations freely available on Theia-hydroweb
 836 (<http://hydroweb.theia-land.fr/>) and median amplitude of the time series. Dots are operational
 837 VSs (from currently flying missions and updated in near real time) and squares are research VSs
 838 (identified as reanalysis in table W). VSs rounded in black are drawn in d and e; b) month of
 839 maximum SWE for the mean monthly time series at each VS; c) month of the minimum SWE
 840 for the mean monthly time series; d) composite time series of the VSs close one to each other on
 841 the lower Negro River, VSs NEGRO_KM1444, NEGRO_KM1420 and NEGRO_KM1404, e)

842 time series on the Amazon middle reach and Amazon lower reach composed of Jason-2 and
843 Jason-3 observation at VS AMAZONAS_KM1534 and AMAZONAS_KM0397 respectively.

844

845 Owing to its relatively dense spatial cover (see **Figure 5**), satellite altimetry has been
846 used for deriving the altimetric profiles of rivers throughout the basin. These profiles, computed
847 for low and high waters for the Negro River from T/P VSs (Frappart et al., 2005) and ENVISAT
848 VSs (Leon et al., 2006), indicated a lower slope for the Negro River over more than 500 km
849 (from its mouth to upstream reaches) than for the Solimões River (confirmed by Callède et al.,
850 2013). Such a difference explains the strong backwater effect that occurs in the lower section of
851 the Negro River and alters the time of peak and low flows. Other backwater effects, mainly from
852 the Amazon main stem on its tributaries, were evident in the river profiles from satellite
853 altimetry. However sparse in time, satellite altimetry observations now provide a dense enough
854 network to monitor extreme events such as those that occurred in 2005 and 2010 in the AB
855 (Frappart et al., 2012; J. S. Da Silva et al., 2012).

856 A straightforward application of these profiles is to derive the spatiotemporal variations
857 of the water surface slope. While former studies focused on the spatial variations of the surface
858 water gradient, a first try to estimate the temporal variations of the Amazon main stem slope was
859 performed in Birkett et al. (2002) using VSs from the T/P mission. They revealed changes in the
860 sign of the rate of slope variation that were explained by the river not reaching equilibrium.
861 Although the slopes from Birkett et al. (2002) compared well with slopes from the Shuttle Radar
862 Topography Mission (SRTM) Digital Elevation Model (DEM) - a snapshot of profiles and slopes
863 in February 2000 (LeFavour & Alsdorf, 2005) - and with gauge data (Calmant et al., 2013), these
864 breaks in slope variation rate were not found in profiles extracted from more recent and complete
865 altimetric databases (Calmant et al., 2016). Paris et al. (2016) estimated two different time series
866 of slopes from satellite altimetry in the lower Negro River: the first was calculated using a daily
867 interpolation of upstream and downstream SWE time series, providing a daily slope time series,
868 and the second was calculated using the mean climatology of upstream and downstream VSs.
869 Although the stage to discharge relationship was improved when considering the variation of
870 slope with time estimated through both methods, it is the monthly means that provided the best
871 improvement. This illustrates the difficulty in inferring slopes from non-daily uncertain
872 observations.

873 By coupling satellite altimetry and a hydrologic and hydraulic model through stage to
874 discharge rating curves, Paris et al. (2016) provided a map of estimated bottom of river in the
875 entire AB using data from ENVISAT and Jason-2 missions. This map was then used by
876 Garambois et al. (2017) on a reach of the Xingu River to parameterize a hydraulic model. Such
877 cases where the satellite ground-track crosscuts several times the same river reach allow a more
878 refined analysis of water surface slope. This occurs in sinuous rivers flowing from north to south
879 (or the contrary) like the Xingu River, a right margin tributary of the Amazon River (**Figure 2**).
880 Given these conditions, the authors verified that the presence of an obstacle in the river bed
881 produces temporal changes in water surface slope observed by satellite altimetry. Brêda et al.
882 (2019) proposed a benchmark of methods of altimetric data assimilation, ranging from direct
883 insertion to a hydraulically based Kalman filter, to improve bathymetry estimates of the Madeira
884 River. They concluded that satellite altimetry can be used for better constraining SWE and flood
885 inundation simulations. An analysis of SWE from the ENVISAT mission revealed water passing

886 from the Negro River to the Solimões River through their interconnected floodplains at high
887 stages (J. S. Da Silva et al., 2012).

888 The capacity to observe channel-floodplain connectivity through altimetry was
889 investigated by Park (2020). By observing seasonal changes in SWE in rivers and surrounding
890 floodplains, they separated the role of channelized flows and of overbanks flows, which
891 contributes to surface water storage and smooths the channelized-induced topography. The
892 floodplain located between the Madre-de-Dios, the Beni, the Guapore and the Mamore rivers in
893 the upper Maderia basin was characterized using ENVISAT and SARAL data (Ovando et al.,
894 2018). Water level differences between the frequently flooded regions, with no direct connection
895 to the Andes, and the regions subject to sporadic though large flood events were distinguished.

896 Alsdorf et al. (2000, 2005, 2007) applied for the first time interferometric SAR (InSAR)
897 in the central Amazon floodplains and showed that the water flows in the floodplains are
898 dynamic in space and time, changing the direction with the flood wave of the river. Before the
899 flood, the flows are controlled by the local topography and the surface water elevation in the
900 floodplain is not equivalent to the river level (Alsdorf et al., 2007). By assuming that the water
901 surface in the floodplain is equivalent to those in the main channel, estimates of water storage
902 derived from flood routing can be overestimated, as shown by Alsdorf (2003). H. C. Jung et al.
903 (2010) compared temporal changes in floodplain water in the Amazon and Congo river basins.
904 While the Amazon River is connected by many channels to the floodplains and has complex
905 flow patterns, the Congo Rivers (and especially the Cuvette Centrale) have sparse connections
906 with interfluvial areas and flow patterns that are not well defined and have diffuse boundaries.
907 The patterns of water surface variations in the floodplains located on the Tapajós and Solimões
908 rivers were examined by C. Wang et al. (2011) and Cao et al. (2018), respectively. The most
909 recent SAR missions allowed monitoring of smaller water bodies. Recently, Fleischmann et al.
910 (2020) produced SWE time series in the complex Negro River interfluvial wetlands from
911 Sentinel3-A data. For the first time, they reported < 1 m water level variations in these complex
912 areas. Their results show that satellite altimetry can help understanding the hydraulic behavior of
913 complex ungaged areas and help validate hydrologic and hydraulics models.

914 Through direct assessment or combination with other RS products, satellite altimetry can
915 be used to derive non-measured hydrological variables. Pfeffer et al. (2014) were able to infer
916 the varying exchanges between surface water and the groundwater base-level from 491
917 ENVISAT VSs located all over the basin. Estimates of deviations from groundwater base-level
918 reached up to 5 m. Frappart et al. (2012) made a joint use of satellite altimetry and inundation
919 extent to derive variations of surface continental water storage (see Section 5). These two
920 variables were used in Frappart et al. (2019) to estimate the spatiotemporal variability of
921 groundwater storage in the AB. de Oliveira Campos et al. (2001) and M. V. Silva et al. (2019)
922 found signatures of global climatic events such as ENSO and sea surface temperature variations
923 in the T/P and Jason-2 SWE time series, respectively. Since the SWE estimates are now
924 delivered in near real time, rating curves that relate SWE with discharge and depth, have been
925 the focus of several studies (see details in Section 6.2). These rating curves were either computed
926 using local gauges (Zakharova et al., 2006) or model outputs (Getirana et al., 2012; Leon et al.,
927 2006). By constraining the rating curve parameters into Manning-realistic bounds, Paris et al.
928 (2016) showed that discharges predicted from satellite altimetry are comparable to those
929 measured in situ. The original SWE time series or their conversion into discharge offer an

930 independent tool to validate hydrological models (Paris et al., 2016) and their rainfall inputs, and
931 in situ data (J. S. Da Silva et al., 2014).

932 With its disruptive technology based on swath altimetry, almost-global coverage and joint
933 observation of SWE, River width and slope, the SWOT mission, due to be launched in 2022,
934 will permit an unprecedented observation of SWE all over the AB. As highlighted by
935 Biancamaria et al. (2016), SWOT observation of SWE will permit a better monitoring of
936 transboundary waters and wetlands in the AB. Dedicated to sample all rivers wider than 100 m
937 and lakes larger than 250 x 250 m, the mission will permit a consequent reduction of global and
938 regional models, noteworthy through data assimilation (Emery et al., 2020; Wongchuig et al.,
939 2020). The estimate of discharge from altimetry will benefit from SWOT data, both thanks to the
940 global coverage and the observation of slopes, allowing a better constraining of uncertain
941 hydraulics (Wilson et al., 2015).

942 Thanks to more than twenty years of studies, EO datasets, especially satellite altimetry,
943 have been revealed as an unprecedented tool to monitor continental watersheds and their
944 droughts and floods (Lopez et al., 2020). The current satellite altimetry missions opened the era
945 of operational monitoring from space at large scale, and this will be of critical importance in the
946 coming decades in the large tropical transboundary watershed that is the AB. With almost two
947 thousand VSs distributed all over the basin and available for free on websites, and potentially
948 hundreds more, satellite altimetry can favorably complement the traditional in situ network,
949 whose location usually depends on the proximity to a city or town. However, to operationally
950 monitor non-open waters such as permanently or seasonally flooded vegetated floodplains
951 remains challenging. In fact, few lakes and reservoirs are monitored by altimetry routinely in the
952 AB though more could be (Crétaux et al., 2011; Crétaux & Birkett, 2006). The forthcoming
953 missions will benefit from past research to improve the accuracy of SWE time series and
954 promote its use for monitoring more local phenomena, such as floodplain-channel exchanges.
955 Although limited due to availability of appropriate data, InSAR datasets help characterize
956 floodplains/rivers connectivity and dynamics. The global coverage of the forthcoming SWOT
957 mission will increase greatly our understanding on the global water cycle and should allow a
958 better quantification of past and current inter-mission biases, helping turning satellite altimetry
959 archives into a unique climatic dataset and understanding the impacts of climate change and
960 human activities on the basin. Such a task will benefit of the ongoing VASHYB project
961 (Validation of Altimetric Satellites for HYdrology in Brazil,
962 <https://swot.jpl.nasa.gov/documents/1054/>), which aims to validate SAR and InSAR
963 observations. The SWOT mission will dramatically increase our capacity to model the AB and
964 the variations of its water cycle, thanks to the new capacity to monitor hydrological variables
965 (height, width, slope, and associated discharge) of hundreds of rivers 100 m wide (Biancamaria
966 et al., 2016). The centimetric accuracy in SWE and slope (Desai, 2018) should provide new
967 insights on water fluxes in the AB. Since the main limitation for a broader use of satellite
968 altimetry remains its relatively low temporal sampling, future missions such as the SMASH
969 mission (SMall Altimetry Satellites for Hydrology, Blumstein et al., 2019), broadcasted together
970 with the current constellation, should help tackle this issue.

971

972 **4.2. Surface water extent**

973 Characterizing the extent and variation of surface water bodies and aquatic ecosystems,
974 which include rivers, streams, lakes, wetlands, as well as seasonally inundated floodplains,
975 forests and savannas, is of primary importance to the study of the water, energy and
976 biogeochemical cycles of the Amazon River basin (Junk, 1997; Melack et al., 2009). Indeed,
977 covering about 20% of basin's surface area, with large temporal variability, the surface waters of
978 the Amazon play a key role in the climate and in the maintenance of biodiversity. Amazon
979 surface waters are a major source and sink of carbon dioxide (Abril et al., 2014; Amaral et al.,
980 2020; Raymond et al., 2013) and the largest natural geographic source of methane in the tropics
981 (Kirschke et al., 2013; Melack et al., 2004; Pangala et al., 2017; Pison et al., 2013). In this
982 context, understanding the dynamics of surface water extent is of primary importance to Amazon
983 hydrology, biogeochemistry processes and their link with climate, for effective management of
984 water and fisheries resources (see Section 6.3) and for a disaster management for cities which are
985 under flood risk (e.g., Iquitos, Porto Velho, Rio Branco, Cruzeiro do Sul). This is particularly
986 true in the context of current global changes that impact the AB (see Section 6.4), with intense
987 drought and flood events that recently affected large areas of this region (E. A. Davidson et al.,
988 2012; Jiménez-Muñoz et al., 2013; Marengo et al., 2008, 2011). In addition, monitoring the
989 variations of surface water hydrological conditions is key to support the development of models
990 of the Amazon water cycle and its surface hydrology (see Section 6.2).

991 Characterizing the distribution and quantifying seasonal and interannual variations in the
992 extent of surface waters at the scale of the AB is a challenge given their large variety and
993 variability, and the presence of cloud cover and forest vegetation. Early estimates of the
994 distribution of surface water for large areas were based on static databases from aeronautical
995 charts and aerial photographs, which often reflected the maximum open water extent (Cogley,
996 2013; E. Matthews & Fung, 1987) and did not provide information on their temporal and spatial
997 variations. The Global Lakes and Wetlands Database (Lehner & Döll, 2004) estimates the extent
998 of floodplains and wetlands in the AB of $\sim 300\text{-}350 \times 10^3 \text{ km}^2$, but with large uncertainties (N. C.
999 Davidson et al., 2018). The advent of satellite observations now allow monitoring the large-scale
1000 dynamic of surface waters, including those in the AB (Alsdorf et al., 2007; Prigent et al., 2007)
1001 enabling progress on understanding of the associated physical, biogeochemical, environmental
1002 and ecological processes.

1003 Different RS-based techniques, using observations made in a wide range of the
1004 electromagnetic spectrum (visible, infrared, and microwave; Melack et al., 2004; Prigent et al.,
1005 2016), have been developed, with varying degrees of success, to derive quantitative estimates of
1006 the extent and dynamics of surface waters and aquatic systems in the Amazon (**Table 4**). They
1007 encompass a wide range of spatial and temporal resolutions, often based on a trade-off between
1008 temporal and spatial coverages. Observations with low spatial resolution (e.g., $\sim 10\text{-}50 \text{ km}$ from
1009 passive microwave sensors) are generally limited to the detection of relatively large inundated
1010 areas, or regions where the cumulative area of small areas represents a fairly large portion of the
1011 satellite footprint. They have the advantage of frequent temporal coverage, sometimes daily.
1012 High-resolution observations (e.g., $<100 \text{ m}$ from SAR for instance) provide information at a fine
1013 spatial scale but have low temporal frequency, often limiting observations over large areas to a
1014 few times per season. Optical and infrared observations offer good spatial and temporal
1015 resolution but have limited capabilities in the tropical Amazon region as they are unable to
1016 penetrate clouds and dense vegetation.

1017

1018 **Table 4.** Summary of RS-based approaches developed to monitor the extent of surface water in
 1019 the Amazon (non-exhaustive list). References, sensor/satellite name, product name (when
 1020 available), original area of study, spatial/temporal resolution and time span of data availability
 1021 are shown.

RS Approaches	References	Sensors/Satellites (product name)	Original Area of Study	Spatial/temporal resolution	Time span
Passive Microwaves	Giddings and Choudhury (1989)	SMMR on Nimbus 7	4 major river basins of SA	~25km / Monthly	1979-1985
	Sippel et al., (1994)	SMMR on Nimbus 7	Central Amazon and floodplains	~25km/ Monthly	1979-1985
	Sippel et al., (1998)	SMMR on Nimbus 7	Amazon River and tributaries	~25km/ Monthly	1979-1985 (and 1902-1995 reconstruction)
	Hamilton et al., (2002)	SMMR on Nimbus 7	6 major floodplains over SA.	~25km/ Monthly	1979-1987
	Brakenridge et al., (2007)	AMSR/E on Aqua	Global	~25km/ daily	2002-2011
	Parrens et al., (2017)	SMOS (SWAF)	AB	~25-50km/ 3-day	2009-present
Active Microwaves	Hess et al., (2003)	SAR on JERS-1	Central Amazon	100m/Sep-Oct 95 and May-Jun 96	Sept-Oct 95 and May-Jun 96
	Bourrel et al., (2009)	SAR on ERS-2 / RADARSAT	Bolivian Amazon	2 RADARSAT (50m)/ 3 ERS (15m) images	1996–1998
	Arnesen et al., (2013)	ScanSAR mode on ALOS/PALSAR	Lower Amazon River floodplain	100m/ Twelve ScanSAR images	2007-2010
	Ferreira-Ferreira et al., (2015)	SAR on ALOS/PALSAR	Central Amazon floodplain	12.5m / 13 ScanSAR fine beam images	2007-2010
	Hess et al., (2015)	SAR on JERS-1	AB	100m/ Sept-Oct 1995 and May-Jun 1996	Sept-Oct 1995 and May-Jun 1996
	Chapman et al., (2015)	ScanSAR mode on ALOS/PALSAR	AB	100m / 323 ScanSAR images	2007-2010
	Ovando et al., (2016, 2018)	ScanSAR mode on ALOS/PALSAR and MODIS reflectance	Bolivian Amazon wetlands	100m/Forty-five ScanSAR and 500m/ 8-day MODIS images	2007-2009 and 2001-2014
	Park et Latrubesse (2017)	SAR on ALOS/PALSAR	Amazon floodplain (Miratuba)	12-350m / 19 images	2006-2008
	Pinel (2019)	SAR on ALOS/PALSAR	Amazon/Solimoes River (Janauaca)	30m/ 23 images	2007-2011
	Resende et al. (2019)	SAR on ALOS/PALSAR	Central Amazon	25m / 56 images	2006-2011
	Rosenqvist et al. (2020)	ScanSAR on ALOS-2 PALSAR-2	AB	50m / Yearly minimum and maximum	2014-2017
Optical and infrared	Yamazaki et al. (2015)	Landsat (G3WBM)	Global	90m / 4 scenes of surface body freq. at 5-year interval	1990-2010
	Pekel et al. (2016)	Landsat (GSW)	Global	30m/ Surface water occurrence	1984-2015

	Allen et al., (2018)	Landsat (GRWL)	Global	30m / static widths and areas	--
	Souza et al (2019)				
Multi-satellite techniques	Prigent et al., (2007, 2020)	SSMI/AVHRR/ERS (GIEMS)	Global	~25km/ monthly	1992-2016
	Schroeder et al., (2015)	Landsat	AB	30m/Surface water changes	1985-2017
	Aires et al., (2013)	GIEMS/JERS-1 SAR	Central Amazon	500m/ monthly	1993-2007
	Fluet-Chouinard et al., (2015)	GIEMS downscalled (named GIEMS-D15)	Global	500m/ max./min./average	1993-2007
	Aires et al., (2017)	GIEMS downscalled (named GIEMS-D15)	Global	90m/ monthly	1993-2007
	Parrens et al. (2019)	SMOS downscalled (named SWAF-HR)	AB	1km/ 3-day	2010-2016

1022

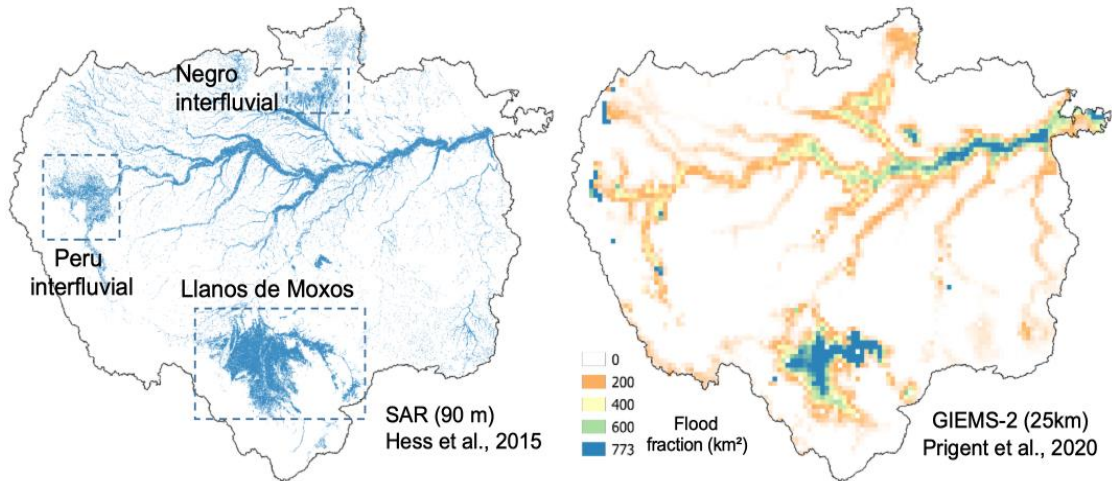
1023 Passive microwave observations have demonstrated their usefulness for observing
1024 surface water and flood extent and provided some of the first estimates of Amazon surface water
1025 extent from satellite (Giddings & Choudhury, 1989) as reviewed in Kandus et al. (2018).
1026 Emissivities (and brightness temperatures) are sensitive to the presence of surface water
1027 (Choudhury, 1991; Sippel et al., 1994) with a decrease in emissivity in both linear polarizations
1028 (horizontal and vertical) and an increase for the difference in polarization, especially at low
1029 frequencies, due to the different dielectric properties between water, soil and vegetation. Surface
1030 water and inundation patterns in the large floodplains of the central AB (Sippe et al., 1998) and
1031 South America (Hamilton et al., 2002) were derived by analysis of the 37-GHz polarization
1032 difference observed by the Scanning Multichannel Microwave Radiometer (SMMR; Nimbus-7
1033 satellite, 1979-1987). By developing a relationship between the total flooded area along the
1034 Amazon river main stem and the monthly means of river stage at Manaus, they provided the first
1035 94-year reconstruction of flooded area from the river stage in situ record, estimating the long-
1036 term mean of the flooded area along the Amazon River main stem to be ~ 47000 km². Those
1037 studies have been followed by passive microwave-derived products of surface water extent over
1038 the AB, using Special Sensor Microwave/Imager (SSM/I), Advanced Microwave Scanning
1039 Radiometer (AMSR-E; Brakenridge et al., 2007) and most recently Soil Moisture Ocean Salinity
1040 (SMOS) observations (Parrens et al., 2017). Parrens et al. (2017) used the microwave L-band
1041 (1.4 GHz) observations from 2010 to 2017 to map the temporal evolution of the Amazon water
1042 bodies at coarse spatial resolution (~50 km) and weekly temporal resolution (product named
1043 SWAF) with the ability, thanks to the L-Band frequency, to better retrieve water under dense
1044 canopy. Passive microwave observations have inherent limitations because of their ground
1045 footprints in the typical order of 25-50 km, and their relatively low spatial resolution is often
1046 insufficient to observe small water bodies.

1047 Multi-satellite methodologies that combine the complementary strengths of different
1048 types of satellite observations to retrieve surface water extent and their dynamics expand the
1049 information provided by passive microwave radiometers (**Table 4**). Though designed originally
1050 for global scale applications, these approaches have been evaluated in the AB. The Global
1051 Inundation Extent from Multi-Satellite (GIEMS, Papa et al., 2010; Prigent et al., 2007, 2016,

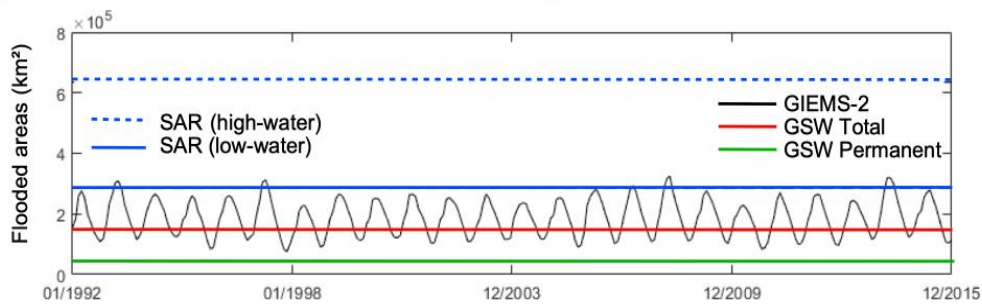
1052 2020) or the Surface Water Microwave Product Series (SWAMPS) Inundated Area Fraction
1053 (Schroeder et al., 2015) detect and quantify multi-decadal variability of surface water extent over
1054 tropical environments (Frappart et al., 2008; Papa et al., 2008, 2013). The current version of
1055 GIEMS is available at ~25 km spatial resolution on a monthly basis for 1992 to 2015 (GIEMS-2,
1056 Prigent et al., 2020, **Figure 6a**), while SWAMPS offers current and near-real time information
1057 (Jensen et al., 2018). The use of these passive microwave-derived datasets helped reveal the
1058 sources and characteristics of the flood pulse and annual flood wave along the Amazon River
1059 and major tributaries. They contributed to show at basin scale the water extent seasonality, with a
1060 high flood season in May-June and low flood season in November in the central Amazon
1061 floodplain. At basin-scale, Amazon surface water extent (**Figure 6b**) varies from ~100,000 km²
1062 (low season) to almost ~400,000 km² (high season), but with a large interannual variability,
1063 mainly driven by droughts (1998, 2005, 2010) or floods (1997, 2014) extreme events (Papa et al.,
1064 2010; Prigent et al., 2020). However, the maximum surface water extent from GIEMS and
1065 SWAMPS are lower than those from SAR estimates (**Figure 6b**).

1066 Prigent et al. (2007) showed that seasonal flooding differed between the north and south
1067 part of the basin due to seasonal differences in precipitation. Papa et al. (2008) reported a phase
1068 lag in precipitation, flood extent and peak flows at the basin scale, suggesting as in Richey et al.
1069 (1989), that floodplains in large basins such as the Amazon can store large volume of water and
1070 alter the water transport. Richey et al. (1989) applied a simple water routing scheme and
1071 estimated that up to 30% of the discharge of the Amazon River is routed through the floodplains.
1072 However, studies such as Getirana et al. (2012), based on large-scale hydrological model that
1073 used GIEMS to evaluate their floodplains simulations, suggested instead that the actual value
1074 might be more below 5%. Furthermore, Sorribas et al. (2020) reported that the ratio between
1075 river-floodplain discharge and basin discharge ranged between 5 and 40%, which is comparable
1076 to the range estimated from observations by Richey et al. (1989) and Alsdorf et al. (2010) who
1077 used gravimetric and imaging satellite methods to estimate the amounts of water seasonally
1078 filling and draining from the mainstem Amazon floodplain. Hence, there is a need to better
1079 understand the processes that control Amazon inundations in order to quantify the various fluxes
1080 across floodplain environments, as is evident in applications of regional-scale flooding models
1081 (Rudorff et al., 2014b).

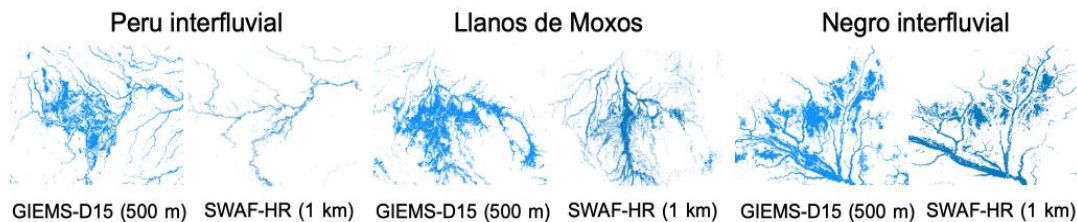
(a) Maximum flood extent at basin scale



(b) Basin-scale surface water extent variability



(c) Maximum flood extent at regional scale (downscaling)



1082

1083 **Figure 6.** Surface water extent of the AB. (a) Map of maximum wetland and surface water extent
 1084 (high water season) from JERS-1 SAR (Hess et al., 2015) and map of annual maximum surface
 1085 water extent (fraction in km^2 for each 773 km^2 pixel) averaged over 1992– 2015 from GIEMS2
 1086 (Prigent et al., 2020). (b) Basin-scale monthly mean surface water extent variability for 1992–
 1087 2015 from GIEMS2 (solid black line) along with estimates of JERS-1 SAR-derived wetland and
 1088 flooded area for high-water (dashed blue line) and low-water (solid blue line) seasons. Also
 1089 shown are the Global Surface Water (GSW, Pekel et al., 2016) permanent surface water extent
 1090 (green line, GSW permanent) and the total (permanent plus transitory) surface water extent at
 1091 maximum (red line, GSW Total). (c) Map of maximum surface water extent at regional scale
 1092 (boxes in (a) indicate the locations) from GIEMS-D15 (Fluet-Chouinard et al., 2015) and
 1093 SWAF-HR (Parrens et al., 2019).

1094

1095 Synthetic aperture radars are active radar instruments that measure the backscatter of the
 1096 observed surface at an angle of incidence (off-nadir), regardless of cloud cover, and allow
 1097 delineation of open surface waters and inundated area with vegetation with a typical spatial
 1098 resolution of 10-100 m (Behnamian et al., 2017; Hess et al., 1990; Kasischke et al., 1997) The
 1099 Spaceborne Imaging Radar-C (SIR-C) experiment provided high quality, multi-band and multi-
 1100 polarization data for the Amazon that led to the development of new approaches using SAR.
 1101 Alsdorf et al. (2000) demonstrated the ability of interferometric analyses to detect centimeter-
 1102 scale variations in slope across the Amazon rivers and floodplains (see Section 4.1). Hess et al.
 1103 (1995) developed algorithms to detect inundation and vegetation within Amazon wetlands that
 1104 benefitted from modeling of interactions between vegetation and radar, including the double-
 1105 bounce effect, also done as part of SIR-C (Y. Wang et al., 1995). Understanding derived from
 1106 this led to use of data provided by the Japan Earth Resources Satellite-1 (JERS-1) to produce the
 1107 first high-resolution wetland map for the central Amazon region under low-water and high-water
 1108 conditions at 100-m resolution (Hess et al., 2003). These results were validated with airborne,
 1109 high-resolution, videography transects throughout the imaged area (Hess et al., 2003). Hess et
 1110 al., (2003) found that 17% of the 1.77 million km² study area is occupied by wetlands, of which
 1111 96% are inundated at high water and 26% at low water. Flooded forests accounted for nearly
 1112 70% of the overall wetland area, but proportions of the wetland habitats showed large regional
 1113 variations related to floodplain geomorphology. Those new estimates of large inundated area
 1114 were of major importance to understand the outgassing of methane and carbon dioxide from
 1115 Amazon flooded areas (see Section 6.3).

1116 The JERS-1 SAR estimates were extended to the entire wetlands of the lowland AB
 1117 (region < 500 m asl) (**Figure 6a**; Hess et al., 2015), currently one of the standards for comparison
 1118 with other satellite-derived products. It estimates flooded extent (**Figure 6b**) to be of $\sim 2.85 \times 10^5$
 1119 km² for low water season (Oct-Nov 1995) and of $\sim 6.34 \times 10^5$ km² for high water season (May-July
 1120 1996). An interesting comparison is one made for the central corridor of the AB (Prigent et al.,
 1121 2007) between GIEMS and the 100 m resolution L-band JERS-1 SAR mosaic of Hess et al.
 1122 (2003) for low water (September-October 1995) and high water (May-June 1996). For both
 1123 seasons, the spatial structures are similar but estimates of the surface water extent observed by
 1124 SAR (118,000 km² for the low water season, 243,000 km² for the high water season) are larger
 1125 than the area estimated by GIEMS (105,000 km² for the low water season, 171,000 km² for the
 1126 high water season). Thanks to its better spatial resolution, the SAR estimates are capable to
 1127 discriminate smaller water bodies than GIEMS (typically water bodies smaller than 80 km² i.e,
 1128 10% of a GIEMS pixel), especially for the low water season. For the entire AB, the basin-wide
 1129 estimates from GIEMS do not match the basin-wide SAR (**Figure 6a** and **b**) as reported in Hess
 1130 et al. (2015) which suggested that global datasets derived from lower-resolution sensors or
 1131 optical sensors capture less than 25% of the wetland area mapped by the SAR.

1132 The use of multi-temporal SAR coverage, such as the ScanSAR mode of
 1133 ALOS/PALSAR, provide variations of flood extent at the scale of floodplain units, e.g., Curuai
 1134 floodplain along lower Amazon River (Arnesen et al., 2013), Mamiraua floodplain (Ferreira-
 1135 Ferreira et al., 2015) or inundation patterns in central Amazon (Pinel et al., 2019; Resende et al.,
 1136 2019). Rosenqvist et al. (2020) generated annual maximum and minimum inundation extent
 1137 maps over the AB using ALOS-2/PALSAR-2 ScanSAR, in line with previous inundation maps

1138 by L-band JERS-1 and ALOS/PALSAR radar classifications of the inundation (Chapman et al.,
1139 2015). At the regional scale, Bourrel et al. (2009) mapped the floods in the Bolivian Amazon
1140 from SAR C-Band microwave data of RADARSAT and ERS-2. Over the same region, the
1141 surface water dynamics of the Bolivian Amazon wetlands (Ovando et al., 2018), as well as the
1142 characterization of extreme flood events (Ovando et al., 2016) were investigated by combining
1143 ALOS/PALSAR SAR observations with MODIS multi-temporal flood maps and altimetry-
1144 derived water level variations (ENVISAT & SARAL). Other SAR satellite missions, such as the
1145 Copernicus Sentinel-1 SAR (launched in 2014), which offer a global revisit of 6-12 days, have
1146 not been yet fully exploited in the AB but offers new opportunities for mapping the spatial and
1147 temporal variations of surface waters at a fine scale in tropical environments. The near-future
1148 launch of SAR satellites, such as NISAR and SWOT (Prigent et al., 2016), will offer new
1149 opportunities to monitor Amazon surface water with dedicated sensors.

1150 Optical and infrared imagery observations (e.g., Landsat, SPOT, QuickBird, Ikonos,
1151 AVHRR, MODIS, Sentinel 2A/B) offer high spatial and temporal resolutions (~1-500 m, sub-
1152 daily to weekly) but in tropical environments they are generally limited by the inability to
1153 penetrate clouds and dense vegetation. Therefore, assembling cloud-free coverage during the
1154 rising flood season of the central AB remains challenging (Asner, 2001; Hess et al., 2015; Klein
1155 et al., 2015). Nevertheless, classification of optical imagery using water indexes and related
1156 methods, as reviewed by Huang et al. (2018), enables to estimate flood frequency based on
1157 temporal maps of surface water cover, and despite the limitations from vegetation canopy and
1158 cloud cover, this type of data can be of value to monitor open surface water. Several studies
1159 (**Table 4**) based on Landsat observations created global databases of the area of rivers (Global
1160 River Widths from Landsat -GRWL; Allen & Pavelsky, 2018) and surface water (Pekel et al.,
1161 2016; Yamazaki et al., 2015) which can be used at the AB scale. Based on the decadal-scale
1162 monitoring of Landsat missions, the Global Surface Water dataset (GSW, Pekel et al., 2016) uses
1163 three million images over 32 years (from 1984 to 2015) at a 30 m spatial resolution to derive a
1164 monthly record of water presence in classifying each Landsat pixel as open water, land, or non-
1165 valid observation using an expert system. In the AB, GSW estimates of surface water extent
1166 (permanent and total as the sum of permanent and transitory water bodies) are lower than the
1167 estimates from other RS-based technique such as SAR or GIEMS (**Figure 6b**) and comparison of
1168 GSW with GIEMS-D3 (see further below) found seasonal water bodies in savannas and forest
1169 floodplains were not detected properly (Filipe Aires et al., 2018). C. M. Souza et al. (2019)
1170 developed another Landsat classification to estimate long-term changes in Amazon surface
1171 waters revealing the recent increase in areas associated to hydropower lakes. Recent satellite
1172 missions such as Sentinel 2A/B (since 2015, with 10 m spatial resolution at 5–10-day intervals,
1173 Pham-Duc et al., 2020) or programs such as the RapidEye (since 2008, 5 m spatial resolution and
1174 a temporal resolution of 1–5.5 days, Garousi-Nejad et al., 2019) or the PlanetScope (CubeSats,
1175 since 2014, with 3–5 m spatial resolution and daily revisit time; Cooley et al., 2019)
1176 constellations might bring new opportunities to study fine scale surface water extent of the
1177 Amazon.

1178 In order to take advantage of the complementary strengths of various observations, for
1179 instance the low resolution but long term estimates of passive microwave versus the high
1180 resolution but limited in time observations from SAR, a downscaling methodology combining
1181 both estimates has been developed to retrieve monthly central Amazon at ~500 m spatial for the
1182 1993-2007 period (Filipe Aires et al., 2013). Several other studies based on downscaling

1183 approaches using a floodability index provide high resolution maps of surface water extent over
 1184 the Amazon, such as GIEMS-D15 (Fluet-Chouinard et al., 2015; ~500 m spatial resolution and
 1185 its 1-km adaptation as in Reis et al., 2019) and GIEMS-D3 (Aires et al., 2017, 90m). Similarly,
 1186 Parrens et al. (2019) proposed a downscaling methodology based on multi-source RS data
 1187 (SMOS SWAF; combined with a global DEM and GSW dataset) to map Amazon inland water
 1188 under vegetation at ~1 km spatial resolution every 3 days for the 2010–2016 (named SWAF-
 1189 HR). **Figure 6c** shows maps of maximum surface water extent from GIEMS-D15 and SWAF-
 1190 HR for three regions, including interfluvial wetlands. Such observations are valuable to wetland
 1191 conservation decisions, as the timing and duration of inundation often determine ecological
 1192 characteristics and the provision of ecosystem services. For instance, Reis et al. (2019) classified
 1193 Amazon wetlands according to the timing and duration (months per year) of inundation detected
 1194 with GIEMS-D15, and their link to precipitation regimes. It revealed that permanently inundated
 1195 wetlands account for the largest area and are mainly floodplains located in the lowlands of the
 1196 catchment. Seasonally inundated wetlands varied in the duration of inundation reflecting
 1197 different rainfall and hydrological regimes. These regional differences in inundation
 1198 characteristics are important to conservation planning and wetland management especially in the
 1199 context of anthropogenic interventions such as dams and waterway construction.

1200 Finally, new RS techniques and methodologies are continuing to be developed and can
 1201 help monitor the surface water extent of the AB. The potential for Global Navigation Satellite
 1202 System-Reflectometry (GNSS-R) has been explored (Chew & Small, 2020; Jensen et al., 2018;
 1203 Rodriguez-Alvarez et al., 2019) using Cyclone GNSS (CYGNSS) constellation of GNSS-R
 1204 satellites and a simple forward model that demonstrate how surface reflectivity measured by
 1205 CYGNSS can capture flooding dynamic over the region.

1206 In Section 5.1 “Methods for Measuring Area” of Alsdorf et al. (2007), the authors
 1207 suggested that *“Perhaps the best opportunity in the next few years for routine measurements of*
 1208 *inundated area will result from the Japan Aerospace Exploration Agency’s ALOS mission”*.
 1209 More than a decade later, it is worth noting that the extent and variability of surface water of the
 1210 Amazon are still one of the most studied variables of the hydrological cycle, but that studies
 1211 using ALOS observations remain recent and limited. Further studies and new observations are
 1212 required to fully characterize Amazon surface water extent and the processes that drive the
 1213 patterns and dynamic. In particular, polarimetric and interferometric L-band SAR data from the
 1214 forthcoming NASA/ISRO L-band SAR mission and the Ka-band Radar Interferometer (KaRIn)
 1215 swath observations from the forthcoming SWOT mission will be capable of enhanced
 1216 monitoring and comprehensive survey of large-scale surface water extent and dynamics of the
 1217 AB.

1218

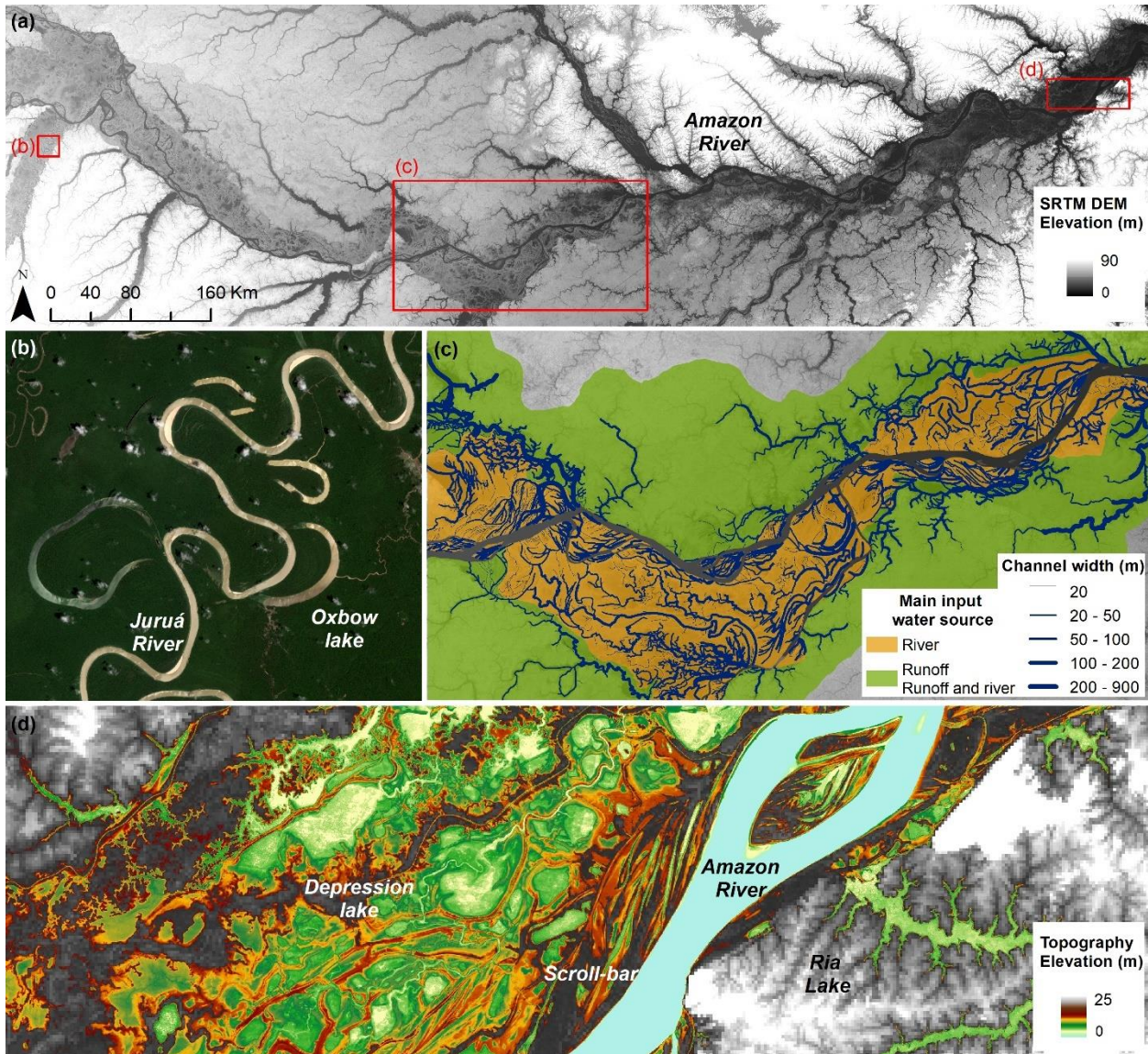
1219 **4.3. Floodplain and river channels topography**

1220 Along the Amazon River, the floodplain has many lakes and channels that vary in extent,
 1221 depth, and connectivity (Hess et al., 2015; Rudorff et al., 2014b; Trigg et al., 2012). This
 1222 complex topography affects the water flow through river-floodplain water exchanges, which in
 1223 turn, are important for carbon, nutrients, and sediment fluxes (Melack et al., 2009). Accurate
 1224 topographic information is essential for the characterization of the surface water in the
 1225 floodplain, particularly for hydraulic numerical modeling (Baugh et al., 2013; Paiva, Buarque, et

1226 al., 2013; Rudorff et al., 2014a). Furthermore, topographic mapping is required for understanding
1227 the morphology and morphodynamics of the river channels and lakes. The SRTM DEM is a
1228 global topographic dataset generated from C-band interferometry (Farr et al., 2007) and has been
1229 widely used in hydraulic simulations and geomorphic characterization of the Amazon
1230 floodplains (**Figure 7a**). However, the data are affected by vegetation cover, and has errors such
1231 as absolute bias, speckle noise (granular aspect in the image due to the random presence of pixels
1232 with extreme values), and stripe noise (Rodríguez et al., 2006). It is also not capable of
1233 describing bathymetry of inland water bodies as it observed surface water elevation only once.

1234 The application of topographic data, such as SRTM DEM, together with radar (e.g.,
1235 RADAM, JERS-1) and optical (e.g., Landsat) images allowed the geomorphological
1236 characterization of floodplains and river channels of the AB. Sippel et al. (1992) described lakes
1237 of different shapes based on RADAM maps along different sections of the main stem
1238 Solimoes/Amazonas rivers and their major tributaries. Latrubesse & Franzinelli (2002) and
1239 Mertes et al. (1996), described geomorphologically distinct regions along the upper and middle
1240 reach of the Amazon River. Scroll-bar topography, which forms long and narrow lakes, and
1241 oxbow lakes, located in abandoned river meanders, are dominant in the upstream reaches
1242 (Mertes et al., 1996; **Figure 7**). Downstream reaches are characterized by large, shallow lakes
1243 formed by the overbank deposition of fine sediments in a very flat floodplain topography
1244 (Latrubesse & Franzinelli, 2002; Mertes et al., 1996; **Figure 7**). Active deposition of sediments
1245 across the floodplains was also identified and described by Lewin et al. (2017) using RS data.
1246 Constantine et al. (2014), Peixoto et al. (2009) and Rozo et al. (2012) characterized the channel's
1247 migration of rivers and floodplains. Sediment supplies play an important role in the evolution of
1248 Amazonian rivers, as the rivers with high sediment loads experience faster meander migration
1249 and higher cutoff rates than rivers with lower sediment loads (Constantine et al., 2014). Large
1250 and rapid geomorphological changes can also arise due to anthropogenic pressures such as
1251 livestock and channel irrigation. These may be the causes of the progressive erosion of a channel
1252 along the lower Amazon River that captured almost all discharge from the lower Araguari River,
1253 which previously had flowed directly to the Atlantic Ocean (E. S. dos Santos et al., 2018;
1254 described in more details in Section 6.4).

1255



1256

1257 **Figure 7.** (a) SRTM DEM in central Amazon. (b) Oxbow lakes in Juruá River (Sentinel-2,
 1258 October of 2020). (c) Channel width in the floodplain (Adapted from Trigg et al., 2012). (d)
 1259 Topography elevation of the floodplain channels and lakes (Adapted from Fassoni-Andrade,
 1260 Paiva, Rudorff, et al., 2020).

1261

1262 In order to improve the applicability of SRTM data to hydraulic modeling of the AB,
 1263 various techniques were developed such as the removal of the vegetation height (Baugh et al.,
 1264 2013; O’Loughlin et al., 2016; Paiva, Buarque, et al., 2013; Paiva, Collischonn, et al., 2011;
 1265 Pinel et al., 2015; Rudorff et al., 2014a; Yamazaki et al., 2017), the interferometric bias (Pinel et
 1266 al., 2015; Rudorff et al., 2014a), as well as smoothing as pit removal (Yamazaki, Baugh, et al.,
 1267 2012). Despite the better topographic representation achieved by these methods, topographic
 1268 information below the water surface cannot be recovered from SRTM. Also, SRTM dataset
 1269 relies on one only overpass in February 2000. Therefore, some processes, such as infilling and

1270 drainage of the floodplain, may not be well represented in the numerical models. River
1271 bathymetry is also key information that is not systematically resolved. Recently Brêda et al.
1272 (2019) demonstrated the potential of assimilating satellite altimetry data into hydraulic models
1273 for its estimation. To estimate the topography in seasonally flooded areas, Bonnet et al. (2008)
1274 combined SWE with flood extents derived from JERS-1 images to estimate a bathymetric DEM
1275 of the Curuai floodplain. Park et al. (2020) related water depth and a flood frequency map,
1276 derived from surface water mapping, to infer the Curuai bathymetry. Fassoni-Andrade, Paiva,
1277 Rudorff, et al. (2020) developed and applied a systematic method to estimate floodplain
1278 topography using a combination of flood frequency maps derived from optical RS and ancillary
1279 in situ water level data archives (**Figure 7d**). This was the first systematic and extensive mapping
1280 of a seasonally flooded area in a wetland, showing floodplain depths less than 5 m (15 m) in low
1281 (high) water, and that active storage volume in the open-water floodplain varies 104.3 km^3 on
1282 average each year. This dataset was complemented over permanently flooded regions by a
1283 compilation of digitized nautical charts from the Brazilian Navy. Recently, Fassoni-Andrade et
1284 al. (2021) applied this methodology to the Amazon estuary showing the morphology of the
1285 intertidal floodplain.

1286 The bathymetric information in permanently flooded areas relies on in situ field surveys.
1287 Among the studies cited here, only a few obtained in situ bathymetric information (Bonnet et al.,
1288 2008; Fricke et al., 2019; Pinel et al., 2015). Additional studies with detailed bathymetry include
1289 Lesack & Melack (1995), Barbosa et al. (2006), Panosso et al. (1995), and Trigg et al. (2012). As
1290 part of the first hydrological budget of an Amazon floodplain lake, Lesack & Melack (1995)
1291 surveyed the lake's bathymetry, which was subsequently used in the hydrological model of Ji et
1292 al. (2019). Panosso et al. (1995) conducted a bathymetric survey of Lake Batata, located near the
1293 confluence of the Trombetas River and the Amazon River. This lake received tailings from
1294 bauxite processing and the estimate was used for conservation and recovery studies. Barbosa et
1295 al. (2006) conducted an extensive bathymetric survey of the Lake Grande do Curuai floodplain,
1296 in the eastern AB. The bathymetry was used to estimate volume, in hydraulic simulation
1297 (Rudorff et al., 2014a) and topographic assessment (Fassoni-Andrade, Paiva, & Fleischmann,
1298 2020). Trigg et al. (2012) illustrated the first systematic characterization of floodplain channels
1299 in central Amazon based on Landsat imagery and field survey (**Figure 7c**). Floodplain channel
1300 widths vary considerably (10–1000 m), and channel depths are related to the local amplitude of
1301 the Amazon river flood wave (~10 m), and deeper when subject to local runoff.

1302 Many advances have been made to characterize the topography of rivers and floodplains
1303 using RS techniques, among the promising prospects for new DEMs (eg.. The L-band reduces
1304 the systematic positive bias of vegetation due to its ability of penetrating the canopy. Images
1305 from the NISAR mission, a bi-band SAR satellite to be launched in 2022 with global coverage
1306 and revisiting periods of 12 days will improve the availability of L-band radar data. The SWOT
1307 mission will simultaneously measure the SWE and water extent, opening up new opportunities to
1308 create and improve new techniques. New unexplored data from ICESat-2 satellite (launched in
1309 2018) could be useful for topography estimation and validation.

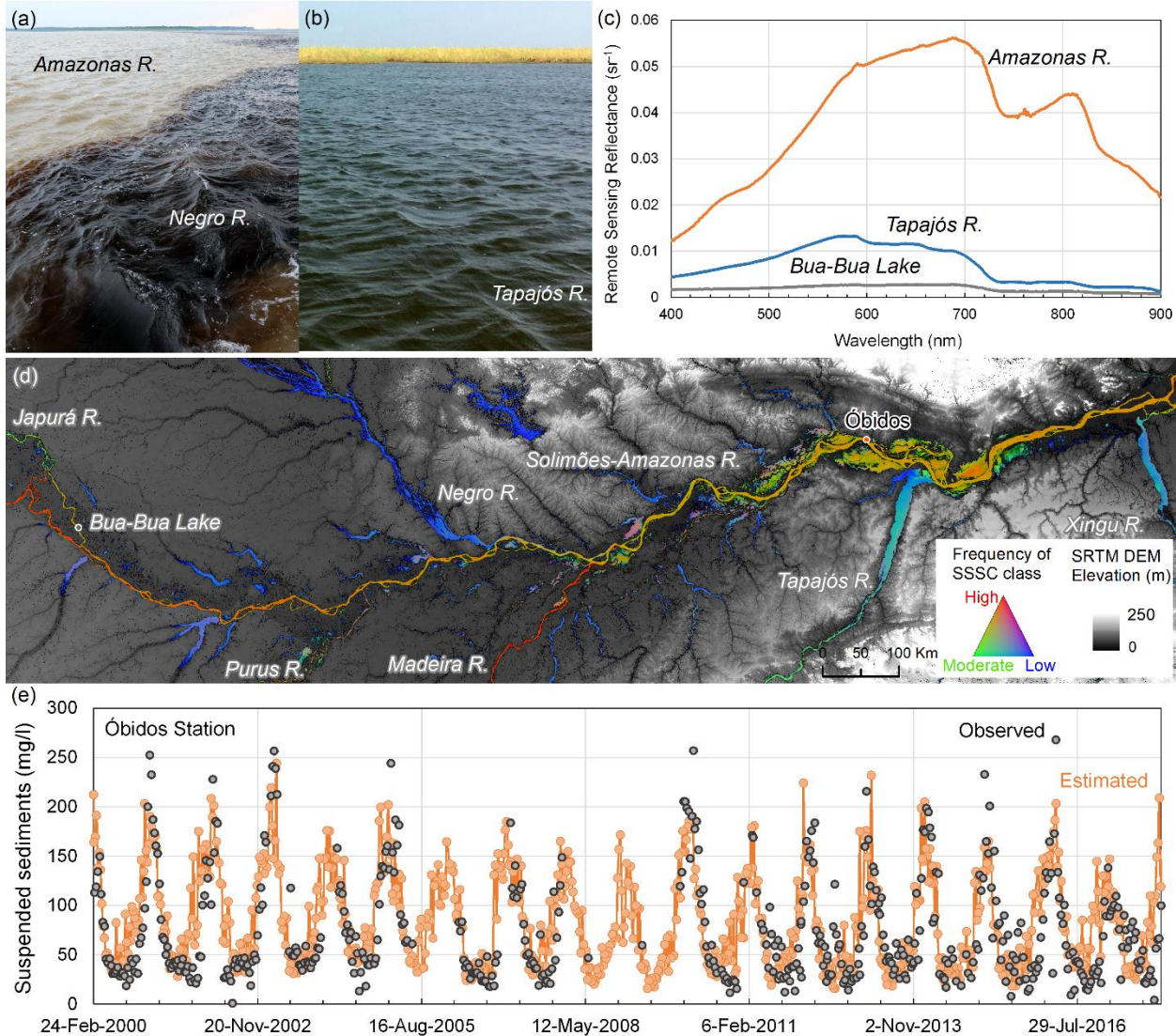
1310

1311 **4.4. Water quality: Sediments, chlorophyll and colored dissolved organic matter**

1312 According to their physical and chemical water characteristics, rivers of the AB are
1313 classified into three types: white, black, and clear-waters rivers (Junk et al., 2011; Sioli, 1956).
1314 Nutrient-rich whitewater rivers, such as Madeira and Solimões rivers, which account for 98% of
1315 Amazon River's sediment discharge to the Atlantic Ocean are dominated by inorganic sediments
1316 mainly originated from the Andes (Almeida et al., 2015; Meade, 1994). Blackwater rivers (e.g.
1317 Negro River; **Figure 8a**) are rich in dissolved organic matter derived from podzolic soils (Bouchez
1318 et al., 2011). Clear-water rivers (e.g. Tapajós River; **Figure 8b**) are characterized by nutrient-
1319 poor, low sediment, and dissolved organic matter concentration (Junk et al., 2015). The water-type
1320 diversity and the pathways throughout the Amazon floodplain have significant implications for
1321 floodplain lakes and contribute to their high biodiversity (Junk et al., 2011; Thom et al., 2020).

1322 A feasible way to monitor the aquatic system's biogeochemical properties and water paths
1323 between the rivers and floodplain lakes is through satellite RS. The interaction between
1324 electromagnetic radiation and water bodies, described by radiative transfer theory (Kirk, 2010;
1325 Mobley, 1994), allows the development and calibration of algorithms for estimating optically
1326 active constituents (OACs: Total Suspended Sediments -TSS; Phytoplankton pigments such as
1327 Chlorophyll-a - Chl-a - and Phycocyanin; and Colored Dissolved Organic Matter – CDOM) in the
1328 water bodies. These OACs influence the underwater light field and, therefore, the inherent (e.g.,
1329 absorption and backscattering coefficient) and apparent optical properties (e.g., Remote Sensing
1330 Reflectance – R_{rs}) of the water bodies.

1331



1332

1333 **Figure 8.** a) Examples of white and black, and b) clear waters. c) Examples of spectra of three
 1334 water types (Source: Labisa; <http://www.dpi.inpe.br/labisa/>): white water - Amazon River (TSS
 1335 of 288.5 mg L⁻¹; Chl-a of 2.0 µg L⁻¹; aCDOM in 440 nm of 1.3 m⁻¹); clear water - Tapajós River
 1336 (TSS 5.7 mg L⁻¹; Chl-a of 10.8 µg L⁻¹; aCDOM in 440 nm of 1.2 m⁻¹); black water - Bua-Bua
 1337 Lake (TSS 7.4 mg L⁻¹; Chl-a of 3.6 µg L⁻¹; aCDOM in 440 nm of 2.9 m⁻¹). d) Spatial variability
 1338 of suspended sediments in the central Amazon (Adapted from Fassoni-Andrade & Paiva, 2019).
 1339 e) Suspended sediment time-series in situ (observed) and satellite-based MODIS (estimated)
 1340 obtained from the HYBAM monitoring system (<http://hidrosat.ana.gov.br>).

1341

1342 There are significant challenges applying RS to monitoring of AB aquatic ecosystems: i)
 1343 frequent cloud cover makes it difficult to acquire images; ii) the optical complexity of the waters
 1344 that flow throughout the AB, characterized by high variability in the concentration of the OACs;
 1345 iii) the lack of sensors with high radiometric, spectral, spatial resolution and signal-to-noise ratio
 1346 to detect the small changes in upwelling radiance from the water column; and iv) the difficulty of

1347 using RS in narrow rivers and small lakes. These challenges have existed since the beginning of
1348 RS applications to study of Amazonian aquatic ecosystems in the early 1980s, that focused on
1349 calibration/validation of algorithms based on in situ data. These methods were based mostly on
1350 empirical approaches (Bayley & Moreira, 1978; Bradley, 1980; Mertes et al., 1993), with
1351 acceptable accuracy limited in time and space to the dataset for which the algorithm was developed
1352 (M. W. Matthews, 2011; Odermatt et al., 2012). In the last decade, efforts have been made to adapt
1353 ocean color protocols (Mueller et al., 2003) to acquire inherent optical properties (IOPs) of the
1354 Amazonian waters (L. A. S. de Carvalho et al., 2015; M. P. F. Costa et al., 2013; Jorge et al., 2017;
1355 Maciel, Barbosa, et al., 2020; Pinet et al., 2017; Valerio et al., 2018), allowing for the development
1356 of semi-analytical algorithms (SAA). As the apparent optical properties (AOPs) are proportional
1357 to the IOPs, SAA uses an inversion process based on radiative transfer theory to obtain IOPs from
1358 the AOPs. Once the IOPs are known, they are used to retrieve the OAC concentrations. Therefore,
1359 SAA algorithms better identify each constituent contribution, providing more comprehensive
1360 temporal and spatial coverage (Dekker, 1993; Novoa et al., 2017).

1361 The flourishing of satellite RS in the second decade of the 21st century is due to two crucial
1362 technological advances. First, a new generation of sensors was better designed to study complex
1363 aquatic environments, with improved spectral and radiometric resolution (Landsat-8, Sentinel-2,
1364 CBERS-04A). Second, the unprecedented increase in computing performance and data storage has
1365 improved image processing capability. However, the low radiometric resolution provided by
1366 sensors onboard earlier Landsat (Landsat-5 and Landsat-7) satellites has not prevented the
1367 development of studies taking advantage of the substantial temporal database available (1972 to
1368 now) as reported in Lobo et al. (2015) and Montanher et al. (2018).

1369 In preparation for new sensors, studies of spectral behavior of Amazon water types among
1370 a wide range of OAC concentrations have been done (C. C. F. Barbosa, 2005; Nobrega, 2002;
1371 Rudorff, 2006). Those spectra were organized into a spectral library linked to OACs data to create
1372 reference spectra for water types classification (Lobo et al., 2012). The spectral library is an input
1373 to a Spectral Angle Mapper algorithm for deriving water type maps from Hyperion and Medium
1374 Resolution Imaging Spectrometer (MERIS) images acquired simultaneously with field campaigns,
1375 with reasonable accuracies (48% and 67% for Hyperion and MERIS respectively). This updated
1376 library was applied to classify Brazilian water types (E. F. F. da Silva et al., 2020). In proof of
1377 concept studies, MODIS images from AQUA and TERRA satellites were successfully used for
1378 estimating Chl-a (Novo et al., 2006) and TSS (Espinoza-Villar et al., 2018; Fassoni-Andrade &
1379 Paiva, 2019; Marinho et al., 2018; J. M. Martinez et al., 2009) in Amazonian water bodies with a
1380 size compatible with the spatial resolution of the sensors.

1381 Chl-a estimation, a proxy for phytoplankton abundance, remains challenging in the
1382 Amazon floodplain lakes due to high TSS masking chl-a spectral features (Z.-P. Lee et al., 2016)
1383 at some times (C. C. F. Barbosa et al., 2009, 2015; Bourgoin et al., 2007; R. D. Ferreira et al.,
1384 2013; Maciel et al., 2019). A spectral mixture algorithm can overcome this problem in some cases
1385 (Novo et al., 2006; Rudorff et al., 2006). Highest chlorophyll concentrations were observed in low
1386 water periods (November and December) in the middle reach of the Amazon floodplain, as a result
1387 of lakes enriched by dissolved nutrients in less turbid waters (Novo et al., 2006). However, the
1388 empirical nature of those algorithms prevents their wide application. Therefore, new approaches
1389 have been investigated, including the use of semi-analytical algorithms (Flores Júnior, 2019).
1390 CDOM retrieval based on satellite imagery is scarce in Amazon lakes since the isolation of CDOM

1391 signature from the water leaving signal is complex in turbid waters (Kutser et al., 2016). M. P. da
 1392 Silva et al. (2019) proposed an empirical algorithm for estimating CDOM absorption at 440nm
 1393 from Sentinel-2/MSI images. **Table 5** presents a summary of these studies.

1394 There are many studies on sediment retrieval from satellite data. These studies are mainly
 1395 focused on TSS estimates for rivers (Bernini et al., 2019; Espinoza-Villar et al., 2018; Kilham &
 1396 Roberts, 2011; Lobo et al., 2015; Maciel et al., 2019; Maciel, Novo, et al., 2020; Montanher et al.,
 1397 2014; Park & Latrubesse, 2014; Villar et al., 2013; Yopez et al., 2018) rather than for Amazon
 1398 floodplain lakes (Alcântara et al., 2009; Fassoni-Andrade & Paiva, 2019; Maciel et al., 2019;
 1399 Rudorff et al., 2006, 2007). Most of them are based on empirical algorithms, and only recently,
 1400 some semi-analytical algorithms became available (**Table 5**). The HYBAM observatory provides
 1401 an example of systematically derived TSS concentration using empirical algorithms from MODIS
 1402 at 16 stations (TSS time-series; <http://hidrosat.ana.gov.br>) in the main sediment-contributing
 1403 rivers, including Amazon-Andean rivers in Peru and Bolivia (Espinoza-Villar et al., 2018; R.
 1404 Espinoza Villar et al., 2012; J. M. Martinez et al., 2009; Villar et al., 2013). **Figure 8e** is an
 1405 example of a suspended sediment time-series obtained from the HYBAM monitoring system in
 1406 Amazon River between 1999 and 2017 and illustrates substantial variability of TSS concentration,
 1407 ranging from 25 up to 250 mg L⁻¹.

1408 Montanher et al. (2014) mapped TSS in five Amazonian rivers using multiple regression
 1409 and observed that regional-calibrated algorithms performed better than global algorithms due to
 1410 changes in optical properties of rivers. Park & Latrubesse (2014) also observed that calibrating a
 1411 separate empirical algorithm for low and high-water seasons provided better results for the
 1412 Amazonian river waters. High variability in the OACs in floodplain lakes makes algorithm
 1413 parametrizations difficult. For example, in the Curuai floodplain (lower reach of the AB), TSS
 1414 concentrations can vary from ~5 mg L⁻¹ in the high-water season up to 1000 mg L⁻¹ in the low
 1415 water season due to sediment resuspension by winds. Despite those issues, recent work provide
 1416 successful TSS estimates in the floodplains of the lower Amazon River (Maciel et al., 2019;
 1417 Maciel, Novo, et al., 2020).

1418 TSS trends have been documented in the Amazon River (J. M. Martinez et al., 2009;
 1419 Montanher et al., 2018) and the Madeira River (Latrubesse et al., 2017; Li et al., 2020) that
 1420 might be related to dam construction (see Section 6.4 for details). RS data in AB were also used
 1421 to evaluate siltation impacts caused by artisanal gold mining in the Tapajós River basin (Lobo et
 1422 al., 2015, 2016; see Section 6.4 for details). Furthermore, Fassoni-Andrade & Paiva (2019)
 1423 mapped for the first time the spatial-temporal pattern of sediment in clear, white, and black water
 1424 of the Amazon rivers (**Figure 8d**). Despite errors in the empirical model, temporally filtered
 1425 reflectance in red and infrared revealed sediment variations in rivers and lakes. Therefore, it was
 1426 possible to characterize hydrological processes, such as backwater effects, overbank flow, and
 1427 sediment resuspension in lakes. It was observed that depression lakes of the middle reach receive
 1428 sediments-rich water by overbank flow during the flood, and resuspension of sediments occurs in
 1429 the low water period, as previously documented (Bourgoin et al., 2007). In ria lakes, the main
 1430 water source comes from the local basin (surface runoff and local rainfall) with river inflows
 1431 adding sediment during the low water period.

1432

1433 **Table 5.** OACs algorithms for the AB. OAC range refers to the minimum and maximum values;
 1434 Algorithm Type (AT) refers to Empirical (E) or Semi-Analytical (SAA). In algorithm equation

1435 column, f_{phy} refers to phytoplankton fraction from Linear Mixture Model, $R_{rs}(\lambda)$ is the RS
 1436 reflectance, $p(\lambda)$ is water reflectance. R^2 is the coefficient of determination, SE is the Standard
 1437 Error, MSE is the mean square error, %NMSE is the normalized mean squared error, MAPE is
 1438 the Mean Absolute Percentage Error, RMSE is the root mean square error, PE is the percentage
 1439 error. For the equations of statistical metrics, the reader is referred to each reference.

Study Area	Sensor Name	OAC	OAC Range	AT	Algorithm Equation	Validation Statistical Results	Reference
Low Amazon	MODIS Terra	Chl-a	10-120 μgL^{-1}	E	$Chl = 3.9 * e^{0.0175 * f_{phy}}$	$R^2 = 0.76$ SE = 19 μgL^{-1}	(Novo et al., 2006)
Mamirauá Sustainable Development Reserve	Sentinel-2	CDOM	~1 – 6 m^{-1}	E	$a_{cdom}(440) = 4.39 \frac{B2}{B3} + 0.59 \frac{B6}{B5} - 6.67$	$R^2 = 0.75$ MSE = 0.53 m^{-1} %NMSE = 15.12%	(M. P. da Silva et al., 2019)
Curuai Lake	Sentinel-2 and Landsat-8	TSS and TSI	7-43.5 mgL^{-1} (TSS) 3.4-33.8 mgL^{-1} (TSI)	E	$\ln(TSS_{OLI}) = 9.656 + 1.672 * \ln(R_{rs}(550))$ $\ln(TSI_{OLI}) = 10.73 + 2.08 * \ln(R_{rs}(550))$ $\ln(TSS_{MSI}) = 8.318 + 1.336 * \ln(R_{rs}(550))$ $\ln(TSI_{MSI}) = 8.447 + 1.511 * \ln(R_{rs}(550))$	$R^2 = 0.71$, MAPE = 16.81%, RMSE = 3.54 $R^2 = 0.86$, MAPE = 18.08, RMSE = 1.97 $R^2 = 0.69$, MAPE = 16.67, RMSE = 3.58 $R^2 = 0.81$, MAPE = 18.62, RMSE = 3.1	(Maciel et al., 2019)
Curuai Lake	WFI CBERS-4	TSS	9-28 mgL^{-1}	SAA	$TSS = \frac{293.930 * p550}{1 - p/0.345} + 1.341$	$R^2 = 0.75$ MAPE = 27.08% RMSE = 5.73 mgL^{-1}	(Maciel et al., 2019)
Tapajós River	Landsat-5/TM LISS-III	TSS	~0 – 120 mgL^{-1}	E	$p_{surf(Red)} = 2.64 * (TSS - 2.27)^{0.45}$	$R^2 = 0.94$ RMSE = 1.39 mgL^{-1}	(Lobo et al., 2015)
Solimões River	MODIS	TSS	50-700 mgL^{-1}	E	$TSS = 759.12 * \left(\frac{p_{nir}}{p_{red}}\right)^{1.92}$	$r = 0.89$ RMSE = 70.23 mgL^{-1}	(Villar et al., 2018)
Orinoco River	Landsat-8	TSS	~25-210 mgL^{-1}	E	$TSS = 1.35512 * p_{nir} * 1000 - 2.9385$	$R^2 = 0.94$ MAPE = 19.8% RMSE = 12.8 mgL^{-1}	(Yepez et al., 2018)
Madeira River	MODIS	TSS	25-622 mgL^{-1}	E	$TSS = 1020 * \left(\frac{p_{nir}}{p_{red}}\right)^{2.94}$	$r = 0.79$	(Villar et al., 2013)
Amazon River	MODIS	TSS	7-130 mgL^{-1}	E	TSS Fraction from spectral unmixing model	RE = 10 mgL^{-1} (estimated)	(Kilham & Roberts, 2011)
Amazon White water rivers	Landsat-5	TSS	0-3561 mgL^{-1}	E	Multiple regression	$R^2 = 0.76$	(Montanher et al., 2014)
Madeira River	TriOS Ramses (In situ)	TSS	0-450 mgL^{-1}	SAA	Relationship between <i>backscattering coefficient</i> at 550nm and TSS	$R^2 = 0.7345$	(Bernini et al., 2019)
Amazon white water rivers	TriOS Ramses (In situ)	TSS	5-620 mgL^{-1}	E	$TSS = 20.41 * (p_{860})^{1.173}$	$R^2 = 0.89$	(J. Martinez et al., 2015)
Amazon rivers and lakes	MODIS Terra and Aqua	TSS	0-600 mgL^{-1}	E	$TSS = \exp^{20 * p_{red} + 7.68 * p_{nir} + 0.31 * \frac{p_{red}}{p_{nir}}}$	$R^2 = 0.7$ RMSE = 75.6 mgL^{-1}	(Fassoni-Andrade & Paiva, 2019)

1440

1441 One of the main challenges regarding water color RS is identifying and separating each
 1442 constituent contribution from the water column emerging signal. The high sediment
 1443 concentrations, which can mask the contributions of Chl-a and CDOM, makes this challenge
 1444 especially significant in Amazonian waters. The semi-analytical approach, which has performed
 1445 well in other complex waters (Gholizadeh et al., 2016; Werdell et al., 2018; Zheng & DiGiacomo,
 1446 2017), is an alternative to overcome this challenge. However, it depends on sensors with spectral,
 1447 radiometric, and spatial characteristics suitable for inland waters for calibrating high-performance
 1448 algorithms. Initial applications of this approach in Amazonian waters, using Landsat-8/OLI,

1449 Sentinel-2/MSI, and Sentinel-3/OLCI data, have shown promising results (Bernini et al., 2019; L.
 1450 A. S. de Carvalho et al., 2015; Jorge et al., 2017; Maciel, Barbosa, et al., 2020). Furthermore,
 1451 hyperspectral sensors missions such as NASA's Plankton, Aerosol, Cloud, ocean Ecosystem
 1452 (PACE; Werdell et al., 2019) and recently launched ones such as PRISMA (Giardino et al., 2020;
 1453 Niroumand-Jadidi et al., 2020) may help to overcome this challenge. Due to the extensive temporal
 1454 variability in the constituent concentration, a promising approach is to integrate hybrid and semi-
 1455 analytical algorithms to obtain adequate accuracy in a wide range of OACs concentration. To cope
 1456 with the frequent cloud coverage and obtain data compatible with aquatic dynamics, the
 1457 concomitant use of inter-calibrated sensors data (Landsat-8/OLI, Sentinel-2/MSI, Sentinel-
 1458 3/OLCI, CBERS-4A/MUX), called the virtual constellation, can be a solution. In this sense, two
 1459 ongoing initiatives are the Brazil Data Cube project
 1460 (<http://brazildatacube.dpi.inpe.br/portal/explore>) and the Harmonized Landsat Sentinel (Claverie
 1461 et al., 2018), which propose to provide intercalibrated data from different sensors. Moreover, to
 1462 investigate dynamic processes in aquatic ecosystems, high spatiotemporal resolution nanosatellites
 1463 represent a promising tool for understanding the short-term responses of floodplain lakes' biota to
 1464 hydrological changes (Maciel, Novo, et al., 2020; Nagel et al., 2020).

1465 All the improvements in RS technologies in the last decades have supported more accurate
 1466 algorithms for suspended sediment retrieval in the AB. However, as demonstrated in **Table 5**, Chl-
 1467 a and CDOM estimates are still a challenge in those optically complex waters. The accurate
 1468 retrieval of Chl-a and CDOM is dependent on precise RS data, which demands the inversion of
 1469 those OACs. In this sense, new sensors with high radiometric and spectral resolution are
 1470 imperative. Finally, more robust techniques, such as semi-analytical algorithms, machine learning
 1471 approaches, and cloud computing platforms (e.g., Google Earth Engine), can improve water
 1472 quality RS studies in the AB.

1473

1474 **5. Total water storage and groundwater storage**

1475 Water mass redistribution is a key parameter needed to understand the climate system
 1476 and its temporal variations at monthly to multi-decadal time-scales. Over land, it corresponds to
 1477 the continuous exchange of water masses between surface (i.e., rivers, lakes, wetlands, snow
 1478 cover, and mountain glaciers) and sub-surface (soil moisture and groundwater) storages, and
 1479 with the atmosphere and the ocean through rainfall, evapotranspiration, and runoff. Total water
 1480 storage is the sum of the water contained in the different hydrological reservoirs. The importance
 1481 of surface water in the AB was presented in Section 4. Groundwater storage also plays a major
 1482 role in the hydrology of the AB and exerts a large influence on climate variability and rainforest
 1483 ecosystems (Pokhrel et al., 2013). Strong memory effects of the Amazon groundwater system
 1484 propagate climate anomalies over the region for several years (Frappart et al., 2019; Miguez-
 1485 Macho & Fan, 2012; Pfeffer et al., 2014).

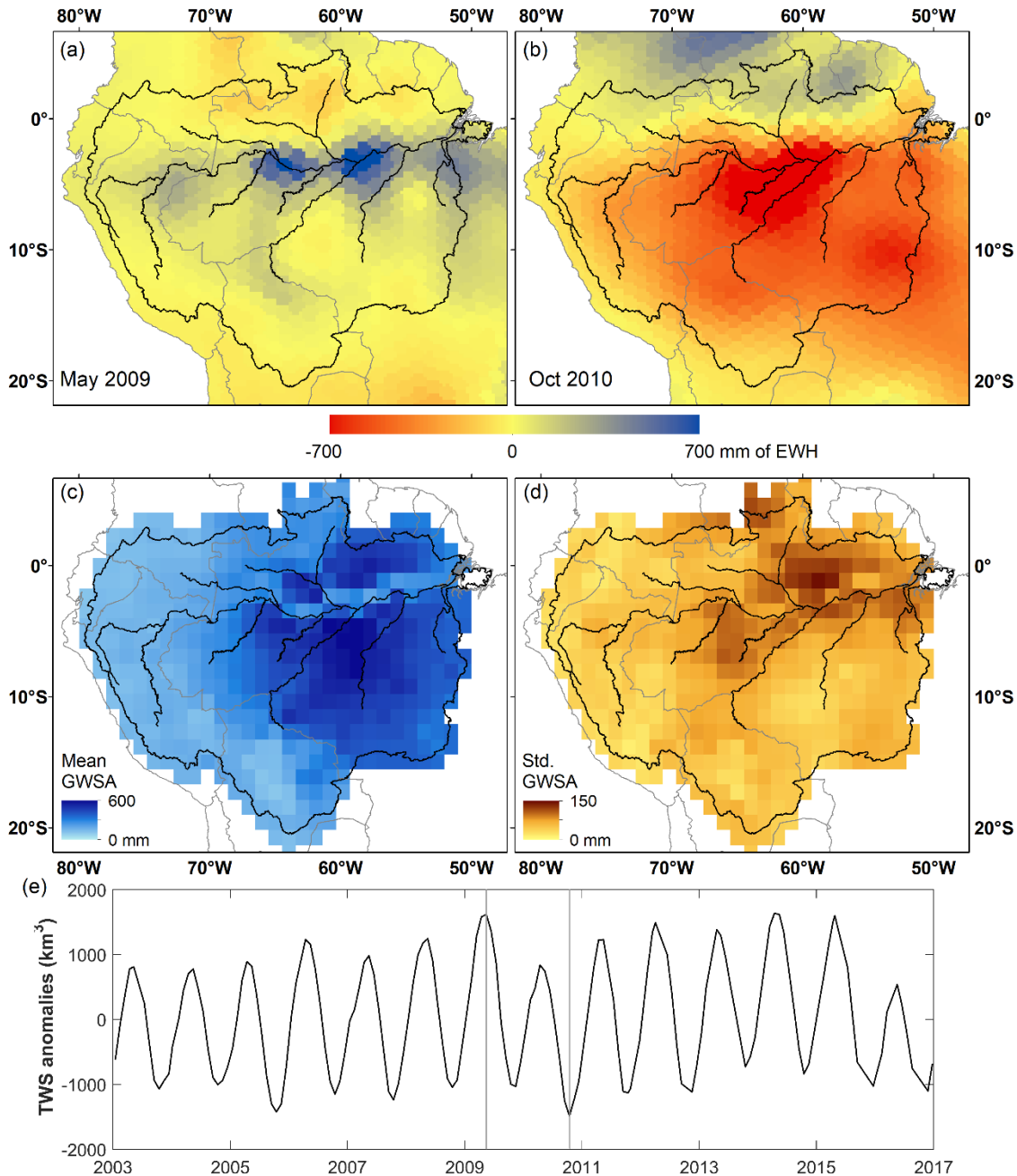
1486 The GRACE mission, in operation from March 2002 to June 2017, and the GRACE
 1487 Follow-On mission (GRACE FO), in orbit since May 2018, enable the monitoring of the spatio-
 1488 temporal changes of Terrestrial Water Storage (TWS) (Tapley et al., 2004). Its temporal anomaly
 1489 is derived from GRACE observations which measure the very small variations in the Earth's
 1490 gravity field (Tapley et al., 2004). GRACE-derived TWS Anomaly (TWSA) observations, in
 1491 spite of their coarse spatial resolution of ~200-300 km, have been widely used to analyze the

1492 impact of climate variability and global changes on the water masses redistribution over land
1493 (Tapley et al., 2019), and groundwater storages in combination with external observations
1494 (Frappart & Ramillien, 2018).

1495 Over the whole AB, GRACE-derived TWS annual amplitude was found to range from
1496 300 to 450 mm (**Figure 9**; J. L. Chen et al., 2009; Crowley et al., 2008; Frappart, Seoane, et al.,
1497 2013; Xavier et al., 2010). This range corresponds to twice the annual amplitude of surface water
1498 storage of the whole basin (Frappart et al., 2012; Ndehedehe & Ferreira, 2020), meaning that the
1499 annual amplitude of the subsurface storage variations (soil moisture and groundwater) also
1500 represents half of the TWS annual amplitude. Large variations of this value were observed
1501 among the major Amazon sub-basins depending on the extent of floodplains (Frappart et al.,
1502 2011, 2019; Papa et al., 2013). Rainfall and GRACE-based TWSA were found to be highly
1503 correlated in the AB and its major sub-basins (over 2003-2010), even at interannual time-scales
1504 with Pearson's correlation coefficients generally higher than 0.7 (except in the basins located in
1505 the Andes) with a time-lag varying from 0 to 3 months (Frappart, Ramillien, et al., 2013;
1506 Ndehedehe & Ferreira, 2020). Similar results were obtained between TWSA and river discharges
1507 over the same time spans (Frappart, Ramillien, et al., 2013). Good agreement was also observed
1508 between TWS and satellite-derived surface water extent (from GIEMS), rainfall, and discharge
1509 over various time-span (Papa et al., 2008; Prigent et al., 2007, 2012; Tourian et al., 2018). These
1510 studies revealed the complexity of water transport among the different sub-basins of the Amazon
1511 with the presence of hysteresis in the relationship between surface water extent and TWSA.

1512 The analysis of the spatio-temporal patterns of TWS changes provided new information
1513 on the impact of the extreme climate events (exceptional droughts and floods which occurred in
1514 2005, 2010, 2012-2015, and 2009, 2012, respectively) on land water storage in the whole AB or
1515 in its major sub-basins (J. L. Chen et al., 2009, 2010; Espinoza et al., 2013; V. G. Ferreira et al.,
1516 2018; Frappart, Ramillien, et al., 2013). Examples of maps of difference in TWSA between a
1517 given month and its climatological mean are presented in **Figure 9a-b** for May 2009, and
1518 October 2010, respectively. These months were chosen as they correspond to the extremum of
1519 these climate events (droughts of 2005, 2010, and 2015, flood of 2009). This information has
1520 revealed to be complementary to what can be obtained using spatialized rainfall and in situ water
1521 levels and discharges. For instance, the patterns of minimum TWSA during the droughts of 2005
1522 and 2010 were found to be in good coincidence across the basin with the areas with large fire
1523 activity (Aragão et al., 2008; Zeng et al., 2008) and of considerable tree mortality (Phillips et al.,
1524 2009) as reported in Frappart, Ramillien, et al. (2013). TWSA also helped, jointly with
1525 hydrological modeling, to characterize the recent extreme droughts which occurred in the
1526 Amazon, highlighting the importance of the interactions between subsurface and surface water
1527 storages to mitigate the deficit in surface reservoirs (Chaudhari et al., 2019).

1528



1529

1530 **Figure 9.** Maps of TWSA during two extreme events (a) the flood in May 2009, and (b) the
 1531 drought in October 2010. Mean annual changes in groundwater storage anomaly - GWSA (c)
 1532 and associated standard deviation (d) over 2003–2010 (adapted from Frappart et al., 2019). (e)
 1533 Time series of GRACE-based TWSA (km^3) over the AB between 2003-2016. The vertical lines
 1534 show the months of maximum (May 2009) and minimum (October 2010) values.

1535

1536 A direct approach to estimate GW storage anomalies is to remove the contribution of the
 1537 different hydrological compartments from GRACE-based TWSA as follows:

1538

$$\Delta GW = \Delta TWS - \Delta SW - \Delta SM - \Delta CW - \Delta SWE \quad (2)$$

1540

1541 where Δ represents the anomaly of water storage in the different hydrological
 1542 compartments, SW is the surface water storage, SM is the soil moisture or water contained in the
 1543 root zone, CW is the water contained in the canopy, and SWE is the snow water equivalent. This
 1544 latter term was neglected in the studies performed in the AB as no reliable information on this
 1545 water storage was available. In most of the cases, water from the other compartments (SW and
 1546 SM) are provided by model outputs and/or in situ measurements. For the Amazon, it is necessary
 1547 to accurately take into account the SW component as it represents around half of the TWSA
 1548 (Frappart et al., 2012, 2019). Using external information from hydrological models for SW, SM,
 1549 and CW, groundwater storage anomalies were estimated over 2003-2015, revealing a strong link
 1550 between geological properties and GW storage: the largest groundwater storage capacity in
 1551 Brazil was found in regions with the highest permeability of the rock layers (e.g., the Guarani
 1552 and Alter do Chão aquifers; Hu et al., 2017). But in these cases, SW storage was limited to river
 1553 storage, neglecting the storage in the extensive floodplains of the AB. In order to adequately take
 1554 into account the contribution of SW components, methodologies were developed to estimate SW
 1555 storage variations from RS observations (Frappart et al., 2008, 2012; Ndehedehe & Ferreira,
 1556 2020). SW storage anomalies were obtained by combining surface water extent (generally from
 1557 GIEMS, see Section 4.2) and altimetry-based time series of water levels (see Section 4.1) over
 1558 rivers and floodplains. Frappart et al. (2012) estimated the monthly variations of SW storage at
 1559 the basin scale during the 2005 drought and found that the amount of water stored in the river
 1560 and floodplains of AB during this extreme event was 130 km^3 (70%) below its 2003–2007
 1561 average, representing almost a half of the anomaly of minimum TWS as estimated by GRACE.

1562 Using this newly external information on SW storage variations, along with SM storage
 1563 estimates from hydrological models, GW storage anomalies were first estimated over 2003-2004
 1564 in the Negro River Basin, one of the largest tributaries to the AB (Frappart et al., 2011). The
 1565 spatial pattern of the annual amplitude of GW anomalies agrees well with the regional
 1566 hydrogeological maps and the amplitude are consistent with observations of water level at local
 1567 wells and altimetry-based time series of water levels in two adjacent wetlands where the
 1568 groundwater table reaches the surface during the whole hydrological cycle (Frappart et al.,
 1569 2011).

1570 This approach was then extended to the whole AB over 2003-2010, using about 1000
 1571 ENVISAT RA-2 altimetry VSs of surface water elevation (Frappart et al., 2019). SW storage
 1572 over the entire basin had an annual amplitude ranging between 900 and 1300 km^3 (Frappart et
 1573 al., 2012). GW estimates had good agreement with scarce in situ groundwater observations and
 1574 low-water maps of GW table (Frappart et al., 2008). At basin-scale, the results have realistic
 1575 spatial patterns when compared to hydrogeological maps of Brazil (e.g., porosity maps, aquifer
 1576 boundaries, GW recharge). The seasonal amplitude of GW was estimated to contribute between
 1577 20 to 35% of the GRACE-derived TWS amplitude in the AB (Frappart et al., 2019). The impact
 1578 of the 2005 extreme drought on GW storage was also observed and lasted several years (Frappart
 1579 et al., 2019).

1580 Radar altimetry was used to estimate low-water maps of GW table in the central part of
 1581 the AB (Frappart et al., 2008). Owing to the connection between surface and groundwater during
 1582 the low water period in the alluvial plains of the central Amazon (54°-70° W, 0°-5°S), annual
 1583 lower water levels of 593 altimetry VSs were interpolated to generate yearly maps of
 1584 groundwater base level (GWBL) between 2003 and 2009. The results show that GWBL is
 1585 governed by the surface topography and that several years were needed for GWBL to recover
 1586 from the extreme drought of 2005 (Pfeffer et al., 2014).

1587 The recent launch of the GRACE Follow-On (GRACE-FO) offers an opportunity to
 1588 extend the monitoring of TWS and GWS changes after 2018. Despite a lack of data between
 1589 October 2017 (end of GRACE operation) and May 2018 (launch of GRACE-FO), two decades
 1590 of TWSA will be soon available, allowing analysis of the impact of multi-year climatic events
 1591 such as ENSO on land and ground water storages. The major drawbacks of these data are their
 1592 low spatial (~200 km) and temporal (1 month) temporal resolutions which are not sufficient to
 1593 study the dynamics of fast hydrological events. To overcome these drawbacks, the GRACE-FO
 1594 payload contains advanced versions of the sensors present on-board GRACE and a novel laser
 1595 ranging interferometer (LRI), measuring the satellite-to-satellite distance in parallel with
 1596 the K-band radar instrument. The LRI is expected to be 26-times more accurate than the K-
 1597 band radar instrument on-board GRACE (Tapley et al., 2019). This better expected accuracy is
 1598 likely to improve the quality and the spatial resolution of the retrieved TWSA. New approaches
 1599 based on the use of Kalman filter were developed to increase the TWSA temporal resolution to
 1600 quasi-daily without degrading the spatial resolution (Ramillien et al., 2015, 2020).

1601

1602 **6. Integrative and interdisciplinary studies**

1603 RS data have provided breakthrough advances in understanding of the AB's hydrology
 1604 and associated aquatic environments. In Sections 2 to 5 we have presented and discussed
 1605 scientific advances for individual components. In this Section we introduce research agendas that
 1606 have benefited from the integration of observations from multiple components of the Amazon
 1607 water cycle. These include the computation of the water budget (6.1), application of hydrological
 1608 models (6.2), understanding of aquatic ecosystems (6.3) and past and ongoing environmental
 1609 changes over the AB (6.4).

1610

1611 **6.1. Water budget**

1612 In order to better understand the complex hydrological processes in the AB, it is
 1613 necessary to monitor each component of the water cycle, and to understand how these
 1614 components link and interact. Thus, studying the AB water budget (WB) requires use of a large
 1615 variety of observations, especially because the AB includes complex local environments (e.g.,
 1616 floodplains) and processes (e.g., soil moisture and canopy transpiration) which are difficult to
 1617 characterize by satellite observations.

1618 Among the WB literature, the AB has been one major region among global analyses of
 1619 the water cycle (Munier & Aires, 2018; Pan et al., 2012; Sahoo et al., 2011; Y. Zhang et al.,
 1620 2018) or the main focus of the analysis (Azarderakhsh et al., 2011; Builes-Jaramillo & Poveda,
 1621 2018; Moreira et al., 2019; P. T. S. Oliveira et al., 2014). Most WB studies used only one

1622 satellite product for each water component (Azarderakhsh et al., 2011; Builes-Jaramillo &
1623 Poveda, 2018; Maeda et al., 2015; Moreira et al., 2019; P. T. S. Oliveira et al., 2014; Rodell et
1624 al., 2011). Use of a multiplicity of the satellite products for each water component can reduce
1625 uncertainties, through an approach that is based on observations only (Filipe Aires, 2014) or
1626 integrating model simulations and re-analyses (Pan et al., 2012; Y. Zhang et al., 2018).

1627 Continuous quality improvement and increased use of satellite products, associated with
1628 more sophisticated integration techniques, have allowed better characterization the water cycle.
1629 WB analyses have been used to i) directly estimate a missing water component such as *ET*
1630 (Maeda et al., 2017; Rodell et al., 2011), *R* (Azarderakhsh et al., 2011; P. T. S. Oliveira et al.,
1631 2014), and terrestrial water storage change *dS* (Moreira et al., 2019); ii) diagnose the
1632 hydrological coherence of a combination of RS-based estimates and investigating discrepancies
1633 (Builes-Jaramillo & Poveda, 2018; Moreira et al., 2019; P. T. S. Oliveira et al., 2014); and iii) to
1634 optimize RS-based estimates to obtain a hydrologically coherent water cycle (Munier & Aires,
1635 2018; Pan et al., 2012; Pan & Wood, 2006; Pellet et al., 2021; Sahoo et al., 2011). The three
1636 main uses of WB closure are detailed in the following paragraphs.

1637 When estimating missing water components, the objective can be to investigate seasonal
1638 patterns (Azarderakhsh et al., 2011; Moreira et al., 2019) and more complex features such as
1639 trends and impacts due to land use and land cover changes (P. T. S. Oliveira et al., 2014). The
1640 studies provide uncertainties for their estimates based on the relative uncertainties of the other
1641 components (Rodell et al., 2011). When focusing on *ET*, the literature stresses that *ET* is
1642 controlled by both *P* and radiation without being limited by one of these two (Maeda et al.,
1643 2017); but the seasonality remains unclear due to large uncertainty in *P*. Nevertheless, the
1644 indirect estimation of *ET* has been used by Rodell et al. (2011) to evaluate model *ET* outputs
1645 over the Tocantins basin and the authors concluded that much effort are still required on the *ET*
1646 modeling.

1647 Diagnosing WB coherency by combining RS products is a useful tool to assess the
1648 quality of the RS products. For instance, Moreira et al. (2019) demonstrated that the MSWEP
1649 and GLEAM datasets reduce the WB imbalance. P. T. S. Oliveira et al. (2014) showed that
1650 recent versions of the TMPA also improve WB closure compared to older versions. Builes-
1651 Jaramillo & Poveda (2018) have jointly evaluated the surface and atmospheric water balances
1652 over the Amazon, and their diagnostic of the discrepancy between various ET estimate showed
1653 that RS-based ET products balance better the WB than the model and reanalysis outputs. As
1654 reported in Builes-Jaramillo & Poveda (2018) and Moreira et al. (2019), the WB imbalance
1655 relates at sub-basin to the drainage area and the climatic conditions (i.e. tropical or mountainous)
1656 which impact the signal-to-noise ratio of each water component.

1657 Several studies have used the WB closure as a constraint for the optimization of satellite
1658 estimates, jointly for each water component. Pan & Wood (2006) developed an optimization of
1659 the satellite products using an assimilation scheme within a land surface model at the basin scale.
1660 This method has then been applied to the AB (Pan et al., 2012; Sahoo et al., 2011). Zhang et al.
1661 (2018) extended this scheme to the pixel scale by considering only simulated R. Similarly, Aires
1662 (2014) described several approaches to integrate satellite observation (simple weighting, optimal
1663 interpolation, post-filtering and neural networks) with the WB closure constraint but without the
1664 use of surface or hydrological models to obtain an observational database. Munier & Aires
1665 (2018) investigated AB hydrology using this framework, and Pellet et al. (2021) added inter-

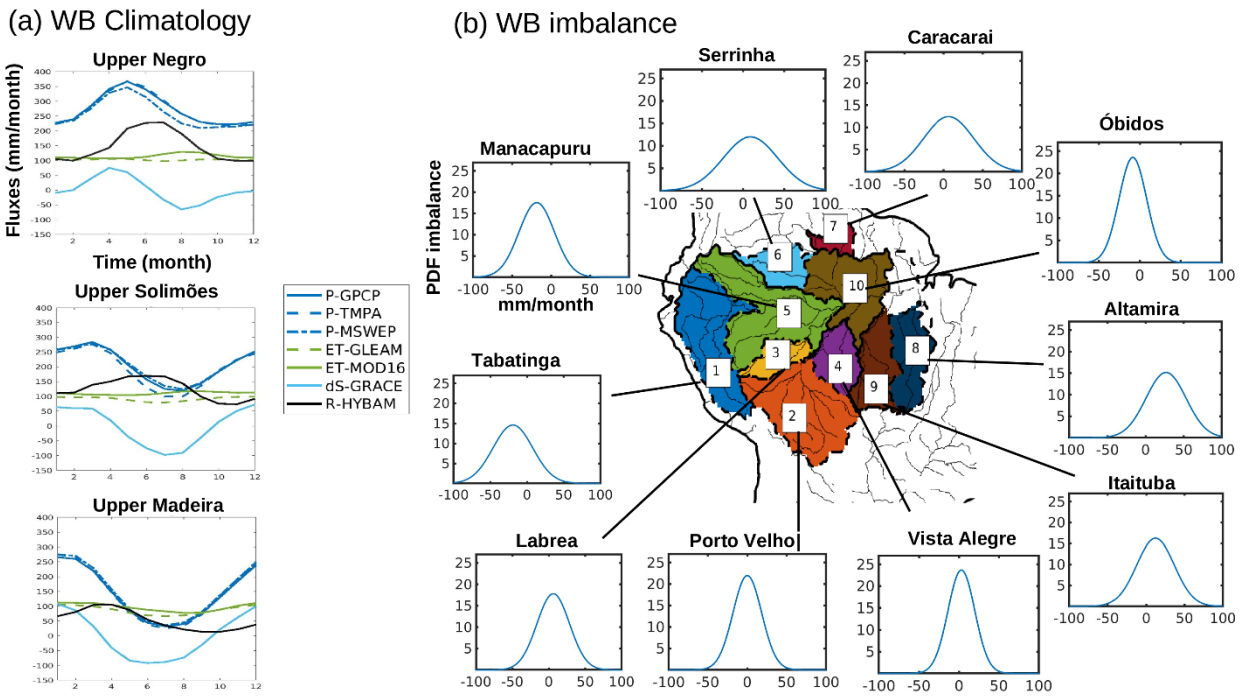
1666 basins constraints on the budget closure using river discharges over several stations in the basin.
 1667 This technical framework allows for the optimization of the satellite datasets and can be used to
 1668 develop new tools in hydrology such as the assimilation of GRACE data (Y. Zhang et al., 2018).
 1669 For instance, in Pellet et al. (2021), the spatial patterns of P , ET and dS were used to estimate the
 1670 river discharge along the river network.

1671 The estimation of the uncertainty of each water component is one of the main objectives
 1672 of a WB analysis. Such characterizations are generally component- and site-specific. For
 1673 instance, Moreira et al. (2019) extensively evaluated the satellite estimate uncertainty of P and
 1674 ET using in situ data (i.e., 300 precipitation gauges and fourteen eddy-covariance monitoring
 1675 sites), however this approach is limited due to the sparsity of the observation network. Sahoo et
 1676 al. (2011) used the distance to non-satellite estimate while Y. Zhang et al. (2018) and Pellet et al.
 1677 (2021) used the spread of the satellite as a proxy for uncertainty. Azarderakhsh et al. (2011) or
 1678 Munier and Aires (2018) used a literature review based on RS expertise to quantify the
 1679 uncertainties of the satellite products. Studies generally assume a value of 5% to 10% of error for
 1680 R while dS errors from GRACE are often computed following the specifications for leakage and
 1681 measurement covariance errors (Rodell et al., 2004). All the studies agree in the relatively high
 1682 contribution of the P estimate in the total WB imbalance (~40%). Moreira et al. (2019) and P. T.
 1683 S. Oliveira et al. (2014) found a positive bias in P when comparing them to in situ data, but all
 1684 the integration approaches (Pan et al., 2012; Pellet et al., 2021; Sahoo et al., 2011) result in an
 1685 increased P estimate. Furthermore, Moreira et al. (2019) considered that dS is the second
 1686 contributor to the WB imbalance (~25%) while Sahoo et al. (2011) and Pellet et al. (2021) found
 1687 a higher contribution from ET (~30%). All the optimization strategies have shown that the WB
 1688 can be balanced within the range of the RS-based uncertainties.

1689 **Figure 10a** represents the climatology of the four water components in three basins and
 1690 using several datasets for each water component. The three basins are: northern Negro catchment
 1691 upstream of the Serrinha station, the central basin upstream of the Manacapuru station (including
 1692 the drainage area upstream of the Tabatinga station) and the southern basin upstream of the
 1693 Fazenda (Fz) Vista Alegre station (including the drainage area upstream of Porto-Velho station).
 1694 The climatological season (i.e., annual cycle) of all the water components are represented in
 1695 mm/month. All satellite products have bias and uncertainties, but this multi-component analysis
 1696 can isolate the spatial patterns over the AB. For instance, the annual cycles of the WB differ on
 1697 the northern and southern basins. As reported in the literature (Espinoza, Sörensson, et al., 2019;
 1698 Marengo, 2005), over southern basin, P is driven by the monsoon with a peak in January and has
 1699 larger seasonal variations (e.g. min-max range) and lower annual average than on the northern
 1700 basin, where P peaks in May. The P seasonality drives R over all basins (north and south) with a
 1701 time-lag of one-two months. Over the central-western basin, R can be higher than P for a
 1702 particular month and P - R peak is about 4 months related to the runoff and river discharge travel
 1703 times inside the basin (Sorribas et al., 2020). dS is in phase with P in the southern basin, but
 1704 shows a particular season over the Negro and Branco river basins: dS is equal to zero during the
 1705 dry season and a linear transition exists between maximum and minimum. Over these basins, dS
 1706 become negative while R was increasing, and reached its maximum 2 months later. This
 1707 illustrates the effect of water storage in floodplain before releasing it into the river. ET seasonal
 1708 variation is weaker but ET peak seems to be in phase with P over southern basin arguing for a
 1709 water-limited behavior while ET peak follows the P minimum month in northern basin of an

1710 energy-limited system (Maeda et al., 2017). In Pellet et al. (2021), the correction of ET based on
 1711 the closure of the water cycle enhances the water limitation regime over the central AB and the
 1712 energy limitation over the northern AB. In the south, during dry months (JJA), ET is higher than
 1713 P , and water that evaporates is provided by the soil storage which continues to lose water until
 1714 November. For this season, the role of ET on the water cycle is relatively more important in the
 1715 dry season than in the rainy season (Marengo, 2005).

1716



1717

1718 **Figure 10.** a) seasonal climatology of all the water component: precipitation (P),
 1719 evapotranspiration (ET), water storage change (dS) and discharge measured at in situ gauges (R)
 1720 described by one or multiple datasets. b) Probability Density Function (PDF) of the resulting WB
 1721 imbalances are shown at sub-basin scale (right). PDF provides the bias and variance of the
 1722 imbalance.

1723

1724 To investigate the overall WB imbalance related to the bias and uncertainty of the all the
 1725 water components, **Figure 10b** shows the Probability Density Function (PDF) of these
 1726 imbalances at sub-basins scale. Spatially, there is a gradient in the mean of the PDF between the
 1727 western and southern sub-basins. Western sub-basins have a lack of water (negative bias in the
 1728 PDF), while southern sub-basins have an excess of water (positive bias). This gradient was
 1729 reported by Builes-Jaramillo & Poveda (2018). Furthermore, the variance of the WB imbalance
 1730 increases from south to north with the annual mean of P suggesting that a large part of imbalance
 1731 is due to P (Moreira et al., 2019; Pellet et al., 2021). The optimization strategy based on the
 1732 closure of the WB leads to a bigger correction of the water component over western and central
 1733 sub-basins (Pellet et al., 2021).

1734 The remaining precipitation uncertainties of the globally calibrated satellite products are
 1735 mainly due to the increase of the precipitation measurement errors by satellite products during
 1736 the rainy season, and the lack of in situ gauges used in calibration (Moreira et al., 2019). The AB
 1737 hydrology could benefit from the use of a dedicated network of precipitation gauges such as
 1738 HYBAM Observatory Precipitation (J. C. Espinoza Villar, Ronchail, et al., 2009; Guimberteau et
 1739 al., 2012) to obtain a regionally-calibrated satellite product for precipitation. Its gauges density
 1740 over the AB is higher than the global gridded rainfall dataset generally used to calibrate satellite
 1741 products (Guimberteau et al., 2012).

1742 Estimating *ET* in the AB remains a challenge (see Section 3). In **Figure 10**, the use of
 1743 different *ET* datasets can lead to a difference of 30-50 mm/month which represent up to 50% of
 1744 the *ET* value. Following Moreira et al. (2019), the establishment of generic methods for
 1745 estimating uncertainties is of importance for improving our understanding of the terrestrial water
 1746 cycle. As for *P*, one source of the improvement will be the extensive use and increase of an eddy
 1747 covariance network to better understand the uncertainties in *ET* models.

1748 One technical improvement in the WB based optimization approach might come with the
 1749 spatial resolution of the analysis. WB analysis has been mostly done at the basin scale over the
 1750 AB (Munier & Aires, 2018; Sahoo et al., 2011) even if several studies have been conducted in
 1751 sub-basins defined by river discharge stations (Azarderakhsh et al., 2011; Pellet et al., 2021).
 1752 Using topography information, it should be possible to consider the runoff over land and
 1753 downscale the satellite products while closing the WB at a pixel level. The satellite datasets
 1754 could even be downscaled temporally to obtain a better time resolution.

1755 As discussed in Section 5, attempts have been made to decompose the TWS from
 1756 GRACE into its surface (Frappart et al., 2012; Papa et al., 2013) and groundwater (Frappart et
 1757 al., 2019) components. Such decomposition could also be attempted within a full terrestrial WB
 1758 analysis, especially when reliable soil moisture satellite estimates over the AB will become
 1759 available. As mentioned in Section 4, long-term surface water datasets would also be necessary
 1760 (Filipe Aires et al., 2017; Parrens et al., 2019; Prigent et al., 2020).

1761 The GRACE-FO mission launched in 2018, extension of the TRMM data record with the
 1762 GPM mission, and the launch of the SWOT mission will provide a comprehensive set of new
 1763 observations. The continuity of these satellite missions monitoring the water components is
 1764 mandatory to improve our understanding of spatial hydrology patterns through more precise WB
 1765 analyses, and assess potential long-term trends.

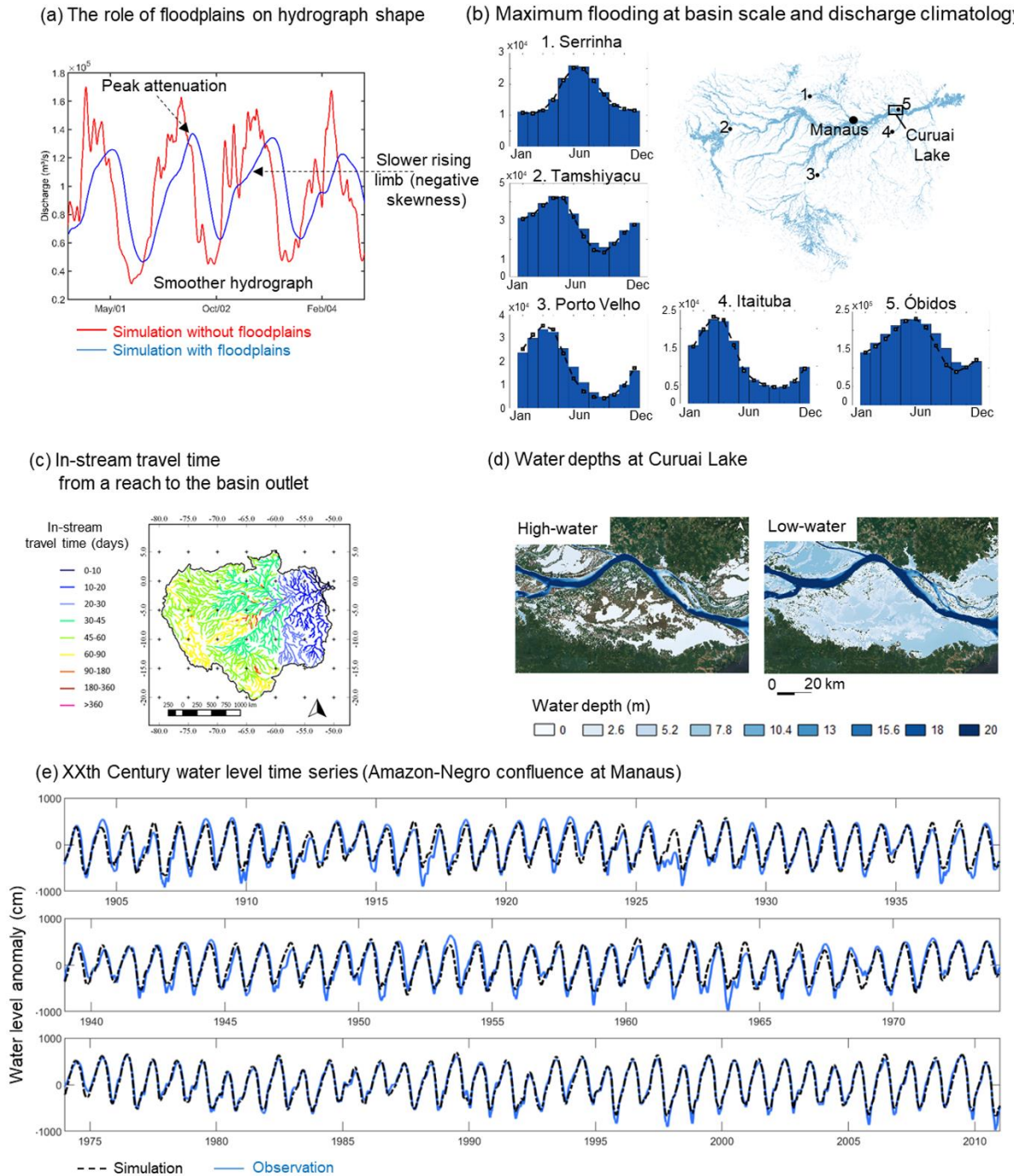
1766

1767 **6.2. Modeling the Amazon water cycle and its wetlands**

1768 Hydrologic and hydraulic models represent the water cycle storages and fluxes through a
 1769 set of mathematical equations. Such process-based models are suitable tools to understand
 1770 Amazon hydrological processes such as river-floodplain water exchange and groundwater-
 1771 surface water interactions (Miguez-Macho & Fan, 2012; Paiva, Buarque, et al., 2013) and past
 1772 floods and droughts (Wongchuig et al., 2017), to estimate variables in ungauged regions (e.g.,
 1773 distributed river discharge for the last century; Wongchuig et al., 2019), and to perform scenarios
 1774 of hydrological alteration due to deforestation, flow regulation by reservoirs, and climate change
 1775 (M. E. Arias et al., 2020; Guimberteau et al., 2017; Júnior et al., 2015; Lima et al., 2014; Mohor

1776 et al., 2015; Pokhrel et al., 2014; Pontes et al., 2019; Sorribas et al., 2016; Zed Zulkafli et al.,
1777 2016).

1778 During the last decades, many models have been applied in the Amazon at different
1779 scales, from reach (i.e., more detailed studies addressing a few kilometers long river-floodplain
1780 area) to the whole basin scale. Because of the basin's remoteness and vast dimensions, RS
1781 datasets are usually adopted as either forcings (e.g., precipitation), a priori information to
1782 estimate parameter values (e.g., topographic data), validation, or calibration/assimilation data
1783 (e.g., discharge, river water levels). A major distinction can be made between (i) hydrological
1784 models that simulate vertical processes as evapotranspiration, soil water infiltration and runoff
1785 generation mechanisms, and (ii) hydraulic models of surface waters, which represent flow
1786 propagation along rivers and floodplains with physically-based equations, and allow the
1787 computation of variables such as surface water elevation and slope, river discharge, and surface
1788 water extent and storage (**Figure 11**). More recently, the so-called hydrologic- hydraulic models
1789 have been developed to couple the strengths of both approaches (Fleischmann et al., 2020; Hoch
1790 et al., 2016; Paiva, Buarque, et al., 2013), and there may be cases where simplified inundation
1791 schemes are represented within hydrologic models to estimate wetland flooding dynamics. **Table**
1792 **6** summarizes the differences between the two approaches.



1793

1794 **Figure 11.** Recent applications of hydrologic and hydraulic models in the AB have added
 1795 insights into the role of river floodplains on (a) hydrograph shape (Fleischmann et al., 2016) and
 1796 (c) in-stream travel times (Sorribas et al., 2020), and provided the estimation of (b) long-term
 1797 discharge climatology (Paiva, Buarque, et al., 2013), (c) long-term water level time series
 1798 (example for the location of Manaus; Wongchuig et al., 2019), and (d) floodplain water depths
 1799 (example for the Curuai Lake, 2014 high and low water seasons; Rudorff et al., 2014a).

1800

1801 **Table 6.** Summary of main differences between hydrologic and hydraulic models of surface
 1802 waters, with examples of model applications in the AB. Some examples are provided in both
 1803 categories since they refer to hydrologic-hydraulic models.

	Hydrological models	Hydraulic models of surface waters
Main simulated process	Vertical processes (e.g., evapotranspiration, soil water infiltration and runoff generation mechanisms) and groundwater dynamics	River-floodplain interaction (e.g., floodplain storage, backwater effects)
Main forcing (boundary conditions)	Precipitation	River discharge, river water level and precipitation
Main output variables	Water balance, evapotranspiration, soil water and groundwater storage, river discharges	Inundation maps, river-floodplain water depths, longitudinal water levels along rivers, river discharges
Typical scientific outcomes	Quantification of water balance components, water storage partition between surface and subsurface reservoirs, evapotranspiration dynamics, impacts of human alteration on water balance components (e.g., changes in precipitation partition into <i>ET</i> and runoff)	Floodplain water storage and residence time, water travel times across river-floodplain systems, rating curves (water level-discharge relationships) for operational use, impacts of human alteration on flood dynamics
Examples of studies	Beighley et al., 2009; Coe et al., 2002; M. H. Costa & Foley, 1997; Cuartas et al., 2012; Miguez-Macho & Fan, 2012; Paiva, Buarque, et al., 2013; Vörösmarty et al., 1989	Fleischmann et al., 2020; Garambois et al., 2017; Getirana et al., 2012; Miguez-Macho & Fan, 2012; Paiva, Buarque, et al., 2013; Paris et al., 2016; Pinel et al., 2019; Rudorff et al., 2014a; Sorribas et al., 2020; Trigg et al., 2009; Wilson et al., 2007; Yamazaki, Lee, et al., 2012

1804

1805 The first generation of models in the Amazon involved the development of large scale
 1806 hydrological models, starting with the studies by Vörösmarty et al. (1989), Costa and Foley
 1807 (1997) and Coe et al. (2002). With the advent of RS datasets and higher computational capacity,
 1808 several models have been developed, improving the physical representation of hydrological
 1809 processes, increasing the model spatial resolution and moving from monthly to daily estimates
 1810 (Beighley et al., 2009; Coe et al., 2008; Luo et al., 2017; Miguez-Macho & Fan, 2012; Paiva,
 1811 Buarque, et al., 2013). These models usually adopt the following RS-based input data:
 1812 precipitation with the TMPA product (Collischonn et al., 2008; Getirana et al., 2012; Zubieta et
 1813 al., 2015), and more recently GPM-IMERG (Zubieta et al., 2017) and MSWEP (Beck, Van Dijk,
 1814 et al., 2017); landscape properties including terrain lengths and slopes, based on DEMs (most
 1815 studies using SRTM DEM); and land use and vegetation maps (global maps as FAO, or regional
 1816 ones as the Brazilian RadamBrasil soil maps). The most common validation datasets from RS are

1817 water level from satellite altimetry (Section 4.1), surface water extent (Section 4.2), and total
1818 water storage (Section 5).

1819 These model applications deepened our comprehension of the water partition between
1820 soil, surface water and groundwater, and acted as laboratories to improve global hydrological
1821 models, which in turn are fundamental elements of Earth System models. The assessment of land
1822 surface and global hydrological models in the Amazon has been a standard procedure in
1823 geoscientific model development and in model intercomparison projects (Alkama et al., 2010;
1824 Bertrand Decharme et al., 2008; Getirana et al., 2012, 2014; Getirana, Peters-Lidard, et al., 2017;
1825 Guimberteau et al., 2014, 2017; Pilotto et al., 2015; Towner et al., 2019; Yamazaki, Baugh, et
1826 al., 2012; Yamazaki et al., 2011; Z. Zulkafli et al., 2013). At the basin scale, the fraction of the
1827 total water storage corresponding to surface waters was estimated as 56%, 41% and 27% by
1828 Paiva, Buarque, et al. (2013), Getirana et al. (2017) and Pokhrel et al. (2013), respectively. These
1829 values have been compared to RS-based estimates (Frappart et al., 2012, 2019; Papa et al.,
1830 2013). Furthermore, basin-scale average *ET* estimated as 2.39 to 3.26 mm/day by an ensemble of
1831 land surface models (Getirana et al., 2014), and as 2.72 mm/day by Paiva, Buarque, et al. (2013),
1832 were slightly lower than values by basin-scale RS (Paca et al., 2019) and an in situ eddy-
1833 covariance network (M. H. Costa et al., 2010), which estimated values of 3.11 to 3.58 mm/day
1834 across a gradient from southern dry to equatorial wet Amazon forests. The role of soil water
1835 storage to sustain dry season *ET* in the Amazon was shown by modeling experiments at local
1836 (Fang et al., 2017) and basin scale (Getirana et al., 2014). Some studies addressed the role of
1837 groundwater and soil storage on the water balance, and the importance of its representation into
1838 hydrological models. Applications at headwater basins showed the predominance of groundwater
1839 on headwater water storage (Cuartas et al., 2012; Niu et al., 2017), in agreement with in situ
1840 monitoring studies (Hodnett et al., 1997). Miguez-Macho & Fan (2012) suggested the same
1841 pattern at the whole basin scale. Their model also indicated an important two-way feedback
1842 between floodwater and groundwater, and the existence of large areas not subject to surface
1843 flooding across the basin, but where a high water table level would be responsible for keeping
1844 high soil water content year-round. The simulation of multiple soil layers in the ORCHIDEE
1845 land surface model, in contrast to a simple 2-layer “bucket” model, was also shown to improve
1846 the representation of the soil water dynamics and the total water storage in the Amazon,
1847 especially for the drier regions in the southern sub-basins (Guimberteau et al., 2014).

1848 Among hydraulic models of surface waters, a pioneer study by Wilson et al. (2007) is one
1849 of the first hydraulic modeling experiments performed over large domains. The authors applied
1850 the LISFLOOD-FP model to a 260 km reach of the Solimões River, and estimated the river-
1851 floodplain water exchange as at least 40% of the river volume in that reach. For a relatively
1852 different reach in the Central Amazon (from São Paulo de Olivença to Óbidos), Richey et al.
1853 (1989) estimated this ratio as 30% based on a simpler routing method, while Sorribas et al.
1854 (2020) estimated a value of 40% for the AB system, based on large scale hydraulic modeling
1855 (see below). The authors also found the model accuracy to be higher for the high water period, as
1856 has been also reported by recent studies (Pinel et al., 2019; Rudorff et al., 2014a), likely due to
1857 misrepresentation of the terrain heterogeneities and small disconnected lakes during the dry
1858 season. Furthermore, since the river-floodplain water exchange often occurs through floodplain
1859 channels and breached levees that hinder its conceptualization as a simple overbanking flow
1860 (Trigg et al., 2012), hydraulic models have the challenge to estimate effective channel
1861 parameters that represent these complex processes (Fleischmann et al., 2018; Trigg et al., 2009).

1862 Other applications at reach or floodplain lake scale were developed by Bonnet et al. (2008,
1863 2017), Ji et al. (2019), Trigg et al. (2009) and Wilson et al. (2007), and addressed the relative
1864 role of local runoff and river inflow as the main water input, ranging from local runoff-
1865 dominated systems in the Lago Calado (Ji et al., 2019; Lesack & Melack, 1995) to river-
1866 dominated ones in the Curuai (**Figure 11d**) and Janauacá systems (Bonnet et al., 2008, 2017;
1867 Pinel et al., 2019; Rudorff et al., 2014b, 2014a), through either channelized or diffuse flow
1868 patterns. In the case of Curuai and Janauacá, the Amazon or Solimões river was responsible for
1869 82% and 93% of the floodplain annual influxes, respectively (Bonnet et al., 2017; Rudorff et al.,
1870 2014b).

1871 The first basin-scale inundation model was introduced by Coe et al. (2002), and
1872 numerous hydrologic models were developed and coupled to inundation schemes afterwards
1873 (Coe et al., 2008; Getirana et al., 2012; Getirana, Peters-Lidard, et al., 2017; Hoch et al., 2016;
1874 Luo et al., 2017; Miguez-Macho & Fan, 2012; Paiva, Buarque, et al., 2013; Yamazaki et al.,
1875 2011; Yamazaki, Lee, et al., 2012). The models featured varying degrees of physics
1876 representation, with the simulation of floodplains moving from simple storage components to
1877 dynamic hydraulic schemes, which can represent relevant processes such as backwater effects.
1878 For hydraulic models, additional RS-based information required as input data includes river
1879 channel geometry as width, and floodplain topography from DEMs (mainly SRTM and its
1880 derivatives with vegetation removal to represent the bare terrain; see Baugh et al. (2013),
1881 O’Loughlin et al. (2016), Yamazaki et al. (2019) and Fassoni-Andrade, Paiva, Rudorff, et al.
1882 (2020). For local scale hydraulic models, additional parameterization usually involves the
1883 definition of floodplain roughness based on land cover maps (Pinel et al., 2019; Rudorff et al.,
1884 2014a). RS validation datasets are typically surface water elevation and surface water extent
1885 (Hall et al., 2011; Schumann et al., 2009).

1886 These hydraulic model applications revealed the combination of backwater effects and
1887 floodplain storage to drive the flood wave behavior along Amazon rivers (Paiva, Buarque, et al.,
1888 2013), causing strong attenuation and delay up to 2.5 months. Floodplain storage is also
1889 responsible for the general negative hydrograph skewness in the main Amazon rivers, with a
1890 slower rising and a faster falling limb (Fleischmann et al., 2016; **Figure 11a**). Sorribas et al.
1891 (2020) used particle tracking methods to estimate surface water travel times along the AB as 45
1892 days (median), with 20% of Amazon river waters flowing through floodplains (**Figure 11c**).
1893 While basin-scale applications have employed 1D models (longitudinal direction along rivers),
1894 the necessity of representing the 2D diffuse flow in floodplains, especially during receding
1895 waters, was highlighted by Alsdorf et al. (2005), who combined interferometry data with a
1896 simple continuity-based model to show that floodplain storage changes decrease with distance
1897 from the main channel. Generally, the water level in the river-floodplain system is not horizontal,
1898 and the river-floodplain is not homogeneously mixed (Alsdorf et al., 2007), as assumed by
1899 several 1D models. While a proper characterization of the complex river-floodplain interactions
1900 with hydraulic models has been done at local scales (Pinel et al., 2019; Rudorff et al., 2014a), it
1901 is still to be developed for the regional scale – for instance, to be able to infer hyperresolution
1902 (e.g., 30 m spatial resolution) flooding patterns for the whole central Amazon at weekly to
1903 monthly resolution. Finally, the full coupling between hydrologic and hydraulic models has been
1904 suggested to improve the representation of the floodplain-upland interactions, for instance
1905 through a more proper representation of open water evaporation in flooded areas (Getirana,
1906 Kumar, et al., 2017). However, recent studies have suggested that this process has relatively low

1907 impact on the total *ET* estimates because of the general energy-limited (and not water-limited)
1908 *ET* in the Amazon (Fleischmann et al., 2020; Paiva, Buarque, et al., 2013). A different
1909 conclusion is expected for semi-arid wetlands (Fleischmann et al., 2018).

1910 Regional scale validation of inundation models has been done with surface water extent
1911 (Getirana et al., 2012; Luo et al., 2017; Paiva, Collischonn, et al., 2013; Wilson et al., 2007;
1912 Yamazaki et al., 2011) based on the products by Hess et al. (2003), GIEMS from Prigent et al.
1913 (2007), and more recently with the SWAF database (Parrens et al., 2017) (see Section 4.2 for a
1914 description of these products). Although the flooding seasonal cycle is usually well captured by
1915 most models, estimates usually diverge in terms of magnitude (Fleischmann et al., 2020), and the
1916 fusion between different techniques is likely the optimal solution. However, more detailed
1917 validation experiments, for instance with maps based on SAR data, are needed, although many
1918 SAR data classifications were already developed for individual Amazon wetlands (Section 4.2).
1919 A recent application used ALOS/PALSAR imagery for a local scale model validation in the
1920 Janauacá floodplain system (Pinel et al., 2019).

1921 Regarding surface water elevation, hydraulic models are typically capable of representing
1922 anomalies, but estimates of absolute values tend to be less accurate (Fleischmann et al., 2019).
1923 The hundreds of virtual stations available (see Section 4.1) have provided breakthrough
1924 improvements of modelling systems, especially in terms of distributed model validation with
1925 dozens of virtual stations (Fleischmann et al., 2020; Getirana, Peters-Lidard, et al., 2017; Paiva,
1926 Buarque, et al., 2013) and recent model calibration and assimilation (Brêda et al., 2019; A. M.
1927 Oliveira et al., 2021). Validation exercises yielded Nash-Sutcliffe coefficients higher than 0.6 for
1928 60% of the 212 ENVISAT virtual stations assessed by Paiva, Buarque, et al. (2013), and
1929 amplitude errors lower than 0.8 m and absolute bias lower than 2.3 m for most of the stations
1930 analyzed by Yamazaki, Lee, et al. (2012). The combination of satellite altimetry with a hydraulic
1931 model for an ungauged reach of the Xingu River led Garambois et al. (2017) to propose the
1932 concept of hydraulic visibility through RS datasets, i.e., the capability of current and future
1933 satellite altimetry data to properly estimate river hydraulic variables. Altimetry data were shown
1934 to be relevant for the understanding of the hydraulic functioning of ungauged braided reaches in
1935 Amazonian rivers, especially along stretches with heterogeneous bed morphology and strong
1936 downstream control, which have major effects on surface water elevation and slope (Birkett et
1937 al., 2002).

1938 The main output variables that have been addressed by hydrologic-hydraulic models are
1939 *ET*, soil water storage, river discharge, surface water elevation, and surface water extent.
1940 However, other variables are also important for an effective understanding of the water cycle,
1941 and need to be better constrained within modeling systems. For instance, only a few studies have
1942 addressed simulated water velocity (C. M. Dias et al., 2011; Fassoni-Andrade, 2020; Pinel et al.,
1943 2019) and flood storage (Fleischmann et al., 2020; Getirana, Kumar, et al., 2017; Paiva, Buarque,
1944 et al., 2013) in the Amazon wetlands, which are fundamental variables to understand flood
1945 dynamics, even though the latter (flood storage) was already estimated by different RS methods
1946 (see Section 5).

1947 As there are still uncertainties in both models and RS estimates, model calibration and data
1948 assimilation (DA) techniques have been developed to improve model predictability, based on the
1949 optimal combination/analysis of these two. Model calibration was performed with satellite
1950 altimetry by Getirana et al. (2013) and A. M. Oliveira et al. (2021), showing the benefits of using

1951 such datasets toward model general improvement in terms of discharge estimation. In turn, the
 1952 evaluation of DA techniques (mainly the Kalman Filter-based methods) within the Amazon
 1953 involved many experiments with RS data (e.g. satellite altimetry), from reach to regional scale
 1954 (Brêda et al., 2019; Emery et al., 2018; Garambois et al., 2017; Paiva, Collischonn, et al., 2013).
 1955 These studies showed the applicability of such methods to improve model estimates and
 1956 representation of the water cycle in general. The usefulness of DA schemes for better estimating
 1957 discharges was demonstrated for forecasting (Paiva, Collischonn, et al., 2013), comprehension of
 1958 past extreme events (Wongchuig et al., 2019), and near-real time discharge estimation (Paris et al.,
 1959 2016). The study by Wongchuig et al. (2019) was the first to show discharge estimation in a
 1960 spatially distributed way for the last 100 years (**Figure 11e**), estimating extreme drought and flood
 1961 events in unrecorded locations. They follow a general pattern of significant trend of increasing
 1962 drought events in the south and flood events in the western and northwestern regions of the
 1963 Amazon (Callède et al., 2004; Correa et al., 2017; J. C. Espinoza Villar, Guyot, et al., 2009; Lopes
 1964 et al., 2016; Molina-Carpio et al., 2017). RS data other than discharge and water levels can also
 1965 be used through DA and could be applied in the Amazon, e.g., soil moisture (Baguis & Roulin,
 1966 2017; Crowley et al., 2008; Massari et al., 2015); terrestrial water storage change (Khaki et al.,
 1967 2018, 2019) and flooded water extent. Additionally, the forthcoming SWOT mission will provide
 1968 breakthrough information for hydraulic modeling of the Amazon rivers. Many studies have been
 1969 discussing the utility of the mission to better estimate hydraulic variables in the Amazon, from
 1970 reach (lower Madeira River; Brêda et al., 2019) to the basin scale (Emery et al., 2020; Wongchuig
 1971 et al., 2020). New frameworks for the incorporation of satellite altimetry water levels will set up
 1972 the development of the next generation of hydraulic models for the AB, aiming at better
 1973 representing local processes as water surface heterogeneities that occur due to hydraulic controls
 1974 as channel width reductions (Garambois et al., 2017; Montazem et al., 2019; Pujol et al., 2020).

1975 Most model applications in Amazon wetlands focused either on parts of the central
 1976 Amazon floodplains or the whole AB. The simulation of river floodplains is still poorly
 1977 performed over complex, dynamic river systems as in the Andes foothills, which are associated
 1978 to multiple alluvial fans, wetlands disconnected from the main river in terms of surface waters
 1979 but connected through groundwater (e.g., the groundwater-fed backswamp forests; Hamilton et
 1980 al., 2007), and relatively quick hydrographs, which in turn hamper RS-based monitoring. In
 1981 addition to river floodplains, other types of wetlands exist in the AB, which are often named as
 1982 interfluvial wetlands (Junk et al., 2011). They combine endogenous and exogenous flooding
 1983 processes to different degrees (Bourrel et al., 2009), and are more subject to local rainfall and
 1984 less connected to adjacent rivers (V. Reis et al., 2019). They are associated with varying
 1985 vegetation and ecosystem types (e.g., savanna, forest, grasslands). While 1D hydraulic models
 1986 have proven satisfactory to simulate flooding along river floodplains (Trigg et al., 2009),
 1987 interfluvial wetlands require a 2D simulation to properly capture the wetland diffuse flow.
 1988 Fleischmann et al. (2020) provided a first model assessment focusing on the Negro interfluvial
 1989 wetlands, which are associated to neotectonic events and savanna environment within the
 1990 Amazon rainforest (Rossetti et al., 2017), and thus largely differ from the central Amazon in
 1991 terms of flooding, vegetation and soil characteristics. Belger et al. (2011) used a time series of
 1992 Radarsat images and in situ measurements of water level and local rainfall to estimate changes in
 1993 inundation in an interfluvial wetland in the Negro basin. 1D models were shown to be unrealistic
 1994 for simulating surface water elevation in these areas. Future studies should further address the
 1995 hydrology of these complex wetland systems, including the Llanos de Moxos (Hamilton et al.,

1996 2004; Ovando et al., 2018), Roraima (Hamilton et al., 2002) and Peruvian (Kvist & Nebel, 2001)
 1997 interfluvial wetlands, aiming at better understanding the hydrological differences between
 1998 floodplains and interfluvial wetlands, which in turn will improve our understanding of the
 1999 various particular Amazon ecosystems relying on them, and the differences in terms of river-
 2000 wetland connectivity.

2001 The downstream part of the AB remains relatively unexplored in terms of hydraulic
 2002 modelling and RS. This can be explained by the intricate dynamics of the estuary, which has
 2003 energetic behaviour over a broad range of timescales from the intra-daily tides propagating
 2004 upstream from the Atlantic Ocean through the Amazon delta to the seasonal-to-interannual
 2005 timescales driven by the hydrology of the basin. Moreover, tidal effects remain sensible up to
 2006 about 900 km upstream of the river mouth (Kosuth et al., 2009). One of the challenges in the
 2007 hydraulic continuum of the lower Amazon is the understanding of the relative roles of the
 2008 upstream forcing and of the oceanic influence in shaping the spatial and temporal patterns of
 2009 variability of water level, flow velocity and flooding extent along the course of the estuary.
 2010 Promising initiatives have been made to model this complex estuary, mostly relying on coastal
 2011 ocean circulation models, either in two-dimensional configurations (Gabioux et al., 2005; Gallo
 2012 & Vinzon, 2005), or more recently through full-blown tri-dimensional modeling (Molinas et al.,
 2013 2020). These studies in particular shed light on the distinct behaviour of the tidal waves during
 2014 their upstream propagation in the Amazon estuary. However, to date a comprehensive, high-
 2015 resolution hydraulic modeling framework embracing the complex geometry of the whole
 2016 hydraulic continuum of the lower Amazon, and accounting for the full range of interactions
 2017 between oceanic and riverine forcing factors, is lacking. This can be explained, at least partly, by
 2018 the fact that the monitoring of water level variability is instrumental in the success of a hydraulic
 2019 modeling of the lower Amazon for calibration/validation purposes; however, spaceborne
 2020 altimetry has been hardly used in the Amazon estuary.

2021 Finally, new EO data as SWOT-derived water levels (Biancamaria et al., 2016), channel
 2022 water widths (G. H. Allen & Pavelsky, 2018; Yamazaki et al., 2014), floodplain topography
 2023 (Fassoni-Andrade, Paiva, Rudorff, et al., 2020), and soil moisture estimates (SMOS, SMAP), as
 2024 well as new precipitation datasets (e.g., rainfall estimation using soil moisture data as the
 2025 SM2RAIN Brocca et al., 2013, 2014), gravimetry missions (GRACE-FO), and techniques to
 2026 retrieve groundwater storages (e.g., Frappart et al., 2019), open great opportunities for the next
 2027 decade of hydrological and hydraulic modeling development in the AB. A major goal of the
 2028 Amazon modeling community should be to move towards hyper resolution models, capable of
 2029 providing locally relevant estimates everywhere (Bierkens et al., 2015; Fleischmann et al., 2019;
 2030 Wood et al., 2011), as well as better representing all processes within the water cycle, including
 2031 groundwater dynamics which has been misrepresented in most surface water-oriented
 2032 hydrological models (Miguez-Macho & Fan, 2012; Sutanudjaja et al., 2018). Such modeling
 2033 systems could then be coupled to models of other processes, as recently done by researchers
 2034 aiming at understanding flooding impacts on photosynthesis and biosphere in general (Castro et
 2035 al., 2018), feedbacks between surface waters and atmosphere (M. J. Santos et al., 2019),
 2036 sediment exports and floodplain trapping (Fagundes et al., 2021; Rudorff et al., 2017), carbon
 2037 storage and emissions through wetlands and uplands (Hastie et al., 2019; Lauerwald et al., 2020),
 2038 and dynamics of biogeochemistry cycles at the basin scale or over wetlands (Guilhen et al.,
 2039 2020). All these efforts will require additional RS data, and will move forward our predictability
 2040 of the effects of ongoing environmental changes in the AB.

2041

2042 **6.3. Aquatic ecosystems**

2043 Floodplains are the largest aquatic system in the AB, support a diverse biota and are
2044 important to the biogeochemistry and economy (Hess et al., 2015; Junk, 1997; Junk et al., 2011;
2045 Melack et al., 2009). Amazon floodplains contain thousands of lakes, thousands of km² of
2046 vegetated wetlands and are characterized by large seasonal and inter-annual variations in depth
2047 and extent of inundation. Hydrological conditions are central to the ecological structure and
2048 function of these aquatic ecosystems, and floodplain hydrology is complex because it combines
2049 local inputs and regional-scale fluxes with large spatial variability. Applications of innovations
2050 in RS and hydrological measurements and modeling to the investigation of Amazon floodplains
2051 have led to advances in understanding of the ecology of floodplains, in general.

2052 Key aspects of hydrology relevant to floodplain ecosystems in the Amazon and elsewhere
2053 are the amplitude, duration, frequency, and predictability of variations in discharge and
2054 inundation (Melack & Coe, 2021). Two conceptual frameworks of general relevance to river
2055 systems were motivated by studies in the Amazon. Junk et al. (1989) emphasized the flood pulse
2056 and defined floodplains in terms of river stage, associated physical and chemical conditions, and
2057 adaptations of organisms to these conditions; Junk (1997) elaborated these concepts for the central
2058 Amazon. Mertes (1997) examined hydrologic aspects of inundation of floodplain systems with
2059 RS and simple models, and introduced the concept of the perirheic zone, the mixing zone of
2060 water from the river and local catchment. Both these conceptual developments are supported by
2061 hydrological measurements of Amazon floodplain lakes, the first by Lesack & Melack (1995),
2062 subsequent modeled by Ji et al. (2019) and Bonnet et al. (2008, 2017). Floodplains play an
2063 important role in the carbon balance and nitrogen biogeochemistry of the AB and are sites of
2064 large fluxes of methane and carbon dioxide to the troposphere and high rates of aquatic plant
2065 production. Studies designed to estimate the magnitude and variability of gas fluxes and
2066 productivity in the Amazon have combined RS with field data in innovative ways applicable to
2067 aquatic ecosystems in general. Melack et al. (2004) used habitat-specific methane fluxes in
2068 combination with seasonal changes in the surface water extent of the aquatic habitats derived
2069 from active and passive microwave RS to estimate regional methane fluxes. On the mainstem
2070 Solimões-Amazonas rivers and their fringing floodplains, annual methane emissions were
2071 estimated to vary between approximately 0.7 to 2.4 TgC yr⁻¹ (Melack et al., 2004). Furthermore,
2072 methane fluxes per m² were higher during lower water levels than during high water in an
2073 Amazon floodplain lake, and fluxes in proximity to vegetation were higher than those from
2074 habitats in open water (P. M. Barbosa et al., 2020). Richey et al. (2002) and Melack (2016) also
2075 used estimates of surface water extent to calculate carbon dioxide fluxes. Guilhen et al. (2020)
2076 estimated N₂O emissions from denitrification in Amazonian wetlands by adapting a simple
2077 denitrification model forced by open water surface extent from the Soil Moisture and Ocean
2078 Salinity (SMOS) satellite, and reported a pattern in denitrification linked to inundation.

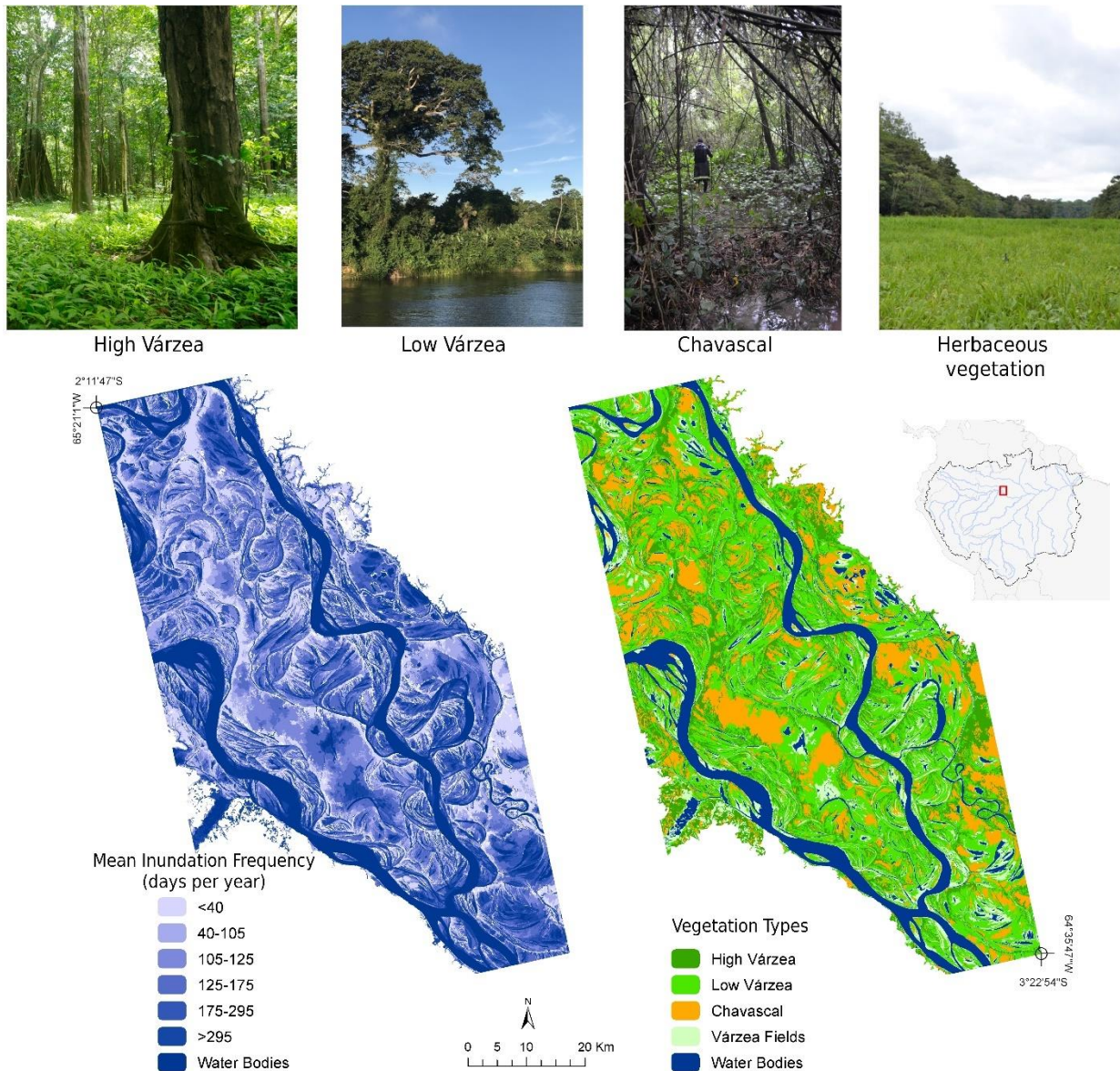
2079 Seminal approaches with RS data were used to delineate inundated area and extent of
2080 flooded forests, open water and herbaceous plants (e.g., Hamilton et al., 2002; Hess et al., 1995,
2081 2003, 2015); Section 4.2) and used to improve estimates of seasonal and interannual variations in
2082 methane fluxes. As described in Section 4.2, new satellite-borne sensors and remote-sensing
2083 products can now be used to update such approaches (e.g., Parrens et al., 2019; Prigent et al.,
2084 2020). These data can be combined with remotely sensed changes in aquatic habitats, recent field

2085 measurements (e.g., Amaral et al., 2020; P. M. Barbosa et al., 2020), and modeling (e.g., Potter
2086 et al., 2014) to significantly improve estimates of emissions. More generally, the vegetative-
2087 hydrologic classification scheme used in these analyses meets the criteria for a “functional
2088 parameterization” of wetlands (Sahagian & Melack, 1998), with classes suitable for
2089 biogeochemical and biodiversity applications

2090 The primary productivity of aquatic plants is often high but challenging to measure,
2091 especially for herbaceous plants with large seasonal and spatial variations. On Amazon
2092 floodplains, productivity of herbaceous aquatic plants is strongly influenced by hydrological
2093 variations (Engle et al., 2008; Junk, 1997). For instance, growth of herbaceous aquatic plants in
2094 floodplain lakes follows water level variation. Extending field measurements of plant
2095 productivity to a regional scale was first done by M. Costa (2005) using SAR estimates of plant
2096 biomass. Lower values were found in regions where plants developed only in the beginning of
2097 the flood season, and higher values in areas closer to the Amazon River, where the availability
2098 and influence of nutrient-rich water is greater. Further work by T. S. F. Silva et al. (2010) and T.
2099 S. F. Silva et al. (2013) used C-band SAR combined and optical data to investigate responses of
2100 horizontal expansion and vertical growth of herbaceous plants to variations in the flooded area
2101 and water level in two large floodplains along the Amazon River. Over the period from 1970 to
2102 2011 vertical growth varied by a factor of 2 and maximum annual cover varied by a factor 1.5.
2103 Years with exceptionally large changes in water level resulted in the highest productivity
2104 because horizontal expansion and vertical growth were both enhanced.

2105 The productivity of Amazon aquatic ecosystems is also related to nutrient supply and
2106 optical conditions within the water (Melack & Forsberg, 2001). Applications of satellite-borne
2107 imaging spectrometers to the optically complex waters of the Amazon have revealed chlorophyll
2108 and suspended sediment levels (e.g., C. C. F. Barbosa et al., 2009; Novo et al., 2006; Section
2109 4.4), which are related to planktonic productivity. Other studies employing data from optical
2110 sensors have been used to describe aquatic vegetation (e.g., Josse et al., 2007; Novo &
2111 Shimabukuro, 1997; Wittmann et al., 2002), and indicate fluvial dynamics (Constantine et al.,
2112 2014; Mertes et al., 1995), both important aspects of aquatic ecosystems. However, observations
2113 with optical RS are frequently impeded by cloud cover or smoke, and forest canopies are often
2114 too dense to allow detection of flooding. Alternatively, time series of SAR data are available for
2115 several subregions within the AB and can be used to generate high-resolution maps of vegetation
2116 and inundation. For example, Ferreira-Ferreira et al. (2015) used a hydrologically-based time
2117 series of ALOS/PALSAR-1 SAR data to distinguish between land cover classes and map water
2118 extent and mean flood duration (**Figure 12**). The authors depicted the uneven distribution of
2119 flooded areas at different water levels, i.e., some water level stages result in large expansions of
2120 the inundated areas while other stages have less effect.

2121



2122

2123 **Figure 12.** Major vegetation types and estimated mean flood duration maps in the Mamirauá
 2124 Sustainable Development Reserve, Central Amazon, Brazil (Adapted from Ferreira-Ferreira et
 2125 al., 2015). The maps were based on a time series of ALOS/ PALSAR-1 image data comprising
 2126 nine dates between 2007 and 2010 chosen to provide the largest and most uniform range of water
 2127 level conditions within the available imagery for the area. The water bodies were derived from
 2128 the flood class of 365 days per year on average, i.e., permanent water bodies. More details on
 2129 Ferreira-Ferreira et al. (2015).

2130

2131 Complex flow patterns, revealed by interferometric SAR analyses (Alsdorf et al., 2007),
 2132 and differences in sources of water, evident in hydrological models (Bonnet et al., 2017; Ji et al.,
 2133 2019), account, in part, for the variations in nutrients, suspended sediments, and productivity
 2134 (Forsberg et al., 2017). A further example of how advances in hydrological modeling contributed

2135 to the understanding of Amazon floodplains is provided by Rudorff et al. (2014a, 2014b). They
2136 added a simple model of hydrological balance to the LISFLOOD-FP hydraulic flooding model
2137 and applied it over 15 years. This work also emphasized the importance of detailed topography
2138 which they derived from a combination of data from the SRTM with extensive echo-sounding.
2139 The model simulated well changes in water level, flooding extent, and river-floodplain flows.
2140 Rudorff et al. (2017) combined these results with measurements of suspended sediments to
2141 demonstrate variations in sediments supply and loss from the floodplain.

2142 Variations in the distribution and inundation of floodplain habitats play a key role in the
2143 ecology and production of many commercially important fish in Amazonia. Lobón-Cerviá et al.
2144 (2015) demonstrated that number of fish species and their abundance were directly related to
2145 presence of flooded forests and inversely related to distance from the river. Arantes et al. (2018)
2146 used both Landsat and SAR data to characterize aquatic habitats and found that spatial patterns
2147 of fish biodiversity on Amazon floodplains were associated with forest cover and landscape
2148 gradients. Additional examples of connections between fisheries and fish ecology are provided in
2149 Melack et al. (2009) and Melack et al. (2021).

2150 Tree phenology on both fertile, eutrophic floodplains (várzea) and nutrient-poor,
2151 oligotrophic floodplains (igapó) follow variations in inundation (Junk et al., 2010). Seasonal
2152 inundation also provides connectivity that is critical for gamma diversity (Thomaz et al., 2007;
2153 Ward et al., 2002). Avian diversity varies among the aquatic habitats (Cintra, 2015; Laranjeiras
2154 et al., 2021). At the community level on large river floodplains, birds and fishes have more stable
2155 communities in environments with rhythmic annual floods (Jardine et al., 2015; Luz-Agostinho
2156 et al., 2009). In a floodplain lake near the confluence of Amazon and Negro rivers, for instance,
2157 Röpké et al. (2017) detected an abrupt and persistent change in fish assemblage structure that
2158 lasted for more than a decade after the extreme drought of 2005.

2159 Disturbances of the natural variations of flooded area, hydrological connectivity or land
2160 cover are disruptive for wetland systems. Resende et al. (2019) used SAR RS to assess the
2161 impacts of the Balbina dam to the downstream igapó forests in the Uatumã River. The authors
2162 showed that 12% of the floodplain forests died because of the altered flood pulse and another
2163 29% of the remaining living forest stands may be undergoing mortality. Schöngart et al. (2021)
2164 provide further evidence for changes in floodplain forests below the Balbina dam over 35 years.
2165 Castello et al. (2018) combined fisheries data and habitat coverage derived from SAR analyses to
2166 determine effects of land cover change on fishery yields. They showed that removal of flooded
2167 forests can reduce fish yields and that other floodplain habitats cannot replace forest removal to
2168 improve fish yields.

2169 Several challenges and knowledge gaps remain in the linkage of hydrology to the
2170 functioning of aquatic ecosystems in the AB and elsewhere. Wet soil without standing can have
2171 high rates of biogeochemical processes such as methane release. While difficult to detect with
2172 RS, models offer promise if operating at the correct scales. Streams and small rivers as well as
2173 ponds can release disproportionately high amounts of carbon dioxide, but their surface areas are
2174 seldom known; high spatial resolution RS products will help alleviate this problem. Interfluvial
2175 and savanna wetlands, often inundated by rain rather than rivers, are not well represented by
2176 basin-scale hydrological models and will require fine-scale topographic data combined with
2177 multi-temporal RS of inundation. Within the AB, particularly large data gaps exist in the Llanos

2178 de Moxos (Bolivia), peatlands in the Pastaza-Marañón foreland basin (Peru), and coastal
2179 freshwater wetlands.

2180

2181 **6.4. Environmental changes**

2182 In the last decades, the Amazon has been subject to large environmental changes.
2183 Extensive rainforest areas have been deforested, being converted to pasturelands, croplands, or
2184 mining. These land cover changes alter the partitioning of precipitation into evapotranspiration,
2185 surface runoff and deep drainage, transport of sediments, river discharge and river color, and
2186 influence the processes of formation of rainfall in Amazonia. At the same time, forest areas have
2187 been flooded by artificial dams to produce hydropower, affecting flood pulses downstream of the
2188 dam, while the forests' ecohydrology has adapted to the flood patterns. RS has been an important
2189 tool to detect and map these environmental changes and their impacts on the hydrological cycle.

2190 The role of deforestation on the AB hydrological cycle could only be understood after
2191 large-scale mapping of land use and land cover (LULC) in Amazonia. The first of these maps
2192 were produced by Cardille et al. (2002). They merged RS imagery from AVHRR with
2193 agricultural census data to produce a spatially-explicit LULC map for the Amazon and Tocantins
2194 basins for 1995. Based on this dataset and agricultural census data for 1960, M. H. Costa et al.
2195 (2003) evaluated how land use increases in the upper Tocantins basin affected its discharge from
2196 1949-1969 to 1979-1999. Although precipitation did not change significantly from the former to
2197 the latter period, the annual mean discharge increased by 24% ($P < 0.02$), while the rainy season
2198 discharge increased by 28% ($P < 0.01$), and seasonal peaks occurred about one month earlier.
2199 Such variations could be credited both to reduced ET and reduced infiltration during the rainy
2200 season. The reduction in evapotranspiration is a consequence of three factors: the increased
2201 albedo reduces the net radiation at the surface; the reduced roughness length decreases
2202 atmospheric turbulence, weakening vertical motions; and the reduced root depth leaves less soil
2203 moisture available to plants. Additional factors that can also influence local evapotranspiration
2204 include compaction of the soil surface or sub-surface and reduction of leaf area index through
2205 grazing (M. H. Costa, 2005).

2206 Other LULC maps were produced for the Brazilian Amazon using similar techniques
2207 (Leite et al., 2011 for 1940-1995; L. C. P. Dias et al., 2016 for 1940-2012). Purely RS products
2208 are available for more recent periods, like the MODIS MOD44 tree cover product (2002-recent),
2209 Landsat-based PRODES (1988-recent, <http://www.obt.inpe.br/prodes/>) and TerraClass (2004-
2210 2014, <https://www.terraclass.gov.br/>) official government products for the Brazilian Amazon,
2211 and MapBiomass for the Pan-Amazonia (1985-recent, <https://mapbiomas.org/>). Several authors
2212 have used these datasets to study the effects of LULC changes on the hydrological regime of
2213 several of the Amazon tributaries and the Amazon-Cerrado arc-of-deforestation as a whole (M.
2214 E. Arias et al., 2018; Cavalcante et al., 2019; Coe et al., 2011; Levy et al., 2018; Panday et al.,
2215 2015), generally finding increased mean and low-flow discharge with deforestation.

2216 In addition to river discharge, LULC changes may also affect the precipitation,
2217 particularly during the beginning and end of the rainy season. The first evidence of this was
2218 provided by Butt et al. (2011). They compared four Landsat-based land cover maps from 1975 to
2219 2005 against the rainy season onset dates calculated from daily rain gauge data, concluding that,
2220 for stations that lie inside the major deforested area, the rainy season's onset has significantly

2221 shifted to, on average, 11 days (and up to 18 days) later in the year over the last three decades.
2222 However, for stations that lie in areas that have not been heavily deforested, the onset has not
2223 shifted significantly. Recent studies confirmed these results. Repeating the same analysis for
2224 southern Amazonia from 1974 to 2012, and after removing regional trends and interannual
2225 variability, Leite-Filho et al. (2019) confirmed a delay in the onset of 1.2–1.7 days per each 10%
2226 increase in deforestation. In addition, the probability of occurrence of dry spells in the early and
2227 late rainy season is higher in areas with greater deforestation.

2228 Moreover, using daily rainfall data from the Tropical Rainfall Measurement Mission
2229 3B42 product and the L. C. P. Dias et al. (2016) 1-km land-use dataset, Leite-Filho et al. (2020)
2230 evaluated the quantitative effects of deforestation on the onset, demise, and length of the rainy
2231 season in southern Amazon for 1998–2012. After removing the effects of geographical position
2232 and year, they verified a relationship between onset, demise, and length of the rainy season and
2233 deforestation. Onset delays $\sim 0.4 \pm 0.12$ day, demise advances $\sim 1.0 \pm 0.22$ day, and length
2234 decreases $\sim 0.9 \pm 0.34$ day per each 10% deforestation increase relative to the existing forested
2235 area ($P < 10^{-5}$ in all three trends).

2236 Another breakthrough owned to RS was identifying the “deforestation breeze” effect,
2237 which affects rainfall distribution. Khanna et al. (2017) used remotely-sensed land-use,
2238 precipitation, and cloudiness data combined with a regional climate model, finding that small-
2239 scale deforestation patches trigger thermally-driven atmospheric circulation cells in Rondônia.
2240 This circulation creates a precipitation anomaly dipole over the deforested area, with enhanced
2241 precipitation downwind and suppressed precipitation upwind in the thermal cell's descending
2242 branch. The observed dipole in Rondônia is substantial, with the precipitation change in the two
2243 regions being $\pm 25\%$ of the deforested area mean.

2244 Although several techniques to infer surface water and channel properties from RS have
2245 been developed in recent years (as described in Section 4), there are still relatively few studies
2246 that apply these techniques to assess how anthropic and natural environmental changes affect
2247 these properties in the AB. Latrubesse et al. (2017) used tree cover data from Hansen et al.
2248 (2013), Landsat images, and RS estimates of TSS of Park & Latrubesse (2014) to investigate the
2249 current and potential impacts of dams in the basin. They found that the Santo Antônio and Jirau
2250 dams caused a 20% reduction in mean surface suspended sediment concentration in the Madeira
2251 River, despite unusually high flood discharges in the years analyzed after their start-of-operation.
2252 They also used Landsat images to calculate channel migration rates for each sub-basin, finding
2253 an average migration rate of $0.02 \pm 20\%$ channel widths per year.

2254 Satellite retrieval of TSS has also been used to document trends in the Amazon River's
2255 main stem, although there is no apparent consensus on the causes of the observed trends. Such
2256 techniques allow for expansion and extrapolation of field datasets, being especially useful in the
2257 Amazon since runoff and TSS are poorly correlated at the Amazon River's lowest reaches due to
2258 asynchronism of the peak water discharges of the Solimões, Madeira, and Negro rivers (Filizola
2259 & Guyot, 2009). J. M. Martinez et al. (2009) used 18 TSS sampling campaigns from 1995 to
2260 2003 and MODIS images to obtain a 12-year (1995–2007) continuous series of TSS at the
2261 Óbidos station, the last gauge station in the Amazon river before it reaches the Atlantic Ocean.
2262 They find a 20% increase in sediment discharge in the period with no discernible trends in water
2263 discharge and cite changes in land use and rainfall patterns as likely explanations. Recently, Li et
2264 al. (2020) used similar techniques to obtain an updated (1996–2018) time series of TSS and find

2265 that sediment loading increased until 2007 but decreased afterward. They infer that this reversal
2266 is due to decreased sediment contribution from the Madeira river after the construction of the
2267 Santo Antônio and Jirau dams in the late 2000s, in agreement with Latrubesse et al. (2017).

2268 Montanher et al. (2018) used similar techniques to generate an extended 32-year (1984-
2269 2016) time series of suspended sediment transport (SST, the product of TSS by river discharge).
2270 They argued that there is a recurrent pattern of SST rising and falling in cycles likely associated
2271 with climate fluctuations and that trends such as those observed by J. M. Martinez et al. (2009)
2272 are a consequence of short time series. However, SST depends on river discharge variability, and
2273 J. M. Martinez et al. (2009) and Li et al. (2020) found no trends in river discharge in their shorter
2274 time series.

2275 Some studies also investigated the impact of mining on suspended solids in sub-basins of
2276 the Amazon. Artisanal and small-scale mining, especially gold, is common in some regions, such
2277 as the Tapajós River basin. These small mining operations often use low-end techniques such as
2278 water jets and dredges that can cause proportionally high land degradation levels and water
2279 contamination (Lobo et al., 2018). They are also often illegal and unregistered, making RS an
2280 important tool for identifying and mapping these activities. The only publicly available dataset
2281 (to our knowledge) on mining areas in the AB is the TerraClass project, which is based on visual
2282 interpretation of Landsat images and is available only for a few years between 2004-2014. Lobo
2283 et al. (2018) combined multiple datasets to develop an automated classification method that can
2284 distinguish between industrial and small-scale mining and ore types based on Sentinel-2. They
2285 found that in 2017 64% of the total mining area in the several key mining regions in the basin
2286 was comprised of small-scale gold and tin mining.

2287 Lobo et al. (2015) estimated total suspended solids (TSS) in the Tapajós River basin
2288 based on Landsat images. They found that increases in TSS are strongly associated with reported
2289 increases in mining activity at seasonal and decadal timescales. Lobo et al. (2016) updated the
2290 Landsat-based identification of mining areas from the TerraClass project. They described the
2291 evolution of mining areas in the same basin, identifying different eras of mining impacts on TSS
2292 related to the introduction of different technologies and variations in the gold price. Comparing
2293 sub-basins with different kinds of land alteration, they also indicated that mining activities have a
2294 much higher effect on TSS than deforestation for agricultural purposes.

2295 Landsat images have also been used to document and understand a major hydro-
2296 morphological event in the Amazon: the recent capture of almost all of the water flow from the
2297 Araguari River by the Amazon River (E. S. dos Santos et al., 2018). The Araguari is a large
2298 river, with an average annual discharge $>1000 \text{ m}^3 \text{ s}^{-1}$, which used to flow directly to the Atlantic
2299 Ocean until the rapid formation of the Urucurituba channel connecting it to the Amazon River in
2300 the early 2010s. The initial headwater migration of the proto-Urucurituba was likely associated
2301 with deforestation for buffalo farming around 2007. The first connection to the Araguari was
2302 attributed to a high flow event in 2011. The rapid growth of the channel, which increased in
2303 width by about 5 m per month until 2015, is likely a consequence of complex hydro-
2304 morphodynamic processes related to tidal currents and estuarine deposition that ultimately led to
2305 the blockage of the Araguari River mouth. This channel's formation caused large changes in the
2306 hydraulic pattern, sediment dynamics, and ecosystems in the Araguari estuary, being the first
2307 known observation of estuarine distributary network development by headwater erosion.

2308 RS techniques contributed input, calibration, and validation data to many models that
2309 provided important insights on the consequences of environmental changes in the AB (see
2310 Section 6.2). These models can integrate hydrological, hydraulic, climate, and land-use processes
2311 and are important tools in many studies investigating the impacts of past and future changes in
2312 the environment. A main application of these models is to analyze future scenarios (e.g., climate
2313 change, deforestation). Another application is attributing the effects of different processes in the
2314 variability of the observed data.

2315 Sorribas et al. (2016) examined climate change projections on discharge and inundation
2316 extent in the AB using the regional hydrological model MGB with 1-dimensional river hydraulic
2317 and water storage simulation in floodplains forced by five GCMs IPCC's Fifth Assessment
2318 Report CMIP5. The model was validated against a mix of in situ and RS data. Results indicate an
2319 increased mean and maximum river discharge for large rivers draining the Andes in the
2320 northwest contributes to increased mean and maximum discharge and inundation extent over
2321 Peruvian floodplains and Solimões River in western Amazonia. In contrast, decreased river
2322 discharges (mostly dry season) are projected for eastern basins and decreased inundation at low
2323 water in the central and lower Amazon.

2324 With the renewed interest in the last decades in constructing hydroelectric dams in the
2325 AB (Castello & Macedo, 2016), many modeling studies attempted to quantify the environmental
2326 impacts of new and existing dam projects. Forsberg et al. (2017) used several models to evaluate
2327 the impacts of six planned dams in the Andean region of the Amazon. Since a sizable portion of
2328 sediment production in the basin occurs in this region, these dams are predicted to reduce the
2329 basin-wide supply of sediments, phosphorus, and nitrogen by 64%, 51%, and 23%, respectively.
2330 Along with changes in nutrient and sediment supply, mercury dynamics and flood pulse
2331 attenuation are projected by the authors to cause major impacts on downstream aquatic and
2332 floodplain fertility and channel geomorphology. Indeed, Resende et al. (2019) found massive
2333 tree mortality in floodplain forests (igapó) downstream of the Balbina reservoir using SAR
2334 images, with about 40% of the igapó 49 km downstream of the reservoir either dead or
2335 undergoing mortality.

2336 Expected environmental changes in the basin, such as deforestation and climate change,
2337 can also significantly impact hydropower production itself, often leading to generation well
2338 below the dam's expected capacity. Most recent dam designs follow a run-of-the-river concept,
2339 avoiding the large environmental impacts of enormous reservoirs from older designs but making
2340 power generation more dependent on river discharge variations (M. H. Costa, 2020). M. E. Arias
2341 et al. (2020) combine a land-use and a hydrological model to assess the direct impacts of climate
2342 change and deforestation on hydropower production of existing and planned dams in the Tapajós
2343 basin. Although decreasing evapotranspiration from deforestation tends to increase annual mean
2344 discharge, reduced water retention increases surface runoff and flash flows during the rainy
2345 season and reduces discharge during the dry season. Since turbines are normally working at
2346 maximum capacity in the rainy season, this excess flow is wasted, and generation in the dry
2347 season is reduced. M. E. Arias et al. (2020) find that projected climate change and deforestation
2348 combined can delay peak energy generation by a month (worsening the mismatch between peak
2349 production and consumption), reduce dry season generation by 4-7% and increase interannual
2350 variability of power production by 50-69%.

2351 Deforestation has the indirect effect of reducing precipitation and delaying the onset of
 2352 the rainy season, which further illustrates the dependency of hydropower generation on forests.
 2353 Stickler et al. (2013) combine land-use, hydrological, and climate models to assess the direct and
 2354 indirect effects of deforestation alone on hydropower generation of the Belo Monte energy
 2355 complex in the Xingu River basin. They find that when considering only the direct effects of
 2356 deforestation on river flow, a 20-40% deforestation of the basin would lead to a 4-12% increase
 2357 in mean discharge with similar increases in power generation. However, when the climate effects
 2358 of deforestation of the Amazon region were considered, rainfall inhibition in the basin
 2359 counterbalanced the direct effects and led to a 6-36% reduction in discharge. Under the business-
 2360 as-usual deforestation scenario for 2050 (40% of the Amazon forest removed), they simulated
 2361 that power generation was reduced to 25% of maximum plant output.

2362

2363 **7. Synthesis of scientific advances, future challenges and priorities**

2364 The various achievements of more than three decades of scientific advances on the
 2365 hydrology of the AB with satellite data, along with the development of new RS techniques, and
 2366 some selected research opportunities, are summarized in **Table 7** and **Table 8**. Section 7.1
 2367 presents the main findings obtained in the AB, which has been a RS laboratory for hydrology
 2368 advancement. Section 7.2 highlights how these experiences can be used to foster the
 2369 understanding of the water cycle in other large river basins worldwide. Section 7.3 discusses the
 2370 knowledge gaps and research opportunities on AB waters, thanks to an unprecedented and
 2371 continued monitoring of AB with upcoming and future satellite missions. Finally, Section 7.4
 2372 discusses how to move forward from scientific advances toward more sustainable water
 2373 resources and risk management, and Section 7.5 highlights recommendations for future studies
 2374 on Amazon waters from space.

2375

2376 **Table 7.** Synthesis of scientific advances in understanding the Amazon hydrology with RS

Variable	Seminal developments in RS performed in Amazon	Breakthrough lessons about Amazon / General hydrology learnt from RS	Knowledge gaps and new opportunities for the Amazon
Precipitation	1) Spatial distribution of rainfall at regional scale (Espinoza et al. 2009). 2) Rain trend over the last few decades (Paca et al. 2020).	1) Spatial distribution of "hot-spot" regions (Chavez & Takahashi, 2017; Espinoza et al., 2015). 2) Reduced rainfall over main rivers (Paiva et al., 2011). 3) Rainforest inducted early wet season onset (Wright et al., 2017).	1) Improved algorithms for orographic rains (Dinku et al., 2011; Toté et al., 2015). 2) Strategic network of rain gauges. 3) Low-cost satellite constellation (Peral et al., 2019).

Evapotranspiration	<ol style="list-style-type: none"> 1) Water flux estimates in the tropics at large scales (Fisher et al., 2009). 2) Observational data for model calibration and validation and multi-model assessments (Rocha et al., 2009; Goncalves et al., 2013). 	<ol style="list-style-type: none"> 1) Understanding of environmental drivers and <i>ET</i> seasonality basin-wide, with more energy limitation and small seasonality in the wettest parts (central Amazon), and the opposite in southern ones. 2) Decreasing <i>ET</i> due to deforestation and cropland expansion (Spera et al., 2016; Zemp et al., 2017; Oliveira et al., 2019). 	<ol style="list-style-type: none"> 1) Modeling high spatial resolution (< 30 m) <i>ET</i> estimates on long time series (> 40 yr). 2) Combining surface energy balance (SEB) models and models less dependent on land cover parameterization. 3) New data fusion techniques using multiple RS sources (multispectral, thermal and microwave) to reduce the cloud cover effects on SEB approaches.
Surface water elevation (SWE)	<ol style="list-style-type: none"> 1) Large scale water level and slope estimates by radar altimetry (Guskowska et al 1990; Birkett et al 2002). 2) Water level changes from interferometry estimates (Alsdorf et al 2000; 2007). 3) Monitoring of SWE and level-discharge rating curves in ungauged rivers (Silva et al 2014; Paris et al 2016). 	<ol style="list-style-type: none"> 1) Characterization of water level variation in rivers and wetland forests (Birkett et al 2002; Alsdorf et al 2003, 2007). 2) River-floodplain connectivity (Park et al 2020, Alsdorf et al 2003). 3) Flood storage in river-wetland systems (Frappart et al 2005, Alsdorf, 2003). 	<ol style="list-style-type: none"> 1) 2D characterization of water levels (SWOT swath data; Biancamaria et al 2016). 2) Finer spatio-temporal resolution for water level and slope. 3) New techniques for fusion with local to regional modeling (Yamazaki et al 2011; Paiva et al 2013).
Surface water extent	<ol style="list-style-type: none"> 1) First large scale extent and variability of surface water and inundations in floodplains (Sippel et al., 1994; Hess et al. 2003). 2) Relationship between surface water extent and discharge (Sippel et al., 1998). 3) High resolution floodplains dynamic and discrimination of aquatic vegetation types for large area (Ferreira-Ferreira 2015). 	<ol style="list-style-type: none"> 1) Seasonal and interannual inundation patterns in the AB (Hamilton et al., 2004; Hess et al., 2015, Aires et al., 2017). 2) Contribution of inland water and floodplains variability to the Amazon Carbon cycle and emissions (Richey et al., 2002, Raymond et al. 2013, Melack et al., 2004). 	<ol style="list-style-type: none"> 1) Finer spatio-temporal resolution of surface water and floodplain inundation extent variability with SWOT and NISAR. 2) New development of fusion techniques with IA to combine various RS observations (visible, IR, microwave, GNSS-R). 3) Ensure long term observations to monitor climate/anthropogenic changes.
Floodplain and river channels topography	<ol style="list-style-type: none"> 1) Adjustment of Digital Elevation Models (Yamazaki et al 2012, Baugh 2013). 2) Topography estimates in seasonally flooded areas (Fassoni et al 2020). 	<ol style="list-style-type: none"> 1) Characterization of floodplain channels and lakes (Sippel 1997, Trigg 2012; Fassoni 2020). 2) Assessment of river channel migration (Constantine et al., 2014; Santos et al., 2018). 	<ol style="list-style-type: none"> 1) Characterization of topography in flooded forests. 2) Long term estimation to monitor geomorphological changes in floodplain and river channels.
Water quality: Sediments, chlorophyll and colored dissolved organic matter	<ol style="list-style-type: none"> 1) Estimates of sediment concentration in rivers (Bayley & Moreira, 1978; Mertes et al., 1993), chlorophyll in floodplain lakes (Novo, 2006), and colored dissolved organic material in lakes (M. P. da Silva et al., 2019). 2) Semi-analytical algorithms for water quality estimates (Bernini et al. 2019, Maciel et al. 2020, Sander de Carvalho et al. 2015). 	<ol style="list-style-type: none"> 1) Spatiotemporal dynamics maps of the underwater light field and optically active constituents (Novo et al. 2006, Martinez et al. 2009, Maciel et al. 2019, 2020; Fassoni et al., 2019). 2) Extended time-series of suspended sediments in the Amazon Region (Montanher et al. 2018, Martinez et al. 2009, Li et al. 2020). 	<ol style="list-style-type: none"> 1) Evaluation of phytoplankton community dynamics using RS as a proxy for biodiversity indicator in Amazon waters. 2) Robust algorithms for CDOM and Chlorophyll-a retrieval in optically complex inland waters.

<p>Total water storage (TWS) and groundwater storage (GWS)</p>	<p>1) Large scale estimates of the TWS using GRACE data (Tapley et al., 2004). 2) Determination of GWS changes using RS products and model outputs (Frappart et al., 2011).</p>	<p>1) Spatial signatures of droughts and floods in TWS (Chen et al., 2009). 2) Spatio-temporal signatures of droughts on surface water storage (Frappart et al., 2012; Papa et al., 2013). 3) Temporal variations of GWS (Frappart et al., 2019).</p>	<p>1) More accurate estimates of surface water storage from SWOT will improve the determination of GWS anomalies. 2) Long-term monitoring of TWS and GWS (GRACE and GRACE-FO).</p>
---	---	---	--

2377

2378

2379

Table 8. Synthesis of scientific advances in multidisciplinary and integrative efforts in understanding of the AB hydrology and ecosystems

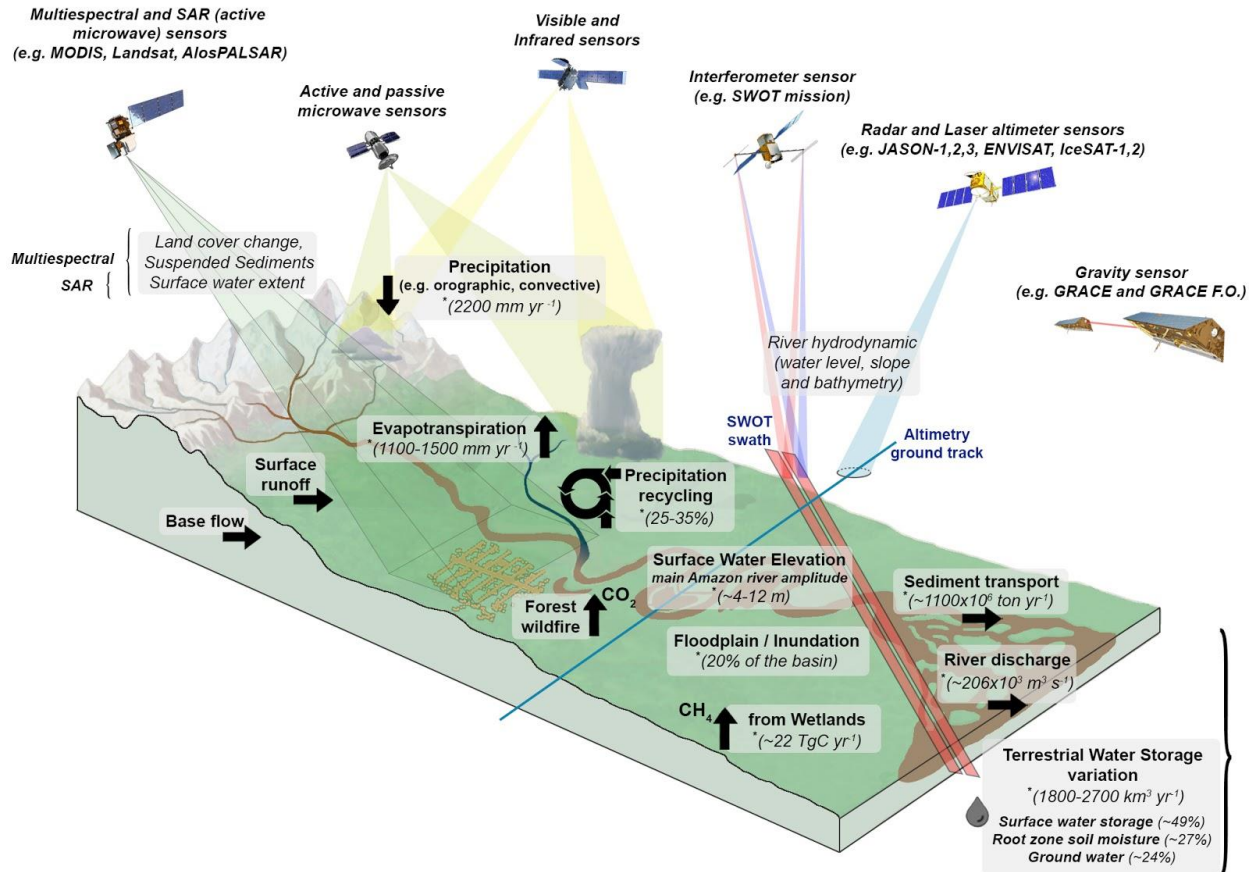
	<p>Breakthrough lessons about Amazon / General hydrology learnt</p>	<p>Knowledge gaps and new opportunities for the Amazon</p>
<p>Water budget</p>	<p>1) Sub-basin scale water cycle analysis (Azarderakhsh et al. 2011). 2) Water budget closure enforcement (Pan et al 2012). 3) Continuous river discharge estimate based on water cycle closure with satellite estimate.</p>	<p>1) Finer spatio-temporal resolution of the water budget analysis using river map information. 2) Sensitivity of the closure to the water component bias in particular ET estimate. 3) Groundwater exchange estimate might be obtained at fine scale in constraining the water cycle at the surface.</p>
<p>Modeling the Amazon water cycle and its wetlands</p>	<p>1) River-floodplain hydrodynamic interactions at local and large scales (Wilson et al., 2007; Paiva et al., 2013; Rudorff et al., 2014; Sorribas et al 2020). 2) Groundwater dynamics across scales and climates, and floodplain-groundwater interaction (Miguez-Macho & Fan, 2012). 3) TWS components (surface, subsurface) at basin scale (Paiva et al., 2013; Pokhrel et al, 2013).</p>	<p>1) Finer spatio-temporal resolution of flood dynamics, considering sedimentation processes, in diverse wetland types (floodplains and interfluvial). 2) Better parameterization of groundwater processes across the AB. 3) Lack of convergence among water storage partition (e.g., divergent estimates of surface water fraction).</p>
<p>Aquatic ecosystems</p>	<p>1) Integration of temporal and spatial variations of inundation and associated aquatic habitats into estimation of carbon dioxide and methane fluxes to the atmosphere (Richey et al. 2002; Melack et al. 2004). 2) Areal estimation of major aquatic habitats in Amazon, and seasonal and interannual variations in the areas (Melack and Hess 2010; Hess et al. 2015). 3) Biomass and growth of aquatic plants on floodplains (Costa 2010, Silva et al. 2014).</p>	<p>1) Extent of saturated soils under forests and in riparian corridors. 2) Modeling of inundation variations in interfluvial wetlands and savanna wetlands. 3) Areal extent of streams and small rivers, especially in Andean region. 4) High-resolution topographic data on floodplains.</p>
<p>Environmental changes</p>	<p>1) Effects of changes in land use on the river discharge (Costa et al. 2003). 2) Influence on changes in land use on onset of the rainy season (Butt et al. 2011; Leite-Filho et al. 2019) and duration of the rainy season (Leite-Filho et al. 2020).</p>	<p>1) Need to better understand the interactions between local changes in land use and large-scale climate mechanisms on the water cycle of the AB. 2) Initiate monitoring of forest degradation in its different forms, so that the long-term effects on forest hydrology can be studied. 3) Apply existing techniques to assess changes in water and floodplain properties caused by anthropic changes (land use change, damming, mining).</p>

2380

2381 **7.1. The Amazon Basin as a remote sensing laboratory for hydrology**

2382 As the largest river basin in the world, characterized by strong hydrological signals in
 2383 precipitation, evapotranspiration, water storage change and discharge, the AB has been an ideal
 2384 laboratory for the seminal development of RS techniques and their applications to foster our
 2385 understanding of hydrological processes. **Table 7** summarizes for various hydrological variables
 2386 key seminal developments made in the RS field over AB along with breakthrough lessons learnt
 2387 regarding AB hydrological functioning. Additionally, **Figure 13** illustrates the major
 2388 characteristics of AB hydrological storages and fluxes as characterized by RS observations and
 2389 analyses. Over the past decades, the need to understand the ongoing environmental changes in
 2390 the AB, that could impact the global water, energy and carbon cycles, has motivated a series of
 2391 multidisciplinary and integrative efforts that foster scientific advances in our understanding of
 2392 AB hydrology and ecosystems (**Table 8**).

2393



2394

2395 **Figure 13.** Schematic illustration of the integrated hydrological processes of the water cycle in
 2396 the AB. The main sensors on board orbiting satellites that have helped measure these processes
 2397 are indicated. The annual estimates of each component averaged over the entire basin are shown.
 2398 The references (*) related to these estimates are provided along the text in Section 7.1.

2399

2400 Advances in precipitation estimates from RS have allowed the characterization of the
2401 spatial and temporal distributions of rainfall at local to regional scale over AB and provide
2402 records long enough to assess rainfall trends over the last few decades (**Table 7** and **Table 2** for
2403 developed precipitation products). The average rainfall in the AB was estimated as 2200 mm yr⁻¹
2404 (**Figure 3**), and the heaviest rainfall occurs in hot-spot regions in the Andes mountain ranges
2405 initiated by convection processes altered by the topography, where rainfall can reach values
2406 higher than 6000 mm yr⁻¹ (Chavez & Takahashi, 2017; Espinoza et al., 2015; **Figure 3**). Large-
2407 scale analysis of RS-derived precipitation revealed the effect of winds over large water bodies
2408 that causes reduced rainfall over these areas (Paiva et al., 2011).

2409 RS observations were key to providing the first large-scale estimates of
2410 evapotranspiration in tropical regions, especially over AB, and also provided unprecedented
2411 observational data for the evaluation, calibration and validation of models (**Table 2**).
2412 Furthermore, RS allowed the characterization of *ET* temporal and spatial variability over the AB
2413 (**Figure 4**) and the understanding of its environmental drivers, revealing contrasting regimes
2414 between the more energy-limited ones in the equatorial part of the basin, and more water-limited
2415 regimes in the southern areas (Maeda et al., 2017). AB annual average evapotranspiration is
2416 estimated as 1100 to 1500 mm yr⁻¹ (based on SSEBop, MOD16, PML, and GLEAM global
2417 models - **Figure 4**, and water balance by Builes-Jaramillo & Poveda (2018), with higher rates in
2418 the northern portions, as in the Negro River basin, decreasing towards the southern parts (Baker
2419 et al., 2020; Maeda et al., 2017). Various RS-based approaches result in significant divergences
2420 in the estimation of evapotranspiration over AB (**Figure 4** and **Figure 10**). For instance, RS-
2421 based *ET* annual rates at the AB scale were 15-37% higher than those obtained from water
2422 balances (Baker et al., 2020).

2423 The characterization of continental water surfaces, including their elevation and extent,
2424 was possible thanks to adaptations of satellite techniques not primarily designed for applications
2425 to hydrology or inland water monitoring. A striking example is that of altimetry satellite
2426 missions, initially designed for the observation of the ocean, but with promising applications to
2427 the large rivers of the Amazon (Guzkowska et al., 1990) and with the potential to derive SWE of
2428 rivers and lakes. Since then, various altimetry databases for the global monitoring of lakes and
2429 rivers have been developed (**Table 3**). The SAR differential interferometry technique, originally
2430 developed in geophysics, was also tested and applied for the first time in central Amazon
2431 floodplains to characterize SWE changes (Alsdorf et al., 2000). Both altimetry and SAR
2432 techniques were important to characterize SWE variations in AB rivers and their connectivity
2433 with the floodplains (Park, 2020). The water surface gradient of the Amazon River varies both
2434 spatially and temporally, with values ranging from 1.5 cm km⁻¹ (800–1020 km upstream) to 4.0
2435 cm km⁻¹ (2900–4000 km upstream; Birkett et al., 2002). The monomodal flood pulse of the main
2436 Amazon River is well captured with radar altimetry (~4-12 m amplitude; **Figure 5**). This pulse
2437 controls the SWE variations in the central Amazon floodplains. During the annual flood, the
2438 SWE variations in rivers and adjacent floodplains, as seen from SAR or altimetry, are similar
2439 (Alsdorf et al., 2007), but connectivity is reduced during the low-water period (Park, 2020) as the
2440 flows are controlled by the local topography (Alsdorf et al., 2007) and SWE in both
2441 environments is not always equivalent (Alsdorf, 2003).

2442 The first large-scale surface water extent mapping from RS was also carried out for the
2443 AB (Sippel et al., 1994). Many estimates and databases, using a wide range of sensors, have been
2444 developed since then at different spatial and temporal scales (**Table 4**). These include innovative
2445 high resolution mapping of wetlands and flooded vegetation using L-band SAR (Hess et al.,
2446 2003), which provided the first estimates of flood extent in the entire Amazon wetlands, ranging
2447 between 285×10^3 and 635×10^3 km² in periods of low (Oct-Dec) and high waters (Apr-Jun),
2448 respectively (Hess et al., 2015; **Figure 6**). Significant differences among various RS-based
2449 estimates of surface water extent exist over AB (**Figure 6**), with in general lower maximum
2450 flooded area found by coarse scale products as compared to SAR-derived maps. Seminal
2451 approaches with RS data were used to delineate AB large-scale surface water area and extent of
2452 flooded forests, open water and herbaceous plants, revealing their complex seasonal and
2453 interannual patterns influenced by local and regional-scale variability (Filipe Aires et al., 2017;
2454 Hamilton et al., 2004; Hess et al., 2015; Melack & Hess, 2010). While the width of the Amazon
2455 River floodplain is similar throughout the central Amazon, the area of flooded forest decreases
2456 from upstream to downstream, where both the number and size of open water lakes increases
2457 (Hess et al., 2015; Mertes et al., 1996).

2458 Mapping surface water extent in the AB, in combination with field data, enabled
2459 pioneering regional estimates of methane emissions (**Table 7**), with an estimate of methane
2460 emissions of ~ 22 Tg C yr⁻¹ for the lowland basin (Melack et al., 2004). The spatial configuration
2461 of the Amazon floodplain habitats in relation to vegetation types is related to flooding patterns
2462 (**Figure 13**; Ferreira-Ferreira et al., 2015). Herbaceous aquatic plants on central Amazon
2463 floodplains have a growth related to water level variation and the flood extent (M. Costa, 2005;
2464 T. S. F. Silva et al., 2013). Furthermore, the increasing effect of dams in the AB has been
2465 assessed through analyses of flood extent dynamics (Li et al., 2020; C. M. Souza et al., 2019)
2466 and impacts on tree mortality (Resende et al., 2019).

2467 The first morphometric characterization in AB using RS data showed that 11% of the
2468 floodplain along the Amazon River and lower reaches of major tributaries is covered with lakes
2469 (Sippel et al., 1992). In fact, the floodplain topography along the Amazon River is complex with
2470 several channels and lakes connected to the river (Latrubesse, 2012; Mertes et al., 1996).
2471 Floodplain channel widths vary largely (10–1000 m), and channel depths are tied closely to the
2472 local amplitude of the Amazon River flood pulse (Trigg et al., 2012; **Figure 7**). The recent
2473 capture of almost all of the water flow from the Araguari River by the Amazon River, the first
2474 known observation of estuarine distributary network development by headwater erosion, was
2475 also documented with RS techniques (E. S. dos Santos et al., 2018). The need for accurate
2476 topographic data for hydrological applications was emphasized in several studies in the central
2477 Amazon (Baugh et al., 2013; Wilson et al., 2007; Yamazaki, Baugh, et al., 2012), in which key
2478 improvements such as vegetation removal were made. Global DEMs still do not accurately
2479 represent the floodplain topography, but surface water extent data combined with WSE allowed
2480 the first topographic mapping in seasonally flooded areas in the central Amazon (Fassoni-
2481 Andrade, Paiva, Rudorff, et al., 2020). In these areas 75% of the open-water areas have depth of
2482 less than 2 m (8 m) in the low (high) water period (Fassoni-Andrade, Paiva, Rudorff, et al.,
2483 2020).

2484 The Amazon River exports the largest sedimentary supply to the world's ocean ($1.1 \times$
2485 10^9 tons per year; (Armijos et al., 2020; **Figure 13**). Several seminal studies and algorithm

2486 developments using RS to characterize water composition of rivers and lakes were primarily
 2487 conducted in AB (see **Table 5**), such as the pioneering estimates of sediment concentration in
 2488 rivers (Bayley & Moreira, 1978; Mertes et al., 1993), chlorophyll in floodplain lakes (Novo et
 2489 al., 2006) and colored dissolved organic material (M. P. da Silva et al., 2019). The spatio-
 2490 temporal pattern of these components is related to SWE variations and mixing processes from
 2491 different sources. The shallow depths during the low water period and the large area of
 2492 floodplain lakes favor conditions for sediment resuspension (Bourgoin et al., 2007; Fassoni-
 2493 Andrade & Paiva, 2019; **Figure 8**). The mapping of chlorophyll in floodplain lakes showed
 2494 higher pigment concentrations during the low water season (Novo et al., 2006). Increasing trends
 2495 in sediment concentration in rivers were linked to changes in land use (J. M. Martinez et al.,
 2496 2009; Amazon River) and the impact of mining (Lobo et al., 2015, 2016; Tapajós River).
 2497 Conversely, the construction of the Santo Antônio and Jirau dams seems to have contributed to a
 2498 reduction of sediment concentration in the Madeira River (Latrubesse et al., 2017; Li et al.,
 2499 2020).

2500 Due to large spatial and temporal changes of freshwater stored in surface, soil root zone
 2501 and aquifers, AB is the ideal laboratory to explore measurements of gravity field variations from
 2502 the GRACE satellite mission and derive TWS variations, linked to the redistribution of water
 2503 mass over the continental surfaces (**Figure 9**). The first GRACE-derived estimates of TWS
 2504 variations (Tapley et al., 2004) and groundwater storage changes (Frappart et al., 2011) were
 2505 presented for the AB. TWS change in the AB is estimated as $\sim 1800\text{-}2700 \text{ km}^3 \text{ yr}^{-1}$ (**Figure 13**)
 2506 with different contributions from surface water storage ($\sim 49\%$), root zone soil moisture ($\sim 27\%$),
 2507 and groundwater ($\sim 24\%$) (Frappart et al., 2019). The residence time of the water stored in the
 2508 AB, i.e., the average time that the water remains in the AB before leaving by runoff or
 2509 evapotranspiration, was estimated at two months (Tourian et al., 2018). GRACE data helped to
 2510 monitor periods of extreme droughts (e.g., 2009) and floods (e.g., 2005, 2010; J. L. Chen et al.,
 2511 2009), quantify water deficit during such events (Frappart et al., 2012), understand groundwater
 2512 dynamics across different scales and climates, and the interaction between floodplains and
 2513 groundwater (Miguez-Macho & Fan, 2012).

2514 RS has proven to be a great complement to in situ observations that have traditionally
 2515 been used to calibrate/assimilate and validate hydrologic and hydrodynamic models (**Table 6** and
 2516 **Figure 11**). In the case of the AB, the pioneering development or application of models have
 2517 provided major understanding of basin-wide river-floodplain systems (Coe et al., 2002; Paiva,
 2518 Buarque, et al., 2013; Rudorff et al., 2014a; Sorribas et al., 2020; Trigg et al., 2009; Wilson et
 2519 al., 2007; Yamazaki et al., 2011), the role of groundwater in hydrological buffering and
 2520 headwater basin dynamics (Cuartas et al., 2012), and partitioning of total water storage (Paiva,
 2521 Buarque, et al., 2013; Pokhrel et al., 2013). The study by Wilson et al. (2007) was one of the first
 2522 large scale hydraulic models developed, while with the first large-scale hydrologic-
 2523 hydrodynamic model of the AB by Paiva, Buarque, et al. (2013) it was possible to represent
 2524 physical processes such as the backwater effects in the main river and the attenuation of the flood
 2525 wave due to water storage in the floodplains. Applications of two-dimensional models in a reach
 2526 of the Amazon River showed that the floodplain receives large amounts of water from the river,
 2527 and small increases in peak discharge promote large changes in this flow (Rudorff et al., 2014b).
 2528 Recently, Sorribas et al. (2020) estimated, using an innovative hydrological tracking model,
 2529 surface water travel times along the AB as 45 days (median), with 20% of Amazon River waters
 2530 flowing through floodplains. Furthermore, with the integration of RS data and hydrological

2531 modeling, the assessment of past floods and droughts was possible (Frappart et al., 2012;
2532 Wongchuig et al., 2019).

2533 RS techniques were also important for understanding how the hydrological cycle
2534 responds to environmental changes. Long-term changes in discharge could be attributed to
2535 changes in land cover via changes in evapotranspiration, as first shown for the Tocantins River
2536 (M. H. Costa et al., 2003). The average annual discharge increased by 24% between 1949-1986
2537 and 1979-1998, associated with increased agricultural land use in the basin (from 30% to 49%).
2538 The presence of the forest was established as important for determining precipitation patterns
2539 both in and outside the region. The deep roots, low albedo and high *ET* rates of the rainforest
2540 induce the wet season onset to be several weeks before what it would be without it, in a
2541 mechanism dubbed ‘shallow convection moisture pump’ (Wright et al., 2017). The changes in
2542 land-surface fluxes caused by deforestation were found to cause reductions in precipitation
2543 totals, delays on the rainy season onset and longer dry spells during the wet season, with negative
2544 consequences for hydropower generation, regional agriculture and the resilience of the forest
2545 itself (M. E. Arias et al., 2020; Butt et al., 2011; M. H. Costa, 2020; Leite-Filho et al., 2020;
2546 Spera et al., 2014; Stickler et al., 2013).

2547

2548 **7.2. The benefits of the lessons learnt in the Amazon to understand the hydrology of other** 2549 **large tropical river basins**

2550 AB can be seen as a RS laboratory for fostering the understanding of the water cycle and
2551 hydrology in general. While these advances have prompted the scientific understanding of AB
2552 hydrology, they have also set up new developments, techniques and analysis that contribute to a
2553 better understanding of the hydrological cycle of other large basins worldwide, and at the global
2554 scale. Without being exhaustive, we discuss here some key studies that benefit from such
2555 advances and how they have contributed to hydrological progress in other regions. In particular,
2556 as the second largest river basin in the world, with similar environmental characteristics as AB
2557 such as extensive floodplains and dense forests, the Congo River Basin is the new frontier of
2558 tropical hydrological research (Alsdorf et al., 2016), gaining more scientific attention in recent
2559 years and benefiting from the lessons learnt from AB hydrology. The “Hydrologic Research in
2560 the Congo Basin” conference in Washington, D.C (USA) in 2018 delineated new research
2561 opportunities for the basin. This effort to gather African and international communities around a
2562 joint objective of a better understanding of the Congo basin response to climate change led to an
2563 extensive monograph (Alsdorf et al., 2021) that indicates the usefulness of RS and model
2564 methodologies built for AB.

2565 The first development of satellite altimetry datasets (Section 4.1) in AB was turned into
2566 freely available global datasets providing long-term WSE at thousands of virtual stations (**Table**
2567 **3**) enabling the characterization of the surface hydrology variability from altimetry in the Congo
2568 basin (Paris et al., 2020), Indian inland waters (Ghosh et al., 2017) and the Niger River basin
2569 (Normandin et al., 2018). The integration of satellite altimetry and hydrological modeling had
2570 seminal advances in the AB, including model validation and development of rating curves for
2571 near real-time monitoring of discharges from the space (Section 6.2), that were further performed
2572 in other tropical basins as the Congo (Paris et al., 2020), Tsiribihina in Madagascar

2573 (Andriambelason et al., 2020), Niger (Fleischmann et al., 2018), and Ogooué (Bogning et al.,
2574 2020).

2575 Studies based on initial RS developments in the Amazon further performed comparative
2576 hydrology approaches, for instance by studying jointly the floodplain dynamics in the central
2577 Amazon, the Congo and the Brahmaputra wetlands with SAR (H. C. Jung et al., 2010),
2578 highlighting the unique features of each of these river systems. AB, with its extensive river
2579 floodplains, largely contrasts with Congo Cuvette Centrale, mainly dominated by interfluvial
2580 wetlands, with less river-wetland interaction (H. C. Jung et al., 2010). Following studies using
2581 SAR observations to map flood and wetlands extent and distinguish vegetation types in AB
2582 (Section 4.2), seasonal flooding dynamics, water level variations and vegetation types over the
2583 Congo basin were derived from JERS-1 (Å. Rosenqvist & Birkett, 2002) or ALOS-PALSAR
2584 SAR and Envisat altimetry data (Kim et al., 2017).

2585 The development of large scale, multi-satellite RS techniques to monitor surface water
2586 storage variability, with initial techniques and analysis developed and assessed for AB (Sections
2587 4.1 and 5) were further applied to the Orinoco River in South America (Frappart et al., 2015), to
2588 study droughts in the Ganges-Brahmaputra River (Papa et al., 2015) and to quantify the relative
2589 contribution of surface and groundwater variations in the Mekong (Pham-Duc et al., 2019), the
2590 Chad (Pham-Duc et al., 2020) and the Congo (M. Becker et al., 2018; Yuan et al., 2017) basins.

2591 Given the global relevance in terms of climate and ecosystems, the presence of large
2592 floodplains and dimensions in accordance with the resolution of coarse scale models, many
2593 advances and developments of land surface and hydrological models were first assessed over AB
2594 (Section 6.2), especially the introduction of basin-scale inundation schemes that were later
2595 introduced to other river basins (Andriambelason et al., 2020; Paris et al., 2020), at continental
2596 scale (Siqueira et al., 2018) and at the global scale (Alkama et al., 2010; B Decharme et al.,
2597 2012; Yamazaki et al., 2011). Recent advances in large-scale sediment transport using RS
2598 observations and modeling followed a similar path, with pioneering works in AB (Section 4.4)
2599 being followed by progress for all South America (Fagundes et al., 2021).

2600

2601 **7.3. Tackling the current knowledge gaps with future satellite missions**

2602 This review shows the tremendous achievements made during more than three decades of
2603 scientific advance on the hydrology and the water cycle of the AB with the help of RS. It also
2604 helped to identify the various knowledge gaps remaining to promote a comprehensive
2605 understanding of the AB hydrology. Here, we summarize these knowledge gaps (**Table 7** and
2606 **Table 8**), present the new research opportunities with the upcoming and future satellite missions.

2607 Regarding RS-based precipitation, current algorithm challenges involve the definition of
2608 dynamic thresholds of temperature brightness in IR sensors, and processing of MW data to avoid
2609 confusing the summit of the Andes snowy peaks with cold clouds (Dinku et al., 2011; Toté et al.,
2610 2015). Better algorithms for the detection of solid precipitation are necessary for improved
2611 understanding of local processes in AB headwaters in the Andes mountains (Hurley et al., 2015;
2612 Levizzani et al., 2011; Peng et al., 2014). In situ observations are fundamental for the calibration
2613 of remote sensors, therefore a strategic network of traditional stations and ground-based radars in
2614 key points of the AB must necessarily be part of a future agenda. Finally, new low-cost

2615 technologies such as nanosatellites have proven to be viable while maintaining scientific
2616 requirements, which should continue to be encouraged for future missions (Peral et al., 2019).

2617 RS models can reasonably estimate average *ET* rates in the AB, but correctly
2618 representing *ET* seasonality is still a challenge, as well as understanding differences among
2619 individual *ET* components as soil evaporation, transpiration and interception. More studies are
2620 needed to disentangle the controls of *ET* across the basin (water and energy limitation, and
2621 vegetation phenology), since multiple drivers operate simultaneously (Maeda et al., 2017).
2622 Besides, a major knowledge gap is the difference between *ET* in Amazon uplands and wetlands,
2623 and the effect of open water evaporation on the regional climate. Current satellite-based models
2624 need to minimize the use of parameterization (or better constrain it), while the accuracy of input
2625 data must be improved. A major limitation of SEB models is their requirement of clear sky
2626 conditions, which may be improved by the use of microwave data (Holmes et al., 2018) and the
2627 combination with other types of *ET* models as those based on vegetation index models. In situ
2628 measurements are fundamental to achieve this goal, yet today there are only eight flux towers
2629 with publicly available data in the AB. For vegetation index-based models (e.g., MOD16,
2630 GLEAM), improving the understanding of soil water deficit controls on *ET* across the basin is
2631 also necessary, given the high dependence of these products on soil moisture content. Some
2632 breakthrough ongoing and future missions will provide a new understanding of *ET* dynamics in
2633 AB. The ECOSTRESS is addressing the response of vegetation to water deficit with
2634 unprecedented details, while the VIIRS collects visible and infrared imagery, extending the time
2635 series from its predecessor MODIS and improving its estimates, and the FLEX mission will map
2636 vegetation fluorescence, a proxy of photosynthetic activity and vegetation stress and health. The
2637 continuity of the Landsat missions will ensure the development of long-term *ET* at high spatial
2638 scale, while the GRACE-FO mission will provide new data for water balance approaches to
2639 estimate *ET*. This will ultimately allow us to model *ET* at high spatial resolution (< 30 meters)
2640 and for long time periods (> 40 years).

2641 The surface water bodies and aquatic ecosystems of AB are still challenging the current
2642 available RS observations. Despite the substantial progress in the last decades, there are still
2643 limitations. Currently, there is a trade-off over AB between spatial and temporal resolutions in
2644 satellite observations, with generally high temporal sampling associated with lower spatial
2645 resolution and vice-versa. Therefore, there is a need for finer spatio-temporal resolution to
2646 adequately monitor water extent, level and slope of the surface water and floodplain inundation.
2647 There is also a need to improve the accuracy of these estimates in order to understand more local
2648 phenomena, such as floodplain-river exchanges and dynamics or the complex flooding processes
2649 of extensive interfluvial areas. Similarly, only few lakes and reservoirs in AB are monitored
2650 routinely from space, using altimetry for instance. The context of the AB, with dense vegetation
2651 and cloud cover, makes it still challenging to monitor surface waters such as permanently or
2652 seasonally flooded forests and floating herbaceous plants.

2653 The forthcoming NASA/ISRO L-band SAR mission, with its combination of radar
2654 wavelengths and polarizations and 12-day orbit passes, will help to precisely measure small
2655 changes of SWE in AB, including areas with standing vegetation. Furthermore, with its
2656 technology based on swath altimetry from the KaRIn, quasi-global coverage and joint
2657 observation of surface water elevation, extent, river width and slope, the SWOT mission, to be
2658 launched in 2022, will permit an unprecedented monitoring of AB surface water and rivers at

2659 100 m resolution in two horizontal dimensions. The centimetric accuracy in SWE and slope
2660 (Desai, 2018) will help to better characterize freshwater fluxes in the AB. The current satellite
2661 altimetry missions, especially the Copernicus program, is now setting the era of operational
2662 monitoring from space at large scale for the coming decades, with clear benefits for large tropical
2663 transboundary watersheds such as AB. With nearly two thousand virtual stations distributed over
2664 the basin, potentially hundreds more, freely available on multiple websites, conventional satellite
2665 altimetry can favorably complement the traditional and necessary in situ network. Since the main
2666 limitation for a broader use of current satellite altimetry remains its relatively low temporal
2667 sampling, future missions in development, such as SMASH (Blumstein et al., 2019), broadcasted
2668 together with the current constellation, should help to tackle this issue. Further developments in
2669 satellite observations are nevertheless required to fully characterize AB surface water extent and
2670 elevation and should combine, in the future, the benefits of SWOT swath global measurements
2671 with high temporal sampling of SMASH-like constellation, into a SWOT-like satellite
2672 constellation providing global and daily observations.

2673 Besides the concept of new satellite missions, it is worth noticing that the upcoming
2674 unprecedented availability of information regarding AB surface water extent and elevations will
2675 challenge the current analysis capabilities. New development of analysis tools or fusion
2676 techniques with artificial intelligence to combine various RS observations (visible, IR, MW,
2677 GNSS-R) are needed. Similarly, new techniques for fusion with local to regional modeling, data
2678 assimilation and better constraining of uncertain hydraulics should also dramatically increase our
2679 capacity to model the AB and the variations of its water cycle.

2680 Floodplain and river channel topography have not yet been fully characterized in the AB,
2681 despite recent efforts with local and regional estimates, preventing a better understanding of
2682 habitats related to flood pulse and limiting the accuracy of hydraulic models. In addition, the
2683 association between sediment concentration in rivers and channel migration is still poorly
2684 understood (Constantine et al., 2014). The development of new techniques and RS data for
2685 topography mapping are needed. The main challenge is vegetation removal, as many sensors do
2686 not have the ability to penetrate vegetation. LiDAR and altimetric data, such as ICESat-2
2687 (launched in 2018), which allow bare earth mapping, have still been little exploited in the AB for
2688 this task. Furthermore, NISAR and SWOT satellites will open opportunities with more accurate
2689 estimates of the surface water extent and distributed SWE over water bodies. Thus, new
2690 methodologies for topographic mapping, such as the waterline method (Salameh et al., 2019) and
2691 Flood2Topo (Fassoni-Andrade, Paiva, & Fleischmann, 2020) can be better developed.

2692 White, black and clear water rivers of AB have particular characteristics with large
2693 variation of COA (sediment, chlorophyll and CDOM). Despite the development of many
2694 algorithms for estimating these components, little has been explored to implement those
2695 algorithms to address scientific questions, as also reported by Topp et al. (2020) worldwide.
2696 Sediment concentration estimates could be better exploited to assess the effects of dams, mining,
2697 and land use changes in the AB. In addition, the characterization of natural processes, such as the
2698 spatio-temporal variation of phytoplankton in lakes, has not been widely explored. On the other
2699 hand, there are still technical challenges for these estimates using RS data, such as the high cloud
2700 cover in the AB. The main challenge is the discretization of the COA spectra, which can be
2701 partially overcome with new sensors with high radiometric and spectral resolution.

2702 The recent launch of the GRACE-FO mission offers an opportunity to extend the
2703 monitoring of TWS and GWS changes over more than two decades, allowing to start analyzing
2704 the impact of multi-year climatic events such as ENSO on land and groundwater storages over
2705 AB. The major drawbacks of these data remain their low spatial and temporal (~200 km and 1
2706 month) resolutions which are not sufficient to study the dynamics of more local and rapid
2707 hydrological events. To overcome these drawbacks, the GRACE-FO payload contains advanced
2708 versions of the sensors used on-board GRACE, allowing a better expected accuracy to improve
2709 the quality and the spatial resolution of the retrieved TWSA. Combined with new
2710 methodological approaches based on the use of Kalman filter, it should increase the TWSA
2711 temporal resolution to quasi-daily without degrading the spatial resolution (Ramillien et al.,
2712 2015, 2020). With the upcoming availability of SWOT observations, unprecedented and finer
2713 estimates of surface water storage over large areas will improve the determination of GWS
2714 anomalies and will allow us to better understand the interactions between flood dynamics and
2715 aquifer recharge in the AB. Groundwater exchange in the AB, which remains poorly
2716 characterized with satellites, should also benefit from the integration of these new observations,
2717 and could be further estimated in better constraining the water budget at the surface. A
2718 comprehensive set of observations dedicated to hydrology, with the continuity of the current
2719 satellite missions, is mandatory to improve our understanding of hydrology patterns through
2720 more precise water budget analyses and to assess long-term trends.

2721 Given the uncertainties in both hydrological models and RS estimates, model calibration
2722 and data assimilation techniques have been recently developed by incorporating mainly water
2723 level (satellite altimetry) data and, to a lesser extent, GRACE TWS. Other variables to be better
2724 assimilated are flood extent and storage, soil moisture and evapotranspiration. While most
2725 hydrologic and hydraulic model applications have been used to estimate variables such as
2726 evapotranspiration, soil water storage, river discharge, surface water elevation and extent, new
2727 studies must investigate other variables such as water velocity and flood storage. There is also a
2728 lack of convergence among water storage partitions (e.g., divergent estimates of surface water
2729 fraction), which must be addressed by better constraining models with EO observations, and by
2730 performing model intercomparison projects. On the other hand, while the Amazon wetlands were
2731 mainly studied for the central Amazon river floodplains, other types of wetlands do exist, as the
2732 interfluvial ones in large areas of the Llanos de Moxos, Pacaya-Samiria and Negro, and deserve
2733 more efforts from the hydrological community, especially considering their particular flood
2734 dynamics, more dependent on local rainfall. Furthermore, high resolution 2D modelling of the
2735 full Amazon mainstem mapping velocity fields and detailed river-floodplain interactions was
2736 still not explored. The downstream part of the AB also remains relatively unexplored in terms of
2737 hydrodynamic modelling and RS, e.g., the relative roles of the upstream forcing and the oceanic
2738 influence on the dynamics of the river-estuary-ocean continuum. In addition to a better
2739 representation of hydrological processes, e.g., groundwater dynamics which is poorly
2740 represented in surface hydrology-oriented models, the future of hydrologic-hydrodynamic
2741 models is largely dependent on the growing availability of new EO data. These include SWOT-
2742 derived water levels and discharges, channel water widths, floodplain topography, soil moisture
2743 (e.g., SMOS, SMAP), precipitation (e.g., SM2RAIN), gravimetry (GRACE-FO), and techniques
2744 to retrieve groundwater storages (e.g., Frappart et al., 2019). These data will promote the basis
2745 for modeling estimates at high temporal and spatial resolution, aiming ultimately at providing
2746 locally relevant hydrological estimates everywhere (Bierkens et al., 2015; Wood et al., 2011).

2747 While most major components of the water cycle have been relatively well addressed in
2748 the literature as shown along this review, soil moisture stands out as the less reliable component.
2749 This relates to the difficulty to retrieve this variable under densely vegetated areas (Prigent et al.,
2750 2005). The relatively poor performance of current soil moisture datasets (e.g., SMAP, AMSR-E
2751 and SMOS) on these environments is well known, even when products are combined (Y. Y. Liu
2752 et al., 2011) or merged (F Aires et al., 2005; Kolassa et al., 2016). Most soil moisture-oriented
2753 studies were performed with hydrological models and in situ data, in a few headwater locations.
2754 Moreover, there is an inherent ambiguity in passive microwave observations between water-
2755 saturated soils and surface waters. As a consequence, the large surface water fraction in AB
2756 affects the soil moisture retrievals by this type of observations. This ambiguity in the satellite
2757 observation has triggered the development of a product such as SMOS-based surface water
2758 product (Parrens et al., 2017). There is an urgent need to better monitor soil moisture at different
2759 spatial-temporal resolutions in the AB, especially considering its major role in controlling the
2760 Amazon forest dynamics and phenology, evapotranspiration, and the water cycle in general. This
2761 observation supports the development of SMOS-HR, the High Resolution follow-on mission of
2762 SMOS, which is currently undergoing feasibility study by the French space agency and which
2763 goal is to ensure continuity of L-band measurements while increasing the spatial resolution to
2764 ~10 km without degrading the radiometric sensitivity and keeping the revisit time of 3 days
2765 unchanged.

2766 Similarly, river discharge, which is historically one of the first hydrological variables that
2767 has been observed in situ is still not properly measured from space. This review stresses that
2768 there is a need to accurately estimate river discharge using RS in AB with fine spatial and
2769 temporal resolution. River discharge has already been estimated indirectly by RS data (e.g.,
2770 Brakenridge et al., 2007; LeFavour & Alsdorf, 2005; Tarpanelli et al., 2013; Zakharova et al.,
2771 2006), but still poorly complements the current in situ network of AB. Upcoming missions, such
2772 as SWOT, in combination with current satellite missions, will soon help us move toward a more
2773 comprehensive monitoring of river discharge in AB.

2774 The ongoing and future environmental alterations in the AB urge the understanding of the
2775 basin hydrology under the perspective of a changing system. The long term effects of multiple
2776 human impacts (land use change, climate change, damming, mining, fires) on the Amazon must
2777 be better understood. Changes in land-atmosphere feedback due to deforestation will affect the
2778 AB water cycle, but the extent is still under debate. There is relatively little understanding of
2779 how these interact, especially in terms of how the impact of land-use changes in local climate
2780 can be different under large scale meteorological conditions that are changing with the global
2781 climate (e.g., Leite-Filho et al., 2020) and how these would affect the land and water ecosystems
2782 in the basin. Furthermore, techniques to map forest degradation and discern primary and
2783 secondary vegetation are still relatively new, and the impacts of those subtler but pervasive land-
2784 use changes on AB hydrology is yet to be understood. Finally, although the influence of the
2785 Amazon forest on the hydroclimate outside the AB has been increasingly documented, the
2786 consequences of its deforestation and degradation outside the basin is yet to be understood.

2787 Furthermore, the proliferation of dams in tropical basins as the Amazon, Congo and
2788 Mekong require basin-scale planning and analysis tools to foster mutual benefits in
2789 understanding these changes (e.g. Latrubesse et al., 2017; Schmitt et al., 2019; Winemiller et al.,
2790 2016), and RS data stand out as powerful tool to monitor large scale impacts of existing man-

2791 made reservoirs (e.g., Resende et al., 2019), and infer their characteristics, such as water level
 2792 and stage-area-volume relationships (e.g., Fassoni-Andrade, Paiva, & Fleischmann, 2020; Gao et
 2793 al., 2012). Better data and knowledge of these impacts are also the base for better hydro-
 2794 geomorphological models that could be used to quantify the expected impacts of planned
 2795 reservoirs and therefore aid in creating designs that minimize environmental impacts.

2796

2797 **7.4. How to use RS-based scientific advances to foster water resources management in the** 2798 **Amazon basin?**

2799 While the AB served as an important laboratory for RS development that produced
 2800 significant scientific advances related to its hydrological processes in the last decades (**Table 7**
 2801 and **Table 8**), the Amazon currently undergoing extensive anthropogenic pressure (Section 6.4),
 2802 and urgently calls for better basin-scale water resources planning and new environment
 2803 monitoring tools. RS has the potential to democratize essential information for decision makers,
 2804 for instance to monitor "politically ungauged" regions where information is not publicly
 2805 available (Gleason & Durand, 2020). Although RS is now a reality and documented knowledge
 2806 on the AB is much better than decades ago, there is still an open road to move all these advances
 2807 towards effective applications in decision making and water resources management.

2808 Deforestation and fire monitoring may be the most advanced and promising example in
 2809 the context of AB environmental management. Since 1988, satellite-based monitoring systems
 2810 using MODIS, Landsat and CBERS imagery as the DETER (Diniz et al., 2015,
 2811 <http://www.obt.inpe.br/OBT/assuntos/programas/amazonia/deter/>), PRODES
 2812 (<http://www.obt.inpe.br/OBT/assuntos/programas/amazonia/prodes/>), Imazon
 2813 (<https://imazon.org.br/categorias/boletim-do-desmatamento/>) and Queimadas
 2814 (<http://queimadas.dgi.inpe.br/queimadas/portal>) have been systematically supporting local
 2815 governments and NGOs on the monitoring and control of deforestation and fires. Technical
 2816 advances made it possible to monitor deforestation in near real time, on the scale of days, weeks,
 2817 or months. However, institution building, along with related civil-society engagement, is still
 2818 needed to facilitate effective actions within complex government frameworks and bridge the gap
 2819 between technology and policy towards deforestation reduction (Finer et al., 2018).

2820 Amazon neighborhood countries have mature Water Resources Agencies, Geology and
 2821 Hydrometeorological Services as the ANA, the Peruvian and Bolivian National Meteorology and
 2822 Hydrology Services (SENAMHIs) and the Brazilian Geological Survey (CPRM). These
 2823 institutions have dedicated efforts on the challenging task of systematic in situ monitoring of
 2824 Amazon vast territory and rivers and promoting open hydrological datasets. In this sense, RS is
 2825 starting to be incorporated into operational monitoring (e.g., SIPAM <http://hidro.sipam.gov.br/>,
 2826 Hidrosat, J. C. Carvalho et al., 2015; near real-time flood simulations at sub-daily scale, Llauca
 2827 et al., 2021). In particular, precipitation has been widely monitored through RS data by multiple
 2828 meteorological agencies, while other water cycle variables have received less attention. These
 2829 organizations have been developing technical reports about the national situation and water
 2830 resources planning including the AB (e.g., Water Resources Situation Report, Agência Nacional
 2831 de Águas, 2019a; National Water Security Plan, Agência Nacional de Águas, 2019b; flow
 2832 forecasts at national level and at hourly and daily scale by SENAMHI Peru available at:
 2833 <https://www.senamhi.gob.pe/?&p=pronostico-caudales>). Currently, they are mostly supported by

2834 the national hydrometeorological networks that are still scarce and could be greatly enhanced
2835 with the data and knowledge produced by RS. Some of these countries also have advanced Water
2836 Resources Laws and regulation, such as the Brazilian National Water Resources Management
2837 System created by Law 9433, 1997 (Brasil, 1997), but most of the efforts on the development
2838 and implementation of such regulation is devoted to river basins in more densely populated
2839 regions and not in the context of the complexity of the international/transboundary and larger
2840 river basin of the world. Also, even though AB is in the epicenter of international scientific
2841 discussion, it appears not to be the main focus of technical and scientific developments on the
2842 water resources field in the Amazon countries, as revealed by recent synthesis of advances from
2843 Brazilian water community (Paiva, 2020).

2844 Most flooding studies in the Amazon have aimed at understanding ecosystem services
2845 and the natural system (Sections 4.2 and 6.2), but many Amazon urban centers are under flood
2846 risk (e.g., Amazon River at Iquitos, Madeira River at Porto Velho, Acre River at Rio Branco,
2847 Juruá river at Cruzeiro do Sul), and suffer annually from overbanking flow (Fleischmann et al.,
2848 2020). While this paper is being drafted, the Brazilian Acre state is recovering from a
2849 humanitarian crisis caused by floods at Acre River at Rio Branco and Juruá River at Cruzeiro do
2850 Sul, enhanced by the COVID-19 pandemic. Thus, the several developed flood monitoring tools
2851 could be translated into effective flood risk mapping and real-time monitoring for disaster
2852 management. International initiatives such as the Copernicus Emergency Management Service
2853 (<https://emergency.copernicus.eu/>) and the International Charter “Space and Major Disasters”
2854 (<https://disasterscharter.org/>) have the potential to provide important EO data for real-time
2855 disaster management. Furthermore, the transboundary character of many Amazon sub-basins
2856 (e.g., Madeira River, with floods at Porto Velho in Brazil being partially generated in upstream
2857 Bolivian reaches) makes RS data a fundamental tool to fulfill the disparity in data availability
2858 among countries. On the other hand, in many areas of the Amazon, droughts have a larger
2859 societal impact than floods, given the adaptation of livelihoods to the annual flooding regime,
2860 and the interruption of provision of goods and general transport through rivers during extremely
2861 dry periods (Zeng et al., 2008). Recent technical efforts include evaluation of hydrological
2862 forecasts from physically based hydrological models supported by RS (Section 6.2),
2863 development of site specific statistical forecasting and real-time monitoring systems (e.g. SACE
2864 system from <http://www.cprm.gov.br/sace/>; systems available for the Madeira, Acre, Xingu,
2865 Branco and some reaches of the Amazon mainstem), prototypes of hydrological model based
2866 monitoring systems (e.g. South America River Discharge Monitor - SARDIM
2867 <https://sardim.herokuapp.com/>; G. G. dos Reis et al., 2020), global flood forecast systems (e.g.
2868 GLOFAS, Alfieri et al., 2013) and efforts on monitoring and alerts of natural hazards by centers
2869 as CEMADEN from Brazil (Centro Nacional de Alerta e Monitoramento de Desastres Naturais).
2870 Drought monitor systems based on in situ and RS-based observations and local community
2871 interpretation (e.g., ANA Drought Monitor <http://monitordesecas.ana.gov.br/>) are evolving and
2872 there are no operational hydrological forecasting systems at the AB, national or continental
2873 scales (Fan et al., 2016).

2874 Impacts from human activities may propagate through the Amazon River network and
2875 neighbor countries, since the ongoing developments of hydropower projects and agricultural
2876 expansion alter the hydrological, sediments and ecosystem dynamics (Anderson de Castro et al.,
2877 2018; Forsberg et al., 2017). Recent research has explored integrated planning looking for the
2878 best hydropower development solutions (Almeida et al., 2020; Winemiller et al., 2016), while

2879 organizations as the Amazon Cooperation Treaty Organization aim at promoting sustainable
 2880 development of the AB with the participation of its neighborhood countries. However, current
 2881 national scale policies and regulation do not promote fully integrated water resources planning,
 2882 as new projects are usually accessed individually. RS can definitely encourage a common and
 2883 transparent understanding of AB water related issues.

2884 The RS scientific community has now the challenge to promote knowledge, datasets and
 2885 applications on water-environmental changes, aiming at enhanced water resources management
 2886 and planning. Potential pathways include: (i) training decision makers and multiple stakeholders
 2887 on the language of RS (e.g., Applied Remote Sensing Training Program - ARSET
 2888 <https://appliedsciences.nasa.gov/what-we-do/capacity-building/arset>); (ii) encouraging local
 2889 engagement by bridging the gap between RS based science and in situ and traditional knowledge
 2890 (Runde et al., 2020); (iii) initiatives of science communication and citizen science (Buytaert et
 2891 al., 2014; e.g. www.amazoniacienciaciudadana.org/, <https://www.ufrgs.br/conexoesamazonicas/>,
 2892 <https://ipam.org.br/biblioteca/?biblioteca=artigos-cientificos>,
 2893 <https://amazon.org.br/categorias/outros/>, <https://infoamazonia.org/>) (iii) development of open
 2894 access datasets focused on specific applications (e.g. aquatic ecosystem conservation,
 2895 Venticinque et al., 2016); (iv) developing monitoring systems focused on environmental changes
 2896 and water related disasters; (v) developing open hydrological repositories (e.g. HYBAM,
 2897 <https://hybam.obs-mip.fr/>, SERVIR-Amazonia, <https://servir.ciat.cgiar.org/>); (vi) developing a
 2898 basin-scale research agenda focused on directly supporting water resources decision making (e.g.
 2899 scenarios of hydropower development; Almeida et al., 2020).

2900

2901 **7.5. Recommendations**

2902 Based on the knowledge gaps and the perspectives presented in the previous sections, we
 2903 provide the following recommendations for the future studies on Amazon waters from space.

2904 **Recommendation 1: Observations**

2905 Current limitations of satellite data for AB are often related to the space-time resolution
 2906 (e.g., SWE and slope, surface water extent, ET), time span (e.g., surface water extent, TWS,
 2907 GWS, ET, topography) and accuracy (e.g., surface water extent, GWS anomalies). The largest
 2908 limitations so far in monitoring the AB hydrology from space refer to soil moisture and river
 2909 discharge, which have been poorly addressed due to vegetation interference in sensors or by the
 2910 nature of the variable, respectively, which hampers its estimation from the space. The increasing
 2911 availability of long term archives of RS datasets should be ensured by national space and water
 2912 agencies, in complement to existing in situ monitoring networks, which are fundamental to
 2913 properly calibrate and validate RS estimates. Latency time of RS data distribution (e.g.,
 2914 precipitation and SWE) should be reduced to a few hours to be used by water/risk management.
 2915 Ensuring satellite observation to be archived into climatic datasets can foster the understanding
 2916 the impacts of climate change and human activities on the basin.

2917 **Recommendation 2: Models, algorithms and integration**

2918 Technical limitations are related to the development of algorithms (e.g., orographic rains,
 2919 CDOM and chlorophyll retrieval, water budget closure, hydrodynamic models), and data fusion
 2920 (e.g., ET, SWE, surface water extent). The recognition of uncertainties in multiple RS data and

2921 trade-offs between temporal and spatial resolution point to the need of more integrative
 2922 approaches, e.g., for mapping long term flooding and evapotranspiration patterns at high spatio-
 2923 temporal resolutions, and artificial intelligence will play a major role in this. The better coupling
 2924 of EO datasets with hydrological-hydraulic models and land surface models (e.g., data
 2925 assimilation, spatiotemporal interpolation) is also a necessary step forward in Earth System
 2926 modeling, by considering the dynamic aspect of AB hydrology.

2927 **Recommendation 3: Characterization of hydrological processes in a changing Amazon**

2928 Upcoming and future satellite observations will bring new opportunities for the AB
 2929 regarding the characterization of natural processes, including phytoplankton in waters, floodplain
 2930 topography, aquatic ecosystems, groundwater dynamics, as well as the monitoring of
 2931 anthropogenic environmental changes. The development of long term datasets is fundamental to
 2932 understand Amazon hydrological processes across multiple decades. While RS data currently
 2933 focus on a set of a few hydrological variables, there are many others that require more attention
 2934 from the hydrologic community, such as river discharge and water velocity, surface and
 2935 groundwater storage, soil moisture, CDOM and Chlorophyll-a. Most studies in the AB also focus
 2936 on a few areas (e.g., the várzea environment in the central Amazon floodplains), and many other
 2937 complex river-wetland systems or streams and small rivers, especially in Andean region, also
 2938 require attention.

2939 **Recommendation 4: Towards the use of RS to support sustainable science in AB**

2940 The AB harbors an incredibly large and still poorly known biodiversity, which provides
 2941 massive ecosystem services for the globe, as well as some of the most complex and intriguing
 2942 river-wetland systems in the world. While EO through satellites has provided breakthrough
 2943 scientific advances on the comprehension of the AB water cycle in the last decades, the
 2944 forthcoming years with the new hydrology-oriented missions will provide a new milestone on
 2945 the monitoring of Amazon waters from space. Advance knowledge from RS should be translated
 2946 into valuable information and indicators to support environmental governance and sustainable
 2947 science in AB. RS has the potential to democratize essential information for decision makers,
 2948 moving towards a more sustainable future for the largest basin in the world.

2949

2950 **Acknowledgments**

2951 We thank Thiago Laranjeiras and the Mamirauá Institute for Sustainable Development for
 2952 providing the photographs in **Figure 1**. We thank Dr. Mark Trigg and Dr. Conrado Rudorff for
 2953 providing topographic mapping of the Amazon floodplain (**Figure 7**) and flood maps for the
 2954 Curuai Lake (**Figure 11**), respectively.

2955 A.C.F-A is supported by EOSC-SYNERGY project (grant number 857647). A.S.F. is supported
 2956 by the CNPq via grants 141161/2017-5 and 201148/2019-6. J.M.M. received support from
 2957 NASA (Contract NNX17AK49G) and US National Science Foundation (Division of
 2958 Environmental Biology, grant number 1753856). F.P., A.P., F.F., F.D., J.F.F. and S.C. received
 2959 support from CNES (SWOT-ST project SWOT for SOUTH AMERICA, ID: 6018-4500066497).
 2960 FF and FP also received support from CNES (SWOT-ST project SWOT Wetlands Hydrology
 2961 Monitoring). F.P., A.P., F.F., F.D. and S.C. are supported by the IRD Groupement De Recherche
 2962 International SCaHyLab. S.W. and J.C.E. are supported by the French AMANECER-MOPGA

2963 project funded by ANR and IRD (ref. ANR-18-MPGA-0008). V.P was partially supported by the
 2964 JSPS Kakenhi (N°16H06291) and the French Centre National d'Etudes Spatiales (CNES). G.A.
 2965 received support from CNPq, process 142230/2017-0. A.A.M is supported from CNPq, process
 2966 number 141979/2017-8. A.R. is supported by the ANA and by the CAPES Foundation, grant
 2967 number 88881.178687/2018-01.

2968 **Data Availability Statement**

2969 This is a review paper, for which no new data was generated. Data supporting the figures are
 2970 available via the cited references.

2971

2972 **References**

- 2973 Abe, C. A., Lobo, F. L., Novo, E. M. L. de M., Costa, M., & Dibike, Y. (2019). Modeling the effects of
 2974 land cover change on sediment concentrations in a gold-mined Amazonian basin. *Regional*
 2975 *Environmental Change*, *19*, 1801–1813. <https://doi.org/10.1007/s10113-019-01513-8>
- 2976 Abril, G., Martinez, J. M., Artigas, L. F., Moreira-Turcq, P., Benedetti, M. F., Vidal, L., et al. (2014).
 2977 Amazon River carbon dioxide outgassing fuelled by wetlands. *Nature*, *505*(7483), 395–398.
 2978 <https://doi.org/10.1038/nature12797>
- 2979 Aceituno, P. (1988). On the Functioning of the Southern Oscillation in the South American Sector. Part I:
 2980 Surface Climate. *Monthly Weather Review*, *116*(3), 505–524. [https://doi.org/10.1175/1520-0493\(1988\)116<0505:OTFOTS>2.0.CO;2](https://doi.org/10.1175/1520-0493(1988)116<0505:OTFOTS>2.0.CO;2)
- 2982 Adderio, L. P. D., Puca, S., Vulpiani, G., Petracca, M., San, P., & Dietrich, S. (2020). RAINBOW : An
 2983 Operational Oriented Combined IR-Algorithm, 1–21.
- 2984 Adler, R. F., Huffman, G. J., & Keehn, P. R. (1994). Global tropical rain estimates from microwave-
 2985 adjusted geosynchronous IR data. *Remote Sensing Reviews*.
 2986 <https://doi.org/10.1080/02757259409532262>
- 2987 Agência Nacional de Águas. (2019a). *Conjuntura dos recursos hídricos no Brasil 2019*. Brasília.
 2988 Retrieved from <http://conjuntura.ana.gov.br/static/media/conjunturacompleto.bb39ac07.pdf>
- 2989 Agência Nacional de Águas. (2019b). *Plano Nacional de Segurança Hídrica*. Brasília. Retrieved from
 2990 <http://arquivos.ana.gov.br/pnsh/pnsh.pdf>
- 2991 Aires, F, Prigent, C., & Rossow, W. B. (2005). Sensitivity of satellite microwave and infrared
 2992 observations to soil moisture at a global scale: 2. Global statistical relationships. *Journal of*
 2993 *Geophysical Research: Atmospheres*, *110*(D11).
 2994 <https://doi.org/https://doi.org/10.1029/2004JD005094>
- 2995 Aires, Filipe. (2014). Combining Datasets of Satellite-Retrieved Products. Part I: Methodology and Water
 2996 Budget Closure. *Journal of Hydrometeorology*, *15*(4), 1677–1691. <https://doi.org/10.1175/JHM-D->

- 2997 13-0148.1
- 2998 Aires, Filipe, Papa, F., & Prigent, C. (2013). A long-term, high-resolution wetland dataset over the
 2999 amazon basin, downscaled from a multiwavelength retrieval using SAR data. *Journal of*
 3000 *Hydrometeorology*, *14*(2), 594–607. <https://doi.org/10.1175/JHM-D-12-093.1>
- 3001 Aires, Filipe, Miolane, L., Prigent, C., Pham, B., Fluet-Chouinard, E., Lehner, B., & Papa, F. (2017). A
 3002 global dynamic long-term inundation extent dataset at high spatial resolution derived through
 3003 downscaling of satellite observations. *Journal of Hydrometeorology*, *18*(5), 1305–1325.
 3004 <https://doi.org/10.1175/JHM-D-16-0155.1>
- 3005 Aires, Filipe, Prigent, C., Fluet-Chouinard, E., Yamazaki, D., Papa, F., & Lehner, B. (2018). Comparison
 3006 of visible and multi-satellite global inundation datasets at high-spatial resolution. *Remote Sensing of*
 3007 *Environment*, *216*(2018), 427–441. <https://doi.org/10.1016/j.rse.2018.06.015>
- 3008 Alcântara, E., Barbosa, C., Stech, J., Novo, E., & Shimabukuro, Y. (2009). Improving the spectral
 3009 unmixing algorithm to map water turbidity Distributions. *Environmental Modelling and Software*,
 3010 *24*(9), 1051–1061. <https://doi.org/10.1016/j.envsoft.2009.02.013>
- 3011 Alfieri, L., Burek, P., Dutra, E., Krzeminski, B., Muraro, D., Thielen, J., & Pappenberger, F. (2013).
 3012 GloFAS - global ensemble streamflow forecasting and flood early warning. *Hydrology and Earth*
 3013 *System Sciences*, *17*(3), 1161–1175. <https://doi.org/10.5194/hess-17-1161-2013>
- 3014 Alkama, R., Decharme, B., Douville, H., Becker, M., Cazenave, A., Sheffield, J., et al. (2010). Global
 3015 evaluation of the ISBA-TRIP continental hydrological system. Part I: Comparison to GRACE
 3016 terrestrial water storage estimates and in situ river discharges. *Journal of Hydrometeorology*.
 3017 <https://doi.org/10.1175/2010JHM1211.1>
- 3018 Allen, G. H., & Pavelsky, T. (2018). Global extent of rivers and streams. *Science*, *361*(6402), 585–588.
 3019 <https://doi.org/10.1126/science.aat063>
- 3020 Allen, R. G., Tasumi, M., & Trezza, R. (2007). Satellite-Based Energy Balance for Mapping
 3021 Evapotranspiration with Internalized Calibration (METRIC)—Model. *Journal of Irrigation and*
 3022 *Drainage Engineering*, *133*(4), 380–394. [https://doi.org/10.1061/\(asce\)0733-9437\(2007\)133:4\(380\)](https://doi.org/10.1061/(asce)0733-9437(2007)133:4(380))
- 3023 Allen, R. G., Irmak, A., Trezza, R., Hendrickx, J. M. H., Bastiaanssen, W., & Kjaersgaard, J. (2011).
 3024 Satellite-based ET estimation in agriculture using SEBAL and METRIC. *Hydrological Processes*,
 3025 *25*(26), 4011–4027. <https://doi.org/10.1002/hyp.8408>
- 3026 Almeida, R. M., Tranvik, L., Huszar, V. L. M., Sobek, S., Mendonça, R., Barros, N., et al. (2015).
 3027 Phosphorus transport by the largest Amazon tributary (Madeira River, Brazil) and its sensitivity to
 3028 precipitation and damming. *Inland Waters*, *5*(3), 275–282. <https://doi.org/10.5268/IW-5.3.815>
- 3029 Almeida, R. M., Hamilton, S. K., Rosi, E. J., Barros, N., Doria, C. R. C., Flecker, A. S., et al. (2020).

- 3030 Hydropeaking Operations of Two Run-of-River Mega-Dams Alter Downstream Hydrology of the
3031 Largest Amazon Tributary. *Frontiers in Environmental Science*, 8, 120.
3032 <https://doi.org/10.3389/fenvs.2020.00120>
- 3033 Alsdorf, D. (2003). Water Storage of the Central Amazon Floodplain Measured with GIS and Remote
3034 Sensing Imagery. *Annals of the Association of American Geographers*, 93(1), 55–66.
3035 <https://doi.org/10.1111/1467-8306.93105>
- 3036 Alsdorf, D., Melack, J. M., Dunne, T., Mertes, L. A. K., Hess, L. L., & Smith, L. C. (2000).
3037 Interferometric radar measurements of water level changes on the Amazon flood plain. *Nature*,
3038 404(March), 174–177. <https://doi.org/10.1038/35004560>
- 3039 Alsdorf, D., Smith, L. C., & Melack, J. M. (2001). Amazon floodplain water level changes measured with
3040 interferometric SIR-C radar. *IEEE Transactions on Geoscience and Remote Sensing*, 39(2), 423–
3041 431. <https://doi.org/10.1109/36.905250>
- 3042 Alsdorf, D., Birkett, C., Dunne, T., Melack, J., & Hess, L. (2001). Water level changes in a large Amazon
3043 lake measured with spaceborne radar interferometry and altimetry. *Geophysical Research Letters*,
3044 28(14), 2671–2674. <https://doi.org/10.1029/2001GL012962>
- 3045 Alsdorf, D., Dunne, T., Melack, J., Smith, L., & Hess, L. (2005). Diffusion modeling of recessional flow
3046 on central Amazonian floodplains. *Geophysical Research Letters*, 32(21), 1–4.
3047 <https://doi.org/10.1029/2005GL024412>
- 3048 Alsdorf, D., Bates, P., Melack, J., Wilson, M., & Dunne, T. (2007). Spatial and temporal complexity of
3049 the Amazon flood measured from space. *Geophysical Research Letters*, 34(8), 1–5.
3050 <https://doi.org/10.1029/2007GL029447>
- 3051 Alsdorf, D., Han, S. C., Bates, P., & Melack, J. (2010). Seasonal water storage on the Amazon floodplain
3052 measured from satellites. *Remote Sensing of Environment*, 114(11), 2448–2456.
3053 <https://doi.org/10.1016/j.rse.2010.05.020>
- 3054 Alsdorf, D., Beighley, E., Laraque, A., Lee, H., Tshimanga, R., O’Loughlin, F., et al. (2016).
3055 Opportunities for hydrologic research in the Congo Basin. *Reviews of Geophysics*, 54(2), 378–409.
3056 <https://doi.org/10.1002/2016RG000517>
- 3057 Alsdorf, D., Tshimanga, R. M., & Moukandi, G. D. (Eds.). (2021). *Congo Basin Hydrology, Climate, and*
3058 *Biogeochemistry: A Foundation for the Future*. Wiley-AGU.
- 3059 Amaral, J. H. F., Melack, J. M., Barbosa, P. M., MacIntyre, S., Kasper, D., Cortés, A., et al. (2020).
3060 Carbon Dioxide Fluxes to the Atmosphere From Waters Within Flooded Forests in the Amazon
3061 Basin. *Journal of Geophysical Research: Biogeosciences*, 125(3).
3062 <https://doi.org/10.1029/2019JG005293>

- 3063 Anderson, A. B., May, P. H., & Balick, M. J. (1991). The subsidy from nature: palm forests, peasantry,
3064 and development on an Amazon frontier. In *The subsidy from nature: palm forests, peasantry, and*
3065 *development on an Amazon frontier*. Columbia University Press. [https://doi.org/10.1016/0169-](https://doi.org/10.1016/0169-5347(92)90157-7)
3066 [5347\(92\)90157-7](https://doi.org/10.1016/0169-5347(92)90157-7)
- 3067 Anderson de Castro, A., Cuartas, L. A., Coe, M. T., Von Randow, C., Castanho, A., Ovando, A., et al.
3068 (2018). Coupling the terrestrial hydrology model with biogeochemistry to the integrated LAND
3069 surface model: Amazon Basin applications. *Hydrological Sciences Journal*, *63*(13–14), 1954–1966.
3070 <https://doi.org/10.1080/02626667.2018.1538592>
- 3071 Anderson, M. C., Norman, J. M., Diak, G. R., Kustas, W. P., & Mecikalski, J. R. (1997). A two-source
3072 time-integrated model for estimating surface fluxes using thermal infrared remote sensing. *Remote*
3073 *Sensing of Environment*, *60*(2), 195–216. [https://doi.org/10.1016/S0034-4257\(96\)00215-5](https://doi.org/10.1016/S0034-4257(96)00215-5)
- 3074 Andriambeloson, J. A., Paris, A., Calmant, S., & Rakotondraompiana, S. (2020). Re-initiating depth-
3075 discharge monitoring in small-sized ungauged watersheds by combining remote sensing and
3076 hydrological modelling: a case study in Madagascar. *Hydrological Sciences Journal*, *65*(16), 2709–
3077 2728. <https://doi.org/10.1080/02626667.2020.1833013>
- 3078 Angelis, C. F., McGregor, G. R., & Kidd, C. (2004). Diurnal cycle of rainfall over the Brazilian Amazon.
3079 *Climate Research*, *26*(2), 139–149. <https://doi.org/10.3354/cr026139>
- 3080 Aragão, L. E. O. ., Malhi, Y., Barbier, N., Lima, A., Shimabukuro, Y., Anderson, L., & Saatchi, S.
3081 (2008). Interactions between rainfall, deforestation and fires during recent years in the Brazilian
3082 Amazonia. In *Philosophical Transactions of the Royal Society B: Biological Sciences* (Vol. 363, pp.
3083 1779–1785). <https://doi.org/10.1098/rstb.2007.0026>
- 3084 Arantes, C. C., Winemiller, K. O., Petreire, M., Castello, L., Hess, L. L., & Freitas, C. E. C. (2018).
3085 Relationships between forest cover and fish diversity in the Amazon River floodplain. *Journal of*
3086 *Applied Ecology*, *55*(1), 386–395. <https://doi.org/10.1111/1365-2664.12967>
- 3087 Arias, M. E., Lee, E., Farinosi, F., Pereira, F. F., & Moorcroft, P. R. (2018). Decoupling the effects of
3088 deforestation and climate variability in the Tapajós river basin in the Brazilian Amazon.
3089 *Hydrological Processes*, *32*(11), 1648–1663. <https://doi.org/10.1002/hyp.11517>
- 3090 Arias, M. E., Farinosi, F., Lee, E., Livino, A., Briscoe, J., & Moorcroft, P. R. (2020). Impacts of climate
3091 change and deforestation on hydropower planning in the Brazilian Amazon. *Nature Sustainability*,
3092 *3*(6), 430–436. <https://doi.org/10.1038/s41893-020-0492-y>
- 3093 Arias, P. A., Fu, R., Vera, C., & Rojas, M. (2015). A correlated shortening of the North and South
3094 American monsoon seasons in the past few decades. *Climate Dynamics*, *45*(11–12), 3183–3203.
3095 <https://doi.org/10.1007/s00382-015-2533-1>

- 3096 Arias, P. A., Garreaud, R., Poveda, G., Espinoza, J. C., Molina-Carpio, J., Masiokas, M., et al. (2021).
 3097 Hydroclimate of the Andes Part II: Hydroclimate Variability and Sub-Continental Patterns.
 3098 *Frontiers in Earth Science*, 8(February), 666. <https://doi.org/10.3389/feart.2020.505467>
- 3099 Armijos, E., Crave, A., Espinoza, J. C., Filizola, N., Espinoza-Villar, R., Ayes, et al. (2020). Rainfall
 3100 control on Amazon sediment flux: synthesis from 20 years of monitoring. *Environmental Research*
 3101 *Communications*, 2(5), 051008. <https://doi.org/10.1088/2515-7620/ab9003>
- 3102 Arnesen, A. S., Silva, T. S. F. F., Hess, L. L., Novo, E. M. L. M. L. M., Rudorff, C. M., Chapman, B. D.,
 3103 & McDonald, K. C. (2013). Monitoring flood extent in the lower Amazon River floodplain using
 3104 ALOS/PALSAR ScanSAR images. *Remote Sensing of Environment*, 130, 51–61.
 3105 <https://doi.org/10.1016/j.rse.2012.10.035>
- 3106 Arvor, D., Funatsu, B. M., Michot, V., & Dubreui, V. (2017). Monitoring rainfall patterns in the southern
 3107 amazon with PERSIANN-CDR data: Long-term characteristics and trends. *Remote Sensing*, 9(9).
 3108 <https://doi.org/10.3390/rs9090889>
- 3109 Ashouri, H., Hsu, K. L., Sorooshian, S., Braithwaite, D. K., Knapp, K. R., Cecil, L. D., et al. (2015).
 3110 PERSIANN-CDR: Daily precipitation climate data record from multisatellite observations for
 3111 hydrological and climate studies. *Bulletin of the American Meteorological Society*, 96(1), 69–83.
 3112 <https://doi.org/10.1175/BAMS-D-13-00068.1>
- 3113 Asner, G. P. (2001). Cloud cover in Landsat observations of the Brazilian Amazon. *International Journal*
 3114 *of Remote Sensing*, 22, 3855–3862. <https://doi.org/10.1080/01431160010006926>
- 3115 Avila-Diaz, A., Benezoli, V., Justino, F., Torres, R., & Wilson, A. (2020). Assessing current and future
 3116 trends of climate extremes across Brazil based on reanalyses and earth system model projections.
 3117 *Climate Dynamics*, (2017). <https://doi.org/10.1007/s00382-020-05333-z>
- 3118 Aybar, C., Fernández, C., Huerta, A., Lavado, W., Vega, F., & Felipe-Obando, O. (2019). Construction of
 3119 a high-resolution gridded rainfall dataset for Peru from 1981 to the present day. *Hydrological*
 3120 *Sciences Journal*, 0(0), 1. <https://doi.org/10.1080/02626667.2019.1649411>
- 3121 Azarderakhsh, M., Rossow, W. B., Papa, F., Norouzi, H., & Khanbilvardi, R. (2011). Diagnosing water
 3122 variations within the Amazon basin using satellite data. *J. Geophys. Res.*, 116(D24), n/a–n/a.
 3123 <https://doi.org/10.1029/2011JD015997>
- 3124 Baguis, P., & Roulin, E. (2017). Soil moisture data assimilation in a hydrological model: A case study in
 3125 Belgium using large-scale satellite data. *Remote Sensing*, 9(8), 1–26.
 3126 <https://doi.org/10.3390/rs9080820>
- 3127 Baker, J., & Spracklen, D. V. (2019). Climate Benefits of Intact Amazon Forests and the Biophysical
 3128 Consequences of Disturbance. *Frontiers in Forests and Global Change*, 2(August), 1–13.

- 3129 <https://doi.org/10.3389/ffgc.2019.00047>
- 3130 Baker, J., Garcia-Carreras, L., Gloor, M., Marsham, J., Buermann, W., da Rocha, H., et al. (2020).
3131 Evapotranspiration in the Amazon: spatial patterns, seasonality and recent trends in observations,
3132 reanalysis and CMIP models. *Hydrology and Earth System Sciences Discussions*, 1–32.
3133 <https://doi.org/10.5194/hess-2020-523>
- 3134 Balsamo, G., Albergel, C., Beljaars, A., Boussetta, S., Brun, E., Cloke, H., et al. (2015). ERA-
3135 Interim/Land: A global land surface reanalysis data set. *Hydrology and Earth System Sciences*,
3136 *19*(1), 389–407. <https://doi.org/10.5194/hess-19-389-2015>
- 3137 Barahona, D., Molod, A., & Kalesse, H. (2017). Direct estimation of the global distribution of vertical
3138 velocity within cirrus clouds. *Scientific Reports*, *7*(1), 1–11. [https://doi.org/10.1038/s41598-017-](https://doi.org/10.1038/s41598-017-07038-6)
3139 [07038-6](https://doi.org/10.1038/s41598-017-07038-6)
- 3140 Barbosa, C. C. F. (2005). Sensoriamento Remoto da dinâmica da circulação da água do sistema planície
3141 de Curuaí/Rio Amazonas. *Dissertação*, (January 2005), 255.
- 3142 Barbosa, C. C. F., Novo, E. M. L. de M., Melack, J. M., Freitas, R. M. de, & Pereira, W. (2006). A
3143 methodology for analysis of volume and flooded area dynamics: Lago Grande de Curuai várzea as
3144 an example. *Revista Brasileira de Cartografia*, *58*(3), 201–210.
- 3145 Barbosa, C. C. F., de Moraes Novo, E. M. L., Melack, J. M., Gastil-Buhl, M., & Filho, W. P. (2009).
3146 Geospatial analysis of spatiotemporal patterns of pH, total suspended sediment and chlorophyll-a on
3147 the Amazon floodplain. *Limnology*, *11*(2), 155–166. <https://doi.org/10.1007/s10201-009-0305-5>
- 3148 Barbosa, C. C. F., Novo, E., Ferreira, R., Carvalho, L., Cairo, C., Lopes, F., et al. (2015). Brazilian inland
3149 water bio-optical dataset to support carbon budget studies in reservoirs as well as anthropogenic
3150 impacts in Amazon floodplain lakes: Preliminary results. *International Archives of the*
3151 *Photogrammetry, Remote Sensing and Spatial Information Sciences - ISPRS Archives*, *40*(7W3),
3152 1439–1446. <https://doi.org/10.5194/isprsarchives-XL-7-W3-1439-2015>
- 3153 Barbosa, P. M., Melack, J. M., Amaral, J. H. F., MacIntyre, S., Kasper, D., Cortés, A., et al. (2020).
3154 Dissolved methane concentrations and fluxes to the atmosphere from a tropical floodplain lake.
3155 *Biogeochemistry*, *148*(2), 129–151. <https://doi.org/10.1007/s10533-020-00650-1>
- 3156 Barichivich, J., Gloor, E., Peylin, P., Brienen, R. J. W., Schöngart, J., Espinoza, J. C., & Pattayak, K. C.
3157 (2018). Recent intensification of Amazon flooding extremes driven by strengthened Walker
3158 circulation. *Science Advances*, *4*(9). <https://doi.org/10.1126/sciadv.aat8785>
- 3159 Bastiaanssen, W. G. M. (1995). *Regionalization of surface flux densities and moisture indicators in*
3160 *composite terrain: a remote sensing approach under clear skies in Mediterranean climates.*
3161 *Doctoral thesis, Wageningen Agricultural University, Wageningen The Netherlands.*

- 3162 Baugh, C. A., Bates, P. D., Schumann, G., & Trigg, M. A. (2013). SRTM vegetation removal and
3163 hydrodynamic modeling accuracy. *Water Resources Research*, *49*(9), 5276–5289.
3164 <https://doi.org/10.1002/wrcr.20412>
- 3165 Bayley, P. B., & Moreira, J. C. (1978). Preliminary interpretations of aquatic resources in the central
3166 Amazon Basin using Landsat multispectral imagery. In N. de J. Parada (Ed.), *Anais...* (pp. 854–865).
3167 São José dos Campos: Instituto Nacional de Pesquisas Espaciais (INPE). Retrieved from
3168 <http://urlib.net/rep/dpi.inpe.br/marte@80/2008/09.25.13.57>
- 3169 Beck, H. E., Vergopolan, N., Pan, M., Levizzani, V., van Dijk, A. I. J. M., Weedon, G. P., et al. (2017).
3170 Global-scale evaluation of 22 precipitation datasets using gauge observations and hydrological
3171 modeling. *Hydrology and Earth System Sciences*, *21*(12), 6201–6217. [https://doi.org/10.5194/hess-](https://doi.org/10.5194/hess-21-6201-2017)
3172 [21-6201-2017](https://doi.org/10.5194/hess-21-6201-2017)
- 3173 Beck, H. E., Van Dijk, A. I. J. M., Levizzani, V., Schellekens, J., Miralles, D. G., Martens, B., & De Roo,
3174 A. (2017). MSWEP: 3-hourly 0.25° global gridded precipitation (1979–2015) by merging gauge,
3175 satellite, and reanalysis data. *Hydrology and Earth System Sciences*, *21*(1), 589–615.
3176 <https://doi.org/10.5194/hess-21-589-2017>
- 3177 Beck, H. E., Pan, M., Roy, T., Weedon, G. P., Pappenberger, F., van Dijk, A. I. J. M., et al. (2018). Daily
3178 evaluation of 26 precipitation datasets using Stage-IV gauge-radar data for the CONUS. *Hydrology*
3179 *and Earth System Sciences Discussions*, 1–23. <https://doi.org/10.5194/hess-2018-481>
- 3180 Beck, H. E., Wood, E. F., Pan, M., Fisher, C. K., Miralles, D. G., Van Dijk, A. I. J. M., et al. (2019).
3181 MSWep v2 Global 3-hourly 0.1° precipitation: Methodology and quantitative assessment. *Bulletin*
3182 *of the American Meteorological Society*, *100*(3), 473–500. [https://doi.org/10.1175/BAMS-D-17-](https://doi.org/10.1175/BAMS-D-17-0138.1)
3183 [0138.1](https://doi.org/10.1175/BAMS-D-17-0138.1)
- 3184 Becker, A., Finger, P., Meyer-Christoffer, A., Rudolf, B., Schamm, K., Schneider, U., & Ziese, M.
3185 (2013). A description of the global land-surface precipitation data products of the Global
3186 Precipitation Climatology Centre with sample applications including centennial (trend) analysis
3187 from 1901-present. *Earth System Science Data*, *5*(1), 71–99. <https://doi.org/10.5194/essd-5-71-2013>
- 3188 Becker, M., Papa, F., Frappart, F., Alsdorf, D., Calmant, S., da Silva, J. S., et al. (2018). Satellite-based
3189 estimates of surface water dynamics in the Congo River Basin. *International Journal of Applied*
3190 *Earth Observation and Geoinformation*, *66*, 196–209. <https://doi.org/10.1016/j.jag.2017.11.015>
- 3191 Behnamian, A., Banks, S., White, L., Brisco, B., Milard, K., Pasher, J., et al. (2017). Semi-automated
3192 surfacewater detection with synthetic aperture radar data: A wetland case study. *Remote Sensing*, *9*,
3193 1209. <https://doi.org/10.3390/rs9121209>
- 3194 Beighley, R. E., Eggert, K. G., Dunne, T., He, Y., Gummadi, V., & Verdin, K. L. (2009). Simulating

- 3195 hydrologic and hydraulic processes throughout the Amazon River Basin. *Hydrological Processes*,
 3196 23, 1221–1235. <https://doi.org/10.1002/hyp>
- 3197 Belger, L., Forsberg, B. R., & Melack, J. M. (2011). Carbon dioxide and methane emissions from
 3198 interfluvial wetlands in the upper Negro River basin, Brazil. *Biogeochemistry*, 105, 171–183.
 3199 <https://doi.org/10.1007/s10533-010-9536-0>
- 3200 Bercher, N., Dinardo, S., Lucas, B., Fleury, S., Calmant, S., Femenias, P., et al. (2013). A review of
 3201 Cryosat-2/SIRAL applications for the monitoring of river water levels. *ESA Living Planet*
 3202 *Symposium, 1*(September), 1–30. Retrieved from
 3203 <http://ebooks.cambridge.org/ref/id/CBO9781107415324A009>
- 3204 Bernini, H., Borges, H. D., & Martinez, J. (2019). Quasi-Analytical Algorithm Calibration for Retrieval
 3205 of Inherent Optical Properties from Extremely Turbid Waters: The Case of Madeira River Basin. In
 3206 *IGARSS 2019 - 2019 IEEE International Geoscience and Remote Sensing Symposium* (pp. 6150–
 3207 6153). <https://doi.org/10.1109/IGARSS.2019.8897766>
- 3208 Berry, P. A. M., Garlick, J. D., Freeman, J. A., & Mathers, E. L. (2005). Global inland water monitoring
 3209 from multi-mission altimetry. *Geophysical Research Letters*, 32(16).
 3210 <https://doi.org/10.1029/2005GL022814>
- 3211 Biancamaria, S., Lettenmaier, D. P., & Pavelsky, T. M. (2016). The SWOT Mission and Its Capabilities
 3212 for Land Hydrology. *Surveys in Geophysics*, 37(2), 307–337. [https://doi.org/10.1007/s10712-015-](https://doi.org/10.1007/s10712-015-9346-y)
 3213 9346-y
- 3214 Bierkens, M. F. P., Bell, V. A., Burek, P., Chaney, N., Condon, L. E., David, C. H., et al. (2015). Hyper-
 3215 resolution global hydrological modelling: What is next?: “Everywhere and locally relevant” M. F. P.
 3216 Bierkens et al. Invited Commentary. *Hydrological Processes*, 29(2), 310–320.
 3217 <https://doi.org/10.1002/hyp.10391>
- 3218 Birkett, C. M., Mertes, L. A. K., Dunne, T., Costa, M. H., & Jasinski, M. J. (2002). Surface water
 3219 dynamics in the Amazon Basin: Application of satellite radar altimetry. *Journal of Geophysical*
 3220 *Research D: Atmospheres*, 107(20). <https://doi.org/10.1029/2001JD000609>
- 3221 Birkett, C. M., Ricko, M., Beckley, B. D., Yang, X., & Tetrault, R. L. (2017). G-REALM: A
 3222 lake/reservoir monitoring tool for drought monitoring and water resources management. In *AGU*
 3223 *Fall Meeting Abstracts* (Vol. 2017, pp. H23P-02).
- 3224 Blumstein, D., Biancamaria, S., Guérin, A., & Maisongrande, P. (2019). A potential constellation of small
 3225 altimetry satellites dedicated to continental surface waters (SMASH mission). In *AGU Fall Meeting*
 3226 *Abstracts* (Vol. 2019, pp. H43N-2257).
- 3227 Bogning, S., Frappart, F., Blarel, F., Niño, F., Mahé, G., Bricquet, J.-P., et al. (2018). Monitoring Water

- 3228 Levels and Discharges Using Radar Altimetry in an Ungauged River Basin: The Case of the
3229 Ogooué. *Remote Sensing*, 10(2). <https://doi.org/10.3390/rs10020350>
- 3230 Bogning, S., Frappart, F., Paris, A., Blarel, F., Niño, F., Saux Picart, S., et al. (2020). Hydro-climatology
3231 study of the Ogooué River basin using hydrological modeling and satellite altimetry. *Advances in*
3232 *Space Research*. <https://doi.org/https://doi.org/10.1016/j.asr.2020.03.045>
- 3233 Bonnet, M. P., Barroux, G., Martinez, J. M., Seyler, F., Moreira-Turcq, P., Cochonneau, G., et al. (2008).
3234 Floodplain hydrology in an Amazon floodplain lake (Lago Grande de Curuaí). *Journal of*
3235 *Hydrology*, 349(1–2), 18–30. <https://doi.org/10.1016/j.jhydrol.2007.10.055>
- 3236 Bonnet, M. P., Pinel, S., Garnier, J., Bois, J., Resende Boaventura, G., Seyler, P., & Motta Marques, D.
3237 (2017). Amazonian floodplain water balance based on modelling and analyses of hydrologic and
3238 electrical conductivity data. *Hydrological Processes*, 31(9), 1702–1718.
3239 <https://doi.org/10.1002/hyp.11138>
- 3240 Bookhagen, B., & Strecker, M. R. (2008). Orographic barriers, high-resolution TRMM rainfall, and relief
3241 variations along the eastern Andes. *Geophysical Research Letters*, 35(6), L06403.
3242 <https://doi.org/10.1029/2007GL032011>
- 3243 Borma, L. S., Da Rocha, H. R., Cabral, O. M., Von Randow, C., Collicchio, E., Kurzatkowski, D., et al.
3244 (2009). Atmosphere and hydrological controls of the evapotranspiration over a floodplain forest in
3245 the Bananal Island region, Amazonia. *Journal of Geophysical Research: Biogeosciences*, 114(G1).
3246 <https://doi.org/10.1029/2007JG000641>
- 3247 Bosilovich, M. G., & Chern, J. D. (2006). Simulation of water sources and precipitation recycling for the
3248 MacKenzie, Mississippi, and Amazon River basins. *Journal of Hydrometeorology*, 7(3), 312–329.
3249 <https://doi.org/10.1175/JHM501.1>
- 3250 Bouchez, J., Lupker, M., Maurice, L., Perez, M., & Gaillardet, J. (2011). Prediction of depth-integrated
3251 fluxes of suspended sediment in the Amazon River: particle aggregation as a complicating factor.
3252 *Hydrological Processes*, 794(October 2010), 778–794. <https://doi.org/10.1002/hyp.7868>
- 3253 Bourgoin, L. M., Bonnet, M. P., Martinez, J. M., Kosuth, P., Cochonneau, G., Moreira-Turcq, P., et al.
3254 (2007). Temporal dynamics of water and sediment exchanges between the Curuaí floodplain and the
3255 Amazon River, Brazil. *Journal of Hydrology*, 335(1–2), 140–156.
3256 <https://doi.org/10.1016/j.jhydrol.2006.11.023>
- 3257 Bourrel, L., Phillips, L., & Moreau, S. (2009). The dynamics of floods in the Bolivian Amazon Basin.
3258 *Hydrological Processes*, 23, 3161–3167. <https://doi.org/10.1002/hyp.7384>
- 3259 Bradley, J. (1980). *Remote sensing of suspended sediment in Amazonian rivers using satellite*
3260 *multispectral imagery*. Royal Holloway, University of London. Retrieved from

- 3261 <http://isni.org/isni/0000000134753316>
- 3262 Brakenridge, G. R., Nghiem, S. V., Anderson, E., & Mic, R. (2007). Orbital microwave measurement of
3263 river discharge and ice status. *Water Resources Research*, *43*.
3264 <https://doi.org/10.1029/2006WR005238>
- 3265 Brasil. (1997). *Lei nº 9.433, de 8 de janeiro de 1997. Institui a Política Nacional de Recursos Hídricos,*
3266 *cria o Sistema Nacional de Gerenciamento de Recursos Hídricos, regulamenta o inciso XIX do art.*
3267 *21 da Constituição Federal, e altera o art. 1º da Lei nº 8.001, de 13.* Diário Oficial [da] República
3268 Federativa do Brasil, Brasília. Retrieved from http://www.planalto.gov.br/ccivil_03/leis/19433.htm
- 3269 Brêda, J. P. L. F., Paiva, R. C. D., Bravo, J. M., Passaia, O. A., & Moreira, D. M. (2019). Assimilation of
3270 Satellite Altimetry Data for Effective River Bathymetry. *Water Resources Research*, *55*(9), 7441–
3271 7463. <https://doi.org/10.1029/2018wr024010>
- 3272 Brocca, L., Moramarco, T., Melone, F., & Wagner, W. (2013). A new method for rainfall estimation
3273 through soil moisture observations. *Geophysical Research Letters*, *40*(5), 853–858.
3274 <https://doi.org/10.1002/grl.50173>
- 3275 Brocca, L., Ciabatta, L., Massari, C., Moramarco, T., Hahn, S., Hasenauer, S., et al. (2014). Soil as a
3276 natural rain gauge: Estimating global rainfall from satellite soil moisture data. *Journal of*
3277 *Geophysical Research: Atmospheres*, *119*(9), 5128–5141. <https://doi.org/10.1002/2014JD021489>
- 3278 Brocca, L., Filippucci, P., Hahn, S., Ciabatta, L., Massari, C., Camici, S., et al. (2019). SM2RAIN-
3279 ASCAT (2007-2018): Global daily satellite rainfall data from ASCAT soil moisture observations.
3280 *Earth System Science Data*, *11*(4), 1583–1601. <https://doi.org/10.5194/essd-11-1583-2019>
- 3281 Builes-Jaramillo, A., & Poveda, G. (2018). Conjoint Analysis of Surface and Atmospheric Water
3282 Balances in the Andes-Amazon System. *Water Resources Research*, *54*(5), 3472–3489.
3283 <https://doi.org/10.1029/2017WR021338>
- 3284 Butt, N., De Oliveira, P. A., & Costa, M. H. (2011). Evidence that deforestation affects the onset of the
3285 rainy season in Rondonia, Brazil. *Journal of Geophysical Research Atmospheres*, *116*(11), 2–9.
3286 <https://doi.org/10.1029/2010JD015174>
- 3287 Buytaert, W., Zulkafli, Z., Grainger, S., Acosta, L., Alemie, T. C., Bastiaensen, J., et al. (2014). Citizen
3288 science in hydrology and water resources: opportunities for knowledge generation, ecosystem
3289 service management, and sustainable development. *Frontiers in Earth Science*, *2*, 26.
3290 <https://doi.org/10.3389/feart.2014.00026>
- 3291 Callède, J., Guyot, J. L., Ronchail, J., L'Hôte, Y., Niel, H., & De Oliveira, E. (2004). Evolution of the
3292 River Amazon's discharge at Óbidos from 1903 to 1999. *Hydrological Sciences Journal*, *49*(1), 85–
3293 98. <https://doi.org/10.1623/hysj.49.1.85.53992>

- 3294 Callède, J., Cochonneau, G., Alves, F. V., Guyot, J.-L., Guimarães, V. S., & De Oliveira, E. (2010). The
 3295 River Amazon water contribution to the Atlantic Ocean. *Revue Des Sciences de l'eau*, 23(3), 247–
 3296 273. Retrieved from [https://www.erudit.org/en/journals/rseau/2010-v23-n3-](https://www.erudit.org/en/journals/rseau/2010-v23-n3-rseau3946/044688ar/abstract/)
 3297 [rseau3946/044688ar/abstract/](https://www.erudit.org/en/journals/rseau/2010-v23-n3-rseau3946/044688ar/abstract/)
- 3298 Callède, J., Moreira, D. M., & Calmant, S. (2013). Détermination de l'altitude du zéro des stations
 3299 hydrométriques en amazonie brésilienne. Application aux lignes d'eau des Rios Negro, Solimões et
 3300 Amazone. *Revue Des Sciences de l'Eau*, 26(2), 153–171. <https://doi.org/10.7202/1016065ar>
- 3301 Calmant, S., & Seyler, F. (2006). Continental surface waters from satellite altimetry. *Comptes Rendus -*
 3302 *Geoscience*, 338(14–15), 1113–1122. <https://doi.org/10.1016/j.crte.2006.05.012>
- 3303 Calmant, S., Da Silva, J. S., Moreira, D. M., Seyler, F., Shum, C. K., Crétaux, J. F., & Gabalda, G.
 3304 (2013). Detection of Envisat RA2/ICE-1 retracked radar altimetry bias over the Amazon basin rivers
 3305 using GPS. *Advances in Space Research*, 51(8), 1551–1564.
 3306 <https://doi.org/10.1016/j.asr.2012.07.033>
- 3307 Calmant, S., Crétaux, J. F., & Rémy, F. (2016). Principles of Radar Satellite Altimetry for Application on
 3308 Inland Waters. *Microwave Remote Sensing of Land Surfaces: Techniques and Methods*, 175–218.
 3309 <https://doi.org/10.1016/B978-1-78548-159-8.50004-9>
- 3310 Campos-Silva, J. V., Hawes, J. E., Freitas, C. T., Andrade, P. C. M., & Peres, C. A. (2020). Community-
 3311 Based Management of Amazonian Biodiversity Assets. In C. Baldauf (Ed.), *Participatory*
 3312 *Biodiversity Conservation: Concepts, Experiences, and Perspectives* (pp. 99–111). Cham: Springer
 3313 International Publishing. https://doi.org/10.1007/978-3-030-41686-7_7
- 3314 Cao, N., Lee, H., Jung, H. C., & Yu, H. (2018). Estimation of Water Level Changes of Large-Scale
 3315 Amazon Wetlands Using ALOS2 ScanSAR Differential Interferometry, 10(966).
 3316 <https://doi.org/10.3390/rs10060966>
- 3317 Cardille, J. A., Foley, J. A., & Costa, M. H. (2002). Characterizing patterns of agricultural land use in
 3318 Amazonia by merging satellite classifications and census data. *Global Biogeochemical Cycles*,
 3319 16(3), 18-1-18–14. <https://doi.org/10.1029/2000gb001386>
- 3320 Carvalho, J. C., Cochonneau, G., Piscocya, R. de C. C. C. de, Martinez, J., Souza, E. A. De, Antunes, M.
 3321 A., et al. (2015). HIDROSAT - Sistema Integrado para Gerenciamento, Processamento e Difusão de
 3322 Dados Hidrológicos Obtidos a Partir de Monitoramento por Satélites. In *XXI Simpósio Brasileiro de*
 3323 *Recursos Hídricos*. Brasília, DF: ABRH.
- 3324 de Carvalho, L. A. S., Faria Barbosa, C. C., Leão de Moraes Novo, E. M., & de Moraes Rudorff, C.
 3325 (2015). Implications of scatter corrections for absorption measurements on optical closure of
 3326 Amazon floodplain lakes using the Spectral Absorption and Attenuation Meter (AC-S-WETLabs).

- 3327 *Remote Sensing of Environment*, 157, 123–137. <https://doi.org/10.1016/j.rse.2014.06.018>
- 3328 Carvalho, L. M. V., Jones, C., & Liebmann, B. (2004). The South Atlantic Convergence Zone: Intensity,
3329 Form, Persistence, and Relationships with Intraseasonal to Interannual Activity and Extreme
3330 Rainfall. *Journal of Climate*, 17(1), 88–108. [https://doi.org/10.1175/1520-0442\(2004\)017<0088:TSACZI>2.0.CO;2](https://doi.org/10.1175/1520-0442(2004)017<0088:TSACZI>2.0.CO;2)
- 3331
- 3332 Castello, L., & Macedo, M. N. (2016). Large-scale degradation of Amazonian freshwater ecosystems.
3333 *Global Change Biology*, 22(3), 990–1007. <https://doi.org/10.1111/gcb.13173>
- 3334 Castello, L., Hess, L. L., Thapa, R., McGrath, D. G., Arantes, C. C., Renó, V. F., & Isaac, V. J. (2018).
3335 Fishery yields vary with land cover on the Amazon River floodplain. *Fish and Fisheries*, 19, 431–
3336 440. <https://doi.org/10.1111/faf.12261>
- 3337 Cavalcante, R. B. L., Pontes, P. R. M., Souza-Filho, P. W. M., & de Souza, E. B. (2019). Opposite Effects
3338 of Climate and Land Use Changes on the Annual Water Balance in the Amazon Arc of
3339 Deforestation. *Water Resources Research*, 55(4), 3092–3106.
3340 <https://doi.org/10.1029/2019WR025083>
- 3341 Cavalcante, R. B. L., Ferreira, D. B. da S., Pontes, P. R. M., Tedeschi, R. G., da Costa, C. P. W., & de
3342 Souza, E. B. (2020). Evaluation of extreme rainfall indices from CHIRPS precipitation estimates
3343 over the Brazilian Amazonia. *Atmospheric Research*, 238(October 2019), 104879.
3344 <https://doi.org/10.1016/j.atmosres.2020.104879>
- 3345 Chapman, B., McDonald, K., Shimada, M., Rosenqvist, A., Schroeder, R., & Hess, L. (2015). Mapping
3346 Regional Inundation with Spaceborne L-Band SAR. *Remote Sensing*, 7(5), 5440–5470.
3347 <https://doi.org/10.3390/rs70505440>
- 3348 Chaudhari, S., Pokhrel, Y., Moran, E., & Miguez-Macho, G. (2019). Multi-decadal hydrologic change
3349 and variability in the Amazon River basin: Understanding terrestrial water storage variations and
3350 drought characteristics. *Hydrology and Earth System Sciences*, 23(7), 2841–2862.
3351 <https://doi.org/10.5194/hess-23-2841-2019>
- 3352 Chavez, S. P., & Takahashi, K. (2017). Orographic rainfall hot spots in the Andes-Amazon transition
3353 according to the TRMM precipitation radar and in situ data. *Journal of Geophysical Research*.
3354 <https://doi.org/10.1002/2016JD026282>
- 3355 Chen, J. L., Wilson, C. R., Tapley, B. D., Yang, Z. L., & Niu, G. Y. (2009). 2005 drought event in the
3356 Amazon River basin as measured by GRACE and estimated by climate models. *Journal of*
3357 *Geophysical Research: Solid Earth*, 114(5), 1–9. <https://doi.org/10.1029/2008JB006056>
- 3358 Chen, J. L., Wilson, C. R., & Tapley, B. D. (2010). The 2009 exceptional Amazon flood and interannual
3359 terrestrial water storage change observed by GRACE. *Water Resources Research*, 46(12), 1–10.

- 3360 <https://doi.org/10.1029/2010WR009383>
- 3361 Chen, M., Shi, W., Xie, P., Silva, V. B. S., Kousky, V. E., Wayne Higgins, R., & Janowiak, J. E. (2008).
3362 Assessing objective techniques for gauge-based analyses of global daily precipitation. *Journal of*
3363 *Geophysical Research*, 113(D4), D04110. <https://doi.org/10.1029/2007JD009132>
- 3364 Chew, C., & Small, E. (2020). Estimating inundation extent using CYGNSS data: A conceptual modeling
3365 study. *Remote Sensing of Environment*, 246, 111869. <https://doi.org/10.1016/j.rse.2020.111869>
- 3366 Choudhury, B. J. (1991). Passive microwave remote sensing contribution to hydrological variables.
3367 *Surveys in Geophysics*, 12, 63–84. <https://doi.org/10.1007/BF01903412>
- 3368 Christoffersen, B. O., Restrepo-Coupe, N., Arain, M. A., Baker, I. T., Cestaro, B. P., Ciais, P., et al.
3369 (2014). Mechanisms of water supply and vegetation demand govern the seasonality and magnitude
3370 of evapotranspiration in Amazonia and Cerrado. *Agricultural and Forest Meteorology*,
3371 191(February), 33–50. <https://doi.org/10.1016/j.agrformet.2014.02.008>
- 3372 Ciabatta, L., Massari, C., Brocca, L., Gruber, A., Reimer, C., Hahn, S., et al. (2018). SM2RAIN-CCI: A
3373 new global long-term rainfall data set derived from ESA CCI soil moisture. *Earth System Science*
3374 *Data*, 10(1), 267–280. <https://doi.org/10.5194/essd-10-267-2018>
- 3375 Cintra, R. (2015). Spatial distribution and composition of waterbirds in relation to limnological conditions
3376 in the Amazon basin. *Hydrobiologia*, 747, 235–252. <https://doi.org/10.1007/s10750-014-2148-2>
- 3377 Claverie, M., Ju, J., Masek, J. G., Dungan, J. L., Vermote, E. F., Roger, J., et al. (2018). The Harmonized
3378 Landsat and Sentinel-2 surface reflectance data set. *Remote Sensing of Environment*, 219(August),
3379 145–161. <https://doi.org/10.1016/j.rse.2018.09.002>
- 3380 Cleugh, H. A., Leuning, R., Mu, Q., & Running, S. W. (2007). Regional evaporation estimates from flux
3381 tower and MODIS satellite data. *Remote Sensing of Environment*, 106(3), 285–304.
3382 <https://doi.org/10.1016/j.rse.2006.07.007>
- 3383 Coe, M. T., Costa, M. H., Botta, A., & Birkett, C. (2002). Long-term simulations of discharge and floods
3384 in the Amazon Basin. *Journal of Geophysical Research Atmospheres*, 107(20), 1–17.
3385 <https://doi.org/10.1029/2001JD000740>
- 3386 Coe, M. T., Costa, M. H., & Howard, E. A. (2008). Simulating the surface waters of the Amazon River
3387 basin: Impacts of new river geomorphic and flow parameterizations. *Hydrological Processes*,
3388 22(14), 2542–2553. <https://doi.org/10.1002/hyp.6850>
- 3389 Coe, M. T., Costa, M. H., & Soares-Filho, B. S. (2009). The influence of historical and potential future
3390 deforestation on the stream flow of the Amazon River - Land surface processes and atmospheric
3391 feedbacks. *Journal of Hydrology*. <https://doi.org/10.1016/j.jhydrol.2009.02.043>
- 3392 Coe, M. T., Latrubesse, E. M., Ferreira, M. E., & Amsler, M. L. (2011). The effects of deforestation and

- 3393 climate variability on the streamflow of the Araguaia River, Brazil. *Biogeochemistry*, 105(1), 119–
3394 131. <https://doi.org/10.1007/s10533-011-9582-2>
- 3395 Cogley, J. G. (2013). GGHYDRO - Global Hydrographic Data, Release 2.3.1 Trent Technical Note 2003-
3396 1.
- 3397 Collischonn, B., Collischonn, W., & Tucci, C. E. M. (2008). Daily hydrological modeling in the Amazon
3398 basin using TRMM rainfall estimates. *Journal of Hydrology*, 360(1–4), 207–216.
3399 <https://doi.org/10.1016/j.jhydrol.2008.07.032>
- 3400 Constantine, J. A., Dunne, T., Ahmed, J., Legleiter, C., & Lazarus, E. D. (2014). Sediment supply as a
3401 driver of river meandering and floodplain evolution in the Amazon Basin. *Nature Geoscience*,
3402 7(12), 899–903. <https://doi.org/10.1038/ngeo2282>
- 3403 Cooley, S. W., Smith, L. C., Ryan, J. C., Pitcher, L. H., & Pavelsky, T. M. (2019). Arctic-Boreal Lake
3404 Dynamics Revealed Using CubeSat Imagery. *Geophysical Research Letters*, 46(4), 2111–2120.
3405 <https://doi.org/10.1029/2018GL081584>
- 3406 Correa, S. W., Paiva, R. C. D. de, Espinoza, J. C., & Collischonn, W. (2017). Multi-decadal Hydrological
3407 Retrospective: Case study of Amazon floods and droughts. *Journal of Hydrology*, 549, 667–684.
3408 <https://doi.org/10.1016/j.jhydrol.2017.04.019>
- 3409 Coss, S., Durand, M., Yi, Y., Jia, Y., Guo, Q., Tuozzolo, S., et al. (2020). Global River Radar Altimetry
3410 Time Series (GRRATS): New river elevation earth science data records for the hydrologic
3411 community. *Earth System Science Data*, 12(1), 137–150. <https://doi.org/10.5194/essd-12-137-2020>
- 3412 Costa, M. (2005). Estimate of net primary productivity of aquatic vegetation of the Amazon floodplain
3413 using Radarsat and JERS-1. *International Journal of Remote Sensing*, 26(20), 4527–4536.
3414 <https://doi.org/10.1080/01431160500213433>
- 3415 Costa, M. H. (2005). Large-scale hydrological impacts of tropical forest conversion. In M. Bonell & L. A.
3416 S. Bruijnzeel (Eds.), *Forests, Water and People in the Humid Tropics* (pp. 590–597). Cambridge
3417 University Press. <https://doi.org/https://doi.org/10.1017/CBO9780511535666>
- 3418 Costa, M. H. (2020). When more trees mean more power. *Nature Sustainability*, 3(June), 410–411.
3419 <https://doi.org/10.1038/s41893-020-0511-z>
- 3420 Costa, M. H., & Foley, J. A. (1997). Water balance of the Amazon Basin: Dependence on vegetation
3421 cover and canopy conductance. *Journal of Geophysical Research: Atmospheres*, 102(D20), 23973–
3422 23989. <https://doi.org/10.1029/97JD01865>
- 3423 Costa, M. H., & Pires, G. F. (2010). Effects of Amazon and Central Brazil deforestation scenarios on the
3424 duration of the dry season in the arc of deforestation. *International Journal of Climatology*, 30(13),
3425 1970–1979. <https://doi.org/10.1002/joc.2048>

- 3426 Costa, M. H., Botta, A., & Cardille, J. A. (2003). Effects of large-scale changes in land cover on the
3427 discharge of the Tocantins River, Southeastern Amazonia. *Journal of Hydrology*, 283(1–4), 206–
3428 217. [https://doi.org/10.1016/S0022-1694\(03\)00267-1](https://doi.org/10.1016/S0022-1694(03)00267-1)
- 3429 Costa, M. H., Biajoli, M. C., Sanches, L., Malhado, A. C. M., Hutyra, L. R., da Rocha, H. R., et al.
3430 (2010). Atmospheric versus vegetation controls of Amazonian tropical rain forest
3431 evapotranspiration: Are the wet and seasonally dry rain forests any different? *Journal of*
3432 *Geophysical Research*, 115(G4), G04021. <https://doi.org/10.1029/2009JG001179>
- 3433 Costa, M. P. F., Novo, E. M. L. M., & Telmer, K. H. (2013). Spatial and temporal variability of light
3434 attenuation in large rivers of the Amazon. *Hydrobiologia*, 702(1), 171–190.
3435 <https://doi.org/10.1007/s10750-012-1319-2>
- 3436 Crétaux, J. F., & Birkett, C. (2006). Lake studies from satellite radar altimetry. *Comptes Rendus -*
3437 *Geoscience*, 338(14–15), 1098–1112. <https://doi.org/10.1016/j.crte.2006.08.002>
- 3438 Crétaux, J. F., Jelinski, W., Calmant, S., Kouraev, A., Vuglinski, V., Bergé-Nguyen, M., et al. (2011).
3439 SOLS: A lake database to monitor in the Near Real Time water level and storage variations from
3440 remote sensing data. *Advances in Space Research*, 47(9), 1497–1507.
3441 <https://doi.org/10.1016/j.asr.2011.01.004>
- 3442 Crowley, J. W., Mitrovica, J. X., Bailey, R. C., Tamisiea, M. E., & Davis, J. L. (2008). Annual variations
3443 in water storage and precipitation in the Amazon Basin: Bounding sink terms in the terrestrial
3444 hydrological balance using GRACE satellite gravity data. *Journal of Geodesy*, 82(1), 9–13.
3445 <https://doi.org/10.1007/s00190-007-0153-1>
- 3446 Cuartas, L. A., Tomasella, J., Nobre, A. D., Nobre, C. A., Hodnett, M. G., Waterloo, M. J., et al. (2012).
3447 Distributed hydrological modeling of a micro-scale rainforest watershed in Amazonia: Model
3448 evaluation and advances in calibration using the new HAND terrain model. *Journal of Hydrology*,
3449 462–463, 15–27. <https://doi.org/10.1016/j.jhydrol.2011.12.047>
- 3450 Davidson, E. A., & Artaxo, P. (2004). Globally significant changes in biological processes of the Amazon
3451 Basin: Results of the large-scale Biosphere-Atmosphere Experiment. *Global Change Biology*, 10(5),
3452 519–529. <https://doi.org/10.1111/j.1529-8817.2003.00779.x>
- 3453 Davidson, E. A., De Araújo, A. C., Artaxo, P., Balch, J. K., Brown, I. F., Mercedes, M. M., et al. (2012).
3454 The Amazon basin in transition. *Nature*, 481, 312–328. <https://doi.org/10.1038/nature10717>
- 3455 Davidson, N. C., Fluet-Chouinard, E., & Finlayson, C. M. (2018). Global extent and distribution of
3456 wetlands: Trends and issues. *Marine and Freshwater Research*, 69, 620–627.
3457 <https://doi.org/10.1071/MF17019>
- 3458 Debortoli, N. S., Dubreuil, V., Funatsu, B., Delahaye, F., de Oliveira, C. H., Rodrigues-Filho, S., et al.

- 3459 (2015). Rainfall patterns in the Southern Amazon: a chronological perspective (1971–2010).
3460 *Climatic Change*, 132(2), 251–264. <https://doi.org/10.1007/s10584-015-1415-1>
- 3461 Decharme, B., Alkama, R., Papa, F., Faroux, S., Douville, H., & Prigent, C. (2012). Global off-line
3462 evaluation of the ISBA-TRIP flood model. *Climate Dynamics*, 38(7), 1389–1412.
3463 <https://doi.org/10.1007/s00382-011-1054-9>
- 3464 Decharme, Bertrand, Douville, H., Prigent, C., Papa, F., & Aires, F. (2008). A new river flooding scheme
3465 for global climate applications: Off-line evaluation over South America. *Journal of Geophysical*
3466 *Research Atmospheres*, 113(11). <https://doi.org/10.1029/2007JD009376>
- 3467 Dekker, A. G. (1993). *Detection of optical water quality parameters for eutrophic waters by high*
3468 *resolution remote sensing. Management.*
- 3469 Delahaye, F., Kirstetter, P. E., Dubreuil, V., Machado, L. A. T., Vila, D. A., & Clark, R. (2015). A
3470 consistent gauge database for daily rainfall analysis over the Legal Brazilian Amazon. *Journal of*
3471 *Hydrology*, 527, 292–304. <https://doi.org/10.1016/j.jhydrol.2015.04.012>
- 3472 Desai, S. (2018). *Surface Water and Ocean Topography Mission Project - Science Requirements*
3473 *Document. JPL documentD-61923. Jet Propulsion Laboratory.* Retrieved from
3474 https://swot.jpl.nasa.gov/system/documents/files/2176_2176_D-61923_SRD_Rev_B_20181113.pdf
- 3475 Dias, C. M., Pastore, D. H., Borma, L. S., & Bevilacqua, L. (2011). Modelling and numerical simulation
3476 of the velocity field in the Parque Estadual do Cantão (TO), Brazil. *Mathematical and Computer*
3477 *Modelling*, 53(7–8), 1575–1581. <https://doi.org/10.1016/j.mcm.2010.06.021>
- 3478 Dias, L. C. P., Pimenta, F. M., Santos, A. B., Costa, M. H., & Ladle, R. J. (2016). Patterns of land use,
3479 extensification, and intensification of Brazilian agriculture. *Global Change Biology*, 22(8), 2887–
3480 2903. <https://doi.org/10.1111/gcb.13314>
- 3481 Van Dijk, A. I. J. M., & Renzullo, L. J. (2011). Water resource monitoring systems and the role of
3482 satellite observations. *Hydrology and Earth System Sciences*, 15(1), 39–55.
3483 <https://doi.org/10.5194/hess-15-39-2011>
- 3484 Diniz, C. G., d. A. Souza, A. A., Santos, D. C., Dias, M. C., d. Luz, N. C., d. Moraes, D. R. V., et al.
3485 (2015). DETER-B: The New Amazon Near Real-Time Deforestation Detection System. *IEEE*
3486 *Journal of Selected Topics in Applied Earth Observations and Remote Sensing*, 8(7), 3619–3628.
3487 <https://doi.org/10.1109/JSTARS.2015.2437075>
- 3488 Dinku, T., Ceccato, P., & Connor, S. J. (2011). Challenges of satellite rainfall estimation over
3489 mountainous and arid parts of east africa. *International Journal of Remote Sensing*, 32(21), 5965–
3490 5979. <https://doi.org/10.1080/01431161.2010.499381>
- 3491 Drusch, M., Moreno, J., Del Bello, U., Franco, R., Goulas, Y., Huth, A., et al. (2017). The FLuorescence

- 3492 EXplorer Mission Concept-ESA's Earth Explorer 8. *IEEE Transactions on Geoscience and Remote*
3493 *Sensing*, 55(3), 1273–1284. <https://doi.org/10.1109/TGRS.2016.2621820>
- 3494 Durieux, L., Toledo Machado, L. A., & Laurent, H. (2003). The impact of deforestation on cloud cover
3495 over the Amazon arc of deforestation. *Remote Sensing of Environment*, 86(1), 132–140.
3496 [https://doi.org/10.1016/S0034-4257\(03\)00095-6](https://doi.org/10.1016/S0034-4257(03)00095-6)
- 3497 Duvel, J. F., & Kandel, R. S. (1985). Regional-Scale Diurnal Variations of Outgoing Infrared Radiation
3498 Observed by METEOSAT. *Journal of Climate and Applied Meteorology*, 24(4), 335–349.
3499 [https://doi.org/10.1175/1520-0450\(1985\)024<0335:RSDVOO>2.0.CO;2](https://doi.org/10.1175/1520-0450(1985)024<0335:RSDVOO>2.0.CO;2)
- 3500 Eltahir, E. A. B., & Bras, R. L. (1994). Precipitation recycling in the Amazon basin. *Quarterly Journal of*
3501 *the Royal Meteorological Society*, 120(518), 861–880. <https://doi.org/10.1002/qj.49712051806>
- 3502 Emery, C. M., Paris, A., Biancamaria, S., Boone, A., Calmant, S., Garambois, P. A., & Da Silva, J. S.
3503 (2018). Large-scale hydrological model river storage and discharge correction using a satellite
3504 altimetry-based discharge product. *Hydrology and Earth System Sciences*.
3505 <https://doi.org/10.5194/hess-22-2135-2018>
- 3506 Emery, C. M., Biancamaria, S., Boone, A., Ricci, S., Rochoux, M., Pedinotti, V., & David, C. (2020).
3507 Assimilation of wide-swath altimetry observations to correct large-scale river routing model
3508 parameters. *Hydrology and Earth System Sciences Discussions*, 24, 2207–2233.
3509 <https://doi.org/10.5194/hess-2019-242-RC3>
- 3510 Endo, W., Peres, C. A., & Haugaasen, T. (2016). Flood pulse dynamics affects exploitation of both
3511 aquatic and terrestrial prey by Amazonian floodplain settlements. *Biological Conservation*, 201,
3512 129–136. <https://doi.org/10.1016/j.biocon.2016.07.006>
- 3513 Engle, D. L., Melack, J. M., Doyle, R. D., & Fisher, T. R. (2008). High rates of net primary production
3514 and turnover of floating grasses on the Amazon floodplain: Implications for aquatic respiration and
3515 regional CO₂ flux. *Global Change Biology*, 14, 369–381. [https://doi.org/10.1111/j.1365-](https://doi.org/10.1111/j.1365-2486.2007.01481.x)
3516 [2486.2007.01481.x](https://doi.org/10.1111/j.1365-2486.2007.01481.x)
- 3517 Van Der Ent, R. J., Savenije, H. H. G., Schaeffli, B., & Steele-Dunne, S. C. (2010). Origin and fate of
3518 atmospheric moisture over continents. *Water Resources Research*, 46(9), 1–12.
3519 <https://doi.org/10.1029/2010WR009127>
- 3520 Ershadi, A., McCabe, M. F., Evans, J. P., & Wood, E. F. (2015). Impact of model structure and
3521 parameterization on Penman-Monteith type evaporation models. *Journal of Hydrology*, 525, 521–
3522 535. <https://doi.org/10.1016/j.jhydrol.2015.04.008>
- 3523 Espinoza-Villar, R., Martinez, J. M., Armijos, E., Espinoza, J. C., Filizola, N., Dos Santos, A., et al.
3524 (2018). Spatio-temporal monitoring of suspended sediments in the Solimões River (2000-2014).

- 3525 *Comptes Rendus - Geoscience*, 350(1–2), 1–9. <https://doi.org/10.1016/j.crte.2017.05.001>
- 3526 Espinoza, J. C., Ronchail, J., Guyot, J. L., Cochonneau, G., Naziano, F., Lavado, W., et al. (2009). Spatio-
3527 temporal rainfall variability in the Amazon basin countries (Brazil, Peru, Bolivia, Colombia, and
3528 Ecuador). *International Journal of Climatology*, 29(11), 1574–1594.
3529 <https://doi.org/10.1002/joc.1791>
- 3530 Espinoza, J. C., Ronchail, J., Guyot, J. L., Junquas, C., Drapeau, G., Martinez, J. M., et al. (2012). From
3531 drought to flooding: Understanding the abrupt 2010–11 hydrological annual cycle in the Amazonas
3532 River and tributaries. *Environmental Research Letters*, 7(2). [https://doi.org/10.1088/1748-](https://doi.org/10.1088/1748-9326/7/2/024008)
3533 [9326/7/2/024008](https://doi.org/10.1088/1748-9326/7/2/024008)
- 3534 Espinoza, J. C., Ronchail, J., Frappart, F., Lavado, W., Santini, W., & Guyot, J. L. (2013). The Major
3535 Floods in the Amazonas River and Tributaries (Western Amazon Basin) during the 1970–2012
3536 Period: A Focus on the 2012 Flood. *Journal of Hydrometeorology*, 14(3), 1000–1008.
3537 <https://doi.org/10.1175/JHM-D-12-0100.1>
- 3538 Espinoza, J. C., Chavez, S., Ronchai, J., Junquas, C., Takahashi, K., & Lavado, W. (2015). Rainfall
3539 hotspots over the southern tropical Andes: Spatial distribution, rainfall intensity, and relations with
3540 large-scale atmospheric circulation. *Water Resources Research*, 1–27.
3541 <https://doi.org/10.1002/2015WR017096>.Received
- 3542 Espinoza, J. C., Segura, H., Ronchail, J., Drapeau, G., & Gutierrez-Cori, O. (2016). Evolution of wet-day
3543 and dry-day frequency in the western Amazon basin: Relationship with atmospheric circulation and
3544 impacts on vegetation. *Water Resources Research*, 52(11), 8546–8560.
3545 <https://doi.org/10.1002/2016WR019305>
- 3546 Espinoza, J. C., Ronchail, J., Marengo, J. A., & Segura, H. (2019). Contrasting North–South changes in
3547 Amazon wet-day and dry-day frequency and related atmospheric features (1981–2017). *Climate*
3548 *Dynamics*, 52(9–10), 5413–5430. <https://doi.org/10.1007/s00382-018-4462-2>
- 3549 Espinoza, J. C., Sörensson, A. A., Ronchail, J., Molina-Carpio, J., Segura, H., Gutierrez-Cori, O., et al.
3550 (2019). Regional hydro-climatic changes in the Southern Amazon Basin (Upper Madeira Basin)
3551 during the 1982–2017 period. *Journal of Hydrology: Regional Studies*, 26(June), 100637.
3552 <https://doi.org/10.1016/j.ejrh.2019.100637>
- 3553 Espinoza Villar, J. C., Guyot, J. L., Ronchail, J., Cochonneau, G., Filizola, N., Fraizy, P., et al. (2009).
3554 Contrasting regional discharge evolutions in the Amazon basin (1974–2004). *Journal of Hydrology*,
3555 375(3–4), 297–311. <https://doi.org/10.1016/j.jhydrol.2009.03.004>
- 3556 Espinoza Villar, J. C., Ronchail, J., Guyot, J. L., Cochonneau, G., Naziano, F., Lavado, W., et al. (2009).
3557 Spatio-temporal rainfall variability in the Amazon basin countries (Brazil, Peru, Bolivia, Colombia,

- 3558 and Ecuador). *International Journal of Climatology*, 29, 1574–1594.
 3559 <https://doi.org/10.1002/joc.1791>
- 3560 Espinoza Villar, R., Martinez, J. M., Guyot, J. L., Fraizy, P., Armijos, E., Crave, A., et al. (2012). The
 3561 integration of field measurements and satellite observations to determine river solid loads in poorly
 3562 monitored basins. *Journal of Hydrology*, 444–445, 221–228.
 3563 <https://doi.org/10.1016/j.jhydrol.2012.04.024>
- 3564 Fagundes, H. O., Fan, F. M., Paiva, R. C. D., Siqueira, V. A., Buarque, D. C., Kornowski, L. W., et al.
 3565 (2021). Sediment Flows in South America Supported by Daily Hydrologic-Hydrodynamic
 3566 Modeling. *Water Resources Research*, 57(2). <https://doi.org/10.1029/2020wr027884>
- 3567 Fan, F. M., Paiva, R. C. D., & Collischonn, W. (2016). Chapter 2 - Hydrological Forecasting Practices in
 3568 Brazil. In T. E. Adams & T. C. B. T.-F. F. Pagano (Eds.), *Flood Forecasting A Global Perspective*
 3569 (pp. 41–66). Boston: Academic Press. [https://doi.org/https://doi.org/10.1016/B978-0-12-801884-](https://doi.org/https://doi.org/10.1016/B978-0-12-801884-2.00002-5)
 3570 [2.00002-5](https://doi.org/https://doi.org/10.1016/B978-0-12-801884-2.00002-5)
- 3571 Fang, Y., Leung, L. R., Duan, Z., Wigmosta, M. S., Maxwell, R. M., Chambers, J. Q., & Tomasella, J.
 3572 (2017). Influence of landscape heterogeneity on water available to tropical forests in an Amazonian
 3573 catchment and implications for modeling drought response. *Journal of Geophysical Research:*
 3574 *Atmospheres*, 122(16), 8410–8426. <https://doi.org/https://doi.org/10.1002/2017JD027066>
- 3575 Farr, T., Rosen, P., Caro, E., Crippen, R., Duren, R., Hensley, S., et al. (2007). The shuttle radar
 3576 topography mission. *Reviews of Geophysics*, 45(2005), 1–33.
 3577 <https://doi.org/10.1029/2005RG000183>
- 3578 Fassoni-Andrade, A. C. (2020). *Mapping and characterization of the central Amazon river-floodplain*
 3579 *system by remote sensing and hydraulic modeling*. Universidade Federal do Rio Grande do Sul.
- 3580 Fassoni-Andrade, A. C., & Paiva, R. C. D. (2019). Mapping spatial-temporal sediment dynamics of river-
 3581 floodplains in the Amazon. *Remote Sensing of Environment*, 221(March 2018), 94–107.
 3582 <https://doi.org/10.1016/j.rse.2018.10.038>
- 3583 Fassoni-Andrade, A. C., Paiva, R. C. D., Rudorff, C. M., Barbosa, C. C. F., & Novo, E. M. L. de M.
 3584 (2020). High-resolution mapping of floodplain topography from space: A case study in the Amazon.
 3585 *Remote Sensing of Environment*, 251, 112065. <https://doi.org/10.1016/j.rse.2020.112065>
- 3586 Fassoni-Andrade, A. C., Paiva, R. C. D., & Fleischmann, A. S. (2020). Lake topography and active
 3587 storage from satellite observations of flood frequency. *Water Resources Research*, 56(7).
 3588 <https://doi.org/10.1029/2019wr026362>
- 3589 Fassoni-Andrade, A. C., Durand, F., Moreira, D., Azevedo, A., Santos, V., Funi, C., & Laraque, A.
 3590 (2021). Comprehensive bathymetry and intertidal topography of the Amazon estuary. *Earth System*

- 3591 *Science Data*. [https://doi.org/https://doi.org/10.5194/essd-2021-32](https://doi.org/10.5194/essd-2021-32)
- 3592 Fekete, B. M., Looser, U., Pietroniro, A., & Robarts, R. D. (2012). Rationale for monitoring discharge on
3593 the ground. *Journal of Hydrometeorology*, 13(6), 1977–1986. [https://doi.org/10.1175/JHM-D-11-](https://doi.org/10.1175/JHM-D-11-0126.1)
3594 0126.1
- 3595 Ferreira-Ferreira, J., Silva, T. S. F., Streher, A. S., Affonso, A. G., De Almeida Furtado, L. F., Forsberg,
3596 B. R., et al. (2015). Combining ALOS/PALSAR derived vegetation structure and inundation
3597 patterns to characterize major vegetation types in the Mamirauá Sustainable Development Reserve,
3598 Central Amazon floodplain, Brazil. *Wetlands Ecology and Management*, 23(1), 41–59.
3599 <https://doi.org/10.1007/s11273-014-9359-1>
- 3600 Ferreira, R. D., Barbosa, C. C. F., & Novo, E. M. L. de M. (2013). Assessment of in vivo fluorescence
3601 method for chlorophyll-a estimation in optically complex waters (Curuai floodplain, Pará - Brazil).
3602 *Acta Limnologica Brasiliensia*, 24(4), 373–386. <https://doi.org/10.1590/s2179-975x2013005000011>
- 3603 Ferreira, V. G., Montecino, H. C., Ndehedehe, C. E., Heck, B., Gong, Z., de Freitas, S. R. C., &
3604 Westerhaus, M. (2018). Space-based observations of crustal deflections for drought characterization
3605 in Brazil. *Science of the Total Environment*, 644, 256–273.
3606 <https://doi.org/10.1016/j.scitotenv.2018.06.277>
- 3607 Figueroa, S. N., & Nobre, C. A. (1990). Precipitation Distribution over Central and Western Tropical
3608 South America. *Climanálise*, 6, 36–40.
- 3609 Filizola, N., & Guyot, J. (2009). Suspended sediment yields in the Amazon basin: an assessment using the
3610 Brazilian national data set. *Hydrological Processes*, 23, 3207–3215.
3611 <https://doi.org/10.1002/hyp.7394>
- 3612 Finer, M., Novoa, S., Weisse, M. J., Petersen, R., Mascaro, J., Souto, T., et al. (2018). Combating
3613 deforestation: From satellite to intervention. *Science*, 360(6395), 1303–1305.
3614 <https://doi.org/10.1126/science.aat1203>
- 3615 Fisher, J. B., Tu, K. P., & Baldocchi, D. D. (2008). Global estimates of the land-atmosphere water flux
3616 based on monthly AVHRR and ISLSCP-II data, validated at 16 FLUXNET sites. *Remote Sensing of*
3617 *Environment*, 112(3), 901–919. <https://doi.org/10.1016/j.rse.2007.06.025>
- 3618 Fisher, J. B., Malhi, Y., Bonal, D., Da Rocha, H. R., De Araújo, A. C., Gamo, M., et al. (2009). The land-
3619 atmosphere water flux in the tropics. *Global Change Biology*, 15(11), 2694–2714.
3620 <https://doi.org/10.1111/j.1365-2486.2008.01813.x>
- 3621 Fisher, J. B., Melton, F., Middleton, E., Hain, C., Anderson, M., Allen, R., et al. (2017, April 1). The
3622 future of evapotranspiration: Global requirements for ecosystem functioning, carbon and climate
3623 feedbacks, agricultural management, and water resources. *Water Resources Research*. Blackwell

- 3624 Publishing Ltd. <https://doi.org/10.1002/2016WR020175>
- 3625 Fitzjarrald, D. R., Sakai, R. K., Moraes, O. L. L., Cosme de Oliveira, R., Acevedo, O. C., Czikowsky, M.
3626 J., & Beldini, T. (2008). Spatial and temporal rainfall variability near the Amazon-Tapajós
3627 confluence. *Journal of Geophysical Research: Biogeosciences*, *113*(G1), n/a-n/a.
3628 <https://doi.org/10.1029/2007JG000596>
- 3629 Fleischmann, A. S., Paiva, R. C. D., Collischonn, W., Sorribas, M. V., & Pontes, P. R. M. (2016). On
3630 river-floodplain interaction and hydrograph skewness. *Water Resources Research*, *52*(10), 7615–
3631 7630. <https://doi.org/10.1002/2016WR019233>
- 3632 Fleischmann, A. S., Siqueira, V., Paris, A., Collischonn, W., Paiva, R., Pontes, P., et al. (2018).
3633 Modelling hydrologic and hydrodynamic processes in basins with large semi-arid wetlands. *Journal*
3634 *of Hydrology*, *561*, 943–959. <https://doi.org/10.1016/j.jhydrol.2018.04.041>
- 3635 Fleischmann, A. S., Paiva, R., & Collischonn, W. (2019). Can regional to continental river hydrodynamic
3636 models be locally relevant? A cross-scale comparison. *Journal of Hydrology X*, *3*, 100027.
3637 <https://doi.org/10.1016/j.hydroa.2019.100027>
- 3638 Fleischmann, A. S., Paiva, R. C. D., Collischonn, W., Siqueira, V. A., Paris, A., Moreira, D. M., et al.
3639 (2020). Trade-Offs Between 1-D and 2-D Regional River Hydrodynamic Models. *Water Resources*
3640 *Research*, *56*(8). <https://doi.org/10.1029/2019WR026812>
- 3641 Flores Júnior, R. (2019). *Parametrização de algoritmos empíricos e algoritmo quasi-analítico QAA para*
3642 *estimativa de clorofila-a em lagos da várzea do rio Amazonas*. Instituto Nacional de Pesquisas
3643 Espaciais (INPE). Retrieved from <http://urlib.net/rep/8JMKD3MGP3W34R/3SUQ3U2>
- 3644 Fluet-Chouinard, E., Lehner, B., Rebelo, L. M., Papa, F., & Hamilton, S. K. (2015). Development of a
3645 global inundation map at high spatial resolution from topographic downscaling of coarse-scale
3646 remote sensing data. *Remote Sensing of Environment*, *158*, 348–361.
3647 <https://doi.org/10.1016/j.rse.2014.10.015>
- 3648 Forsberg, B. R., Melack, J. M., Dunne, T., Barthem, R. B., Goulding, M., Paiva, R. C. D., et al. (2017).
3649 The potential impact of new Andean dams on Amazon fluvial ecosystems. *PLoS ONE*, *12*(8).
3650 <https://doi.org/10.1371/journal.pone.0182254>
- 3651 Frappart, F., & Ramillien, G. (2018, May). Monitoring groundwater storage changes using the Gravity
3652 Recovery and Climate Experiment (GRACE) satellite mission: A review. *Remote Sensing*.
3653 Multidisciplinary Digital Publishing Institute. <https://doi.org/10.3390/rs10060829>
- 3654 Frappart, F., Seyler, F., Martinez, J. M., León, J. G., & Cazenave, A. (2005). Floodplain water storage in
3655 the Negro River basin estimated from microwave remote sensing of inundation area and water
3656 levels. *Remote Sensing of Environment*, *99*(4), 387–399. <https://doi.org/10.1016/j.rse.2005.08.016>

- 3657 Frappart, F., Calmant, S., Cauhopé, M., Seyler, F., & Cazenave, A. (2006). Preliminary results of
3658 ENVISAT RA-2-derived water levels validation over the Amazon basin. *Remote Sensing of*
3659 *Environment*, 100(2), 252–264. <https://doi.org/10.1016/j.rse.2005.10.027>
- 3660 Frappart, F., Papa, F., Famiglietti, J. S., Prigent, C., Rossow, W. B., & Seyler, F. (2008). Interannual
3661 variations of river water storage from a multiple satellite approach: A case study for the Rio Negro
3662 River basin. *Journal of Geophysical Research Atmospheres*, 113(D21).
3663 <https://doi.org/10.1029/2007JD009438>
- 3664 Frappart, F., Papa, F., Güntner, A., Werth, S., Santos da Silva, J., Tomasella, J., et al. (2011). Satellite-
3665 based estimates of groundwater storage variations in large drainage basins with extensive
3666 floodplains. *Remote Sensing of Environment*, 115(6), 1588–1594.
3667 <https://doi.org/10.1016/j.rse.2011.02.003>
- 3668 Frappart, F., Papa, F., Santos Da Silva, J., Ramillien, G., Prigent, C., Seyler, F., & Calmant, S. (2012).
3669 Surface freshwater storage and dynamics in the Amazon basin during the 2005 exceptional drought.
3670 *Environmental Research Letters*, 7(4). <https://doi.org/10.1088/1748-9326/7/4/044010>
- 3671 Frappart, F., Ramillien, G., & Ronchail, J. (2013). Changes in terrestrial water storage versus rainfall and
3672 discharges in the Amazon basin. *International Journal of Climatology*, 33(14), 3029–3046.
3673 <https://doi.org/10.1002/joc.3647>
- 3674 Frappart, F., Seoane, L., & Ramillien, G. (2013). Validation of GRACE-derived terrestrial water storage
3675 from a regional approach over South America. *Remote Sensing of Environment*, 137, 69–83.
3676 <https://doi.org/10.1016/j.rse.2013.06.008>
- 3677 Frappart, F., Papa, F., Malbeteau, Y., León, J. G., Ramillien, G., Prigent, C., et al. (2015). Surface
3678 Freshwater Storage Variations in the Orinoco Floodplains Using Multi-Satellite Observations.
3679 *Remote Sensing*, 7(1), 89–110. <https://doi.org/10.3390/rs70100089>
- 3680 Frappart, F., Legrésy, B., Niño, F., Blarel, F., Fuller, N., Fleury, S., et al. (2016). An ERS-2 altimetry
3681 reprocessing compatible with ENVISAT for long-term land and ice sheets studies. *Remote Sensing*
3682 *of Environment*, 184, 558–581. <https://doi.org/10.1016/j.rse.2016.07.037>
- 3683 Frappart, F., Papa, F., Güntner, A., Tomasella, J., Pfeffer, J., Ramillien, G., et al. (2019). The spatio-
3684 temporal variability of groundwater storage in the Amazon River Basin. *Advances in Water*
3685 *Resources*, 124(October 2016), 41–52. <https://doi.org/10.1016/j.advwatres.2018.12.005>
- 3686 Fricke, A. T., Nittrouer, C. A., Ogston, A. S., Nowacki, D. J., Asp, N. E., & Souza Filho, P. W. M.
3687 (2019). Morphology and dynamics of the intertidal floodplain along the Amazon tidal river. *Earth*
3688 *Surface Processes and Landforms*, 44(1), 204–218. <https://doi.org/10.1002/esp.4545>
- 3689 Fu, R., Zhu, B., & Dickinson, R. E. (1999). How Do Atmosphere and Land Surface Influence Seasonal

- 3690 Changes of Convection in the Tropical Amazon? *Journal of Climate*, 12(5), 1306–1321.
3691 [https://doi.org/10.1175/1520-0442\(1999\)012<1306:HDAALS>2.0.CO;2](https://doi.org/10.1175/1520-0442(1999)012<1306:HDAALS>2.0.CO;2)
- 3692 Fu, R., Yin, L., Li, W., Arias, P. A., Dickinson, R. E., Huang, L., et al. (2013). Increased dry-season
3693 length over southern Amazonia in recent decades and its implication for future climate projection.
3694 *Proceedings of the National Academy of Sciences of the United States of America*, 110(45), 18110–
3695 18115. <https://doi.org/10.1073/pnas.1302584110>
- 3696 Funatsu, B. M., Dubreuil, V., Claud, C., Arvor, D., & Gan, M. A. (2012). Convective activity in Mato
3697 Grosso state (Brazil) from microwave satellite observations: Comparisons between AMSU and
3698 TRMM data sets. *Journal of Geophysical Research Atmospheres*, 117(16), 1–16.
3699 <https://doi.org/10.1029/2011JD017259>
- 3700 Funk, C., Peterson, P., Landsfeld, M., Pedreros, D., Verdin, J., Shukla, S., et al. (2015). The climate
3701 hazards infrared precipitation with stations - A new environmental record for monitoring extremes.
3702 *Scientific Data*, 2, 1–21. <https://doi.org/10.1038/sdata.2015.66>
- 3703 Gabioux, M., Vinzon, S. B., & Paiva, A. M. (2005). Tidal propagation over fluid mud layers on the
3704 Amazon shelf. *Continental Shelf Research*, 25(1), 113–125.
3705 <https://doi.org/10.1016/j.csr.2004.09.001>
- 3706 Gallo, M. N., & Vinzon, S. B. (2005). Generation of overtides and compound tides in Amazon estuary.
3707 *Ocean Dynamics*, 55(5–6), 441–448. <https://doi.org/10.1007/s10236-005-0003-8>
- 3708 Gao, H., Birkett, C., & Lettenmaier, D. P. (2012). Global monitoring of large reservoir storage from
3709 satellite remote sensing. *Water Resources Research*, 48(9), 1–12.
3710 <https://doi.org/10.1029/2012WR012063>
- 3711 Garambois, P. A., Calmant, S., Roux, H., Paris, A., Monnier, J., Finaud-Guyot, P., et al. (2017).
3712 Hydraulic visibility: Using satellite altimetry to parameterize a hydraulic model of an ungauged
3713 reach of a braided river. *Hydrological Processes*, 31(4), 756–767. <https://doi.org/10.1002/hyp.11033>
- 3714 Garousi-Nejad, I., Tarboton, D. G., Aboutalebi, M., & Torres-Rua, A. F. (2019). *Terrain Analysis*
3715 *Enhancements to the Height Above Nearest Drainage Flood Inundation Mapping Method*. *Water*
3716 *Resources Research* (Vol. 55). <https://doi.org/10.1029/2019WR024837>
- 3717 Garreaud, R. D., & Wallace, J. M. (1997). The diurnal march of convective cloudiness over the Americas.
3718 *Monthly Weather Review*, 125(12), 3157–3171. [https://doi.org/10.1175/1520-0493\(1997\)125<3157:TDMOCC>2.0.CO;2](https://doi.org/10.1175/1520-0493(1997)125<3157:TDMOCC>2.0.CO;2)
- 3719
- 3720 Garstang, M., Massie Jr., H. L., Halverson, J., Greco, S., & Scala, J. (1994). Amazon Coastal Squall
3721 Lines. Part I: Structure and Kinematics. *Monthly Weather Review*, 122(4), 608–622.
3722 [https://doi.org/10.1175/1520-0493\(1994\)122<0608:ACSLPI>2.0.CO;2](https://doi.org/10.1175/1520-0493(1994)122<0608:ACSLPI>2.0.CO;2)

- 3723 Gash, J., Keller, M., Bustamante, M., & Dias, P. S. (2013). *Amazonia and Global Change. Amazonia and*
3724 *Global Change*. <https://doi.org/10.1029/GM186>
- 3725 Gelaro, R., McCarty, W., Suárez, M. J., Todling, R., Molod, A., Takacs, L., et al. (2017). The modern-era
3726 retrospective analysis for research and applications, version 2 (MERRA-2). *Journal of Climate*,
3727 *30*(14), 5419–5454. <https://doi.org/10.1175/JCLI-D-16-0758.1>
- 3728 Getirana, A. C. V., Espinoza, J. C. V., Ronchail, J., & Rotunno Filho, O. C. (2011). Assessment of
3729 different precipitation datasets and their impacts on the water balance of the Negro River basin.
3730 *Journal of Hydrology*, *404*(3–4), 304–322. <https://doi.org/10.1016/j.jhydrol.2011.04.037>
- 3731 Getirana, A. C. V., Boone, A., Yamazaki, D., Decharme, B., Papa, F., & Mognard, N. (2012). The
3732 Hydrological Modeling and Analysis Platform (HyMAP): Evaluation in the Amazon Basin. *Journal*
3733 *of Hydrometeorology*, *13*(6), 1641–1665. <https://doi.org/10.1175/JHM-D-12-021.1>
- 3734 Getirana, A. C. V., Boone, A., Yamazaki, D., & Mognard, N. (2013). Automatic parameterization of a
3735 flow routing scheme driven by radar altimetry data : Evaluation in the Amazon basin. *Water*
3736 *Resources Research*, *49*(1), 614–629. <https://doi.org/10.1002/wrcr.20077>
- 3737 Getirana, A. C. V., Dutra, E., Guimberteau, M., Kam, J., Li, H.-Y., Decharme, B., et al. (2014). Water
3738 Balance in the Amazon Basin from a Land Surface Model Ensemble. *Journal of Hydrometeorology*,
3739 *15*(6), 2586–2614. <https://doi.org/10.1175/JHM-D-14-0068.1>
- 3740 Getirana, A. C. V., Kumar, S., Giroto, M., & Rodell, M. (2017). Rivers and Floodplains as Key
3741 Components of Global Terrestrial Water Storage Variability. *Geophysical Research Letters*, *44*(20),
3742 10,359–10,368. <https://doi.org/10.1002/2017GL074684>
- 3743 Getirana, A. C. V., Peters-Lidard, C., Rodell, M., & Bates, P. D. (2017). Trade-off between cost and
3744 accuracy in large-scale surface water dynamic modeling. *Water Resources Research*, *53*(6), 4942–
3745 4955. <https://doi.org/10.1002/2017WR020519>
- 3746 Gholizadeh, M. H., Melesse, A. M., & Reddi, L. (2016). A comprehensive review on water quality
3747 parameters estimation using remote sensing techniques. *Sensors (Switzerland)*, *16*(8).
3748 <https://doi.org/10.3390/s16081298>
- 3749 Ghosh, S., Thakur, P. K., Sharma, R., Nandy, S., Garg, V., Amarnath, G., & Bhattacharyya, S. (2017).
3750 The Potential Applications of Satellite Altimetry with SARAL/AltiKa for Indian Inland Waters.
3751 *Proceedings of the National Academy of Sciences, India Section A: Physical Sciences*, *87*(4), 661–
3752 677. <https://doi.org/10.1007/s40010-017-0463-5>
- 3753 Giardino, C., Bresciani, M., Braga, F., Fabretto, A., Ghirardi, N., Pepe, M., et al. (2020). First evaluation
3754 of PRISMA Level 1 data for water applications. *Sensors*, (SUBMITTED(August)).
3755 <https://doi.org/10.3390/s20164553>

- 3756 Giddings, L., & Choudhury, B. J. (1989). Observation of hydrological features with Nimbus-7 37 GHz
3757 data, applied to South America. *International Journal of Remote Sensing*, *10*, 1673–1686.
3758 <https://doi.org/10.1080/01431168908903998>
- 3759 Giovannetone, J. P., & Barros, A. P. (2009). Probing regional orographic controls of precipitation and
3760 cloudiness in the Central Andes using satellite data. *Journal of Hydrometeorology*, *10*(1), 167–182.
3761 <https://doi.org/10.1175/2008JHM973.1>
- 3762 Gleason, C. J., & Durand, M. T. (2020). Remote sensing of river discharge: A review and a framing for
3763 the discipline. *Remote Sensing*, *12*(7), 1–28. <https://doi.org/10.3390/rs12071107>
- 3764 Gloor, M., Brienen, R. J. W., Galbraith, D., Feldpausch, T. R., Schöngart, J., Guyot, J.-L., et al. (2013).
3765 Intensification of the Amazon hydrological cycle over the last two decades. *Geophysical Research*
3766 *Letters*, *40*(9), 1729–1733. <https://doi.org/10.1002/grl.50377>
- 3767 Gomis-Cebolla, J., Jimenez, J. C., Sobrino, J. A., Corbari, C., & Mancini, M. (2019). Intercomparison of
3768 remote-sensing based evapotranspiration algorithms over amazonian forests. *International Journal*
3769 *of Applied Earth Observation and Geoinformation*, *80*, 280–294.
3770 <https://doi.org/10.1016/j.jag.2019.04.009>
- 3771 Gonçalves, L. G., Borak, J. S., Costa, M. H., Saleska, S. R., Baker, I., Restrepo-Coupe, N., et al. (2013).
3772 Overview of the large-scale biosphere-atmosphere experiment in amazonia data model
3773 intercomparison project (LBA-DMIP). *Agricultural and Forest Meteorology*, *182–183*, 111–127.
3774 <https://doi.org/10.1016/j.agrformet.2013.04.030>
- 3775 Gosset, M., Kunstmann, H., Zougmore, F., Cazenave, F., Leijnse, H., Uijlenhoet, R., et al. (2016).
3776 Improving rainfall measurement in gauge poor regions thanks to mobile telecommunication
3777 networks. *Bulletin of the American Meteorological Society*, *97*(3), ES49–ES51.
3778 <https://doi.org/10.1175/BAMS-D-15-00164.1>
- 3779 Gruber, A., & Krueger, A. F. (1984). The status of the NOAA outgoing longwave radiation data set.
3780 *Bulletin - American Meteorological Society*, *65*(9), 958–962. [https://doi.org/10.1175/1520-0477\(1984\)065<0958:TSOTNO>2.0.CO;2](https://doi.org/10.1175/1520-0477(1984)065<0958:TSOTNO>2.0.CO;2)
- 3782 Guilhen, J., Al Bitar, A., Sauvage, S., Parrens, M., Martinez, J.-M., Abril, G., et al. (2020). Denitrification
3783 and associated nitrous oxide and carbon dioxide emissions from the Amazonian wetlands.
3784 *Biogeosciences*, *17*(16), 4297–4311. <https://doi.org/10.5194/bg-17-4297-2020>
- 3785 Guimberteau, M., Drapeau, G., Ronchail, J., Sultan, B., Polcher, J., Martinez, J. M., et al. (2012).
3786 Discharge simulation in the sub-basins of the Amazon using ORCHIDEE forced by new datasets.
3787 *Hydrology and Earth System Sciences*, *16*, 911–935. <https://doi.org/10.5194/hess-16-911-2012>
- 3788 Guimberteau, M., Ducharne, A., Ciais, P., Boisier, J. P., Peng, S., De Weirtdt, M., & Verbeeck, H. (2014).

- 3789 Testing conceptual and physically based soil hydrology schemes against observations for the
3790 Amazon Basin. *Geoscientific Model Development*, 7(3), 1115–1136. [https://doi.org/10.5194/gmd-7-](https://doi.org/10.5194/gmd-7-1115-2014)
3791 1115-2014
- 3792 Guimberteau, M., Ciais, P., Ducharne, A., Boisier, J. P., Dutra Aguiar, A. P., Biemans, H., et al. (2017).
3793 Impacts of future deforestation and climate change on the hydrology of the Amazon Basin: a multi-
3794 model analysis with a new set of land-cover change scenarios. *Hydrology and Earth System*
3795 *Sciences*, 21(3), 1455–1475. <https://doi.org/10.5194/hess-21-1455-2017>
- 3796 Guzkowska, M. A. J., Rapley, C. G., Ridley, J. K., Cudlip, W., Birkett, C. M., & Scott, R. F. (1990).
3797 *Developments in inland water and land altimetry: University College of London, Mullard Space*
3798 *Science Laboratory, European Space Agency final contract report 7839/88/F/Fl.*
- 3799 Haghtalab, N., Moore, N., Heerspink, B. P., & Hyndman, D. W. (2020). Evaluating spatial patterns in
3800 precipitation trends across the Amazon basin driven by land cover and global scale forcings.
3801 *Theoretical and Applied Climatology*, (2017). <https://doi.org/10.1007/s00704-019-03085-3>
- 3802 Hall, A. C., Schumann, G. J. P., Bamber, J. L., & Bates, P. D. (2011). Tracking water level changes of the
3803 Amazon Basin with space-borne remote sensing and integration with large scale hydrodynamic
3804 modelling: A review. *Physics and Chemistry of the Earth*, 36(7–8), 223–231.
3805 <https://doi.org/10.1016/j.pce.2010.12.010>
- 3806 Hall, A. C., Schumann, G. J., Bamber, J. L., Bates, P. D., & Trigg, M. A. (2012). Geodetic corrections to
3807 Amazon River water level gauges using ICESat altimetry, 48(6).
3808 <https://doi.org/10.1029/2011WR010895>
- 3809 Hamilton, S. K., Sippel, S. J., & Melack, J. M. (2002). Comparison of inundation patterns among major
3810 South American floodplains. *Journal of Geophysical Research Atmospheres*, 107(20), 1–14.
3811 <https://doi.org/10.1029/2000JD000306>
- 3812 Hamilton, S. K., Sippel, S. J., & Melack, J. M. (2004). Seasonal inundation patterns in two large savanna
3813 floodplains of South America: The Llanos de Moxos (Bolivia) and the Llanos del Orinoco
3814 (Venezuela and Colombia). *Hydrological Processes*, 18(11), 2103–2116.
3815 <https://doi.org/10.1002/hyp.5559>
- 3816 Hamilton, S. K., Kellndorfer, J., Lehner, B., & Tobler, M. (2007). Remote sensing of floodplain
3817 geomorphology as a surrogate for biodiversity in a tropical river system (Madre de Dios, Peru).
3818 *Geomorphology*, 89(1-2 SPEC. ISS.), 23–38. <https://doi.org/10.1016/j.geomorph.2006.07.024>
- 3819 Hansen, M. C., Potapov, P. V., Moore, R., Hancher, M., Turubanova, S. A., Tyukavina, A., et al. (2013).
3820 High-Resolution Global Maps of 21st-Century Forest Cover Change. *Science*, 342(November), 850–
3821 854. <https://doi.org/10.1126/science.1244693>

- 3822 Hastie, A., Lauerwald, R., Ciais, P., & Regnier, P. (2019). Aquatic carbon fluxes dampen the overall
3823 variation of net ecosystem productivity in the Amazon basin: An analysis of the interannual
3824 variability in the boundless carbon cycle. *Global Change Biology*, 25(6), 2094–2111.
3825 <https://doi.org/10.1111/gcb.14620>
- 3826 Heerspink, B. P., Kendall, A. D., Coe, M. T., & Hyndman, D. W. (2020). Trends in streamflow,
3827 evapotranspiration, and groundwater storage across the Amazon Basin linked to changing
3828 precipitation and land cover. *Journal of Hydrology: Regional Studies*, 32(March), 100755.
3829 <https://doi.org/10.1016/j.ejrh.2020.100755>
- 3830 Hersbach, H., Rosnay, P. de, Bell, B., Schepers, D., Simmons, A., Soci, C., et al. (2018). *Operational*
3831 *global reanalysis: progress, future directions and synergies with NWP* (ERA Report). *ERA Report*
3832 *Series*.
- 3833 Hersbach, H., Bell, B., Berrisford, P., Hirahara, S., Horányi, A., Muñoz-Sabater, J., et al. (2020). The
3834 ERA5 global reanalysis. *Quarterly Journal of the Royal Meteorological Society*, (September 2019),
3835 1–51. <https://doi.org/10.1002/qj.3803>
- 3836 Hess, L. L., Melack, J. M., & Simonett, D. S. (1990). Radar detection of flooding beneath the forest
3837 canopy: A review. *International Journal of Remote Sensing*, 11, 1313–1325.
3838 <https://doi.org/10.1080/01431169008955095>
- 3839 Hess, L. L., Melack, J. M., Melack, J. M., Filoso, S., Wang, Y., & Wang, Y. (1995). Delineation of
3840 Inundated Area and Vegetation Along the Amazon Floodplain with the SIR-C Synthetic Aperture
3841 Radar. *IEEE Transactions on Geoscience and Remote Sensing*, 33(4), 896–904.
3842 <https://doi.org/10.1109/36.406675>
- 3843 Hess, L. L., Melack, J. M., Novo, E. M. L. M. L. M., Barbosa, C. C. F. F., & Gastil, M. (2003). Dual-
3844 season mapping of wetland inundation and vegetation for the central Amazon basin. *Remote Sensing*
3845 *of Environment*, 87(4), 404–428. <https://doi.org/10.1016/j.rse.2003.04.001>
- 3846 Hess, L. L., Melack, J. M., Affonso, A. G., Barbosa, C., Gastil-Buhl, M., & Novo, E. M. L. M. (2015).
3847 Wetlands of the Lowland Amazon Basin: Extent, Vegetative Cover, and Dual-season Inundated
3848 Area as Mapped with JERS-1 Synthetic Aperture Radar. *Wetlands*, 35(4), 745–756.
3849 <https://doi.org/10.1007/s13157-015-0666-y>
- 3850 Hoch, J. M., Haag, A. V., van Dam, A., Winsemius, H. C., van Beek, L. P. H., & Bierkens, M. F. P.
3851 (2016). Assessing the impact of hydrodynamics on large-scale flood wave propagation - a case study
3852 for the Amazon Basin. *Hydrology and Earth System Sciences Discussions*, (August), 1–25.
3853 <https://doi.org/10.5194/hess-2016-442>
- 3854 Hodnett, M. G., Vendrame, I., De O. Marques Filho, A., Oyama, M. D., & Tomasella, J. (1997). Soil

- 3855 water storage and groundwater behaviour in a catenary sequence beneath forest in central
3856 Amazonia: I. Comparisons between plateau, slope and valley floor. *Hydrology and Earth System*
3857 *Sciences*, 1(2), 265–277. <https://doi.org/10.5194/hess-1-265-1997>
- 3858 Holmes, T. R. H., Hain, C. R., Crow, W. T., Anderson, M. C., & Kustas, W. P. (2018). Microwave
3859 implementation of two-source energy balance approach for estimating evapotranspiration.
3860 *Hydrology and Earth System Sciences*, 22(2), 1351–1369. [https://doi.org/10.5194/hess-22-1351-](https://doi.org/10.5194/hess-22-1351-2018)
3861 2018
- 3862 Horel, J. D., Hahmann, A. N., & Geisler, J. E. (1989). An investigation of the Annual Cycle of
3863 Convective Activity over the Tropical Americas. *Journal of Climate*, 2(11), 1388–1403.
3864 [https://doi.org/10.1175/1520-0442\(1989\)002<1388:AIOTAC>2.0.CO;2](https://doi.org/10.1175/1520-0442(1989)002<1388:AIOTAC>2.0.CO;2)
- 3865 Hu, K., Awange, J. L., Khandu, Forootan, E., Goncalves, R. M., & Fleming, K. (2017). Hydrogeological
3866 characterisation of groundwater over Brazil using remotely sensed and model products. *Science of*
3867 *the Total Environment*, 599–600, 372–386. <https://doi.org/10.1016/j.scitotenv.2017.04.188>
- 3868 Huang, C., Chen, Y., Zhang, S., & Wu, J. (2018). Detecting, Extracting, and Monitoring Surface Water
3869 From Space Using Optical Sensors: A Review. *Reviews of Geophysics*, 56(2), 333–360.
3870 <https://doi.org/10.1029/2018RG000598>
- 3871 Huffman, G. J., Adler, R. F., Rudolf, B., Schneider, U., & Keehn, P. R. (1995). Global Precipitation
3872 Estimates Based on a Technique for Combining Satellite-Based Estimates, Rain Gauge Analysis,
3873 and NWP Model Precipitation Information. *Journal of Climate*, 8(5), 1284–1295.
3874 [https://doi.org/10.1175/1520-0442\(1995\)008<1284:GPEBOA>2.0.CO;2](https://doi.org/10.1175/1520-0442(1995)008<1284:GPEBOA>2.0.CO;2)
- 3875 Huffman, G. J., Adler, R. F., Arkin, P., Chang, A., Ferraro, R., Gruber, A., et al. (1997). The Global
3876 Precipitation Climatology Project (GPCP) Combined Precipitation Dataset. *Bulletin of the American*
3877 *Meteorological Society*, 78(1), 5–20. [https://doi.org/10.1175/1520-](https://doi.org/10.1175/1520-0477(1997)078<0005:TGPCPG>2.0.CO;2)
3878 0477(1997)078<0005:TGPCPG>2.0.CO;2
- 3879 Huffman, G. J., Adler, R. F., Morrissey, M. M., Bolvin, D. T., Curtis, S., Joyce, R., et al. (2001). Global
3880 precipitation at one-degree daily resolution from multisatellite observations. *Journal of*
3881 *Hydrometeorology*, 2(1), 36–50. [https://doi.org/10.1175/1525-](https://doi.org/10.1175/1525-7541(2001)002<0036:GPAODD>2.0.CO;2)
3882 7541(2001)002<0036:GPAODD>2.0.CO;2
- 3883 Huffman, G. J., Adler, R. F., Bolvin, D. T., Gu, G., Nelkin, E. J., Bowman, K. P., et al. (2007). The
3884 TRMM Multisatellite Precipitation Analysis (TMPA): Quasi-global, multiyear, combined-sensor
3885 precipitation estimates at fine scales. *Journal of Hydrometeorology*, 8(1), 38–55.
3886 <https://doi.org/10.1175/JHM560.1>
- 3887 Huffman, G. J., Adler, R. F., Bolvin, D. T., & Nelkin, E. J. (2010). *The TRMM Multi-satellite*

- 3888 *Precipitation Analysis (TMPA). Chapter 1 in Satellite Rainfall Applications for Surface Hydrology.*
 3889 (M. Gebremichael & F. Hossain, Eds.). Dordrecht: Springer Netherlands.
 3890 <https://doi.org/10.1007/978-90-481-2915-7>
- 3891 Huffman, G. J., Bolvin, D. T., Braithwaite, D., Hsu, K., Joyce, R., & Xie, P. (2015). *Algorithm*
 3892 *Theoretical Basis Document (ATBD) Version 4.5. NASA Global Precipitation Measurement (GPM)*
 3893 *Integrated Multi-satellitE Retrievals for GPM (IMERG)*. Retrieved from
 3894 https://gpm.nasa.gov/sites/default/files/document_files/IMERG_ATBD_V5.2_0.pdf
- 3895 Huffman, G. J., Bolvin, D. T., & Nelkin, E. J. (2015). *Integrated MultisatellitE Retrievals for GPM*
 3896 *(IMERG) technical documentation*. Retrieved from
 3897 https://gpm.nasa.gov/sites/default/files/document_files/IMERG_doc.pdf
- 3898 Huffman, G. J., Bolvin, D. T., & Adler, R. F. (2016). GPCP Version 1.2 One-Degree Daily Precipitation
 3899 Data Set. Boulder, CO: Research Data Archive at the National Center for Atmospheric Research,
 3900 Computational and Information Systems Laboratory. <https://doi.org/10.5065/D6D50K46>
- 3901 Van Huijgevoort, M. H. J., Hazenberg, P., Van Lanen, H. A. J., Teuling, A. J., Clark, D. B., Folwell, S., et
 3902 al. (2013). Global multimodel analysis of drought in runoff for the second half of the twentieth
 3903 century. *Journal of Hydrometeorology*, *14*(5), 1535–1552. [https://doi.org/10.1175/JHM-D-12-](https://doi.org/10.1175/JHM-D-12-0186.1)
 3904 [0186.1](https://doi.org/10.1175/JHM-D-12-0186.1)
- 3905 Hurley, J. V., Vuille, M., Hardy, D. R., Burns, S. J., & Thompson, L. G. (2015). Cold air incursions, $\delta^{18}\text{O}$
 3906 variability, and monsoon dynamics associated with snow days at Quelccaya Ice Cap, Peru. *Journal*
 3907 *of Geophysical Research: Atmospheres*, *120*(15), 7467–7487.
 3908 [https://doi.org/https://doi.org/10.1002/2015JD023323](https://doi.org/10.1002/2015JD023323)
- 3909 Jardine, T. D., Bond, N. R., Burford, M. A., Kennard, M. J., Ward, D. P., Bayliss, P., et al. (2015). Does
 3910 flood rhythm drive ecosystem responses in tropical riverscapes? *Ecology*, *96*(3), 684–692.
 3911 <https://doi.org/10.1890/14-0991.1>
- 3912 Jensen, K., McDonald, K., Podest, E., Rodriguez-Alvarez, N., Horna, V., & Steiner, N. (2018). Assessing
 3913 L-Band GNSS-reflectometry and imaging radar for detecting sub-canopy inundation dynamics in a
 3914 tropical wetlands complex. *Remote Sensing*, *10*(9), 1431. <https://doi.org/10.3390/rs10091431>
- 3915 Ji, X., Lesack, L. F. W., Melack, J. M., Wang, S., Riley, W. J., & Shen, C. (2019). Seasonal and inter-
 3916 annual patterns and controls of hydrological fluxes in an Amazon floodplain lake with a surface-
 3917 subsurface processes model. *Water Resources Research*, *55*(4), 3056–3075.
 3918 <https://doi.org/10.1029/2018WR023897>
- 3919 Jiang, L., Schneider, R., Andersen, O. B., & Bauer-Gottwein, P. (2017). CryoSat-2 altimetry applications
 3920 over rivers and lakes. *Water*, *9*(3), 211. <https://doi.org/10.3390/w9030211>

- 3921 Jiang, S., Ren, L., Hong, Y., Yong, B., Yang, X., Yuan, F., & Ma, M. (2012). Comprehensive evaluation
3922 of multi-satellite precipitation products with a dense rain gauge network and optimally merging their
3923 simulated hydrological flows using the Bayesian model averaging method. *Journal of Hydrology*,
3924 452–453, 213–225. <https://doi.org/10.1016/j.jhydrol.2012.05.055>
- 3925 Jiménez-Muñoz, J. C., Sobrino, J. A., Mattar, C., & Malhi, Y. (2013). Spatial and temporal patterns of the
3926 recent warming of the Amazon forest. *Journal of Geophysical Research Atmospheres*, 118, 5204–
3927 5215. <https://doi.org/10.1002/jgrd.50456>
- 3928 Jimenez, J. C., Marengo, J. A., Alves, L. M., Sulca, J. C., Takahashi, K., Ferrett, S., & Collins, M. (2019).
3929 The role of ENSO flavours and TNA on recent droughts over Amazon forests and the Northeast
3930 Brazil region. *International Journal of Climatology*, (December), 1–20.
3931 <https://doi.org/10.1002/joc.6453>
- 3932 Jorge, D. S. F., Barbosa, C. C. F., de Carvalho, L. A. S., Affonso, A. G., Lobo, F. D. L., & Novo, E. M. L.
3933 D. M. (2017). SNR (Signal-To-Noise Ratio) Impact on Water Constituent Retrieval from Simulated
3934 Images of Optically Complex Amazon Lakes. *Remote Sensing*, 9(7), 644.
3935 <https://doi.org/10.3390/rs9070644>
- 3936 Josse, C., Navarro, G., Encarnación, F., Tovar, A., Comer, P., Ferreira, W., et al. (2007). *Ecological*
3937 *Systems of the Amazon Basin of Peru and Bolivia: Classification and Mapping*. Virginia:
3938 NatureServe.
- 3939 Joyce, R. J., & Xie, P. (2011). Kalman filter-based CMORPH. *Journal of Hydrometeorology*, 12(6),
3940 1547–1563. <https://doi.org/10.1175/JHM-D-11-022.1>
- 3941 Joyce, R. J., Janowiak, J. E., Arkin, P. A., & Xie, P. (2004). CMORPH: A method that produces global
3942 precipitation estimates from passive microwave and infrared data at high spatial and temporal
3943 resolution. *Journal of Hydrometeorology*, 5(3), 487–503. [https://doi.org/10.1175/1525-7541\(2004\)005<0487:CAMTPG>2.0.CO;2](https://doi.org/10.1175/1525-7541(2004)005<0487:CAMTPG>2.0.CO;2)
- 3944
- 3945 Jung, H. C., Hamski, J., Durand, M., Alsdorf, D., Hossain, F., Lee, H., et al. (2010). Characterization of
3946 complex fluvial systems using remote sensing of spatial and temporal water level variations in the
3947 Amazon, Congo, and Brahmaputra rivers. *Earth Surface Processes and Landforms*, 35(3), 294–304.
3948 <https://doi.org/10.1002/esp.1914>
- 3949 Jung, M., Reichstein, M., Ciais, P., Seneviratne, S. I., Sheffield, J., Goulden, M. L., et al. (2010). Recent
3950 decline in the global land evapotranspiration trend due to limited moisture supply. *Nature*,
3951 467(7318), 951–954. <https://doi.org/10.1038/nature09396>
- 3952 Júnior, J. L. S., Tomasella, J., & Rodriguez, D. A. (2015). Impacts of future climatic and land cover
3953 changes on the hydrological regime of the Madeira River basin. *Climatic Change*, 129(1–2), 117–

- 3954 129. <https://doi.org/10.1007/s10584-015-1338-x>
- 3955 Junk, W. J. (1997). *The Central Amazon Floodplain: ecology of a pulsing system. Ecological Studies*
- 3956 (Vol. 126). Berlin: Springer-Verlag.
- 3957 Junk, W. J., Bayley, P. B., & Sparks, R. E. (1989). The flood pulse concept in river-floodplain-systems.
- 3958 *Canadian Journal of Fisheries and Aquatic Sciences*, 106, 110–127.
- 3959 <https://doi.org/10.1371/journal.pone.0028909>
- 3960 Junk, W. J., Piedade, M. T. F., Wittmann, F., Schöngart, J., & Parolin, P. (2010). *Amazonian Floodplain*
- 3961 *Forests: Ecophysiology, ecology, biodiversity and sustainable management. Ecological Studies.*
- 3962 Berlin, Germany: Springer. <https://doi.org/10.1007/978-90-481-8725-6>
- 3963 Junk, W. J., Piedade, M. T. F., Schöngart, J., Cohn-Haft, M., Adeney, J. M., & Wittmann, F. (2011). A
- 3964 classification of major naturally-occurring amazonian lowland wetlands. *Wetlands*, 31(4), 623–640.
- 3965 <https://doi.org/10.1007/s13157-011-0190-7>
- 3966 Junk, W. J., Wittmann, F., Schöngart, J., & Piedade, M. T. F. (2015). A classification of the major
- 3967 habitats of Amazonian black-water river floodplains and a comparison with their white-water
- 3968 counterparts. *Wetlands Ecology and Management*, 23(4), 677–693. [https://doi.org/10.1007/s11273-](https://doi.org/10.1007/s11273-015-9412-8)
- 3969 [015-9412-8](https://doi.org/10.1007/s11273-015-9412-8)
- 3970 Junquas, C., Takahashi, K., Condom, T., Espinoza, J. C., Chavez, S., Sicart, J. E., & Lebel, T. (2018).
- 3971 Understanding the influence of orography on the precipitation diurnal cycle and the associated
- 3972 atmospheric processes in the central Andes. *Climate Dynamics*, 50(11–12), 3995–4017.
- 3973 <https://doi.org/10.1007/s00382-017-3858-8>
- 3974 Kandus, P., Minotti, P. G., Morandeira, N. S., Grimson, R., Trilla, G. G., González, E. B., et al. (2018).
- 3975 Remote sensing of wetlands in South America: Status and challenges. *International Journal of*
- 3976 *Remote Sensing*, 39(4), 993–1016. <https://doi.org/10.1080/01431161.2017.1395971>
- 3977 Kasischke, E. S., Melack, J. M., & Dobson, M. C. (1997). The use of imaging radars for ecological
- 3978 applications - A review. *Remote Sensing of Environment*, 59(2), 141–156.
- 3979 [https://doi.org/10.1016/S0034-4257\(96\)00148-4](https://doi.org/10.1016/S0034-4257(96)00148-4)
- 3980 Khaki, M., Forootan, E., Kuhn, M., Awange, J., Longuevergne, L., & Wada, Y. (2018). Efficient basin
- 3981 scale filtering of GRACE satellite products. *Remote Sensing of Environment*, 204(October 2017),
- 3982 76–93. <https://doi.org/10.1016/j.rse.2017.10.040>
- 3983 Khaki, M., Hoteit, I., Kuhn, M., Forootan, E., & Awange, J. (2019). Assessing data assimilation
- 3984 frameworks for using multi-mission satellite products in a hydrological context. *Science of The*
- 3985 *Total Environment*, 647(October 2017), 1031–1043. <https://doi.org/10.1016/j.scitotenv.2018.08.032>
- 3986 Khand, K., Numata, I., Kjaersgaard, J., & Vourlitis, G. L. (2017). Dry season evapotranspiration

- 3987 dynamics over human-impacted landscapes in the southern Amazon using the landsat-based
3988 METRIC model. *Remote Sensing*, 9(7). <https://doi.org/10.3390/rs9070706>
- 3989 Khanna, J., Medvigy, D., Fueglistaler, S., & Walko, R. (2017). Regional dry-season climate changes due
3990 to three decades of Amazonian deforestation. *Nature Climate Change*, 7(3), 200–204.
3991 <https://doi.org/10.1038/nclimate3226>
- 3992 Kidd, C. (2001). Satellite rainfall climatology: A review. *International Journal of Climatology*, 21(9),
3993 1041–1066. <https://doi.org/10.1002/joc.635>
- 3994 Kidd, C., & Huffman, G. (2011). Global precipitation measurement. *Meteorological Applications*, 18(3),
3995 334–353. <https://doi.org/10.1002/met.284>
- 3996 Kidd, C., & Levizzani, V. (2011). Status of satellite precipitation retrievals. *Hydrology and Earth System
3997 Sciences*, 15(4), 1109–1116. <https://doi.org/10.5194/hess-15-1109-2011>
- 3998 Kidd, C., Kniveton, D. R., Todd, M. C., & Bellerby, T. J. (2003). Satellite Rainfall Estimation Using
3999 Combined Passive Microwave and Infrared Algorithms. *Journal of Hydrometeorology*, 4(6), 1088–
4000 1104. [https://doi.org/10.1175/1525-7541\(2003\)004<1088:SREUCP>2.0.CO;2](https://doi.org/10.1175/1525-7541(2003)004<1088:SREUCP>2.0.CO;2)
- 4001 Kidd, C., Becker, A., Huffman, G. J., Muller, C. L., Joe, P., Skofronick-Jackson, G., & Kirschbaum, D. B.
4002 (2017). So, How Much of the Earth’s Surface Is Covered by Rain Gauges? *Bulletin of the American
4003 Meteorological Society*, 98(1), 69–78. <https://doi.org/10.1175/BAMS-D-14-00283.1>
- 4004 Kilham, N. E., & Roberts, D. (2011). Amazon river time series of surface sediment concentration from
4005 MODIS. *International Journal of Remote Sensing*, 32(10), 2659–2679.
4006 <https://doi.org/10.1080/01431161003713044>
- 4007 Killeen, T. J., Douglas, M., Consiglio, T., Jørgensen, P. M., & Mejia, J. (2007). Dry spots and wet spots
4008 in the Andean hotspot. *Journal of Biogeography*, 34(8), 1357–1373. [https://doi.org/10.1111/j.1365-
2699.2006.01682.x](https://doi.org/10.1111/j.1365-
4009 2699.2006.01682.x)
- 4010 Kim, D., Lee, H., Laraque, A., Tshimanga, R. M., Yuan, T., Jung, H. C., et al. (2017). Mapping spatio-
4011 temporal water level variations over the central Congo River using PALSAR ScanSAR and Envisat
4012 altimetry data. *International Journal of Remote Sensing*, 38(23), 7021–7040.
4013 <https://doi.org/10.1080/01431161.2017.1371867>
- 4014 Kirk, J. T. O. (2010). *Light and Photosynthesis in Aquatic Ecosystems* (3rd ed.). New York: Cambridge
4015 University Press.
- 4016 Kirschke, S., Bousquet, P., Ciais, P., Saunois, M., Canadell, J. G., Dlugokencky, E. J., et al. (2013). Three
4017 decades of global methane sources and sinks. *Nature Geoscience*, 6, 813–823.
4018 <https://doi.org/10.1038/ngeo1955>
- 4019 Klein, I., Dietz, A., Gessner, U., Dech, S., & Kuenzer, C. (2015). Results of the Global WaterPack: A

- 4020 novel product to assess inland water body dynamics on a daily basis. *Remote Sensing Letters*, 6(1).
4021 <https://doi.org/10.1080/2150704X.2014.1002945>
- 4022 Knapp, K. R., Ansari, S., Bain, C. L., Bourassa, M. A., Dickinson, M. J., Funk, C., et al. (2011). Globally
4023 Gridded Satellite observations for climate studies. *Bulletin of the American Meteorological Society*,
4024 92(7), 893–907. <https://doi.org/10.1175/2011BAMS3039.1>
- 4025 Koblinsky, C. J., Clarke, R. T., Brenner, A. C., & Frey, H. (1993). Measurement of river level variations
4026 with satellite altimetry. *Water Resources Research*, 29(6), 1839–1848.
4027 <https://doi.org/10.1029/93WR00542>
- 4028 Kolassa, J., Gentine, P., Prigent, C., & Aires, F. (2016). Soil moisture retrieval from AMSR-E and
4029 ASCAT microwave observation synergy. Part 1: Satellite data analysis. *Remote Sensing of*
4030 *Environment*, 173, 1–14. <https://doi.org/https://doi.org/10.1016/j.rse.2015.11.011>
- 4031 Koren, I., Martins, J. V., Remer, L. A., & Afargan, H. (2008). Smoke Invigoration Versus Inhibition of
4032 Clouds over the Amazon. *Science*, 321(5891), 946–949. <https://doi.org/10.1126/science.1159185>
- 4033 Kosuth, P., Callede, J., Laraque, A., Filizola, N., Guyot, J. L., Seyler, P., et al. (2009). Sea-tide effects on
4034 flows in the lower reaches of the Amazon River. *Hydrological Processes*, 23(November 2008),
4035 3141–3150. <https://doi.org/10.1002/hyp.7387>
- 4036 Kumar, S., Del Castillo-Velarde, C., Prado, J. M. V., Rojas, J. L. F., Gutierrez, S. M. C., Alvarez, A. S.
4037 M., et al. (2020). Rainfall characteristics in the mantaro basin over tropical andes from a vertically
4038 pointed profile rain radar and in-situ field campaign. *Atmosphere*, 11(3).
4039 <https://doi.org/10.3390/atmos11030248>
- 4040 Kustas, W. P., & Norman, J. M. (1999). *Evaluation of soil and vegetation heat flux predictions using a*
4041 *simple two-source model with radiometric temperatures for partial canopy cover. Agricultural and*
4042 *Forest Meteorology* (Vol. 94).
- 4043 Kutser, T., Pascual, G. C., Barbosa, C., & Paavel, B. (2016). Mapping inland water carbon content with
4044 Landsat 8 data. *International Journal of Remote Sensing ISSN:*, (June).
4045 <https://doi.org/10.1080/01431161.2016.1186852>
- 4046 Kvist, L. P., & Nebel, G. (2001). A review of Peruvian flood plain forests: Ecosystems, inhabitants and
4047 resource use. *Forest Ecology and Management*, 150(1–2), 3–26. [https://doi.org/10.1016/S0378-](https://doi.org/10.1016/S0378-1127(00)00679-4)
4048 [1127\(00\)00679-4](https://doi.org/10.1016/S0378-1127(00)00679-4)
- 4049 Laipelt, L., Ruhoff, A. L., Fleischmann, A. S., Bloedow Kayser, R. H., Kich, E. de M., Rocha, H. R. da,
4050 & Usher Neale, C. M. (2020). Assessment of an automated calibration of the SEBAL Algorithm to
4051 estimate dry-season surface-energy partitioning in a Forest-Savanna Transition in Brazil. *Remote*
4052 *Sensing*, 12(7). <https://doi.org/10.3390/rs12071108>

- 4053 Landerer, F. W., Flechtner, F. M., Save, H., Webb, F. H., Bandikova, T., Bertiger, W. I., et al. (2020).
4054 Extending the Global Mass Change Data Record: GRACE Follow-On Instrument and Science Data
4055 Performance. *Geophysical Research Letters*, *47*(12). <https://doi.org/10.1029/2020GL088306>
- 4056 Laranjeiras, T. O., Naka, L. N., Leite, G. A., & Cohn-Haft, M. (2021). Effects of a major Amazonian
4057 river confluence on the distribution of floodplain forest avifauna. *Journal of Biogeography*,
4058 (November), 1–14. <https://doi.org/10.1111/jbi.14042>
- 4059 Latrubesse, E. M. (2012). Amazon lakes. In L. Bengtsson, R. W. Herschy, & R. W. Fairbridge (Eds.),
4060 *Encyclopedia of Lakes and Reservoirs* (pp. 13–26). Springer Verlag. <https://doi.org/10.1007/978-1->
4061 4020-4410-6
- 4062 Latrubesse, E. M., & Franzinelli, E. (2002). The Holocene alluvial plain of the middle Amazon River,
4063 Brazil. *Geomorphology*, *44*(3–4), 241–257. [https://doi.org/10.1016/S0169-555X\(01\)00177-5](https://doi.org/10.1016/S0169-555X(01)00177-5)
- 4064 Latrubesse, E. M., Arima, E. Y., Dunne, T., Park, E., Baker, V. R., D’Horta, F. M., et al. (2017).
4065 Damming the rivers of the Amazon basin. *Nature*. Nature Publishing Group.
4066 <https://doi.org/10.1038/nature22333>
- 4067 Lauerwald, R., Regnier, P., Guenet, B., Friedlingstein, P., & Ciais, P. (2020). How Simulations of the
4068 Land Carbon Sink Are Biased by Ignoring Fluvial Carbon Transfers: A Case Study for the Amazon
4069 Basin. *One Earth*, *3*(2), 226–236. <https://doi.org/10.1016/j.oneear.2020.07.009>
- 4070 Laurance, W. F., & Bruce Williamson, G. (2001). Positive feedbacks among forest fragmentation,
4071 drought, and climate change in the Amazon. *Conservation Biology*, *15*(6), 1529–1535.
4072 <https://doi.org/10.1046/j.1523-1739.2001.01093.x>
- 4073 Lawrence, D., & Vandecar, K. (2015). Effects of tropical deforestation on climate and agriculture. *Nature*
4074 *Climate Change*, *5*(1), 27–36. <https://doi.org/10.1038/nclimate2430>
- 4075 Lee, H., Yuan, T., Yu, H., & Jung, H. C. (2020). Interferometric SAR for Wetland Hydrology: An
4076 Overview of Methods, Challenges, and Trends. *IEEE Geoscience and Remote Sensing Magazine*,
4077 *8*(1), 120–135. <https://doi.org/10.1109/MGRS.2019.2958653>
- 4078 Lee, Z.-P., Shang, S., Lin, G., Chen, J., & Doxaran, D. (2016). On the modeling of hyperspectral remote-
4079 sensing reflectance of high-sediment-load waters in the visible to shortwave-infrared domain.
4080 *Applied Optics*, *55*(7), 1738–1750. <https://doi.org/10.1364/AO.55.001738>
- 4081 LeFavour, G., & Alsdorf, D. (2005). Water slope and discharge in the Amazon River estimated using the
4082 shuttle radar topography mission digital elevation model. *Geophysical Research Letters*, *32*(17), 1–
4083 5. <https://doi.org/10.1029/2005GL023836>
- 4084 Legresy, B., Papa, F., Remy, F., Vinay, G., Van Den Bosch, M., & Zanife, O. Z. (2005). ENVISAT radar
4085 altimeter measurements over continental surfaces and ice caps using the ICE-2 retracking algorithm.

- 4086 *Remote Sensing of Environment*, 95(2), 150–163. <https://doi.org/10.1016/j.rse.2004.11.018>
- 4087 Lehner, B., & Döll, P. (2004). Development and validation of a global database of lakes, reservoirs and
4088 wetlands. *Journal of Hydrology*, 296(1–4), 1–22. <https://doi.org/10.1016/j.jhydrol.2004.03.028>
- 4089 Leite-Filho, A. T., Pontes, V. Y. de S., & Costa, M. H. (2019). Effects of Deforestation on the Onset of
4090 the Rainy Season and the Duration of Dry Spells in Southern Amazonia. *Journal of Geophysical*
4091 *Research: Atmospheres*, 124(10), 5268–5281. <https://doi.org/10.1029/2018JD029537>
- 4092 Leite-Filho, A. T., Costa, M. H., & Fu, R. (2020). The southern Amazon rainy season: The role of
4093 deforestation and its interactions with large-scale mechanisms. *International Journal of*
4094 *Climatology*, 40(4), 2328–2341. <https://doi.org/10.1002/joc.6335>
- 4095 Leite, C. C., Costa, M. H., de Lima, C. A., Ribeiro, C. A. A. S., & Sedyama, G. C. (2011). Historical
4096 reconstruction of land use in the Brazilian Amazon (1940–1995). *Journal of Land Use Science*, 6(1),
4097 33–52. <https://doi.org/10.1080/1747423X.2010.501157>
- 4098 Leite, C. C., Costa, M. H., Soares-Filho, B. S., & De Barros Viana Hissa, L. (2012). Historical land use
4099 change and associated carbon emissions in Brazil from 1940 to 1995. *Global Biogeochemical*
4100 *Cycles*, 26(2). <https://doi.org/10.1029/2011GB004133>
- 4101 Lenters, J. D., & Cook, K. H. (1997). On the origin of the Bolivian high and related circulation features of
4102 the South American climate. *Journal of the Atmospheric Sciences*, 54(5), 656–677.
4103 [https://doi.org/10.1175/1520-0469\(1997\)054<0656:otootb>2.0.co;2](https://doi.org/10.1175/1520-0469(1997)054<0656:otootb>2.0.co;2)
- 4104 Leon, J. G., Calmant, S., Seyler, F., Bonnet, M. P., Cauhopé, M., Frappart, F., et al. (2006). Rating curves
4105 and estimation of average water depth at the upper Negro River based on satellite altimeter data and
4106 modeled discharges. *Journal of Hydrology*, 328(3–4), 481–496.
4107 <https://doi.org/10.1016/j.jhydrol.2005.12.006>
- 4108 Lesack, F. W., & Melack, J. M. (1995). Flooding hydrology and mixture dynamics of lakewater derived
4109 from multiple sources in an Amazon floodplain lake. *Water Resources Research*, 31(2), 329–345.
- 4110 Leuning, R., Zhang, Y. Q., Rajaud, A., Cleugh, H., & Tu, K. (2008). A simple surface conductance model
4111 to estimate regional evaporation using MODIS leaf area index and the Penman-Monteith equation.
4112 *Water Resources Research*, 44(10). <https://doi.org/10.1029/2007WR006562>
- 4113 Levizzani, V., & Cattani, E. (2019, October 1). Satellite remote sensing of precipitation and the terrestrial
4114 water cycle in a changing climate. *Remote Sensing*. MDPI AG. <https://doi.org/10.3390/rs11192301>
- 4115 Levizzani, V., Porcú, F., Marzano, F. S., Mugnai, A., Smith, E. A., & Prodi, F. (2007). Investigating a
4116 SSM/I microwave algorithm to calibrate Meteosat infrared instantaneous rainrate estimates.
4117 *Meteorological Applications*, 3(1), 5–17. <https://doi.org/10.1002/met.5060030102>
- 4118 Levizzani, V., Laviola, S., & Cattani, E. (2011). Detection and measurement of snowfall from space.

- 4119 *Remote Sensing*, 3(1), 145–166. <https://doi.org/10.3390/rs3010145>
- 4120 Levy, M. C., Lopes, A. V., Cohn, A., Larsen, L. G., & Thompson, S. E. (2018). Land use change
4121 increases streamflow across the arc of deforestation in Brazil. *Geophysical Research Letters*, 3520–
4122 3530. <https://doi.org/10.1002/2017GL076526>
- 4123 Lewin, J., Ashworth, P. J., & Strick, R. J. P. (2017). Spillage sedimentation on large river floodplains.
4124 *Earth Surface Processes and Landforms*, 42(2), 290–305. <https://doi.org/10.1002/esp.3996>
- 4125 Lewis, S. L., Brando, P. M., Phillips, O. L., Van Der Heijden, G. M. F., & Nepstad, D. (2011). The 2010
4126 Amazon drought. *Science*, 331(6017), 554. <https://doi.org/10.1126/science.1200807>
- 4127 Li, T., Wang, S., Liu, Y., Fu, B., & Gao, D. (2020). Reversal of the sediment load increase in the Amazon
4128 basin influenced by divergent trends of sediment transport from the Solimões and Madeira Rivers.
4129 *Catena*, 195(December 2019), 104804. <https://doi.org/10.1016/j.catena.2020.104804>
- 4130 Liang, Y. C., Lo, M. H., Lan, C. W., Seo, H., Ummenhofer, C. C., Yeager, S., et al. (2020). Amplified
4131 seasonal cycle in hydroclimate over the Amazon river basin and its plume region. *Nature*
4132 *Communications*, 11(1), 1–11. <https://doi.org/10.1038/s41467-020-18187-0>
- 4133 Liebmann, B., & Smith, C. A. (1996). Description of a complete (interpolated) outgoing longwave
4134 radiation dataset. *Bulletin of the American Meteorological Society*.
- 4135 Lima, L. S., Coe, M. T., Soares Filho, B. S., Cuadra, S. V., Dias, L. C. P., Costa, M. H., et al. (2014).
4136 Feedbacks between deforestation, climate, and hydrology in the Southwestern Amazon:
4137 Implications for the provision of ecosystem services. *Landscape Ecology*, 29(2), 261–274.
4138 <https://doi.org/10.1007/s10980-013-9962-1>
- 4139 Lin, J. C., Matsui, T., Pielke, R. A., & Kummerow, C. (2006). Effects of biomass-burning-derived
4140 aerosols on precipitation and clouds in the Amazon Basin: a satellite-based empirical study. *Journal*
4141 *of Geophysical Research*, 111(D19), D19204. <https://doi.org/10.1029/2005JD006884>
- 4142 Liu, X., Yang, T., Hsu, K., Liu, C., & Sorooshian, S. (2017). Evaluating the streamflow simulation
4143 capability of PERSIANN-CDR daily rainfall products in two river basins on the Tibetan Plateau.
4144 *Hydrology and Earth System Sciences*, 21(1), 169–181. <https://doi.org/10.5194/hess-21-169-2017>
- 4145 Liu, Y. Y., Parinussa, R. M., Dorigo, W. A., De Jeu, R. A. M., Wagner, W., van Dijk, A. I. J. M., et al.
4146 (2011). Developing an improved soil moisture dataset by blending passive and active microwave
4147 satellite-based retrievals. *Hydrology and Earth System Sciences*, 15(2), 425–436.
4148 <https://doi.org/10.5194/hess-15-425-2011>
- 4149 Llauca, H., Lavado-Casimiro, W., León, K., Jimenez, J., Traverso, K., & Rau, P. (2021). Assessing Near
4150 Real-Time Satellite Precipitation Products for Flood Simulations at Sub-Daily Scales in a Sparsely
4151 Gauged Watershed in Peruvian Andes. *Remote Sensing*, 13(4), 826.

- 4152 <https://doi.org/10.3390/rs13040826>
- 4153 Lobo, F., Novo, E. M. L. de M., Barbosa, C. C. F., & Galvão, L. S. (2012). Reference spectra to classify
4154 Amazon water types. *International Journal of Remote Sensing*, 33(11), 3422–3442.
4155 <https://doi.org/10.1080/01431161.2011.627391>
- 4156 Lobo, F., Costa, M. P. F., & Novo, E. M. L. M. (2015). Time-series analysis of Landsat-MSS/TM/OLI
4157 images over Amazonian waters impacted by gold mining activities. *Remote Sensing of Environment*,
4158 157, 170–184. <https://doi.org/10.1016/j.rse.2014.04.030>
- 4159 Lobo, F., Costa, M., Novo, E., & Telmer, K. (2016). Distribution of Artisanal and Small-Scale Gold
4160 Mining in the Tapajós River Basin (Brazilian Amazon) over the Past 40 Years and Relationship with
4161 Water Siltation. *Remote Sensing*, 8(7), 579. <https://doi.org/10.3390/rs8070579>
- 4162 Lobo, F., Souza-Filho, P. W. M., Novo, E. M. L. de M., Carlos, F. M., & Barbosa, C. C. F. (2018).
4163 Mapping mining areas in the Brazilian amazon using MSI/Sentinel-2 imagery (2017). *Remote*
4164 *Sensing*, 10(8). <https://doi.org/10.3390/rs10081178>
- 4165 Lobón-Cerviá, J., Hess, L. L., Melack, J. M., & Araujo-Lima, C. A. R. M. (2015). The importance of
4166 forest cover for fish richness and abundance on the Amazon floodplain. *Hydrobiologia*, 750, 245–
4167 255. <https://doi.org/10.1007/s10750-014-2040-0>
- 4168 Lopes, A. V., Chiang, J. C. H., Thompson, S. A., & Dracup, J. A. (2016). Trend and uncertainty in
4169 spatial-temporal patterns of hydrological droughts in the Amazon basin. *Geophysical Research*
4170 *Letters*, 43(7), 3307–3316. <https://doi.org/10.1002/2016GL067738>
- 4171 Lopez, T., Al Bitar, A., Biancamaria, S., Güntner, A., & Jäggi, A. (2020). On the Use of Satellite Remote
4172 Sensing to Detect Floods and Droughts at Large Scales. *Surveys in Geophysics*.
4173 <https://doi.org/10.1007/s10712-020-09618-0>
- 4174 Luo, X., Li, H. Y., Ruby Leung, L., Tesfa, T. K., Getirana, A., Papa, F., & Hess, L. L. (2017). Modeling
4175 surface water dynamics in the Amazon Basin using MOSART-Inundation v1.0: Impacts of
4176 geomorphological parameters and river flow representation. *Geoscientific Model Development*,
4177 10(3), 1233–1259. <https://doi.org/10.5194/gmd-10-1233-2017>
- 4178 Luz-Agostinho, K. D. G., Agostinho, A. A., Gomes, L. C., Júlio-Jr., H. F., & Fugi, R. (2009). Effects of
4179 flooding regime on the feeding activity and body condition of piscivorous fish in the Upper Paraná
4180 River floodplain. *Brazilian Journal of Biology*, 69, 481–490. <https://doi.org/10.1590/s1519-69842009000300004>
- 4181
- 4182 Maciel, D. A., Novo, E., Sander de Carvalho, L., Barbosa, C., Flores Júnior, R., de Lucia Lobo, F., et al.
4183 (2019). Retrieving Total and Inorganic Suspended Sediments in Amazon Floodplain Lakes: A
4184 Multisensor Approach. *Remote Sensing*, 11(15), 1744. <https://doi.org/10.3390/rs11151744>

- 4185 Maciel, D. A., Novo, E. M. L. de M., Barbosa, C. C. F. C. C. F. C., Martins, V. S. ., Flores Júnior, R.,
4186 Oliveira, A. H., et al. (2020). Evaluating the potential of CubeSats for remote sensing reflectance
4187 retrieval over inland waters. *International Journal of Remote Sensing*, 41(7), 2807–2817.
4188 <https://doi.org/10.1080/2150704X.2019.1697003>
- 4189 Maciel, D. A., Barbosa, C. C. F., Novo, E. M. L. de M., Cherukuru, N., Martins, V. S., Flores Júnior, R.,
4190 et al. (2020). Mapping of diffuse attenuation coefficient in optically complex waters of amazon
4191 floodplain lakes. *ISPRS Journal of Photogrammetry and Remote Sensing*, 170(October), 72–87.
4192 <https://doi.org/10.1016/j.isprsjprs.2020.10.009>
- 4193 Madden, R. A., & Julian, P. R. (1994). Observations of the 40–50-Day Tropical Oscillation—A Review.
4194 *Monthly Weather Review*, 122(5), 814–837. [https://doi.org/10.1175/1520-](https://doi.org/10.1175/1520-0493(1994)122<0814:OOTDTO>2.0.CO;2)
4195 [0493\(1994\)122<0814:OOTDTO>2.0.CO;2](https://doi.org/10.1175/1520-0493(1994)122<0814:OOTDTO>2.0.CO;2)
- 4196 Maeda, E. E., Kim, H., Aragão, L. E. O. C., Famiglietti, J. S., & Oki, T. (2015). Disruption of
4197 hydroecological equilibrium in southwest Amazon mediated by drought. *Geophysical Research*
4198 *Letters*, 42, 7546–7553. <https://doi.org/10.1002/2015GL065252>
- 4199 Maeda, E. E., Ma, X., Wagner, F. H., Kim, H., Oki, T., Eamus, D., & Huete, A. (2017).
4200 Evapotranspiration seasonality across the Amazon Basin. *Earth System Dynamics*, 8(2), 439–454.
4201 <https://doi.org/10.5194/esd-8-439-2017>
- 4202 Manz, B., Páez-Bimos, S., Horna, N., Buytaert, W., Ochoa-Tocachi, B., Lavado-Casimiro, W., &
4203 Willems, B. (2017). Comparative ground validation of IMERG and TMPA at variable
4204 spatiotemporal scales in the tropical Andes. *Journal of Hydrometeorology*, 18(9), 2469–2489.
4205 <https://doi.org/10.1175/JHM-D-16-0277.1>
- 4206 Marengo, J. A. (2005). Characteristics and spatio-temporal variability of the Amazon river basin water
4207 budget. *Climate Dynamics*, 24(1), 11–22. <https://doi.org/10.1007/s00382-004-0461-6>
- 4208 Marengo, J. A., & Espinoza, J. C. (2016). Extreme seasonal droughts and floods in Amazonia: Causes,
4209 trends and impacts. *International Journal of Climatology*, 36(3), 1033–1050.
4210 <https://doi.org/10.1002/joc.4420>
- 4211 Marengo, J. A., Nobre, C. A., Tomasella, J., Cardoso, M. F., & Oyama, M. D. (2008). Hydro-climatic and
4212 ecological behaviour of the drought of Amazonia in 2005. *Philosophical Transactions of the Royal*
4213 *Society B: Biological Sciences*, 363(1498), 1773–1778. <https://doi.org/10.1098/rstb.2007.0015>
- 4214 Marengo, J. A., Tomasella, J., Alves, L. M., Soares, W. R., & Rodriguez, D. A. (2011). The drought of
4215 2010 in the context of historical droughts in the Amazon region. *Geophysical Research Letters*,
4216 38(12), 1–5. <https://doi.org/10.1029/2011GL047436>
- 4217 Marengo, J. A., Souza, C. M., Thonicke, K., Burton, C., Halladay, K., Betts, R. A., et al. (2018). Changes

- 4218 in Climate and Land Use Over the Amazon Region: Current and Future Variability and Trends.
 4219 *Frontiers in Earth Science*. <https://doi.org/10.3389/feart.2018.00228>
- 4220 Marinho, T., Filizola, N., Martinez, J. M., Armijos, E., & Nascimento, A. (2018). Suspended sediment
 4221 variability at the Solimões and negro confluence between May 2013 and February 2014.
 4222 *Geosciences (Switzerland)*, 8(7). <https://doi.org/10.3390/geosciences8070265>
- 4223 Martens, B., Miralles, D. G., Lievens, H., Van Der Schalie, R., De Jeu, R. A. M., Fernández-Prieto, D., et
 4224 al. (2017). GLEAM v3: Satellite-based land evaporation and root-zone soil moisture. *Geoscientific*
 4225 *Model Development*, 10(5), 1903–1925. <https://doi.org/10.5194/gmd-10-1903-2017>
- 4226 Martinez, J., Espinoza-villar, R., Armijos, E., & Moreira, L. S. (2015). The optical properties of river and
 4227 floodplain waters in the Amazon River Basin: Implications for satellite-based measurements of
 4228 suspended particulate matter - Supplementary material. *Journal of Geophysical Research : Earth*
 4229 *Surface*, 1(860), 1–11. <https://doi.org/10.1002/2014JF003404>.Received
- 4230 Martinez, J. A., & Dominguez, F. (2014). Sources of Atmospheric Moisture for the La Plata River
 4231 Basin*. *Journal of Climate*, 27(17), 6737–6753. <https://doi.org/10.1175/JCLI-D-14-00022.s1>
- 4232 Martinez, J. M., Guyot, J. L., Filizola, N., & Sondag, F. (2009). Increase in suspended sediment discharge
 4233 of the Amazon River assessed by monitoring network and satellite data. *Catena*, 79(3), 257–264.
 4234 <https://doi.org/10.1016/j.catena.2009.05.011>
- 4235 Marzano, F. S., Member, S., Palmacci, M., Cimini, D., Giuliani, G., & Turk, F. J. (2004). Multivariate
 4236 Statistical Integration of Satellite Infrared and Microwave Radiometric Measurements for Rainfall
 4237 Retrieval at the Geostationary Scale, 42(5), 1018–1032.
- 4238 Massari, C. (2020, May). GPM+SM2RAIN (2007-2018): quasi-global 25km/daily rainfall product from
 4239 the integration of GPM and SM2RAIN-based rainfall products. Zenodo.
 4240 <https://doi.org/10.5281/zenodo.3854817>
- 4241 Massari, C., Brocca, L., Tarpanelli, A., & Moramarco, T. (2015). *Data assimilation of satellite soil*
 4242 *moisture into rainfall-runoffmodelling: A complex recipe? Remote Sensing (Vol. 7)*.
 4243 <https://doi.org/10.3390/rs70911403>
- 4244 Matthews, E., & Fung, I. (1987). Methane emission from natural wetlands: Global distribution, area, and
 4245 environmental characteristics of sources. *Global Biogeochemical Cycles*, 1, 61–86.
 4246 <https://doi.org/10.1029/GB001i001p00061>
- 4247 Matthews, M. W. (2011). A current review of empirical procedures of remote sensing in Inland and near-
 4248 coastal transitional waters. *International Journal of Remote Sensing*, 32(21), 6855–6899.
 4249 <https://doi.org/10.1080/01431161.2010.512947>
- 4250 Mayta, V. C., Ambrizzi, T., Espinoza, J. C., & Silva Dias, P. L. (2019). The role of the Madden–Julian

- 4251 oscillation on the Amazon Basin intraseasonal rainfall variability. *International Journal of*
 4252 *Climatology*, 39(1), 343–360. <https://doi.org/10.1002/joc.5810>
- 4253 McCabe, M. F., Rodell, M., Alsdorf, D. E., Miralles, D. G., Uijlenhoet, R., Wagner, W., et al. (2017). The
 4254 future of Earth observation in hydrology. *Hydrology and Earth System Sciences*, 21(7), 3879–3914.
 4255 <https://doi.org/10.5194/hess-21-3879-2017>
- 4256 McCorkel, J., Montanaro, M., Efremova, B., Pearlman, A., Wenny, B., Lunsford, A., et al. (2018).
 4257 Landsat 9 Thermal Infrared Sensor 2 Characterization Plan Overview. In *IEEE International*
 4258 *Geoscience and Remote Sensing Symposium* (pp. 8845–8848). Valencia, Spain: IEEE.
- 4259 Meade, R. H. (1994). Suspended sediments of the modern Amazon and Orinoco rivers. *Quaternary*
 4260 *International*, 21(C), 29–39. [https://doi.org/10.1016/1040-6182\(94\)90019-1](https://doi.org/10.1016/1040-6182(94)90019-1)
- 4261 Melack, J. M. (2016). Aquatic ecosystems. In L. Nagy, P. Artaxo, & B. R. Forsberg (Eds.), *Interactions*
 4262 *Between Biosphere, Atmosphere, and Human Land Use in the Amazon Basin* (pp. 117–145).
 4263 Springer. https://doi.org/10.1007/978-3-662-49902-3_1
- 4264 Melack, J. M., & Coe, M. (2021). Amazon floodplain hydrology and implications for aquatic
 4265 conservation. *Aquatic Conservation: Marine and Freshwater Ecosystems*. Retrieved from
 4266 Manuscript ID JHMAS-2020-066.R1
- 4267 Melack, J. M., & Forsberg, B. R. (2001). The Biogeochemistry of the Amazon Floodplain Lakes and
 4268 Associated Wetlands. *The Biogeochemistry of the Amazon Basin and Its Role in a Changing World*.
- 4269 Melack, J. M., & Hess, L. L. (2010). Remote sensing of the distribution and extend of wetlands in the
 4270 Amazon Basin. In J. W.; M. T. F. Piedade, F. Wittmann, J. Schöngart, & P. Parolin (Eds.),
 4271 *Amazonian Floodplain Forests: Ecophysiology, ecology, biodiversity and sustainable management*.
 4272 *Ecological Studies* (Vol. 210, pp. 43–59). Dordrecht: Springer. [https://doi.org/10.1007/978-90-481-](https://doi.org/10.1007/978-90-481-8725-6_3)
 4273 [8725-6_3](https://doi.org/10.1007/978-90-481-8725-6_3)
- 4274 Melack, J. M., Hess, L. L., Gastil, M., Forsberg, B. R., Hamilton, S. K., Lima, I. B. T., & Novo, E. M. L.
 4275 M. (2004). Regionalization of methane emissions in the Amazon Basin with microwave remote
 4276 sensing. *Global Change Biology*, 10, 530–544. <https://doi.org/10.1111/j.1529-8817.2003.00763.x>
- 4277 Melack, J. M., Novo, E. M. L. M., Forsberg, B. R., Piedade, M. T. F. F., & Maurice, L. (2009).
 4278 Floodplain Ecosystem Processes. *Amazonia and Global Change*, (2003), 525–541.
 4279 <https://doi.org/10.1029/2008GM000727>
- 4280 Melack, J. M., Amaral, J. H. F., Kasper, D., Barbosa, P. M., & Forsberg, B. R. (2021). Limnological
 4281 perspectives on conservation of aquatic ecosystems in the Amazon basin. *Aquatic Conservation:*
 4282 *Marine and Freshwater Ecosystems*, 30(12). <https://doi.org/10.1002/aqc.3556>
- 4283 Menenti, M., & Choudhury, B. J. (1993). Parameterization of land surface evaporation by means of

- 4284 location dependent potential evaporation and surface temperature range. In *Exchange Processes at*
4285 *the Land Surface for a Range of Space and Time Scales* (pp. 561–568). Yokohama, Japan: IAHS
4286 Publ.
- 4287 Mertes, L. A. K. (1997). Documentation and significance of the perirheic zone on inundated floodplains.
4288 *Water Resources Research*, 33(7), 1749–1762. <https://doi.org/10.1029/97WR00658>
- 4289 Mertes, L. A. K., Smith, M. O., & Adams, J. B. (1993). Estimating suspended sediment concentrations in
4290 surface waters of the amazon river wetlands from landsat images. *Remote Sensing of Environment*,
4291 43(3), 281–301. [https://doi.org/10.1016/0034-4257\(93\)90071-5](https://doi.org/10.1016/0034-4257(93)90071-5)
- 4292 Mertes, L. A. K., Daniel, D. L., Melack, J. M., Nelson, B., Martinelli, L. A., & Forsberg, B. R. (1995).
4293 Spatial patterns of hydrology, geomorphology, and vegetation on the floodplain of the Amazon river
4294 in Brazil from a remote sensing perspective. *Geomorphology*, 13(1–4), 215–232.
4295 [https://doi.org/10.1016/0169-555X\(95\)00038-7](https://doi.org/10.1016/0169-555X(95)00038-7)
- 4296 Mertes, L. A. K., Dunne, T., & Martinelli, L. A. (1996). Channel-floodplain geomorphology along the
4297 Solimoes-Amazon River, Brazil. *Bulletin of the Geological Society of America*, 108(9), 1089–1107.
4298 [https://doi.org/10.1130/0016-7606\(1996\)108<1089:CFGATS>2.3.CO;2](https://doi.org/10.1130/0016-7606(1996)108<1089:CFGATS>2.3.CO;2)
- 4299 Michel, D., Jiménez, C., Miralles, D. G., Jung, M., Hirschi, M., Ershadi, A., et al. (2016). The
4300 WACMOS-ET project - Part 1: Tower-scale evaluation of four remote-sensing-based
4301 evapotranspiration algorithms. *Hydrology and Earth System Sciences*, 20(2), 803–822.
4302 <https://doi.org/10.5194/hess-20-803-2016>
- 4303 Miguez-Macho, G., & Fan, Y. (2012). The role of groundwater in the Amazon water cycle: 1. Influence
4304 on seasonal streamflow, flooding and wetlands. *Journal of Geophysical Research Atmospheres*,
4305 117(15), 1–30. <https://doi.org/10.1029/2012JD017539>
- 4306 Minnis, P., & Harrison, E. F. (1984). Diurnal Variability of Regional Cloud and Clear-Sky Radiative
4307 Parameters Derived from GOES Data. Part II: November 1978 Cloud Distributions. *Journal of*
4308 *Climate and Applied Meteorology*, 23(7), 1012–1031. [https://doi.org/10.1175/1520-0450\(1984\)023<1012:DVORCA>2.0.CO;2](https://doi.org/10.1175/1520-0450(1984)023<1012:DVORCA>2.0.CO;2)
- 4310 Miralles, D. G., Holmes, T. R. H., De Jeu, R. A. M., Gash, J. H., Meesters, A. G. C. A., & Dolman, A. J.
4311 (2011). Global land-surface evaporation estimated from satellite-based observations. *Hydrology and*
4312 *Earth System Sciences*, 15(2), 453–469. <https://doi.org/10.5194/hess-15-453-2011>
- 4313 Miralles, D. G., Jiménez, C., Jung, M., Michel, D., Ershadi, A., McCabe, M. F., et al. (2016). The
4314 WACMOS-ET project - Part 2: Evaluation of global terrestrial evaporation data sets. *Hydrology and*
4315 *Earth System Sciences*, 20(2), 823–842. <https://doi.org/10.5194/hess-20-823-2016>
- 4316 Mobley, C. D. (1994). *Light and water: radiative transfer in natural waters*. Academic press.

- 4317 Mohammadimanesh, F., Salehi, B., Mahdianpari, M., Brisco, B., & Motagh, M. (2018). Wetland Water
4318 Level Monitoring Using Interferometric Synthetic Aperture Radar (InSAR): A Review. *Canadian*
4319 *Journal of Remote Sensing*, 0(0), 1–16. <https://doi.org/10.1080/07038992.2018.1477680>
- 4320 Mohor, G. S., Rodriguez, D. A., Tomasella, J., & Siqueira Júnior, J. L. (2015). Exploratory analyses for
4321 the assessment of climate change impacts on the energy production in an Amazon run-of-river
4322 hydropower plant. *Journal of Hydrology: Regional Studies*, 4(PB), 41–59.
4323 <https://doi.org/10.1016/j.ejrh.2015.04.003>
- 4324 Molina-Carpio, J., Espinoza, J. C., Vauchel, P., Ronchail, J., Gutierrez Caloir, B., Guyot, J. L., &
4325 Noriega, L. (2017). Hydroclimatology of the Upper Madeira River basin: spatio-temporal variability
4326 and trends. *Hydrological Sciences Journal*, 62(6), 911–927.
4327 <https://doi.org/10.1080/02626667.2016.1267861>
- 4328 Molinas, E., Carneiro, J. C., & Vinzon, S. (2020). Internal tides as a major process in Amazon continental
4329 shelf fine sediment transport. *Marine Geology*, 430(June).
4330 <https://doi.org/10.1016/j.margeo.2020.106360>
- 4331 Montanher, O. C., Novo, E. M. L. de M., Barbosa, C. C. F. F., Rennó, C. D., & Silva, T. S. F. F. (2014).
4332 Empirical models for estimating the suspended sediment concentration in Amazonian white water
4333 rivers using Landsat 5/TM. *International Journal of Applied Earth Observation and*
4334 *Geoinformation*, 29(1), 67–77. <https://doi.org/10.1016/j.jag.2014.01.001>
- 4335 Montanher, O. C., Novo, E. M. L. de M., & Filho, E. D. S. (2018). Temporal trend of the suspended
4336 sediment transport of the Amazon River (1984 – 2016). *Hydrological Sciences Journal*, 63(13–14),
4337 1901–1912. <https://doi.org/10.1080/02626667.2018.1546387>
- 4338 Montazem, A., Garambois, P., Calmant, S., Finaud-Guyot, P., Monnier, J., Medeiros Moreira, D., et al.
4339 (2019). Wavelet-based river segmentation using hydraulic control-preserving water surface
4340 elevation profile properties. *Geophysical Research Letters*, 2019GL082986.
4341 <https://doi.org/10.1029/2019GL082986>
- 4342 Monteith, J. (1965). Evaporation and the Environment in the State and Movement of Water in Living
4343 Organisms. In *Proceedings of the Society for Experimental Biology* (pp. 205–234). Cambridge:
4344 Cambridge University Press.
- 4345 Monteith, J., & Unsworth, M. (2013). *Principles of Environmental Physics: Plants, Animals, and the*
4346 *Atmosphere. Principles of Environmental Physics: Plants, Animals, and the Atmosphere: Fourth*
4347 *Edition* (Fourth). Academic Press. <https://doi.org/10.1016/C2010-0-66393-0>
- 4348 Moreira, A. A., Ruhoff, A. L., Roberti, D. R., Souza, V. de A., da Rocha, H. R., & de Paiva, R. C. D.
4349 (2019). Assessment of terrestrial water balance using remote sensing data in South America. *Journal*

- 4350 *of Hydrology*, 575(May), 131–147. <https://doi.org/10.1016/j.jhydrol.2019.05.021>
- 4351 Mu, Q., Heinsch, F. A., Zhao, M., & Running, S. W. (2007). Development of a global evapotranspiration
4352 algorithm based on MODIS and global meteorology data. *Remote Sensing of Environment*, 111(4),
4353 519–536. <https://doi.org/10.1016/j.rse.2007.04.015>
- 4354 Mu, Q., Zhao, M., & Running, S. W. (2011). Improvements to a MODIS global terrestrial
4355 evapotranspiration algorithm. *Remote Sensing of Environment*, 115(8), 1781–1800.
4356 <https://doi.org/10.1016/j.rse.2011.02.019>
- 4357 Mueller, J. L., Morel, A., Frouin, R., Davis, C. O., Arnone, R. a., Carder, K. L., et al. (2003). Vol 3:
4358 Radiometric Measurements and Data Analysis Protocols. *Ocean Optics Protocols For Satellite*
4359 *Ocean Color Sensor Validation, Revision 4, III*(January), 78.
- 4360 Munier, S., & Aires, F. (2018). A new global method of satellite dataset merging and quality
4361 characterization constrained by the terrestrial water budget. *Remote Sensing of Environment*,
4362 205(October 2017), 119–130. <https://doi.org/10.1016/j.rse.2017.11.008>
- 4363 Nagel, G. W., Novo, E. M. L. de M., & Kampel, M. (2020). Nanosatellites applied to optical Earth
4364 observation: a review. *Revista Ambiente e Agua*, 9(3), 445–458. <https://doi.org/10.4136/1980-993X>
- 4365 Nagy, L., Artaxo, P., & Forsberg, B. R. (2016). *Interactions between Biosphere, Atmosphere and Human*
4366 *Land Use in the Amazon Basin*. (L. Nagy, P. Artaxo, & B. R. Forsberg, Eds.) (1st ed.). Berlin
4367 Heidelberg: Springer. <https://doi.org/10.1007/978-3-662-49902-3>
- 4368 Ndehedehe, C. E., & Ferreira, V. G. (2020). Assessing land water storage dynamics over South America.
4369 *Journal of Hydrology*, 580. <https://doi.org/10.1016/j.jhydrol.2019.124339>
- 4370 Negri, A. J., Adler, R. F., Nelkin, E. J., & Huffman, G. J. (1994). Regional Rainfall Climatologies
4371 Derived from Special Sensor Microwave Imager (SSM/I) Data. *Bulletin of the American*
4372 *Meteorological Society*, 75(7), 1165–1182. [https://doi.org/10.1175/1520-](https://doi.org/10.1175/1520-0477(1994)075<1165:RRCDFS>2.0.CO;2)
4373 [0477\(1994\)075<1165:RRCDFS>2.0.CO;2](https://doi.org/10.1175/1520-0477(1994)075<1165:RRCDFS>2.0.CO;2)
- 4374 Negri, A. J., Anagnostou, E. N., & Adler, R. F. (2000). A 10-yr climatology of amazonian rainfall derived
4375 from passive microwave satellite observations. *Journal of Applied Meteorology*, 39(1), 42–56.
4376 [https://doi.org/10.1175/1520-0450\(2000\)039<0042:AYCOAR>2.0.CO;2](https://doi.org/10.1175/1520-0450(2000)039<0042:AYCOAR>2.0.CO;2)
- 4377 Nguyen, P., Shearer, E. J., Tran, H., Ombadi, M., Hayatbini, N., Palacios, T., et al. (2019). The CHRS
4378 data portal, an easily accessible public repository for PERSIANN global satellite precipitation data.
4379 *Scientific Data*, 6, 1–10. <https://doi.org/10.1038/sdata.2018.296>
- 4380 Niroumand-Jadidi, M., Bovolo, F., & Bruzzone, L. (2020). Water quality retrieval from PRISMA
4381 hyperspectral images: First experience in a turbid lake and comparison with sentinel-2. *Remote*
4382 *Sensing*, 12(23), 1–21. <https://doi.org/10.3390/rs12233984>

- 4383 Niu, J., Shen, C., Chambers, J. Q., Melack, J. M., & Riley, W. J. (2017). Interannual Variation in
4384 Hydrologic Budgets in an Amazonian Watershed with a Coupled Subsurface–Land Surface Process
4385 Model. *Journal of Hydrometeorology*, 18(9), 2597–2617. <https://doi.org/10.1175/JHM-D-17-0108.1>
- 4386 Nobrega, I. W. da. (2002). *Análise espectral de sistemas aquáticos da Amazônia para a identificação de*
4387 *componentes opticamente ativos*. Instituto Nacional de Pesquisas Espaciais (INPE), São José dos
4388 Campos.
- 4389 Norman, J. M., Kustas, W. P., & Humes, K. S. (1995). *Source approach for estimating soil and*
4390 *vegetation energy fluxes in observations of directional radiometric surface temperature*.
4391 *Agricultural and Forest Meteorology* (Vol. 77).
- 4392 Normandin, C., Frappart, F., Diepkilé, A. T., Marieu, V., Mougin, E., Blarel, F., et al. (2018). Evolution
4393 of the Performances of Radar Altimetry Missions from ERS-2 to Sentinel-3A over the Inner Niger
4394 Delta. *Remote Sensing*, 10(6), 833. <https://doi.org/10.3390/rs10060833>
- 4395 Novo, E. M. L. de M., & Shimabukuro, Y. E. (1997). Identification and mapping of the Amazon habitats
4396 using a mixing model. *International Journal of Remote Sensing*, 18, 663–670.
4397 <https://doi.org/10.1080/014311697218999>
- 4398 Novo, E. M. L. de M., de Farias Barbosa, C. C., Freitas, R. M., Shimabukuro, Y. E., Melack, J. M., &
4399 Filho, W. P. (2006). Seasonal changes in chlorophyll distributions in Amazon floodplain lakes
4400 derived from MODIS images. *Limnology*, 7(3), 153–161. [https://doi.org/10.1007/s10201-006-0179-](https://doi.org/10.1007/s10201-006-0179-8)
4401 8
- 4402 Novoa, S., Doxaran, D., Ody, A., Vanhellemont, Q., Lafon, V., Lubac, B., & Gernez, P. (2017).
4403 Atmospheric corrections and multi-conditional algorithm for multi-sensor remote sensing of
4404 suspended particulate matter in low-to-high turbidity levels coastal waters. *Remote Sensing*, 9(1).
4405 <https://doi.org/10.3390/rs9010061>
- 4406 O’Loughlin, F. E., Paiva, R. C. D., Durand, M., Alsdorf, D. E., & Bates, P. D. (2016). A multi-sensor
4407 approach towards a global vegetation corrected SRTM DEM product. *Remote Sensing of*
4408 *Environment*, 182, 49–59. <https://doi.org/10.1016/j.rse.2016.04.018>
- 4409 Odermatt, D., Gitelson, A., Brando, V. E., & Schaepman, M. (2012). Review of constituent retrieval in
4410 optically deep and complex waters from satellite imagery. *Remote Sensing of Environment*,
4411 118(March), 116–126. <https://doi.org/10.1016/j.rse.2011.11.013>
- 4412 Oliveira, A. M., Fleischmann, A. S., & Paiva, R. C. D. (2021). On the contribution of remote sensing-
4413 based calibration to model hydrological and hydraulic processes in tropical regions. *Journal of*
4414 *Hydrology*, 126184. <https://doi.org/https://doi.org/10.1016/j.jhydrol.2021.126184>
- 4415 de Oliveira Campos, I., Mercier, F., Maheu, C., Cochonneau, G., Kosuth, P., Blitzkow, D., & Cazenave,

- 4416 A. (2001). Temporal variations of river basin waters from Topex/Poseidon satellite altimetry.
4417 Application to the Amazon basin. *Comptes Rendus de l'Académie Des Sciences-Series IIA-Earth*
4418 *and Planetary Science*, 333(10), 633–643.
- 4419 de Oliveira, G., Brunzell, N. A., Moraes, E. C., Shimabukuro, Y. E., dos Santos, T. V., von Randow, C.,
4420 et al. (2019). Effects of land-cover changes on the partitioning of surface energy and water fluxes in
4421 Amazonia using high-resolution satellite imagery. *Ecohydrology*, 12(6).
4422 <https://doi.org/10.1002/eco.2126>
- 4423 Oliveira, P. T. S., Nearing, M. A., Moran, M. S., Goodrich, D. C., Wendland, E., & Gupta, H. V. (2014).
4424 Trends in water balance components across the Brazilian Cerrado. *Water Resources Research*,
4425 50(9), 7100–7114. <https://doi.org/10.1002/2013WR015202>
- 4426 Oliveira, R., Maggioni, V., Vila, D., & Morales, C. (2016). Characteristics and diurnal cycle of GPM
4427 rainfall estimates over the Central Amazon region. *Remote Sensing*, 8(7).
4428 <https://doi.org/10.3390/rs8070544>
- 4429 Ovando, A., Tomasella, J., Rodriguez, D. A., Martinez, J. M., Siqueira-Junior, J. L., Pinto, G. L. N., et al.
4430 (2016). Extreme flood events in the Bolivian Amazon wetlands. *Journal of Hydrology: Regional*
4431 *Studies*, 5, 293–308. <https://doi.org/10.1016/j.ejrh.2015.11.004>
- 4432 Ovando, A., Martinez, J. M., Tomasella, J., Rodriguez, D. A., & von Randow, C. (2018). Multi-temporal
4433 flood mapping and satellite altimetry used to evaluate the flood dynamics of the Bolivian Amazon
4434 wetlands. *International Journal of Applied Earth Observation and Geoinformation*, 69(January),
4435 27–40. <https://doi.org/10.1016/j.jag.2018.02.013>
- 4436 Overeem, A., Leijnse, H., & Uijlenhoet, R. (2013). Country-wide rainfall maps from cellular
4437 communication networks. *Proceedings of the National Academy of Sciences of the United States of*
4438 *America*, 110(8), 2741–2745. <https://doi.org/10.1073/pnas.1217961110>
- 4439 Overeem, A., Leijnse, H., & Uijlenhoet, R. (2016). Two and a half years of country-wide rainfall maps
4440 using radio links from commercial cellular telecommunication networks. *Water Resources*
4441 *Research*, 52(10), 8039–8065. <https://doi.org/10.1002/2016WR019412>
- 4442 Paca, V. H. da M., Espinoza-Dávalos, G. E., Hessels, T. M., Moreira, D. M., Comair, G. F., &
4443 Bastiaanssen, W. G. M. (2019). The spatial variability of actual evapotranspiration across the
4444 Amazon River Basin based on remote sensing products validated with flux towers. *Ecological*
4445 *Processes*, 8(1). <https://doi.org/10.1186/s13717-019-0158-8>
- 4446 Paca, V. H. da M., Espinoza-Dávalos, G., Moreira, D., & Comair, G. (2020). Variability of Trends in
4447 Precipitation across the Amazon River Basin Determined from the CHIRPS Precipitation Product
4448 and from Station Records. *Water*, 12(5), 1244. <https://doi.org/10.3390/w12051244>

- 4449 Paccini, L., Espinoza, J. C., Ronchail, J., & Segura, H. (2018). Intra-seasonal rainfall variability in the
4450 Amazon basin related to large-scale circulation patterns: a focus on western Amazon-Andes
4451 transition region. *International Journal of Climatology*, *38*(5), 2386–2399.
4452 <https://doi.org/10.1002/joc.5341>
- 4453 Paiva, R. C. D. de. (2020). Advances and challenges in the water sciences in Brazil : a community
4454 synthesis of the XXIII Brazilian Water Resources Symposium. *Revista Brasileira de Recursos*
4455 *Hídricos*, *5*(50). <https://doi.org/10.1590/2318-0331.252020200136>
- 4456 Paiva, R. C. D. de, Collischonn, W., & Tucci, C. E. M. (2011). Large scale hydrologic and hydrodynamic
4457 modeling using limited data and a GIS based approach. *Journal of Hydrology*, *406*(3–4), 170–181.
4458 <https://doi.org/10.1016/j.jhydrol.2011.06.007>
- 4459 Paiva, R. C. D. de, Buarque, D. C., Clarke, R. T., Collischonn, W., & Allasia, D. G. (2011). Reduced
4460 precipitation over large water bodies in the Brazilian Amazon shown from TRMM data.
4461 *Geophysical Research Letters*, *38*(4). <https://doi.org/10.1029/2010GL045277>
- 4462 Paiva, R. C. D. de, Collischonn, W., Bonnet, M. P., De Gonçalves, L. G. G., Calmant, S., Getirana, A., &
4463 Santos Da Silva, J. (2013). Assimilating in situ and radar altimetry data into a large-scale
4464 hydrologic-hydrodynamic model for streamflow forecast in the Amazon. *Hydrology and Earth*
4465 *System Sciences*, *17*(7), 2929–2946. <https://doi.org/10.5194/hess-17-2929-2013>
- 4466 Paiva, R. C. D. de, Buarque, D. C., Collischonn, W., Bonnet, M. P., Frappart, F., Calmant, S., & Bulhões
4467 Mendes, C. A. (2013). Large-scale hydrologic and hydrodynamic modeling of the Amazon River
4468 basin. *Water Resources Research*, *49*(3), 1226–1243. <https://doi.org/10.1002/wrcr.20067>
- 4469 Pan, M., & Wood, E. F. (2006). Data Assimilation for Estimating the Terrestrial Water Budget Using a
4470 Constrained Ensemble Kalman Filter. *Journal of Hydrometeorology*, *7*(3), 534–547.
4471 <https://doi.org/10.1175/JHM495.1>
- 4472 Pan, M., Sahoo, A. K., Troy, T. J., Vinukollu, R. K., Sheffield, J., & Wood, A. E. F. (2012). Multisource
4473 estimation of long-term terrestrial water budget for major global river basins. *Journal of Climate*,
4474 *25*(9), 3191–3206. <https://doi.org/10.1175/JCLI-D-11-00300.1>
- 4475 Panday, P. K., Coe, M. T., Macedo, M. N., Lefebvre, P., & Castanho, A. D. de A. (2015). Deforestation
4476 offsets water balance changes due to climate variability in the Xingu River in eastern Amazonia.
4477 *Journal of Hydrology*, *523*(February 2015), 822–829. <https://doi.org/10.1016/j.jhydrol.2015.02.018>
- 4478 Pangala, S. R., Enrich-Prast, A., Basso, L. S., Peixoto, R. B., Bastviken, D., Hornibrook, E. R. C., et al.
4479 (2017). Large emissions from floodplain trees close the Amazon methane budget. *Nature*, *552*, 230–
4480 234. <https://doi.org/10.1038/nature24639>
- 4481 Panosso, R. D. F., Muehe, D., & Esteves, F. D. A. (1995). Morphological characteristics of an Amazon

- 4482 floodplain lake (Lake Batata, Para State, Brazil). *Amazonia*, 13(3–4), 245–258.
- 4483 Paola, F. Di, Casella, D., Dietrich, S., Mugnai, A., Ricciardelli, E., Romano, F., et al. (2012). Combined
4484 MW-IR Precipitation Evolving Technique (PET) of convective rain fields, 3557–3570.
4485 <https://doi.org/10.5194/nhess-12-3557-2012>
- 4486 Papa, F., Günther, A., Frappart, F., Prigent, C., Rossow, W. B. B., Güntner, A., et al. (2008). Variations of
4487 surface water extent and water storage in large river basins: A comparison of different global data
4488 sources. *Geophysical Research Letters*, 35(11), L11401. <https://doi.org/10.1029/2008GL033857>
- 4489 Papa, F., Prigent, C., Aires, F., Jimenez, C., Rossow, W. B., & Matthews, E. (2010). Interannual
4490 variability of surface water extent at the global scale, 1993-2004. *Journal of Geophysical Research*
4491 *Atmospheres*, 115(D12). <https://doi.org/10.1029/2009JD012674>
- 4492 Papa, F., Frappart, F., Güntner, A., Prigent, C., Aires, F., Getirana, A. C. V., & Maurer, R. (2013). Surface
4493 freshwater storage and variability in the Amazon basin from multi-satellite observations, 1993-2007.
4494 *Journal of Geophysical Research Atmospheres*, 118(21), 11951–11965.
4495 <https://doi.org/10.1002/2013JD020500>
- 4496 Papa, F., Frappart, F., Malbeteau, Y., Shamsudduha, M., Vuruputur, V., Sekhar, M., et al. (2015).
4497 Satellite-derived surface and sub-surface water storage in the Ganges–Brahmaputra River Basin.
4498 *Journal of Hydrology: Regional Studies*, 4, 15–35.
4499 <https://doi.org/https://doi.org/10.1016/j.ejrh.2015.03.004>
- 4500 Paredes Trejo, F. J., Barbosa, H. A., Peñaloza-Murillo, M. A., Alejandra Moreno, M., & Farías, A.
4501 (2016). Intercomparison of improved satellite rainfall estimation with CHIRPS gridded product and
4502 rain gauge data over Venezuela. *Atmosfera*, 29(4), 323–342.
4503 <https://doi.org/10.20937/ATM.2016.29.04.04>
- 4504 Paris, A., Paiva, R. D. de, Silva, J. S. da, Moreira, D. M., Calmant, S., Garambois, P.-A., et al. (2016).
4505 Stage-discharge rating curves based on satellite altimetry and modeled discharge in the Amazon
4506 basin. *Water Resources Research*, 52, 3787–3814.
4507 <https://doi.org/10.1002/2014WR016618>.Received
- 4508 Paris, A., Calmant, S., Gosset, M., Fleischmann, A., Conchy, T., Bricquet, J.-P., et al. (2020). Monitoring
4509 hydrological variables from remote sensing and modelling in the Congo River basin. *Earth and*
4510 *Space Science Open Archive*, 53. <https://doi.org/10.1002/essoar.10505518.1>
- 4511 Park, E. (2020). Characterizing channel-floodplain connectivity using satellite altimetry: Mechanism,
4512 hydrogeomorphic control, and sediment budget. *Remote Sensing of Environment*, 243(February),
4513 111783. <https://doi.org/10.1016/j.rse.2020.111783>
- 4514 Park, E., & Latrubesse, E. M. (2014). Modeling suspended sediment distribution patterns of the Amazon

- 4515 River using MODIS data. *Remote Sensing of Environment*, 147, 232–242.
4516 <https://doi.org/10.1016/j.rse.2014.03.013>
- 4517 Park, E., Emadzadeh, A., Alcântara, E., Yang, X., & Ho, H. L. (2020). Inferring floodplain bathymetry
4518 using inundation frequency. *Journal of Environmental Management*, 273(July).
4519 <https://doi.org/10.1016/j.jenvman.2020.111138>
- 4520 Parrens, M., Bitar, A. Al, Frappart, F., Papa, F., Calmant, S., Crétaux, J. F., et al. (2017). Mapping
4521 dynamic water fraction under the tropical rain forests of the Amazonian basin from SMOS
4522 brightness temperatures. *Water*, 9(5), 350. <https://doi.org/10.3390/w9050350>
- 4523 Parrens, M., Bitar, A. Al, Frappart, F., Paiva, R., Wongchuig, S., Papa, F., et al. (2019). High resolution
4524 mapping of inundation area in the Amazon basin from a combination of L-band passive microwave,
4525 optical and radar datasets. *International Journal of Applied Earth Observation and Geoinformation*,
4526 81(August 2018), 58–71. <https://doi.org/10.1016/j.jag.2019.04.011>
- 4527 Pearce, F. (2020). Weather makers. *Science*, 368, 1302–1305.
4528 <https://doi.org/10.1126/science.368.6497.1302>
- 4529 Peixoto, J. M. A., Nelson, B. W., & Wittmann, F. (2009). Spatial and temporal dynamics of river channel
4530 migration and vegetation in central Amazonian white-water floodplains by remote-sensing
4531 techniques. *Remote Sensing of Environment*, 113(10), 2258–2266.
4532 <https://doi.org/10.1016/j.rse.2009.06.015>
- 4533 Pekel, J. F., Cottam, A., Gorelick, N., & Belward, A. S. (2016). High-resolution mapping of global
4534 surface water and its long-term changes. *Nature*, 540(7633), 418–422.
4535 <https://doi.org/10.1038/nature20584>
- 4536 Pellet, V., Aires, F., & Yamazaki, D. (2021). Satellite monitoring of the water cycle over the Amazon
4537 using upstream / downstream dependency. Part 2 : Mass-conserved reconstruction of total water
4538 storage change and river discharge. *Water Resources Research*.
- 4539 Peng, B., Shi, J., Ni-Meister, W., Zhao, T., & Ji, D. (2014). Evaluation of TRMM multisatellite
4540 precipitation analysis (tmpa) products and their potential hydrological application at an arid and
4541 semiarid basin in china. *IEEE Journal of Selected Topics in Applied Earth Observations and Remote
4542 Sensing*, 7(9), 3915–3930. <https://doi.org/10.1109/JSTARS.2014.2320756>
- 4543 Penman, H. L. (1948). Natural evaporation from open water, hare soil and grass. *Proceedings of the Royal
4544 Society of London. Series A, Mathematical and Physical Sciences*, 194, 120–146.
4545 <https://doi.org/10.1098/rspa.1948.0037>
- 4546 Peral, E., Tanelli, S., Statham, S., Joshi, S., Imken, T., Price, D., et al. (2019). RainCube: the first ever
4547 radar measurements from a CubeSat in space. *Journal of Applied Remote Sensing*, 13(03), 1.

- 4548 <https://doi.org/10.1117/1.jrs.13.032504>
- 4549 Pfeffer, J., Seyler, F., Bonnet, M.-P., Calmant, S., Frappart, F., Papa, F., et al. (2014). Low-water maps of
4550 the groundwater table in the central Amazon by satellite altimetry. *Geophysical Research Letters*,
4551 *41*(6), 1981–1987. <https://doi.org/10.1002/2013GL059134>
- 4552 Pham-Duc, B., Papa, F., Prigent, C., Aires, F., Biancamaria, S., & Frappart, F. (2019). Variations of
4553 Surface and Subsurface Water Storage in the Lower Mekong Basin (Vietnam and Cambodia) from
4554 Multisatellite Observations. *Water*, *11*(1). <https://doi.org/10.3390/w11010075>
- 4555 Pham-Duc, B., Sylvestre, F., Papa, F., Frappart, F., Bouchez, C., & Crétaux, J. F. (2020). The Lake Chad
4556 hydrology under current climate change. *Scientific Reports*, *10*. [https://doi.org/10.1038/s41598-020-](https://doi.org/10.1038/s41598-020-62417-w)
4557 [62417-w](https://doi.org/10.1038/s41598-020-62417-w)
- 4558 Phillips, O. L., Aragão, L. E. O. C., Lewis, S. L., Fisher, J. B., Lloyd, J., López-González, G., et al.
4559 (2009). Drought sensitivity of the amazon rainforest. *Science*, *323*(5919), 1344–1347.
4560 <https://doi.org/10.1126/science.1164033>
- 4561 Pilotto, I. L., Rodríguez, D. A., Tomasella, J., Sampaio, G., & Chou, S. C. (2015). Comparisons of the
4562 Noah-MP land surface model simulations with measurements of forest and crop sites in Amazonia.
4563 *Meteorology and Atmospheric Physics*, *127*(6), 711–723. [https://doi.org/10.1007/s00703-015-0399-](https://doi.org/10.1007/s00703-015-0399-8)
4564 [8](https://doi.org/10.1007/s00703-015-0399-8)
- 4565 Pinel, S., Bonnet, M.-P., Santos Da Silva, J., Moreira, D., Calmant, S., Satgé, F., & Seyler, F. (2015).
4566 Correction of Interferometric and Vegetation Biases in the SRTMGL1 Spaceborne DEM with
4567 Hydrological Conditioning towards Improved Hydrodynamics Modeling in the Amazon Basin.
4568 *Remote Sensing*, *7*(12), 16108–16130. <https://doi.org/10.3390/rs71215822>
- 4569 Pinel, S., Bonnet, M., Silva, J. S. Da, Sampaio, T. C., Garnier, J., Frago, C. R. J., et al. (2019). Flooding
4570 dynamics within a Amazonian floodplain: Water circulation patterns and inundation duration. *Water*
4571 *Resources Research*, 1–23.
- 4572 Pinet, S. Y. P., Artinez, J. E. A. N. I. M., Uillon, S. Y. O., Runo, B., Artiges, L., & Illar, R. A. U. L. E. S.
4573 V. (2017). Variability of apparent and inherent optical properties of sediment-laden waters in large
4574 river basins – lessons from in situ measurements and bio-optical modeling. *Optics Express*, *25*(8),
4575 283–310.
- 4576 Pison, I., Ringeval, B., Bousquet, P., Prigent, C., & Papa, F. (2013). Stable atmospheric methane in the
4577 2000s: Key-role of emissions from natural wetlands. *Atmospheric Chemistry and Physics*, *13*(23),
4578 11609–11623. <https://doi.org/10.5194/acp-13-11609-2013>
- 4579 Pokhrel, Y. N., Fan, Y., Miguez-Macho, G., Yeh, P. J. F., & Han, S. C. (2013). The role of groundwater
4580 in the Amazon water cycle: 3. Influence on terrestrial water storage computations and comparison

- 4581 with GRACE. *Journal of Geophysical Research Atmospheres*, 118(8), 3233–3244.
4582 <https://doi.org/10.1002/jgrd.50335>
- 4583 Pokhrel, Y. N., Fan, Y., & Miguez-Macho, G. (2014). Potential hydrologic changes in the Amazon by the
4584 end of the 21st century and the groundwater buffer. *Environmental Research Letters*, 9(8), 084004.
4585 <https://doi.org/10.1088/1748-9326/9/8/084004>
- 4586 Pontes, P. R. M., Cavalcante, R. B. L., Sahoo, P. K., Silva Júnior, R. O. d., da Silva, M. S., Dall’Agnol,
4587 R., & Siqueira, J. O. (2019). The role of protected and deforested areas in the hydrological processes
4588 of Itacaiúnas River Basin, eastern Amazonia. *Journal of Environmental Management*, 235, 489–
4589 499. <https://doi.org/10.1016/j.jenvman.2019.01.090>
- 4590 Potter, C., Melack, J. M., & Engle, D. (2014). Modeling methane emissions from amazon floodplain
4591 ecosystems. *Wetlands*, 34, 501–511. <https://doi.org/10.1007/s13157-014-0516-3>
- 4592 Prabhakara, C., Short, D. A., Wiscombe, W., Fraser, R. S., & Vollmer, B. E. (1986). Rainfall over Oceans
4593 Inferred from Nimbus 7 SMMR: Application to 1982–83 El Niño. *Journal of Climate and Applied*
4594 *Meteorology*, 25(10), 1464–1474.
- 4595 Priestley, C. H. B., & Taylor, R. J. (1972). On the Assessment of Surface Heat Flux and Evaporation
4596 Using Large-Scale Parameters. *Monthly Weather Review*, 100(2), 81–92.
4597 [https://doi.org/10.1175/1520-0493\(1972\)100<0081:otaosh>2.3.co;2](https://doi.org/10.1175/1520-0493(1972)100<0081:otaosh>2.3.co;2)
- 4598 Prigent, C. (2010). Precipitation retrieval from space: An overview. *Comptes Rendus - Geoscience*,
4599 342(4–5), 380–389. <https://doi.org/10.1016/j.crte.2010.01.004>
- 4600 Prigent, C., Aires, F., Rossow, W. B., & Robock, A. (2005). Sensitivity of satellite microwave and
4601 infrared observations to soil moisture at a global scale: Relationship of satellite observations to in
4602 situ soil moisture measurements. *Journal of Geophysical Research: Atmospheres*, 110(D7).
4603 <https://doi.org/https://doi.org/10.1029/2004JD005087>
- 4604 Prigent, C., Papa, F., Aires, F., Rossow, W. B., & Matthews, E. (2007). Global inundation dynamics
4605 inferred from multiple satellite observations, 1993–2000. *Journal of Geophysical Research*
4606 *Atmospheres*, 112(12). <https://doi.org/10.1029/2006JD007847>
- 4607 Prigent, C., Papa, F., Aires, F., Jimenez, C., Rossow, W. B., & Matthews, E. (2012). Changes in land
4608 surface water dynamics since the 1990s and relation to population pressure. *Geophysical Research*
4609 *Letters*, 39(8). <https://doi.org/10.1029/2012GL051276>
- 4610 Prigent, C., Lettenmaier, D. P., Aires, F., & Papa, F. (2016). Toward a High-Resolution Monitoring of
4611 Continental Surface Water Extent and Dynamics, at Global Scale: from GIEMS (Global Inundation
4612 Extent from Multi-Satellites) to SWOT (Surface Water Ocean Topography). *Surveys in Geophysics*,
4613 37(2), 339–355. <https://doi.org/10.1007/s10712-015-9339-x>

- 4614 Prigent, C., Jimenez, C., & Bousquet, P. (2020). Satellite-Derived Global Surface Water Extent and
4615 Dynamics Over the Last 25 Years (GIEMS-2). *Journal of Geophysical Research: Atmospheres*,
4616 *125*(3). <https://doi.org/10.1029/2019JD030711>
- 4617 Pujol, L., Garambois, P.-A., Finaud-Guyot, P., Monnier, J., Larnier, K., Mosé, R., et al. (2020).
4618 Estimation of Multiple Inflows and Effective Channel by Assimilation of Multi-satellite Hydraulic
4619 Signatures: The Ungauged Anabranching Negro River. *Journal of Hydrology*.
4620 <https://doi.org/10.1016/j.jhydrol.2020.125331>
- 4621 Ramillien, G., Frappart, F., Gratton, S., & Vasseur, X. (2015). Sequential estimation of surface water
4622 mass changes from daily satellite gravimetry data. *Journal of Geodesy*, *89*(3), 259–282.
4623 <https://doi.org/10.1007/s00190-014-0772-2>
- 4624 Ramillien, G., Seoane, L., Schumacher, M., Forootan, E., Frappart, F., & Darrozes, J. (2020). Recovery of
4625 rapid water mass changes (RWMC) by Kalman filtering of GRACE observations. *Remote Sensing*,
4626 *12*(8), 1299. <https://doi.org/10.3390/RS12081299>
- 4627 von Randow, C., Manzi, A. O., Kruijt, B., de Oliveira, P. J., Zanchi, F. B., Silva, R. L., et al. (2004).
4628 Comparative measurements and seasonal variations in energy and carbon exchange over forest and
4629 pasture in South West Amazonia. *Theoretical and Applied Climatology*, *78*(1–3), 5–26.
4630 <https://doi.org/10.1007/s00704-004-0041-z>
- 4631 von Randow, R. de C. S., Tomasella, J., von Randow, C., de Araújo, A. C., Manzi, A. O., Hutjes, R., &
4632 Kruijt, B. (2020). Evapotranspiration and gross primary productivity of secondary vegetation in
4633 Amazonia inferred by eddy covariance. *Agricultural and Forest Meteorology*, *294*.
4634 <https://doi.org/10.1016/j.agrformet.2020.108141>
- 4635 Raney, R. K. (1998). The delay/Doppler radar altimeter. *IEEE Transactions on Geoscience and Remote*
4636 *Sensing*, *36*(5), 1578–1588. <https://doi.org/10.1109/36.718861>
- 4637 Raymond, P. A., Hartmann, J., Lauerwald, R., Sobek, S., McDonald, C., Hoover, M., et al. (2013). Global
4638 carbon dioxide emissions from inland waters. *Nature*, *503*, 355–359.
4639 <https://doi.org/10.1038/nature12760>
- 4640 Reichle, R. H., Liu, Q., Koster, R. D., Draper, C. S., Mahanama, S. P. P., & Partyka, G. S. (2017). Land
4641 Surface Precipitation in MERRA-2. *Journal of Climate*, *30*(5), 1643–1664.
4642 <https://doi.org/10.1175/JCLI-D-16-0570.1>
- 4643 Reis, G. G. dos, Paiva, R. C. D. de, Brêda, J. P. L. F., & Medeiros, M. S. (2020). SARDIM - UMA
4644 PLATAFORMA PARA ACOMPANHAMENTO HIDROLÓGICO EM TEMPO REAL DOS RIOS
4645 DA AMÉRICA DO SUL. In *II END - Encontro Nacional de Desastres da*. Porto Alegre:
4646 Associação Brasileira de Recursos Hídricos. Retrieved from <http://anais.abrh.org.br/works/7285>

- 4647 Reis, V., Hermoso, V., Hamilton, S. K., Linke, S., & Bunn, S. E. (2019). Characterizing seasonal
4648 dynamics of Amazonian wetlands for conservation and decision making, (December 2018), 1–10.
4649 <https://doi.org/10.1002/aqc.3051>
- 4650 Resende, A. F. de, Schöngart, J., Streher, A. S., Ferreira-Ferreira, J., Piedade, M. T. F., & Silva, T. S. F.
4651 (2019). Massive tree mortality from flood pulse disturbances in Amazonian floodplain forests: The
4652 collateral effects of hydropower production. *Science of the Total Environment*, 659, 587–598.
4653 <https://doi.org/10.1016/j.scitotenv.2018.12.208>
- 4654 Restrepo-Coupe, N., da Rocha, H. R., Hutya, L. R., da Araujo, A. C., Borma, L. S., Christoffersen, B., et
4655 al. (2013). What drives the seasonality of photosynthesis across the Amazon basin? A cross-site
4656 analysis of eddy flux tower measurements from the Brasil flux network. *Agricultural and Forest*
4657 *Meteorology*, 182–183, 128–144. <https://doi.org/10.1016/j.agrformet.2013.04.031>
- 4658 Richey, J. E., Mertes, L. K., Dunne, T., Victoria, R. L., Forsberg, B. R., Tancredi, A. C. N. S., & Oliveira,
4659 E. de. (1989). Sources and routing of the Amazon River flood wave, 3(3), 191–204.
- 4660 Richey, J. E., Melack, J. M., Aufdenkampe, A. K., Ballester, V. M., & Hess, L. L. (2002). Outgassing
4661 from Amazonian rivers and wetlands as a large tropical source of atmospheric CO₂. *Nature*,
4662 416(6881), 617–620. <https://doi.org/10.1038/416617a>
- 4663 Rocha, H. R., Manzi, A. O., Cabral, O. M., Miller, S. D., Goulden, M. L., Saleska, S. R., et al. (2009).
4664 Patterns of water and heat flux across a biome gradient from tropical forest to savanna in Brazil.
4665 *Journal of Geophysical Research: Biogeosciences*, 114(1), 1–8.
4666 <https://doi.org/10.1029/2007JG000640>
- 4667 Rodell, M., Houser, P. R., Jambor, U., Gottschalck, J., Mitchell, K., Meng, C. J., et al. (2004). The Global
4668 Land Data Assimilation System. *Bulletin of the American Meteorological Society*, 85(3), 381–394.
4669 <https://doi.org/10.1175/BAMS-85-3-381>
- 4670 Rodell, M., McWilliams, E. B., Famiglietti, J. S., Beaudoing, H. K., & Nigro, J. (2011). Estimating
4671 evapotranspiration using an observation based terrestrial water budget. *Hydrological Processes*,
4672 25(26), 4082–4092. <https://doi.org/10.1002/hyp.8369>
- 4673 Rodriguez-Alvarez, N., Podest, E., Jensen, K., & McDonald, K. C. (2019). Classifying inundation in a
4674 tropical wetlands complex with GNSS-R. *Remote Sensing*, 11, 1053.
4675 <https://doi.org/10.3390/rs11091053>
- 4676 Rodríguez, E., Morris, C. S., & Belz, J. E. (2006). A Global Assessment of the SRTM Performance.
4677 *Photogrammetric Engineering & Remote Sensing*, 72(3), 249–260.
4678 <https://doi.org/10.14358/PERS.72.3.249>
- 4679 Roerink, G. J., Su, Z., & Menenti, M. (2000). *S-SEBI: A Simple Remote Sensing Algorithm to Estimate*

- 4680 *the Surface Energy Balance. P&s. Chem .Earth (B)* (Vol. 25).
- 4681 Ronchail, J., Cochonneau, G., Molinier, M., Guyot, J. L., De Miranda Chaves, A. G., Guimarães, V., &
 4682 De Oliveira, E. (2002). Interannual rainfall variability in the Amazon basin and sea-surface
 4683 temperatures in the equatorial Pacific and the tropical Atlantic Oceans. *International Journal of*
 4684 *Climatology*, 22(13), 1663–1686. <https://doi.org/10.1002/joc.815>
- 4685 Röpke, C. P., Amadio, S., Zuanon, J., Ferreira, E. J. G., De Deus, C. P., Pires, T. H. S., & Winemiller, K.
 4686 O. (2017). Simultaneous abrupt shifts in hydrology and fish assemblage structure in a floodplain
 4687 lake in the central Amazon. *Scientific Reports*, 7, 40170. <https://doi.org/10.1038/srep40170>
- 4688 Rosenqvist, Å., & Birkett, C. M. (2002). Evaluation of JERS-1 SAR mosaics for hydrological
 4689 applications in the Congo river basin. *International Journal of Remote Sensing*, 23(7), 1283–1302.
 4690 <https://doi.org/10.1080/01431160110092902>
- 4691 Rosenqvist, J., Rosenqvist, A., Jensen, K., & McDonald, K. (2020). Mapping of maximum and minimum
 4692 inundation extents in the amazon basin 2014-2017 with ALOS-2 PALSAR-2 scan SAR time-series
 4693 data. *Remote Sensing*, 12(8). <https://doi.org/10.3390/RS12081326>
- 4694 Rossetti, D. F., Gribel, R., Rennó, C. D., Cohen, M. C. L., Moulatlet, G. M., Cordeiro, C. L. de O., &
 4695 Rodrigues, E. do S. F. (2017). Late Holocene tectonic influence on hydrology and vegetation
 4696 patterns in a northern Amazonian megafan. *Catena*, 158(June), 121–130.
 4697 <https://doi.org/10.1016/j.catena.2017.06.022>
- 4698 Rozo, M. G., Nogueira, A. C. R., & Truckenbrodt, W. (2012). The anastomosing pattern and the
 4699 extensively distributed scroll bars in the middle Amazon River. *Earth Surface Processes and*
 4700 *Landforms*, 37(14), 1471–1488. <https://doi.org/10.1002/esp.3249>
- 4701 Rudorff, C. M. (2006). *Estudo da composição das águas da planície amazônica por meio de dados de*
 4702 *reflectância do sensor hyperion/EO-1 e de espectrômetro de campo visando a compreensão da*
 4703 *variação temporal dos seus constituintes opticamente ativos*. Instituto Nacional de Pesquisas
 4704 Espaciais (INPE), São José dos Campos.
- 4705 Rudorff, C. M., Novo, E. M. L. M., & Galvão, L. S. (2006). Spectral Mixture Analysis of Inland Tropical
 4706 Amazon Floodplain Waters Using EO-1 Hyperion. In *IEEE International Symposium on Geoscience*
 4707 *and Remote Sensing* (pp. 128–133). Denver. <https://doi.org/10.1109/IGARSS.2006.38>
- 4708 Rudorff, C. M., Novo, E. M. L. M., Galvão, L. S., & Pereira Filho, W. (2007). Análise derivativa de
 4709 dados hiperespectrais medidos em nível de campo e orbital para caracterizar a composição de águas
 4710 opticamente complexas na Amazônia. *Acta Amazonica*, 37(2), 269–280.
 4711 <https://doi.org/10.1590/S0044-59672007000200014>
- 4712 Rudorff, C. M., Melack, J. M., & Bates, P. D. (2014a). Flooding dynamics on the lower Amazon

- 4713 floodplain: 1. Hydraulic controls on water elevation, inundation extent, and river-floodplain
 4714 discharge. *Water Resources Research*, 50(1), 619–634. <https://doi.org/10.1002/2013WR014091>
- 4715 Rudorff, C. M., Melack, J. M., & Bates, P. D. (2014b). Flooding dynamics on the lower Amazon
 4716 floodplain: 2. Seasonal and interannual hydrological variability. *Water Resources Research*, 50(1),
 4717 635–649. <https://doi.org/10.1002/2013WR014714>
- 4718 Rudorff, C. M., Dunne, T., & Melack, J. M. (2017). Recent increase of river-floodplain suspended
 4719 sediment exchange in a reach of the lower Amazon River. *Earth Surface Processes and Landforms*.
 4720 <https://doi.org/10.1002/esp.4247>
- 4721 Ruhoff, A. L., Paz, A. R., Aragao, L. E. O. C., Mu, Q., Malhi, Y., Collischonn, W., et al. (2013).
 4722 Evaluation de l’algorithme MODIS d’estimation de l’évapotranspiration globale utilisant des
 4723 mesures de covariance de la turbulence et la modélisation hydrologique dans le bassin du Rio
 4724 Grande. *Hydrological Sciences Journal*, 58(8), 1658–1676.
 4725 <https://doi.org/10.1080/02626667.2013.837578>
- 4726 Runde, A., Hallwass, G., & Silvano, R. A. M. (2020). Fishers’ Knowledge Indicates Extensive
 4727 Socioecological Impacts Downstream of Proposed Dams in a Tropical River. *One Earth*, 2(3), 255–
 4728 268. <https://doi.org/https://doi.org/10.1016/j.oneear.2020.02.012>
- 4729 Saad, S. I., Da Rocha, H. R., Silva Dias, M. A. F., & Rosolem, R. (2010). Can the deforestation breeze
 4730 change the rainfall in Amazonia? A case study for the BR-163 highway region. *Earth Interactions*,
 4731 14(18). <https://doi.org/10.1175/2010EI351.1>
- 4732 Saavedra, M., Junquas, C., Espinoza, J. C., & Silva, Y. (2020). Impacts of topography and land use
 4733 changes on the air surface temperature and precipitation over the central Peruvian Andes.
 4734 *Atmospheric Research*, 234, 104711. <https://doi.org/10.1016/j.atmosres.2019.104711>
- 4735 Sahagian, D., & Melack, J. (1998). *Global Wetland Distribution and Functional Characterization: Trace*
 4736 *Gases and the Hydrologic Cycle*. Royal Swedish Academy of Sciences. Stockholm, Sweden.
- 4737 Sahoo, A. K., Pan, M., Troy, T. J., Vinukollu, R. K., Sheffield, J., & Wood, E. F. (2011). Reconciling the
 4738 global terrestrial water budget using satellite remote sensing. *Remote Sensing of Environment*,
 4739 115(8), 1850–1865. <https://doi.org/10.1016/j.rse.2011.03.009>
- 4740 Salameh, E., Frappart, F., Almar, R., Baptista, P., Heygster, G., Lubac, B., et al. (2019). Monitoring
 4741 Beach Topography and Nearshore Bathymetry Using Spaceborne Remote Sensing: A Review.
 4742 *Remote Sensing*, 11(19). <https://doi.org/10.3390/rs11192212>
- 4743 Salati, E., & Nobre, C. A. (1991). Possible climatic impacts of tropical deforestation. *Climatic Change*,
 4744 19(1–2), 177–196. <https://doi.org/10.1007/BF00142225>
- 4745 Salati, E., & Vose, P. B. (1984). Amazon Basin: A system in equilibrium. *Science*, 225(4658), 129–138.

- 4746 <https://doi.org/10.1126/science.225.4658.129>
- 4747 Salati, E., Dall'Olio, A., Matsui, E., & Gat, J. R. (1979). Recycling of water in the Amazon Basin: An
4748 isotopic study. *Water Resources Research*, *15*(5).
- 4749 Saleska, S. R., da Rocha, H. R., Huete, A. R., Nobre, A. D., Artaxo, P. E., & Shimabukuro, Y. E. (2013).
4750 *LBA-ECO CD-32 Flux Tower Network Data Compilation, Brazilian Amazon: 1999-2006*. Oak
4751 Ridge, Tennessee, USA. <https://doi.org/10.3334/ORNLDAAC/1174>
- 4752 dos Santos, E. S., Lopes, P. P. P., Pereira, H. H. da S., Nascimento, O. de O., Rennie, C. D., Sternberg, L.
4753 da S. L. O., & Cunha, A. C. da. (2018). The impact of channel capture on estuarine hydro-
4754 morphodynamics and water quality in the Amazon delta. *Science of the Total Environment*, *624*,
4755 887–899. <https://doi.org/10.1016/j.scitotenv.2017.12.211>
- 4756 Santos, M. J., Medvigy, D., Silva Dias, M. A. F., Freitas, E. D., & Kim, H. (2019). Seasonal Flooding
4757 Causes Intensification of the River Breeze in the Central Amazon. *Journal of Geophysical*
4758 *Research: Atmospheres*, *124*(10), 5178–5197. <https://doi.org/10.1029/2018JD029439>
- 4759 Satgé, F., Bonnet, M. P., Gosset, M., Molina, J., Hernan Yuque Lima, W., Pillco Zolá, R., et al. (2016).
4760 Assessment of satellite rainfall products over the Andean plateau. *Atmospheric Research*, *167*, 1–14.
4761 <https://doi.org/10.1016/j.atmosres.2015.07.012>
- 4762 Satgé, F., Xavier, A., Zolá, R. P., Hussain, Y., Timouk, F., Garnier, J., & Bonnet, M. P. (2017).
4763 Comparative assessments of the latest GPM mission's spatially enhanced satellite rainfall products
4764 over the main bolivian watersheds. *Remote Sensing*, *9*(4), 1–16. <https://doi.org/10.3390/rs9040369>
- 4765 Satyamurty, P., da Costa, C. P. W., Manzi, A. O., & Candido, L. A. (2013). A quick look at the 2012
4766 record flood in the Amazon Basin. *Geophysical Research Letters*, *40*(7), 1396–1401.
4767 <https://doi.org/10.1002/grl.50245>
- 4768 Satyamurty, P., da Costa, C. P. W., & Manzi, A. O. (2013). Moisture source for the Amazon Basin: A
4769 study of contrasting years. *Theoretical and Applied Climatology*, *111*(1–2), 195–209.
4770 <https://doi.org/10.1007/s00704-012-0637-7>
- 4771 van het Schip, T. I., Overeem, A., Leijnse, H., Uijlenhoet, R., Meirink, J. F., & van Delden, A. J. (2017).
4772 Rainfall measurement using cell phone links: classification of wet and dry periods using
4773 geostationary satellites. *Hydrological Sciences Journal*, *62*(9), 1343–1353.
4774 <https://doi.org/10.1080/02626667.2017.1329588>
- 4775 Schmitt, R. J. P., Bizzi, S., Castelletti, A., Opperman, J. J., & Kondolf, G. M. (2019). Planning dam
4776 portfolios for low sediment trapping shows limits for sustainable hydropower in the Mekong.
4777 *Science Advances*, *5*(10). <https://doi.org/10.1126/sciadv.aaw2175>
- 4778 Schöngart, J., Wittmann, F., Resende, A. F. de, Assahira, C., Lobo, G. de S., Neves, J. R. D., et al. (2021).

- 4779 The shadow of the Balbina dam : A synthesis of over 35 years of downstream impacts on floodplain
4780 forests in Central Amazonia. *Aquatic Conservation: Marine and Freshwater Ecosystems*, (Special
4781 Issue), 1–19. <https://doi.org/10.1002/aqc.3526>
- 4782 Schroeder, R., McDonald, K. C., Chapman, B. D., Jensen, K., Podest, E., Tessler, Z. D., et al. (2015).
4783 Development and evaluation of a multi-year fractional surface water data set derived from
4784 active/passive microwave remote sensing data. *Remote Sensing*, 7(12), 16688–16732.
4785 <https://doi.org/10.3390/rs71215843>
- 4786 Schumann, G., Bates, P. D., Horritt, M. S., Matgen, P., & Pappenberger, F. (2009). Progress in
4787 Integration of Remote Sensing-Derived Flood Extent and Stage Data and Hydraulic Models.
4788 *Reviews of Geophysics*, 47(2008), 1–20. <https://doi.org/10.1029/2008rg000274>
- 4789 Schwatke, C., Dettmering, D., Bosch, W., & Seitz, F. (2015). DAHITI - An innovative approach for
4790 estimating water level time series over inland waters using multi-mission satellite altimetry.
4791 *Hydrology and Earth System Sciences*, 19(10), 4345–4364. [https://doi.org/10.5194/hess-19-4345-](https://doi.org/10.5194/hess-19-4345-2015)
4792 2015
- 4793 Sena, J. A., de Deus, L. A. B., Freitas, M. A. V., & Costa, L. (2012). Extreme Events of Droughts and
4794 Floods in Amazonia: 2005 and 2009. *Water Resources Management*, 26(6), 1665–1676.
4795 <https://doi.org/10.1007/s11269-012-9978-3>
- 4796 Seyler, F., Calmant, S., Silva, J. S. Da, Moreira, D. M., Mercier, F., & Shum, C. K. (2013). From
4797 TOPEX/Poseidon to Jason-2/OSTM in the amazon basin. *Advances in Space Research*, 51(8),
4798 1542–1550. <https://doi.org/10.1016/j.asr.2012.11.002>
- 4799 Sheffield, J., Wood, E. F., Pan, M., Beck, H., Coccia, G., Serrat-Capdevila, A., & Verbist, K. (2018,
4800 December 1). Satellite Remote Sensing for Water Resources Management: Potential for Supporting
4801 Sustainable Development in Data-Poor Regions. *Water Resources Research*. Blackwell Publishing
4802 Ltd. <https://doi.org/10.1029/2017WR022437>
- 4803 Shi, J., Dong, X., Zhao, T., Du, Y., Liu, H., Wang, Z., et al. (2016). The water cycle observation mission
4804 (WCOM): Overview. In *International Geoscience and Remote Sensing Symposium (IGARSS)* (Vol.
4805 2016-November, pp. 3430–3433). Institute of Electrical and Electronics Engineers Inc.
4806 <https://doi.org/10.1109/IGARSS.2016.7729886>
- 4807 Shuttleworth, W. J. (2012). *Terrestrial Hydrometeorology*. *Terrestrial Hydrometeorology*. John Wiley &
4808 Sons. <https://doi.org/10.1002/9781119951933>
- 4809 Silva Dias, M. A. F., Silva Dias, P. L., Longo, M., Fitzjarrald, D. R., & Denning, A. S. (2004). River
4810 breeze circulation in eastern Amazonia: Observations and modelling results. *Theoretical and*
4811 *Applied Climatology*, 78(1–3), 111–121. <https://doi.org/10.1007/s00704-004-0047-6>

- 4812 da Silva, E. F. F., Novo, E. M. L. de M., Lobo, F. de L., Barbosa, C. C. F., Noernberg, M. A., Rotta, L. H.
4813 da S., et al. (2020). Optical water types found in Brazilian waters. *Limnology*.
4814 <https://doi.org/10.1007/s10201-020-00633-z>
- 4815 Silva, H. J. F. da, Gonçalves, W. A., & Bezerra, B. G. (2019). Comparative analyzes and use of
4816 evapotranspiration obtained through remote sensing to identify deforested areas in the Amazon.
4817 *International Journal of Applied Earth Observation and Geoinformation*, 78, 163–174.
4818 <https://doi.org/10.1016/j.jag.2019.01.015>
- 4819 Silva, J. S. Da, Calmant, S., Seyler, F., Rotunno Filho, O. C., Cochonneau, G., & Mansur, W. J. (2010).
4820 Water levels in the Amazon basin derived from the ERS 2 and ENVISAT radar altimetry missions.
4821 *Remote Sensing of Environment*, 114(10), 2160–2181. <https://doi.org/10.1016/j.rse.2010.04.020>
- 4822 Silva, J. S. Da, Seyler, F., Calmant, S., Filho, O. C. R., Roux, E., Araújo, A. A. M., & Guyot, J. L. (2012).
4823 Water level dynamics of Amazon wetlands at the watershed scale by satellite altimetry.
4824 *International Journal of Remote Sensing*, 33(11), 3323–3353.
4825 <https://doi.org/10.1080/01431161.2010.531914>
- 4826 Silva, J. S. Da, Calmant, S., Seyler, F., Moreira, D. M., Oliveira, D., & Monteiro, A. (2014). Radar
4827 altimetry aids managing gauge networks. *Water Resources Management*, 28, 587–603.
4828 <https://doi.org/10.1007/s11269-013-0484-z>
- 4829 Silva Junior, C. H. L., Almeida, C. T., Santos, J. R. N., Anderson, L. O., Aragão, L. E. O. C., & Silva, F.
4830 B. (2018). Spatiotemporal rainfall trends in the Brazilian legal Amazon between the years 1998 and
4831 2015. *Water*, 10(9), 1220. <https://doi.org/10.3390/w10091220>
- 4832 Silva, M. P. da, Sander de Carvalho, L., Novo, E., Jorge, D., & Barbosa, C. (2019). Use of absorption
4833 optical indices to assess seasonal variability of dissolved organic matter in amazon floodplain lakes.
4834 *Biogeosciences Discussions*, 1–20. <https://doi.org/10.5194/bg-2019-324>
- 4835 Silva, M. V., Paris, A., Calmant, S., Cândido, L. A., & Silva, J. S. (2019). Associação do regime
4836 hidrológico do rio xingu com oceanos adjacentes em eventos extremos utilizando dados
4837 altimétricos. *Brazilian Journal of Development*, 5(11). <https://doi.org/10.34117/bjdv5n11-339>
- 4838 Silva, T. S. F., Costa, M. P. F., & Melack, J. M. (2010). Spatial and temporal variability of macrophyte
4839 cover and productivity in the eastern Amazon floodplain: A remote sensing approach. *Remote*
4840 *Sensing of Environment*, 114(9), 1998–2010. <https://doi.org/10.1016/j.rse.2010.04.007>
- 4841 Silva, T. S. F., Melack, J. M., & Novo, E. M. L. M. L. M. (2013). Responses of aquatic macrophyte cover
4842 and productivity to flooding variability on the Amazon floodplain. *Global Change Biology*, 19(11),
4843 3379–3389. <https://doi.org/10.1111/gcb.12308>
- 4844 Sioli, H. (1956). Über natur und mensch im brasilianischen Amazonasgebiet. *Erdkunde*, pp. 89–109.

- 4845 <https://doi.org/http://www.jstor.org/stable/23218158>
- 4846 Sippe, S. J., Hamilton, S. K., Melack, J. M., & Novo, E. M. M. (1998). Passive microwave observations
4847 of inundation area and the area/stage relation in the Amazon River floodplain. *International Journal*
4848 *of Remote Sensing*, 19(16), 3055–3074. <https://doi.org/10.1080/014311698214181>
- 4849 Sippel, S. J., Hamilton, S. K., & Melack, J. (1992). Inundation area and morphometry of lakes on the
4850 Amazon River floodplain, Brazil. *Archiv Für Hydrobiologie*, 123, 385–400.
- 4851 Sippel, S. J., Hamilton, S. K., Melack, J. M., & Choudhury, B. J. (1994). Determination of inundation
4852 area in the Amazon River floodplain using the SMMR 37 GHz polarization difference. *Remote*
4853 *Sensing of Environment*, 48(1), 70–76. [https://doi.org/10.1016/0034-4257\(94\)90115-5](https://doi.org/10.1016/0034-4257(94)90115-5)
- 4854 Siqueira, V. A., Paiva, R. C. D., Fleischmann, A. S., Fan, F. M., Ruhoff, A. L., Pontes, P. R. M., et al.
4855 (2018). Toward continental hydrologic-hydrodynamic modeling in South America. *Hydrology and*
4856 *Earth System Sciences*, 22(9), 4815–4842. <https://doi.org/10.5194/hess-22-4815-2018>
- 4857 Sörensson, A. A., & Ruscica, R. C. (2018). Intercomparison and Uncertainty Assessment of Nine
4858 Evapotranspiration Estimates Over South America. *Water Resources Research*, 54(4), 2891–2908.
4859 <https://doi.org/10.1002/2017WR021682>
- 4860 Sorooshian, S., Hsu, K. L., Gao, X., Gupta, H. V., Imam, B., & Braithwaite, D. (2000). Evaluation of
4861 PERSIANN system satellite-based estimates of tropical rainfall. *Bulletin of the American*
4862 *Meteorological Society*, 81(9), 2035–2046. [https://doi.org/10.1175/1520-](https://doi.org/10.1175/1520-0477(2000)081<2035:EOPSSE>2.3.CO;2)
4863 [0477\(2000\)081<2035:EOPSSE>2.3.CO;2](https://doi.org/10.1175/1520-0477(2000)081<2035:EOPSSE>2.3.CO;2)
- 4864 Sorooshian, S., Gao, X., Hsu, K., Maddox, R. A., Hong, Y., Gupta, H. V., & Imam, B. (2002). Diurnal
4865 variability of tropical rainfall retrieved from combined GOES and TRMM satellite information.
4866 *Journal of Climate*, 15(9), 983–1001. [https://doi.org/10.1175/1520-](https://doi.org/10.1175/1520-0442(2002)015<0983:DVOTRR>2.0.CO;2)
4867 [0442\(2002\)015<0983:DVOTRR>2.0.CO;2](https://doi.org/10.1175/1520-0442(2002)015<0983:DVOTRR>2.0.CO;2)
- 4868 Sorribas, M. V., Paiva, R. C. D., Melack, J. M., Bravo, J. M., Jones, C., Carvalho, L., et al. (2016).
4869 Projections of climate change effects on discharge and inundation in the Amazon basin. *Climatic*
4870 *Change*, 136(3–4), 555–570. <https://doi.org/10.1007/s10584-016-1640-2>
- 4871 Sorribas, M. V., Paiva, R. C. D., Fleischmann, A. S., & Collischonn, W. (2020). *Hydrological Tracking*
4872 *Model for Amazon Surface Waters*. *Water Resources Research* (Vol. 56).
4873 <https://doi.org/10.1029/2019wr024721>
- 4874 Souza, C. M., Kirchhoff, F. T., Oliveira, B. C., Ribeiro, J. G., & Sales, M. H. (2019). Long-term annual
4875 surface water change in the Brazilian Amazon Biome: Potential links with deforestation,
4876 infrastructure development and climate change. *Water (Switzerland)*, 11, 566.
4877 <https://doi.org/10.3390/w11030566>

- 4878 De Souza, E. B., & Ambrizzi, T. (2006). Modulation of the intraseasonal rainfall over tropical Brazil by
4879 the Madden–Julian oscillation. *International Journal of Climatology*, 26(13), 1759–1776.
4880 <https://doi.org/10.1002/joc.1331>
- 4881 Spera, S. A., Cohn, A. S., Vanwey, L. K., Mustard, J. F., Rudorff, B. F., Risso, J., & Adami, M. (2014).
4882 Recent cropping frequency, expansion, and abandonment in Mato Grosso, Brazil had selective land
4883 characteristics. *Environmental Research Letters*, 9(6). [https://doi.org/10.1088/1748-](https://doi.org/10.1088/1748-9326/9/6/064010)
4884 [9326/9/6/064010](https://doi.org/10.1088/1748-9326/9/6/064010)
- 4885 Staal, A., Tuinenburg, O. A., Bosmans, J. H. C., Holmgren, M., Van Nes, E. H., Scheffer, M., et al.
4886 (2018). Forest-rainfall cascades buffer against drought across the Amazon. *Nature Climate Change*,
4887 8, 539–543. <https://doi.org/10.1038/s41558-018-0177-y>
- 4888 Staal, A., Flores, B. M., Aguiar, A. P. D., Bosmans, J. H. C., Fetzer, I., & Tuinenburg, O. A. (2020).
4889 Feedback between drought and deforestation in the Amazon. *Environmental Research Letters*,
4890 15(4). <https://doi.org/10.1088/1748-9326/ab738e>
- 4891 Stammer, D., & Cazenave, A. (2017). *Satellite altimetry over oceans and land surfaces*. (D. Stammer &
4892 A. Cazenave, Eds.), *Satellite Altimetry Over Oceans and Land Surfaces*. CRC Press.
4893 <https://doi.org/10.1201/9781315151779>
- 4894 Stickler, C. M., Coe, M. T., Costa, M. H., Nepstad, D. C., McGrath, D. G., Dias, L. C. P., et al. (2013).
4895 Dependence of hydropower energy generation on forests in the Amazon Basin at local and regional
4896 scales. *Proceedings of the National Academy of Sciences*, 110(23), 9601–9606.
4897 <https://doi.org/10.1073/pnas.1215331110>
- 4898 Su, Z., Schumge, T., Kustas, W. P., & Massman, W. J. (2001). An evaluation of two models for
4899 estimation of the roughness height for heat transfer between the land surface and the atmosphere.
4900 *Journal of Applied Meteorology*, 40(11), 1933–1951. [https://doi.org/10.1175/1520-](https://doi.org/10.1175/1520-0450(2001)040<1933:AEOTMF>2.0.CO;2)
4901 [0450\(2001\)040<1933:AEOTMF>2.0.CO;2](https://doi.org/10.1175/1520-0450(2001)040<1933:AEOTMF>2.0.CO;2)
- 4902 Sun, Q., Miao, C., Duan, Q., Ashouri, H., Sorooshian, S., & Hsu, K. (2018). A Review of Global
4903 Precipitation Data Sets: Data Sources, Estimation, and Intercomparisons. *Reviews of Geophysics*,
4904 56(1), 79–107. <https://doi.org/10.1002/2017RG000574>
- 4905 Sutanudjaja, E. H., van Beek, R., Wanders, N., Wada, Y., Bosmans, J. H. C., Drost, N., et al. (2018).
4906 PCR-GLOBWB 2: a 5arcmin global hydrological and water resources model. *Geoscientific Model*
4907 *Development*, 11(6), 2429–2453. <https://doi.org/10.5194/gmd-11-2429-2018>
- 4908 Talsma, C. J., Good, S. P., Jimenez, C., Martens, B., Fisher, J. B., Miralles, D. G., et al. (2018).
4909 Partitioning of evapotranspiration in remote sensing-based models. *Agricultural and Forest*
4910 *Meteorology*, 260–261, 131–143. <https://doi.org/10.1016/j.agrformet.2018.05.010>

- 4911 Tan, J., Huffman, G. J., Bolvin, D. T., & Nelkin, E. J. (2019). IMERG V06: Changes to the morphing
4912 algorithm. *Journal of Atmospheric and Oceanic Technology*, *36*(12), 2471–2482.
4913 <https://doi.org/10.1175/JTECH-D-19-0114.1>
- 4914 Tang, R., Li, Z. L., Jia, Y., Li, C., Chen, K. S., Sun, X., & Lou, J. (2013). Evaluating one- and two-source
4915 energy balance models in estimating surface evapotranspiration from Landsat-derived surface
4916 temperature and field measurements. *International Journal of Remote Sensing*, *34*(9–10), 3299–
4917 3313. <https://doi.org/10.1080/01431161.2012.716529>
- 4918 Tapiador, F. J., Kidd, C., Levizzani, V., & Marzano, F. S. (2004). A neural networks-based fusion
4919 technique to estimate half-hourly rainfall estimates at 0.1° resolution from satellite passive
4920 microwave and infrared data. *Journal of Applied Meteorology*, *43*(4), 576–594.
4921 [https://doi.org/10.1175/1520-0450\(2004\)043<0576:ANNFTT>2.0.CO;2](https://doi.org/10.1175/1520-0450(2004)043<0576:ANNFTT>2.0.CO;2)
- 4922 Tapiador, F. J., Navarro, A., Levizzani, V., García-Ortega, E., Huffman, G. J., Kidd, C., et al. (2017).
4923 Global precipitation measurements for validating climate models. *Atmospheric Research*, *197*, 1–20.
4924 <https://doi.org/10.1016/j.atmosres.2017.06.021>
- 4925 Tapley, B. D., Bettadpur, S., Ries, J. C., Thompson, P. F., & Watkins, M. M. (2004). GRACE
4926 measurements of mass variability in the Earth system. *Science*, *305*(5683), 503–505.
4927 <https://doi.org/10.1126/science.1099192>
- 4928 Tapley, B. D., Watkins, M. M., Flechtner, F., Reigber, C., Bettadpur, S., Rodell, M., et al. (2019, May).
4929 Contributions of GRACE to understanding climate change. *Nature Climate Change*. Nature
4930 Publishing Group. <https://doi.org/10.1038/s41558-019-0456-2>
- 4931 Tarpanelli, A., Barbetta, S., Brocca, L., & Moramarco, T. (2013). River Discharge Estimation by Using
4932 Altimetry Data and Simplified Flood Routing Modeling, 4145–4162.
4933 <https://doi.org/10.3390/rs5094145>
- 4934 Taylor, C. M., Prigent, C., & Dadson, S. J. (2018). Mesoscale rainfall patterns observed around wetlands
4935 in sub-Saharan Africa. *Quarterly Journal of the Royal Meteorological Society*, *144*(716), 2118–
4936 2132. <https://doi.org/10.1002/qj.3311>
- 4937 Thiemig, V., Rojas, R., Zambrano-Bigiarini, M., & De Roo, A. (2013). Hydrological evaluation of
4938 satellite-based rainfall estimates over the Volta and Baro-Akobo Basin. *Journal of Hydrology*, *499*,
4939 324–338. <https://doi.org/10.1016/j.jhydrol.2013.07.012>
- 4940 Thom, G., Xue, A. T., Sawakuchi, A. O., Ribas, C. C., Hickerson, M. J., Aleixo, A., & Miyaki, C. (2020).
4941 Quaternary climate changes as speciation drivers in the Amazon floodplains. *Science Advances*,
4942 *6*(11). <https://doi.org/10.1126/sciadv.aax4718>
- 4943 Thomaz, S. M., Bini, L. M., & Bozelli, R. L. (2007). Floods increase similarity among aquatic habitats in

- 4944 river-floodplain systems. *Hydrobiologia*, 579(1), 1–13. <https://doi.org/10.1007/s10750-006-0285-y>
- 4945 Topp, S. N., Pavelsky, T. M., Jensen, D., Simard, M., & Ross, M. R. V. (2020). Research trends in the use
4946 of remote sensing for inland water quality science: Moving towards multidisciplinary applications.
4947 *Water (Switzerland)*, 12(1), 1–34. <https://doi.org/10.3390/w12010169>
- 4948 Toté, C., Patricio, D., Boogaard, H., van der Wijngaart, R., Tarnavsky, E., & Funk, C. (2015). Evaluation
4949 of satellite rainfall estimates for drought and flood monitoring in Mozambique. *Remote Sensing*,
4950 7(2), 1758–1776. <https://doi.org/10.3390/rs70201758>
- 4951 Tourian, M. J., Reager, J. T., & Sneeuw, N. (2018). The Total Drainable Water Storage of the Amazon
4952 River Basin: A First Estimate Using GRACE. *Water Resources Research*, 54(5), 1–27.
4953 <https://doi.org/10.1029/2017WR021674>
- 4954 Towner, J., Cloke, H. L., Zsoter, E., Flamig, Z., Hoch, J. M., Bazo, J., et al. (2019). Assessing the
4955 performance of global hydrological models for capturing peak river flows in the Amazon basin.
4956 *Hydrology and Earth System Sciences*. <https://doi.org/10.5194/hess-23-3057-2019>
- 4957 Trenberth, K. E. (2011). Changes in precipitation with climate change. *Climate Research*, 47(1–2), 123–
4958 138. <https://doi.org/10.3354/cr00953>
- 4959 Trigg, M. A., Wilson, M. D., Bates, P. D., Horritt, M. S., Alsdorf, D. E., Forsberg, B. R., & Vega, M. C.
4960 (2009). Amazon flood wave hydraulics. *Journal of Hydrology*, 374(1–2), 92–105.
4961 <https://doi.org/10.1016/j.jhydrol.2009.06.004>
- 4962 Trigg, M. A., Bates, P. D., Wilson, M. D., Schumann, G., & Baugh, C. (2012). Floodplain channel
4963 morphology and networks of the middle Amazon River. *Water Resources Research*, 48(10), 1–17.
4964 <https://doi.org/10.1029/2012WR011888>
- 4965 Turk, F. J., Rohaly, G. D., Jeff, H., Smith, E. A., Marzano, F. S., Mugnai, A., & Levizzani, V. (2000).
4966 Meteorological applications of precipitation estimation from combined SSM/I, TRMM and infrared
4967 geostationary. *Microwave Radiometry and Remote Sensing of the Earth's Surface and Atmosphere*,
4968 (January), 353.
- 4969 Ushio, T., Sasashige, K., Kubota, T., Shige, S., Okamoto, K., Aonashi, K., et al. (2009). A kalman filter
4970 approach to the global satellite mapping of precipitation (GSMaP) from combined passive
4971 microwave and infrared radiometric data. *Journal of the Meteorological Society of Japan*, 87
4972 A(November 2008), 137–151. <https://doi.org/10.2151/jmsj.87A.137>
- 4973 Valerio, A. de M., Kampel, M., Vantrepotte, V., Ward, N. D., Sawakuchi, H. O., Less, D. F. D. S., et al.
4974 (2018). Using CDOM optical properties for estimating DOC concentrations and pCO₂ in the Lower
4975 Amazon River. *Optics Express*, 26(14), A657. <https://doi.org/10.1364/oe.26.00a657>
- 4976 Venticinque, E., Forsberg, B., Barthem, R., Petry, P., Hess, L., Mercado, A., et al. (2016). An explicit

- 4977 GIS-based river basin framework for aquatic ecosystem conservation in the Amazon. *Earth System*
4978 *Science Data*, 8(2), 651–661. <https://doi.org/10.5194/essd-8-651-2016>
- 4979 Vera, C. S., Alvarez, M. S., Gonzalez, P. L. M., Liebmann, B., & Kiladis, G. N. (2018). Seasonal cycle of
4980 precipitation variability in South America on intraseasonal timescales. *Climate Dynamics*, 51(5–6),
4981 1991–2001. <https://doi.org/10.1007/s00382-017-3994-1>
- 4982 Viale, M., Bianchi, E., Cara, L., Ruiz, L. E., Villalba, R., Pitte, P., et al. (2019). Contrasting climates at
4983 both sides of the Andes in Argentina and Chile. *Frontiers in Environmental Science*, 7(May), 1–15.
4984 <https://doi.org/10.3389/fenvs.2019.00069>
- 4985 Vicente, G. A., Scofield, R. A., & Menzel, W. P. (1998). The Operational GOES Infrared Rainfall
4986 Estimation Technique. *Bulletin of the American Meteorological Society*, 79(9), 1883–1893.
4987 [https://doi.org/10.1175/1520-0477\(1998\)079<1883:togire>2.0.co;2](https://doi.org/10.1175/1520-0477(1998)079<1883:togire>2.0.co;2)
- 4988 Villar, R. E., Martinez, J. M., Le Texier, M., Guyot, J. L., Fraizy, P., Meneses, P. R., & Oliveira, E. de.
4989 (2013). A study of sediment transport in the Madeira River, Brazil, using MODIS remote-sensing
4990 images. *Journal of South American Earth Sciences*, 44, 45–54.
4991 <https://doi.org/10.1016/j.jsames.2012.11.006>
- 4992 Villar, R. E., Martinez, J. M., Armijos, E., Espinoza, J. C., Filizola, N., Dos Santos, A., et al. (2018).
4993 Spatio-temporal monitoring of suspended sediments in the Solimões River (2000–2014). *Comptes*
4994 *Rendus - Geoscience*, 350(1–2), 4–12. <https://doi.org/10.1016/j.crte.2017.05.001>
- 4995 Virji, H. (1981). A Preliminary Study of Summertime Tropospheric Circulation Patterns over South
4996 America Estimated from Cloud Winds. *Monthly Weather Review*, 109(3), 599–610.
4997 [https://doi.org/10.1175/1520-0493\(1981\)109<0599:APSOST>2.0.CO;2](https://doi.org/10.1175/1520-0493(1981)109<0599:APSOST>2.0.CO;2)
- 4998 Vörösmarty, C. J., Moore, B., Grace, A. L., Gildea, M. P., Melillo, J. M., Peterson, B. J., et al. (1989).
4999 Continental scale models of water balance and fluvial transport: An application to South America.
5000 *Global Biogeochemical Cycles*, 3(3), 241–265. <https://doi.org/10.1029/GB003i003p00241>
- 5001 Vörösmarty, C. J., Green, P., Salisbury, J., & Lammers, R. B. (2000). Global water resources:
5002 Vulnerability from climate change and population growth. *Science*, 289(5477), 284–288.
5003 <https://doi.org/10.1126/science.289.5477.284>
- 5004 Wanders, N., Bierkens, M. F. P., de Jong, S. M., de Roo, A., & Karssenber, D. (2014). The benefits of
5005 using remotely sensed soil moisture in parameter identification of large-scale hydrological models.
5006 *Water Resources Research*, 50(8), 6874–6891. <https://doi.org/10.1002/2013WR014639>
- 5007 Wang, C., Li, Z., Zhu, J., Yi, H., & Xie, Q. (2011). Flooded forest water level changes in Amazon
5008 measured with ALOS PALSAR polarimetric interferometric SAR data. *Journal of Computational*
5009 *Information Systems*, 7(8), 2922–2930.

- 5010 Wang, G., Cao, X., Cai, X., Sun, J., Li, X., & Wang, H. (2018). A new data assimilation method for high-
5011 dimensional models. *PLoS ONE*, *13*(2), 1–15. <https://doi.org/10.1371/journal.pone.0191714>
- 5012 Wang, Y., Hess, L. L., Filoso, S., & Melack, J. M. (1995). Understanding the radar backscattering from
5013 flooded and nonflooded Amazonian forests: Results from canopy backscatter modeling. *Remote*
5014 *Sensing of Environment*, *54*, 324–332. [https://doi.org/10.1016/0034-4257\(95\)00140-9](https://doi.org/10.1016/0034-4257(95)00140-9)
- 5015 Ward, J. V., Tockner, K., Arscott, D. B., & Claret, C. (2002). Riverine landscape diversity. *Freshwater*
5016 *Biology*, *47*, 517–539. <https://doi.org/10.1046/j.1365-2427.2002.00893.x>
- 5017 Werdell, P. J., McKinna, L. I. W., Boss, E., Ackleson, S. G., Craig, S. E., Gregg, W. W., et al. (2018). An
5018 overview of approaches and challenges for retrieving marine inherent optical properties from ocean
5019 color remote sensing. *Progress in Oceanography*, *160*(January), 186–212.
5020 <https://doi.org/10.1016/j.pocean.2018.01.001>
- 5021 Werdell, P. J., Behrenfeld, M. J., Bontempi, P. S., Boss, E., Cairns, B., Davis, G. T., et al. (2019). The
5022 plankton, aerosol, cloud, ocean ecosystem mission status, science, advances. *Bulletin of the*
5023 *American Meteorological Society*, *100*(9), 1775–1794. <https://doi.org/10.1175/BAMS-D-18-0056.1>
- 5024 Wilson, M. D., Bates, P., Alsdorf, D., Forsberg, B., Horritt, M., Melack, J., et al. (2007). Modeling large-
5025 scale inundation of Amazonian seasonally flooded wetlands. *Geophysical Research Letters*, *34*(15),
5026 4–9. <https://doi.org/10.1029/2007GL030156>
- 5027 Wilson, M. D., Durand, M., Jung, H. C., & Alsdorf, D. (2015). Swath-altimetry measurements of the
5028 main stem Amazon River :, 1943–1959. <https://doi.org/10.5194/hess-19-1943-2015>
- 5029 Winemiller, K. O., McIntyre, P. B., Castello, L., Fluet-Chouinard, E., Giarrizzo, T., Nam, S., et al. (2016).
5030 Balancing hydropower and biodiversity in the Amazon, Congo, and Mekong. *Science*, *351*(6269),
5031 128–129. <https://doi.org/10.1126/science.aac7082>
- 5032 Wittmann, F., Anhuf, D., & Funk, W. J. (2002). Tree species distribution and community structure of
5033 central Amazonian várzea forests by remote-sensing techniques. *Journal of Tropical Ecology*, *18*(6),
5034 805–820. <https://doi.org/10.1017/S0266467402002523>
- 5035 Wongchuig, S. C., de Paiva, R. C. D., Siqueira, V., & Collischonn, W. (2019). Hydrological reanalysis
5036 across the 20th century: A case study of the Amazon Basin. *Journal of Hydrology*, *570*, 755–773.
5037 <https://doi.org/10.1016/j.jhydrol.2019.01.025>
- 5038 Wongchuig, S. C., Paiva, R. C. D. de, Biancamaria, S., & Collischonn, W. (2020). Assimilation of future
5039 SWOT-based river elevations, surface extent observations and discharge estimations into uncertain
5040 global hydrological models. *Journal of Hydrology*, *590*(125473).
5041 <https://doi.org/10.1016/j.jhydrol.2020.125473>
- 5042 Wood, E. F., Roundy, J. K., Troy, T. J., Van Beek, L. P. H., Bierkens, M. F. P., Blyth, E., et al. (2011).

- 5043 Hyperresolution global land surface modeling: meeting a grand challenge for monitoring Earth's
5044 terrestrial water. *Water Resources Research*, 47(5), 1–10. <https://doi.org/10.1029/2010WR010090>
- 5045 Wright, J. S., Fu, R., Worden, J. R., Chakraborty, S., Clinton, N. E., Risi, C., et al. (2017). Rainforest-
5046 initiated wet season onset over the southern Amazon. *Proceedings of the National Academy of*
5047 *Sciences of the United States of America*, 114(32), 8481–8486.
5048 <https://doi.org/10.1073/pnas.1621516114>
- 5049 Wu, J., Lakshmi, V., Wang, D., Lin, P., Pan, M., Cai, X., et al. (2020). The reliability of global remote
5050 sensing evapotranspiration products over Amazon. *Remote Sensing*, 12(14).
5051 <https://doi.org/10.3390/rs12142211>
- 5052 Xavier, L., Becker, M., Cazenave, A., Longuevergne, L., Llovel, W., & Filho, O. C. R. (2010).
5053 Interannual variability in water storage over 2003–2008 in the Amazon Basin from GRACE space
5054 gravimetry, in situ river level and precipitation data. *Remote Sensing of Environment*, 114(8), 1629–
5055 1637. <https://doi.org/10.1016/J.RSE.2010.02.005>
- 5056 Xie, P., Janowiak, J. E., Arkin, P. A., Adler, R., Gruber, A., Ferraro, R., et al. (2003). GPCP pentad
5057 precipitation analyses: An experimental dataset based on gauge observations and satellite estimates.
5058 *Journal of Climate*, 16(13), 2197–2214. <https://doi.org/10.1175/2769.1>
- 5059 Xie, P., Joyce, R., Wu, S., Yoo, S. H., Yarosh, Y., Sun, F., & Lin, R. (2017). Reprocessed, bias-corrected
5060 CMORPH global high-resolution precipitation estimates from 1998. *Journal of Hydrometeorology*,
5061 18(6), 1617–1641. <https://doi.org/10.1175/JHM-D-16-0168.1>
- 5062 Xu, X., Jia, G., Zhang, X., Riley, W. J., & Xue, Y. (2020). Climate regime shift and forest loss amplify
5063 fire in Amazonian forests. *Global Change Biology*, 26(10), 5874–5885.
5064 <https://doi.org/10.1111/gcb.15279>
- 5065 Yamazaki, D., Kanae, S., Kim, H., & Oki, T. (2011). A physically based description of floodplain
5066 inundation dynamics in a global river routing model. *Water Resources Research*, 47(4).
5067 <https://doi.org/10.1029/2010WR009726>
- 5068 Yamazaki, D., Baugh, C. A., Bates, P. D., Kanae, S., Alsdorf, D. E., & Oki, T. (2012). Adjustment of a
5069 spaceborne DEM for use in floodplain hydrodynamic modeling. *Journal of Hydrology*, 436–437,
5070 81–91. <https://doi.org/10.1016/j.jhydrol.2012.02.045>
- 5071 Yamazaki, D., Lee, H., Alsdorf, D. E., Dutra, E., Kim, H., Kanae, S., & Oki, T. (2012). Analysis of the
5072 water level dynamics simulated by a global river model: A case study in the Amazon River. *Water*
5073 *Resources Research*, 48(9), 1–15. <https://doi.org/10.1029/2012WR011869>
- 5074 Yamazaki, D., O'Loughlin, F., Trigg, M. A., Miller, Z. F., Pavelsky, T. M., & Bates, P. D. (2014).
5075 Development of the Global Width Database for Large Rivers. *Water Resources Research*, 50(4),

- 5076 3467–3480. <https://doi.org/10.1002/2013WR014664>
- 5077 Yamazaki, D., Trigg, M. A., & Ikeshima, D. (2015). Development of a global ~90m water body map
5078 using multi-temporal Landsat images. *Remote Sensing of Environment*, *171*, 337–351.
5079 <https://doi.org/10.1016/j.rse.2015.10.014>
- 5080 Yamazaki, D., Ikeshima, D., Tawatari, R., Yamaguchi, T., O’Loughlin, F., Neal, J. C., et al. (2017). A
5081 high-accuracy map of global terrain elevations. *Geophysical Research Letters*, *44*(11), 5844–5853.
5082 <https://doi.org/10.1002/2017GL072874>
- 5083 Yamazaki, D., Ikeshima, D., Sosa, J., Bates, P. D., Allen, G. H., & Pavelsky, T. M. (2019). MERIT
5084 Hydro: A High-Resolution Global Hydrography Map Based on Latest Topography Dataset. *Water*
5085 *Resources Research*, *55*(6), 5053–5073. <https://doi.org/10.1029/2019WR024873>
- 5086 Yang, Z., & Dominguez, F. (2019). Investigating land surface effects on the moisture transport over
5087 South America with a moisture tagging model. *Journal of Climate*, *32*(19), 6627–6644.
5088 <https://doi.org/10.1175/JCLI-D-18-0700.1>
- 5089 Yepez, S., Laraque, A., Martinez, J. M., Sa, J. De, Manuel, J., Castellanos, B., et al. (2018). Retrieval of
5090 suspended sediment concentrations using Landsat-8 OLI satellite images in the Orinoco River
5091 (Venezuela). *Comptes Rendus - Geoscience*, *350*(1–2), 20–30.
5092 <https://doi.org/10.1016/j.crte.2017.08.004>
- 5093 Yilmaz, K. K., Hogue, T. S., Hsu, K. L., Sorooshian, S., Gupta, H. V., & Wagener, T. (2005).
5094 Intercomparison of rain gauge, radar, and satellite-based precipitation estimates with emphasis on
5095 hydrologic forecasting. *Journal of Hydrometeorology*, *6*(4), 497–517.
5096 <https://doi.org/10.1175/JHM431.1>
- 5097 Yuan, T., Lee, H., Jung, H. C., Aierken, A., Beighley, E., Alsdorf, D. E., et al. (2017). Absolute water
5098 storages in the Congo River floodplains from integration of InSAR and satellite radar altimetry.
5099 *Remote Sensing of Environment*, *201*(March), 57–72. <https://doi.org/10.1016/j.rse.2017.09.003>
- 5100 Zakharova, E. A., Kouraev, A. V., Cazenave, A., & Seyler, F. (2006). Amazon River discharge estimated
5101 from TOPEX/Poseidon altimetry. *Comptes Rendus - Geoscience*, *338*(3), 188–196.
5102 <https://doi.org/10.1016/j.crte.2005.10.003>
- 5103 Zemp, D. C., Schleussner, C. F., Barbosa, H. M. J., Van Der Ent, R. J., Donges, J. F., Heinke, J., et al.
5104 (2014). On the importance of cascading moisture recycling in South America. *Atmospheric*
5105 *Chemistry and Physics*, *14*(23), 13337–13359. <https://doi.org/10.5194/acp-14-13337-2014>
- 5106 Zemp, D. C., Schleussner, C. F., Barbosa, H. M. J., Hirota, M., Montade, V., Sampaio, G., et al. (2017).
5107 Self-amplified Amazon forest loss due to vegetation-atmosphere feedbacks. *Nature*
5108 *Communications*, *8*(14681). <https://doi.org/10.1038/ncomms14681>

- 5109 Zeng, N., Yoon, J. H., Marengo, J. A., Subramaniam, A., Nobre, C. A., Mariotti, A., & Neelin, J. D.
5110 (2008). Causes and impacts of the 2005 Amazon drought. *Environmental Research Letters*, 3(1),
5111 014002. <https://doi.org/10.1088/1748-9326/3/1/014002>
- 5112 Zhang, Ke, Kimball, J. S., & Running, S. W. (2016, November 1). A review of remote sensing based
5113 actual evapotranspiration estimation. *Wiley Interdisciplinary Reviews: Water*. John Wiley and Sons
5114 Inc. <https://doi.org/10.1002/wat2.1168>
- 5115 Zhang, Kun, Zhu, G., Ma, J., Yang, Y., Shang, S., & Gu, C. (2019). Parameter Analysis and Estimates for
5116 the MODIS Evapotranspiration Algorithm and Multiscale Verification. *Water Resources Research*,
5117 55(3), 2211–2231. <https://doi.org/10.1029/2018WR023485>
- 5118 Zhang, Y., Pan, M., Sheffield, J., Siemann, A. L., Fisher, C. K., Liang, M., et al. (2018). A Climate Data
5119 Record (CDR) for the global terrestrial water budget: 1984–2010. *Hydrology and Earth System
5120 Sciences*, 22(1), 241–263. <https://doi.org/10.5194/hess-22-241-2018>
- 5121 Zheng, G., & DiGiacomo, P. M. (2017). Remote sensing of chlorophyll-a in coastal waters based on the
5122 light absorption coefficient of phytoplankton. *Remote Sensing of Environment*, 201(September),
5123 331–341. <https://doi.org/10.1016/j.rse.2017.09.008>
- 5124 Zhou, J., & Lau, K. M. (1998). Does a monsoon climate exist over South America? *Journal of Climate*,
5125 11(5), 1020–1040. [https://doi.org/10.1175/1520-0442\(1998\)011<1020:DAMCEO>2.0.CO;2](https://doi.org/10.1175/1520-0442(1998)011<1020:DAMCEO>2.0.CO;2)
- 5126 Zhou, L., Divakarla, M., & Liu, X. (2016). An overview of the joint polar satellite system (JPSS) science
5127 data product calibration and validation. *Remote Sensing*, 8(2). <https://doi.org/10.3390/rs8020139>
- 5128 Zubieta, R., Getirana, A., Espinoza, J. C., & Lavado, W. (2015). Impacts of satellite-based precipitation
5129 datasets on rainfall-runoff modeling of the Western Amazon basin of Peru and Ecuador. *Journal of
5130 Hydrology*, 528, 599–612. <https://doi.org/10.1016/j.jhydrol.2015.06.064>
- 5131 Zubieta, R., Getirana, A., Espinoza, J. C., Lavado-Casimiro, W., & Aragon, L. (2017). Hydrological
5132 modeling of the Peruvian-Ecuadorian Amazon Basin using GPM-IMERG satellite-based
5133 precipitation dataset. *Hydrology and Earth System Sciences*, 21(7), 3543–3555.
5134 <https://doi.org/10.5194/hess-21-3543-2017>
- 5135 Zubieta, R., Saavedra, M., Espinoza, J. C., Ronchail, J., Sulca, J., Drapeau, G., & Martin-Vide, J. (2019).
5136 Assessing precipitation concentration in the Amazon basin from different satellite-based data sets.
5137 *International Journal of Climatology*, 39(7), 3171–3187. <https://doi.org/10.1002/joc.6009>
- 5138 Zulkafli, Z., Buytaert, W., Onof, C., Lavado, W., & Guyot, J. L. (2013). A critical assessment of the
5139 JULES land surface model hydrology for humid tropical environments. *Hydrology and Earth
5140 System Sciences*, 17(3), 1113–1132. <https://doi.org/10.5194/hess-17-1113-2013>
- 5141 Zulkafli, Zed, Buytaert, W., Onof, C., Manz, B., Tarnavsky, E., Lavado, W., & Guyot, J. L. (2014). A

5142 comparative performance analysis of TRMM 3B42 (TMPA) versions 6 and 7 for hydrological
5143 applications over Andean-Amazon river basins. *Journal of Hydrometeorology*, 15(2), 581–592.
5144 <https://doi.org/10.1175/JHM-D-13-094.1>
5145 Zulkafli, Zed, Buytaert, W., Manz, B., Rosas, C. V., Willems, P., Lavado-Casimiro, W., et al. (2016).
5146 Projected increases in the annual flood pulse of the Western Amazon. *Environmental Research*
5147 *Letters*, 11(1). <https://doi.org/10.1088/1748-9326/11/1/014013>
5148